PERFORMANCE ANALYSIS OF ROTARY TOOL MICRO-USM PROCESS

Ph.D. THESIS

by

SANDEEP KUMAR

**DEPARTMENT OF MECHANICAL AND INDUSTRIAL ENGINEERING
INDIAN INSTITUTE OF TECHNOLOGY ROORKEE
ROORKEE-247667 (INDIA)
SEPTEMBER, 2019**

PERFORMANCE ANALYSIS OF ROTARY TOOL MICRO-USM PROCESS

A THESIS

Submitted in partial fulfilment of the requirements for the award of the degree

of

DOCTOR OF PHILOSOPHY

in

MECHANICAL ENGINEERING

by

SANDEEP KUMAR

**DEPARTMENT OF MECHANICAL AND INDUSTRIAL ENGINEERING
INDIAN INSTITUTE OF TECHNOLOGY ROORKEE
ROORKEE-247667 (INDIA)
SEPTEMBER, 2019**

INDIAN INSTITUTE OF TECHNOLOGY ROORKEE

STUDENT'S DECLARATION

I hereby certify that the work presented in the thesis entitled **"PERFORMANCE ANALYSIS OF ROTARY TOOL MICRO-USM PROCESS"** is my own work carried out during a period from December, 2014 to September, 2019 under the supervision of Dr. Akshay Dvivedi, Associate Professor, Department of Mechanical and Industrial Engineering, Indian Institute of Technology Roorkee, Roorkee.

The matter presented in the thesis has not been submitted for the award of any other degree of this or any other Institute.
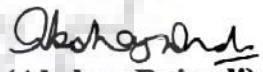
Dated: 16-12-2019

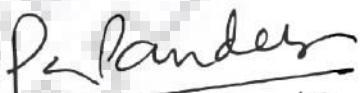**(SANDEEP KUMAR)**

SUPERVISOR'S DECLARATION

This is to certify that the above mentioned work is carried out under my supervision.

Dated:

(Akshay Dvivedi)

The Ph.D. Viva-Voce Examination of **Sandeep Kumar**, Research Scholar, has been held on...16|12|2019......

16.12.19

Chairman, DRC

Signature of External Examiner

This is to certify that the student has made all the corrections in the thesis.

Signature of Supervisor

Head of the Department

i

ACKNOWLEDGEMENT

It is a pleasure to express my feelings to my father **Shri Ilam Singh**, for inculcating moral values and ethics in me. I avail the privilege to pour on paper, my regards to my mother **Smt. Kunwarkali Devi**. Their blessings, love, care, inspiration, seen and unseen blessings kept me sailing through the storms.

A very special expression of positive reception is extended to my brother, sister, brother-in law, nephews and niece.

I express my apology that I could not mention everyone individually. Above all, I would like to express my sincere gratitude from the core of my heart to God Almighty for giving me courage, strength, sound health, and patience to carry out my research. I thank all the souls who helped me in this herculean task. I dedicate this thesis to my grandmother late **Smt. Shanti Devi**.

(Sandeep Kumar)

ABSTRACT

Miniaturization of components is the need of hour because it saves raw material, processing time and energy. Therefore, micro components in the form of microfluidic devices are gaining huge importance in the field of electronics, optics and biotechnology etc. Hard and brittle non-conductive materials such as glass and silicon are the most commonly used materials for the fabrication of microfluidics devices. In recent past, micro-ultrasonic machining (micro-USM) process has emerged as a promising technique for machining of micro features such as microholes and microchannels on hard and brittle materials irrespective of their electrical conductivity. Despite several advantages, micro-USM process has some limitations such as low material removal rate (MRR), high tool wear rate (TWR) and poor form accuracy. The accumulation of abrasive inside the machining zone is the major factor responsible for the abovementioned problems. In past, several attempts have been made to overcome these limitations by augmenting micro-USM process. However, machining of dimensionally accurate, high aspect ratio microfeatures using micro-USM process is still a challenge. Thus, in order to resolve the aforesaid issues, rotary tool micro-USM, a process variant of micro-USM process has been experimentally investigated in the present research endeavor. In rotary tool micro-USM, the tool vibrates and rotates simultaneously and abrasive slurry is pumped between the tool and work material.

The present research work was aimed to enhance the performance (i.e. productivity and accuracy) of micro-USM process by providing modification in the conventional micro-USM system. The modification was provided in the form of rotary motion of tool without making any manufacturing complexity in the micro-USM facility. An extensive experimentation was performed to investigate the effect of tool rotation and other process parameters of micro-USM process on its performance characteristics. Also, multi-criteria optimization was carried out to obtain maximum productivity and accuracy. During experimentation, microholes and microchannels were machined and subsequently characterized using different types of characterization techniques such as optical microscope, stereo zoom microscope, field emission scanning electron microscope (FE-SEM) etc.

The major objectives of the present research work are outlined as follows:

- To develop a rotary tool micro-USM process setup for machining of microfeatures in hard and brittle materials.
- To investigate and analyze the effect of tool materials and their properties on performance of rotary tool micro-USM process.
- To evaluate the performance of rotary tool micro-USM process during machining of microholes and microchannels on borosilicate glass.
- To investigate and analyze the influence of various process parameters of rotary tool micro-USM process during drilling of microholes on hard and brittle materials.
- To investigate the tool wear phenomenon and its effect on form accuracy of microchannels during rotary tool micro-USM process.
- To develop a predictive model of material removal rate for rotary tool micro-USM process.

In the present research work, initially, the experimental setup of rotary tool micro-USM process was designed and fabricated using the in-house facilities. After that pilot experimentation was performed on rotary tool micro-USM process. The objective of pilot experimentation was to select the working range of tool rotation speed and to select the suitable tool material for rotary tool micro-USM process. The one-factor-at-time (OFAT) approach was used in pilot experimentation. The experimental results revealed that tool rotation speed for microhole drilling can be varied from 100 rpm to 500 rpm, whereas for microchannels fabrication, it can be varied from 100 rpm to 600 rpm. Tungsten carbide tool material was found to be suitable candidate tool material for rotary tool micro-USM process due to its high abrasion resistance and better acoustic properties.

After selecting the range of tool rotation speed and tool material, the performance of rotary tool micro-USM process was experimentally evaluated. During performance evaluation, the rotary tool micro-USM process was compared with stationary tool micro-USM process while drilling of microholes and fabrication of microchannels. Experiments were conducted by varying the four micro-USM process parameters. The responses measured in this experimentation were MRR, hole overcut (HOC) for microholes and depth of channel (DOC) and form accuracy for microchannels. The

results revealed that the rotary tool micro-USM process performed better than stationary tool micro-USM process. Thus, rotary tool micro-USM was selected for further experimentation. A qualitative analysis of tool wear and form accuracy during stationary tool and rotary tool micro-USM processes was also carried out with the help of field emission scanning electron microscope (FE-SEM) micrographs. The results revealed that rotary tool micro-USM process exhibits lesser tool wear and better form accuracy as compared to stationary tool micro-USM process.

Subsequently, the rotary tool micro-USM process was employed for drilling of microholes in hard and brittle materials such as glass, silicon and zirconia. The aim of this investigation was to examine the drilling capability of rotary tool micro-USM process for different hard and brittle materials. In order to fulfil this aim, an extensive experimentation was performed on rotary tool micro-ultrasonic drilling (USD) process. Three types of work materials i.e. glass, silicon and zirconia were selected. The experimentation was performed using OFAT approach. The machined surface were analysed qualitatively to investigate the mode of material removal during rotary tool micro-USM of hard and brittle materials. Eventually, desirability approach was used to optimize the responses of rotary tool micro-USM for microhole drilling. The experimental results revealed that rotary tool micro-USM can be employed for drilling of microholes in all type of hard and brittle materials. The machining rate and HOC were found to be higher during drilling of silicon followed by glass and zirconia. Maximum tool wear was observed during machining of zirconia, whereas minimum tool wear was observed when silicon was machined. In all the work materials, pure brittle fracture was observed as the mode of material removal. At optimal parametric settings, microhole of depth 4355 µm was successfully machined in glass using rotary tool micro-USD process.

Tool wear greatly affect the performance of micro-USM process as the shape of the tool governs the shape of machined microfeatures. In order to control the tool wear, an investigation was performed on tool wear and its effect on form accuracy of microchannels during rotary tool micro-USM process. In this investigation, initially, mechanism of tool wear and types of tool wear were identified considering tool, abrasive and workpiece interaction. Thereafter, a geometrical model of tool wear was developed to calculate volumetric wear of tool quantitatively during rotary tool micro-

USM process. Later, the effect of tool wear and other rotary tool micro-USM process parameters were investigated on dimensional and form accuracy of the machined microchannels. The results revealed that rotary tool micro-USM has two types of tool wear i.e. longitudinal wear and edge wear. The form accuracy of microchannels was found to be more affected by edge wear as compared to longitudinal wear. Whereas, the DOC was found to be more affected by longitudinal wear as compared to edge wear. The desired DOC at the best possible form accuracy (i.e. at lowest edge rounding wear) of the microchannel can be obtained by providing longitudinal wear compensation to the tool. The optimal parametric combination of rotary tool micro-USM process provided maximum MRR 2.89 mg/min, DOC 517.48 µm and form accuracy of 87% and minimum width of microchannel 663 µm and TVW 0.017 mm^3. Further, the rotary tool micro-USM process was utilized for machining of complex shaped microchannels to check its machining feasibility for microfluidic applications.

Additionally, an attempt was made on development of material removal rate model for rotary tool micro-USM process considering brittle fracture theory. The model was developed by selecting tetrahedron geometry of abrasive particle. The pure brittle fracture was considered as mode of material removal during development of the model. The developed model was experimentally verified and statistically analysed. The predicted results were in good agreement with the experimental results within the selected range of input parameters. Statistical analysis also conformed the prediction accuracy of the developed model.

TABLE OF CONTENTS

LIST OF FIGURES

xv

LIST OF TABLES

NOMENCLATURE AND ACRONYMS

NOTATION	DESCRIPTION
a	Side length of abrasive
h_1	Height of abrasive
d	Indentation depth
A	Amplitude
f	Frequency of vibration
h_2	Height of abrasive
V_c	Cutting velocity
m	Number of abrasives
A_i	Indentation area
N	Tool rotation speed
n	Number of passes
D_t	Diameter of tool
w	Width of working gap
C	Slurry concentration
m	Mass of abrasive
v	Velocity of abrasive
W_a	Weight of abrasive
ρ_a	Density of abrasive
b	Width of indentation
Δt	Effective machining time
A_c	Cutting area
ρ_w	Density of water
M_a	Material removed by single abrasive
F_{n_1}	Normal load at bottom of work
F_{n_2}	Normal load at side wall of cavity
F_n	Normal load
ρ_a	Density of water
C_L	Length of crack

C_H	Depth of crack
α	Half angle of abrasive particle
C_2	Constant
E	Modulus of elasticity
υ	Poisson's ratio
D_h	Actual diameter of hole
D_{max}	Maximum diameter of hole
D_{min}	Minimum diameter of hole
W_{ie}	Inner edge width
W_{oe}	Outer edge width
D_{Ent}	Entrance diameter of hole
D_{Ext}	Exit diameter of hole
T_w	Thickness of work material
β	Taper angle
$\emptyset$	Tool diameter
B_4C	Boron carbide
SiC	Silicon carbide
Al_2O_3	Aluminium oxide
N_2	Nitrogen dioxide
CO_2	Carbon dioxide

ACRONYM	DESCRIPTION
AJM	Abrasive Jet Machining
AS	Abrasive Size
AWJM	Abrasive Water Jet Machining
CAD	Computer Aided Design
CAM	Computer Aided Manufacturing
CNC	Computerized Numerical Control
CUSM	Chemical-assisted Ultrasonic Machining

DOC	Depth of Channel
EBM	Electron Beam Machining
ECDM	Electro Chemical Discharge Machining
ECM	Electro Chemical Machining
EDM	Electric Discharge Machining
ENIAC	Electronic Numeric Integrator and Computer
EPAMUSM	Electrophoretically Assisted Micro-Ultrasonic Machining
FESEM	Field Emission Scanning Electron Microscope
FIB	Focused Ion Beam
FEM	Finite Element Method
HAZ	Heat Affected Zone
HOC	Hole Overcut
HCS	High Carbon Steel
HSS	High Speed Steel
FA	Form Accuracy
FR	Feed Rate
IBM	Ion Beam Machining
KE	Kinetic Energy
LBM	Laser Beam Machining
LIGA	Lithography, Galvanoformung and Abformung
LASER	Light Amplification Stimulated Emission Radiation
LOC	Lab on Chip
MEMS	Micro Electro Mechanical Systems
MRR	Material Removal Rate
NUAM	Non-contact Ultrasonic Abrasive Machining
OFAT	One-Factor-At-Time
PCD	Poly Crystalline Diamond

PR	Power Rating
PCM	Photochemical Machining
PDMS	Poly Di Methlyl Siloxane
PMMA	Poly Methyl Metha Acrylate
PZT	Piezoelectric Transducer
QC	Quality Characteristic
RIE	Reactive Ion Etching
RS	Rotation Speed
RT-MUSM	Rotary Tool Micro Ultrasonic Machining
RT-MUSD	Rotary Tool Micro Ultrasonic Drilling
SAMMA	Self-Aligned Multilayer Machining and Assembly
SC	Slurry Concentration
SPH	Smooth Particles Hydrodynamics
SEM	Scanning Electron Microscope
SOULE	Self-aligned process combining batch mode ultrasonic machining, lapping and batch mode micro-electro discharge machining
SS	Stainless Steel
TVW	Total Volumetric Wear
UV	Ultra Violate
USAL	Ultrasonic Assisted Lapping
USM	Ultrasonic Machining
UWM	Uniform Wear Method
WC	Tungsten Carbide
WOC	Width of Channel
WEDM	Wire Electric Discharge Machining
WEDG	Wire Electric Discharge Grinding

1.1 Miniaturization

Miniaturization is the need of hour as it saves raw material, energy and space. Miniaturization helps in better conservation of resources and also reduces the adverse effect on environment. The technological developments on miniaturization started in 1947 with invention of transistors. This invention led to the development of integrated circuits (ICs) (Hsu, (2002)) that are the backbone of electronics industry. There are many examples of miniaturized products such as computer, mobile phones, pen drives, microgears, micromolds, microengines (Moges et al., (2017)). Miniaturization has not only reduced the size of the product but also it has significantly reduced the cost of the product (Goldstine and Goldstine, (1996)). Computer is the best example of miniaturization. This difference in space requirement and cost is itself a revolutionary change that has taken place as a result of technology development over a period of time. Thus, because of miniaturization, a paradigm shift has taken place in manufacturing from macro level to micro level (Byrne, (2003)). The advanced manufacturing methods have developed to meet the demand of miniaturized products. The advanced manufacturing methods are capable of machining those materials which are hard, brittle and difficult-to-machine by other methods. But, advanced manufacturing methods require special type of fixtures and tools for micro fabrication. Also, the characterization of machined micro features requires sophisticated precise instruments. To maintain a tight tolerance is always a challenge in micro domain manufacturing. In order to overcome these challenges, an extensive research have been conducted in the domain of micromachining (Refer Figure 1.1).

1.2 Advantages of Miniaturization

Miniaturization has various advantages which are as follows:

- Miniaturized devices requires less space, thus more functional components can be add in a single device.
- Miniaturized systems take lesser analysis time as compared to the large systems.

- Small systems have low mechanical inertia and quick response as compared to large systems. Therefore, these can be used for precision movements.
- Mechanical vibration and thermal distortions are very less in miniaturized systems owing to lesser mass.
- Owing to smaller size, miniaturized devices are particularly suited for biomedical and aerospace applications.
- Miniaturized devices have low thermal expansion even at high working temperatures which results in higher dimensional stability.
- Small systems have low manufacturing costs, transportation cost and operational cost as compared to large systems.
- Miniaturized systems can be mass-produced in batches.

The advancement in the micromachining techniques has led to the development of microfluidic devices. The subsequent section discusses the developments in microfluidics.
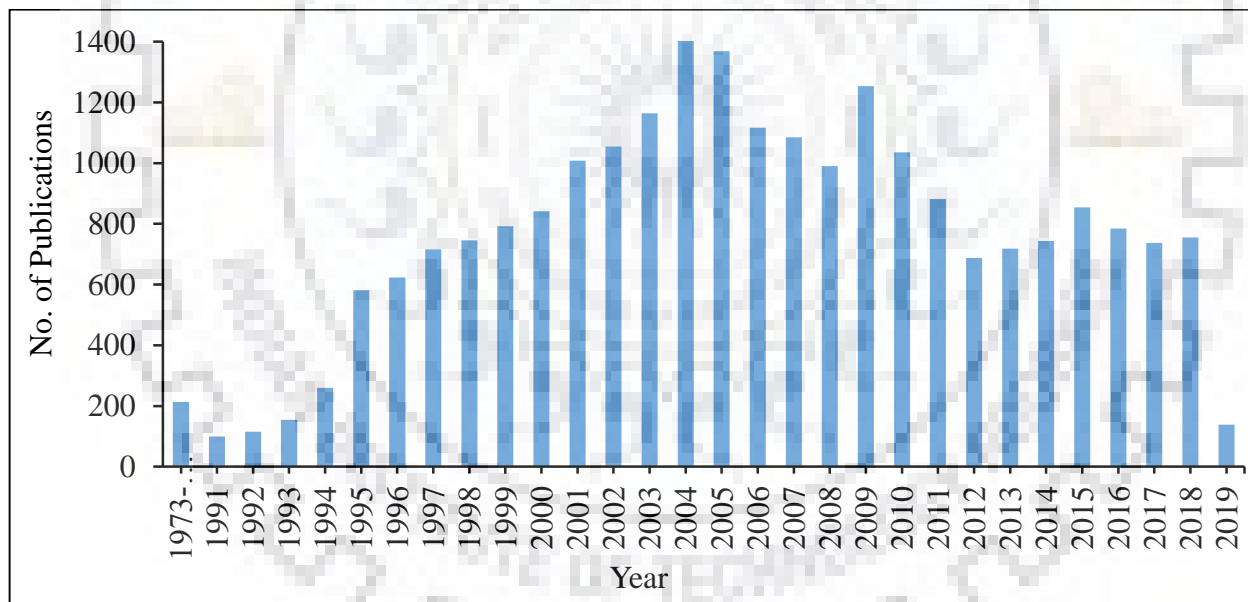
Figure 1.1 Database of publications on micromachining (Scopus on 05/03/2019)

1.3 Developments in Microfluidics

Last decade had witnessed several developments in microfluidics. An evidence for the same can be seen from Figure 1.2, which clearly indicates that more than 35,000 articles containing the word 'microfluidics' have published in the last decade. In spite of that, there is a lack of commercially

available microfluidic devices that can be used in industries (Mark et al., (2010)). This implies that the majority of research work on microfluidics is limited to the laboratories only. The reason being exceptionally high cost of fabrication (Becker, (2009)). Another reason seems to be the lack of coordination between the research community and industries.
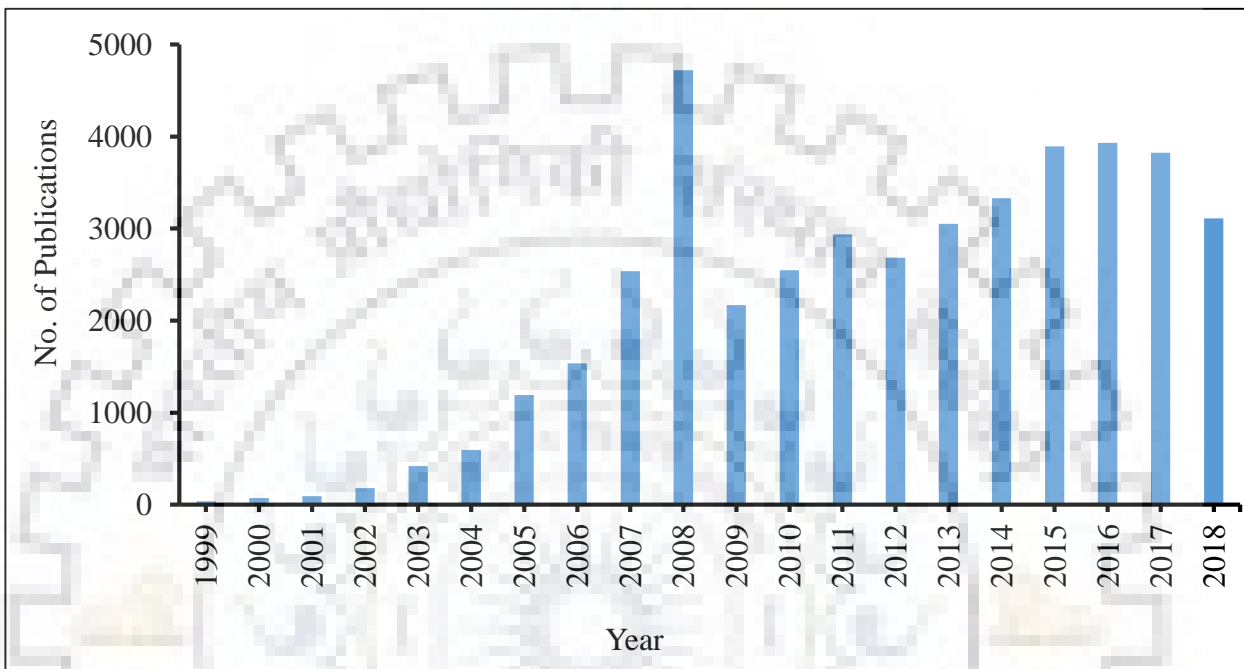
Figure 1.2 Database of publications on microfluidics (Scopus on 05/03/2019)

1.4 Microfluidic Devices

Microfluidic devices are used to control, transfer and manipulate the flow of fluids in a set of microchannels (Casquillas, (2014)). The fluid may be liquid, gas or a mixture of both. These devices use very little amount of fluid that are generally measured in microliter, nanoliter, or even in picoliter quantities. A microfluidic device composed of various components such as micromixers, micropumps, microvalves, and microfilters etc. The flow of fluid in a microfluidic device takes place through microholes and microchannels. A hole is defined as a microhole if its diameter ranges from 1 µm to 999 µm. The function of a through microhole in a microfluidic device is to provide an inlet/outlet to the fluid. The blind microholes are used as reservoirs to store the fluids. A channel is defined as a microchannel if its hydraulic diameter varies in the range of 1 µm to 999 µm. The main function of microchannel is to bring the flowing fluid in contact with its wall and bring fresh fluid in contact with its wall so that new fresh fluid can push the previous

3

fluid away (Kandlikar et al., (2005)). The main advantage of microchannel is its small volume to larger surface area. On decreasing the dimensions of a microchannel, its surface to volume ratio increases (Weibel and Whitessides, (2006)). Higher surface to volume ratio increases the heat transfer. Due to this reason, microchannels are used as micro heat exchanger. A detailed description of different components of a microfluidic device is given below:

- **Micro mixer**

Micro mixers are used to mix two different fluids together and also used to split them into several streams. These streams flow alternatively into the mixing chamber through microchannels. Rapid mixing of fluids is essential in microfluidic systems used in the field of biochemistry analysis, drug delivery and synthesis of acids (Mansur et al., (2008)). Micro mixers assist these complex chemical reaction to complete at faster rate. Micro mixers are of two type i.e. active and passive micro mixers (Hessel et al., (2005); Nguyen and Wu, (2005)). The active micro mixers require external energy in the form of temperature, pressure etc. Whereas, in passive micro mixers no such external energy is required. The mixing depends on the shape and geometry of microchannels. Other applications of micro mixers include mixing operation in foaming, gas absorption, emulsification and reaction etc. (Bayer et al., (2003); Ehrfeld et al., (1999); Hessel et al., (2004); Malek et al., (2007)).

- **Microvalves**

Microvalves are used to vary and control the direction of fluid flowing in a microfluidic system (Cho et al., (2007)). Miccrovalves are categorized as active microvalves and passive microvalves (Oh and Ahn, (2006); Pilarski et al., (2005); Shoji and Esashi, (1994)). As the name suggest, active microvalves works with the help of mechanical/non-mechanical parts with actuators. On the other hand, no actuator is used in passive microvalves. Life sciences applications have huge demand of non-mechanical active microvalves and capillary passive microvalves owing to easy operation and low cost. The actuators/external systems are recommended only when there is no constraint on the size of microfluidic device (Zhang et al., (2007)). The microvalves can be actuated mechanically (Pamble and Towe, (1999)), pneumatically (Studer et al., (2004); Grover et al., (2003); Wheeler et al., (2005)), electrokinetically (Jin et al., (2005)), by phase changes (Baroud et al., (2007); Liow, (2009)) or by introduction of external force (Chen et al., (2008)).

- **Micropumps**

Pumps having a functional dimension of the micrometer range are termed as a micropump. The first miniaturized pump was reported in 1975 by Thomas and Bessman (Thomas and Bessman, (1998)). It was designed for implantation inside the human body. Micropumps are classified into mechanical type and non-mechanical type (Nisar et al., (2008)). Mechanical type micropumps have moving components like check valves and pumping diaphragm. A physical actuator is required to perform pumping function in mechanical micro-pumps. Whereas, non-mechanical type micropumps do not require actuator. The first miniaturized pump was reported in the year 1975. It was designed for implantation inside the human body (Thomas and Bessman, (1998)).

- **Microfilters**

Microfilter is a part of microfluidic device which is used to filter the contaminated fluids such as microorganisms and suspended particles (Baker, (2012)). The filters are specially designed for separating large bacteria, algae, sediments from the process liquid. Microfilters are also used in biochemical analysis for separation of plasma from blood cells (Crowley and Pizziconi, (2005)). But, the microfilters permit the passage of water, monovalent ions and viruses.

The microfluidic devices are generally fabricated on glass and silicon materials and has extensive applications in bio-medical engineering (in point-of-care diagnosis), microelectromechanical systems (MEMS), drug delivery system and lab-on-chip devices for micro total analysis. Moreover, microfluidic systems are used in chemical biology that includes microdiluters (Neils et al., (2004)), gradients (Jauregui et al., (2010)), arrays (Ismagiloy et al., (2001)), droplets (He et al., (2005)), painting cells (Takayama et al., (2001)), gel structures (Zhang, (2004)), study of single cells (Daridon et al., (2001)) and logic gates (Thomson et al., (1998)).

- **Micro heat exchanger**

Micro heat exchangers are also known as the micro heat sinks. The main function of heat sink is to effectively absorb and dissipate the heat from the surroundings using extended surfaces. The micro heat exchanger comprises of a series of microchannels. The micro heat exchanger has the capability to remove high heat flux thereby maintaining the required temperature level (Lee,

(2010); Lowe et al., (2000); Phillise, (1988); Schmidt (2001)) and perform better than typical heat exchanger.

1.5 Materials used in Microfluidics and its Applications

The first microfluidic device was made of silicon using microelectronic technology (Terry et al., (1979)). Nowadays, there are three types of materials i.e. inorganic, polymers, and paper are used for microfluidic devices (Roy et al., (2016)). Inorganic materials include silicon, glass and ceramics (co-fired ceramics and vitroceramics). Polymers are further divided into two subgroups i.e. thermosets and thermoplastics. The paper microfluidics is newly developed technology. Among the above three types of materials, the inorganic materials are wide used in microfluidics. The reason for the same is their superior properties such as thermal resistance, corrosion resistance, high hardness, low thermal conductivity and high dielectric strength. Glass is used in various applications including microelectromechanical systems (MEMS), optical devices, communication devices, fuel cells, and aerospace etc. (Arif et al., (2011); Xiao et al., (2014)). Advanced ceramics such as zirconia is extensively used in several dental applications (i.e. crowns, bridges, inlay etc.), aerospace, automotive components (Arif et al., (2011)) and computer device (i.e. hard disk) (Lee and Choi, (2010)). Silicon wafer is being increasingly used as a raw material for MEMS devices, photonics and semiconductors (Chalker et al., (2005); Subramonian et al., (2015); Lee and Choi, (2010)).

1.6 Challenges in Fabrication of Microfeatures on Hard and Brittle Materials

As mentioned above, hard and brittle materials possess superior properties which make them extremely difficult for machining specifically in micro domain. Both the conventional and non-conventional machining techniques such as lithography, non-conventional and conventional micromachining techniques have been used to machine hard and brittle materials. But, to generate a desired microstructure with desired accuracy and surface finish is still a challenge. Lithography based techniques are either limited to specific material or requires very clean environment during machining. The working environment must be absolutely dust free otherwise that may hinder the working of the developed microfluidic device during analysis. Moreover, it is used for bulk micromachining only. Non-conventional micromachining techniques such as focused ion beam machining, laser machining, abrasive jet machining and ultrasonic machining are used for micro

6

fabrication of hard and brittle materials. The ion beam machining process and laser beam machining process are extremely costly. Moreover, laser produces thermal damage around the machined cavity. Abrasive jet machining process and ultrasonic machining process do not fulfill the surface finish requirements that are needed for microfluidic devices. Conventional micromachining involves direct interaction of tool with work surface in which high cutting force is exerted on the work material. Brittle fracture occurs during machining of hard and brittle which creates non-uniform surfaces which requires additional finishing process. Finishing processes further leads to surface/subsurface damage that reduces the strength and performance of the component. Apart from this, the high cost of manufacturing is also a major challenge in machining of hard and brittle materials.

In order to overcome the challenges encountered in machining of hard and brittle materials, a number of micro manufacturing techniques have been developed by several researchers. The main objective of the researchers was to develop a micromachining facility that can develop intricate profiles and other 3D microstructures on hard and brittle materials without the requirement of clean room facility. Micro-ultrasonic machining is one of such potential processes for fulfilling both the aforesaid requirements.

1.7 Micro-ultrasonic Machining of Hard and Brittle Materials

In the current scenario, a number of manufacturing methods are being increasingly developed for machining of difficult-to-machine hard and brittle materials. The objective of reduction in the cost of manufacturing and increase in the productivity and efficiency of manufacturing methods has motivated the researchers for the development of newer manufacturing methods (Crowley and Pizziconi, (2005)).

Micro-USM process is a cost effective non-conventional machining process. It is mainly used to machine hard and brittle materials irrespective of their electrical conductivity. Glass, quartz, ceramics and silicon are the commonly used work materials in micro-USM process. In micro-USM process, the shape of the micro tool is replicated the work surface. In this process, the material removal takes place by the application of mechanical energy, therefore it does not alter the metallurgical, physical and chemical properties of work materials. It has effectively used for the drilling of microholes as small as 5 μm in diameter on silicon and glass work materials (Sun et al.,

7

(1996ᵃ)). Micro-USM process is comparatively cheaper owing to low setup cost and more environmental friendly as compared to other thermal and chemical type non-conventional micromachining processes. A comparison of micro-USM process with rest of the micromachining methods both conventional and non-conventional is summarized in Table 1.1 (Sun et al., (1996[a]); Gentili et al., (2005); Lin et al., (2017); Jain, (2014)).

Table 1.1 Comparison between micromachining techniques (Sun et al., (1996[a]); Gentili et al., (2005); Lin et al., (2017); Jain, (2014)

Micromachining methods	Minimum dimension	Aspect ratio	Accuracy	Geometric freedom	Roughness	Mass production	Affordability	Thermal damage	Materials
LIGA	++	++	++	±	++	++	-	No	Metals, polymers, ceramics
Bulk surface	+	-	+	-	+	++	-	No	Semiconductors, metals
Soft lithography	+	+	+	±	+	+	++	Yes	Polymer, plastics
Micro drilling, milling and grinding	±	±	±	±	±	±	+	Yes	Metals, polymers
Micro-EDM	±	±	±	++	±	±	+	Yes	Conductive materials
LBM	+	±	±	+	±	+	±	Yes	Metals polymers, ceramics
Micro-ECM	+	±	+	++	++	++	+	Yes	Conductive materials
Micro-USM	±	±	±	±	±	±	++	No	Brittle materials, ceramics
(++) Excellent (+) Good (±) Moderate (-) Poor									

1.8 Motivation

The demand of miniaturized products is increasing exponentially in the area of medical science, engineering and robotics etc. These micro-products are being fabricated by a number of micro manufacturing methods. All the above mentioned applications demand micro products with high degree of accuracy and precision. Moreover, for industrial point of view, an economical and

efficient solution is always needed. These requirements necessitate continuous improvement in the existing micro fabrication techniques. The current investigation was motivated due to the following reasons:

- The microfluidic devices are conventionally made by soft micro machining methods such as molding, embossing and lithography. All these methods have several limitations such as molding and embossing are limited to polymers only. Also, the product made by these methods can be used for low temperature application only. Lithography can be used for machining of glass, but it requires clean environment that renders in high operational costs.
- Microholes and microchannels are the basic features of any microfluidics device. These microfeatures are generally produced on hard and brittle materials. These materials have superior properties which make them difficult-to-machine in micro domain. Although, some non-conventional machining methods are being used for fabrication of microfeatures on hard and brittle materials. But, all these methods have their inherent limitations such as high thermal damage and surface roughness.
- Fabrication of high aspect ratio microfeatures on electrically non-conductive materials is an existing challenge.
- Micro-USM process is used to machine electrically non-conductive material, but it suffers from the problems of debris accumulation (between the tool and workpiece), low material removal rate (MRR), high tool wear and poor dimensional and form accuracy of machined microfeatures. Therefore, there is a need to develop a new method which may overcome the existing problem.
- Majority of research work on micro-USM process is conducted using stationary tool. But, only a few research work has been conducted on study of material removal mechanism and tool wear mechanism in case of micro-USM with tool rotation.

1.9 Organization of Thesis

The present thesis is presented into following eight chapters:

Chapter 1: Introduction

This chapter presents an introduction to microfluidics, the various elements involved in a microfluidic system, the need for micromachining, challenges in micro-fabrication of hard and

brittle materials and comparison between various micromachining techniques. This chapter describe the motivation behind the current research work.

Chapter 2: Literature review and problem formulation

The critical review of previous works (pertaining to present work) is described in this chapter. A state-of-art review on non-conventional micromachining techniques used for micro-fabrication is detailed. Subsequently, in turn, research gaps and opportunities have been identified and problem formulation, objectives, methodology and research work plan is presented.

Chapter 3: Experimental facility and pilot experimentation

This chapter discusses the development of rotary tool micro-USM process facility. The selection of various process parameters, response characteristics and the method of characterizing the response characteristics are also discussed. This chapter also includes the pilot experimentation. The pilot experimentation was performed into three sets. In the first and second set of pilot experiments, the ranges of tool rotation speed were selected for drilling of microhole and fabrication of microchannels for subsequent experimentation. The third set of pilot experiments was performed to select the tool material for subsequent experimentation.

Chapter 4: Performance evaluation of rotary tool micro-USM process

This chapter presents the performance evaluation of rotary tool micro-USM process during machining of microholes and microchannels. This includes the comparative study between stationary tool and rotary tool micro-USM processes during drilling of microholes and fabrication of microchannels.

Chapter 5: Investigations on microhole drilling of hard and brittle materials

This chapter focuses on the experimental investigations on drilling of microholes on hard and brittle materials i.e. glass, silicon and zirconia. In order to obtain desired responses, a desirability based multi-response optimization is also presented in this chapter.

Chapter 6: Investigations on tool wear and its effect on form accuracy of microchannels

This chapter presents an experimental investigation on tool wear and its effect of form accuracy of microchannels. This chapter also includes the development of mathematical model of tool wear to quantify different types of tool wear that prevails in rotary tool micro-USM process.

Chapter 7: Development of mathematical model of material removal rate

This chapter focuses on the development of mathematical model of material removal rate for rotary tool micro-USM process. The predictive model is experimentally verified for machining of borosilicate glass.

Chapter 8: Conclusions and scope for future work

This chapter presents the conclusions drawn from the present research work and future possibilities of the research.

LITERATURE REVIEW AND PROBLEM FORMULATION

This chapter discusses the micromachining processes and their classifications. Subsequently, a comprehensive literature on micro-USM process and its process variants is presented. On the basis of literature, the potential research gaps and opportunities are identified and presented. Eventually, the problem is formulated, it also includes the objective and scope of present work.

2.1 Micromachining

Micromachining can be defined as a machining process in which controlled material is removed from the workpiece surface at micron level to get the desired shape with desired geometrical accuracy (Brinksmeier and preuss, (2012)). This controlled material removal has also been termed as unit removal which means the amount of material removed in one cycle (Masuzawa, (2000)). The material removal at micron level can be obtained through the use of either micro or macro tools (Jain, (2009); Jain, (2010)). The condition for micromachining is that the machined feature size is in micron range (i.e. from 1 μm to 999 μm). In micromachining, a small variation in tool and work material interaction leads to the drastic change in results. Thus, to perform micromachining operations, selection of precise equipment is essential. The components produced by micromachining can be used in applications like microfluidics, micro total analytical systems, actuators, micropumps, lab-on-chip, microheat exchangers, bio-sensors and microfuel cells etc.

2.2 Classification of Micromachining

The micromachining techniques can be broadly classified into following three categories:

1. Lithography based processes
2. Conventional machining processes
3. Non-conventional machining processes

The classification of micromachining techniques is illustrated in Figure 2.1.
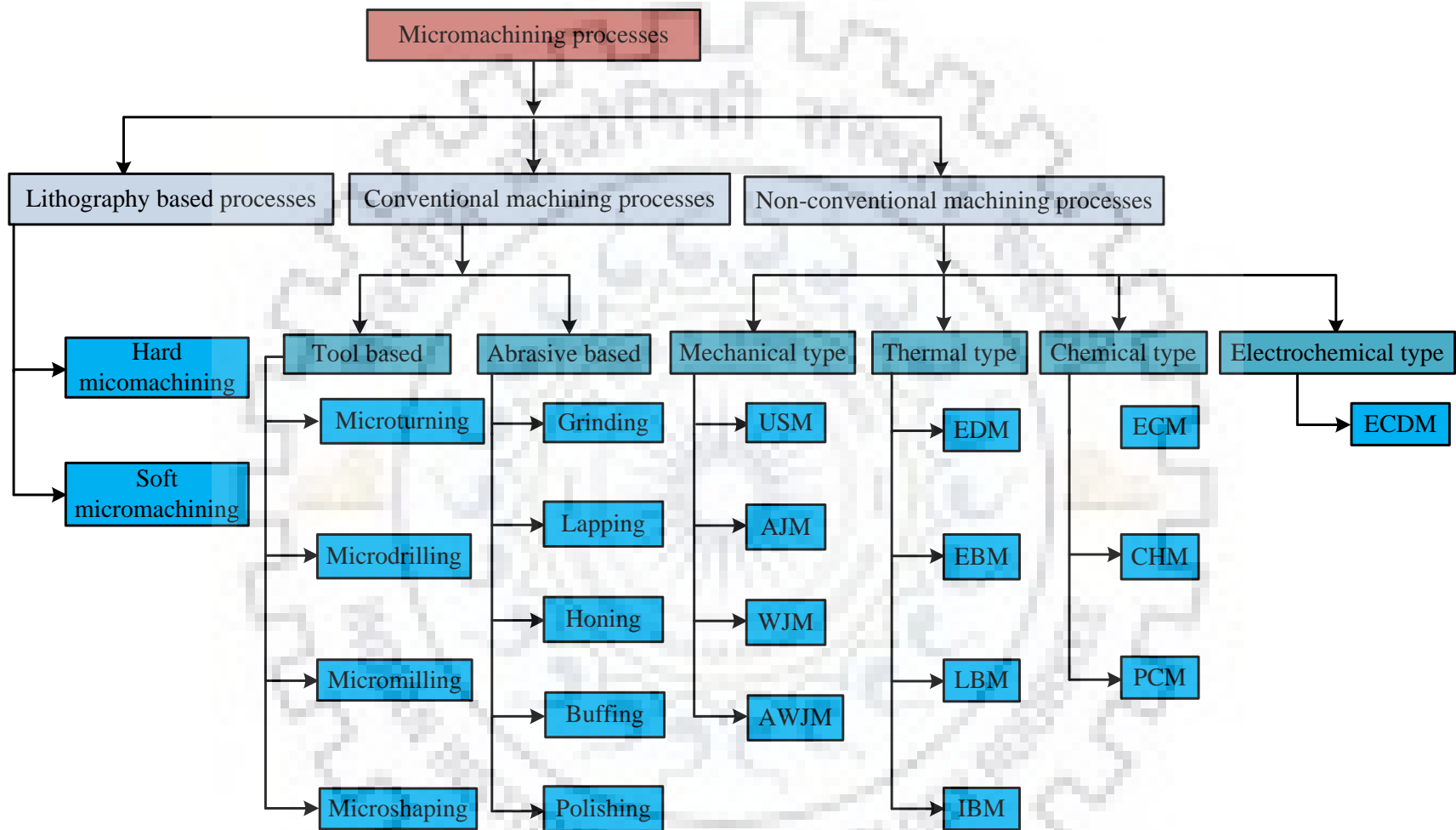
Figure 2.1 Classification of micromachining processes

2.2.1 Lithography based processes

In lithography based processes, a pattern is transferred on photo-sensitive work material by the exposure of radiation using ultra violet (UV) light on the selected area. During lithography, as the work material is exposed to radiation (light), the properties of the work material changes from exposed area to unexposed area. Lithography is divided into two categories named as hard micromachining and soft micromachining.

(i) Hard micromachining

The micromachining processes employed for machining of hard materials such as silicon and glass are called as hard micromachining (Ziaie et al., (2004)). Hard micromachining is divided into three categories such as bulk micromachining, surface micromachining and high aspect ratio micromachining. Bulk micromachining process is used to remove considerable amount of unwanted material from work surface. Surface micromachining is use to achieve good surface finish of the work material. It is used to fabricate MEMS devices, development of cantilevers for chemical detection (Lavrik, (2004)). As the name suggest, high aspect ratio micromachining is used to achieve high aspect ratio in 3D structures. It is generally used to fabricate complex shape bio-medical devices which are otherwise very difficult to fabricate by other means. LIGA comes under the most preferable high aspect ratio macromachining process. LIGA stands for Lithographie (lithography), Galvanoformung (electroplating) and Abformung (molding). It can produce the structures with aspect ratio up to 100:1 with lateral dimension depth of 0.2 μm. The major limitation of these processes is the extremely clean working environment.

(ii) Soft micromachining

Soft micromachining comprises of two methods as molding and embossing. Poly dimethyle siloxane (PDMS) is most commonly used as pattern material in lithography. In this process, a mold is prepare on hard substrate and thereafter, PDMS is poured into the mold and allowed to solidify. The solidified PDMS form a replica of the mold. In the next step, curing is carried out and the solidified PDMS pattern is removed from the mold. Polymer such as polycarbonate and poly methyl metha acrylate are machined using hot embossing. In hot embossing, heat as well as pressure is applied in order to obtain the desired shape. The operational cost of soft

micromachining is low. However, it is limited to the low melting point materials. Also, the material having high viscosity are difficult to make complex microfeatures (Koo et al., (2008)).

2.2.2 Conventional micromachining processes

The micromachining methods which do not have direct contact between the tool and work material are defined as the conventional machining methods. These methods can be grouped into two categories namely cutting group and finishing group. In cutting group is tool based micromachining methods which comprises of micro turning, milling, drilling and shaping. On the other hand, finishing group is abrasive based micromachining methods which comprises of micro grinding and polishing process such as lapping and honing.

(i) Tool based micromachining

As mentioned above, micro level turning, milling, drilling and shaping comes under the category of tool based conventional micromachining processes. These processes are carried out by using a tool with smaller nose radius (in microns). But, the radial force exerted on the work material is the main problem associated with conventional machining at micro level. Owing to high radial force, tool materials such as high carbon steel (HCS), high speed steel (HSS), stainless steel (SS) are not useful for conventional micromachining. In order to resolve this problem, polycrystalline diamond (PCD) inserts and diamond tools are used. The micron size inserts are prepare by using electric discharge machining process (Morgan et al., (2004)). Similarly, micro milling, micro drilling and micro shaping are also carried out using the PCD and diamond tools (Takeuchi et al., (1996)). But, high cost of fabrication of tools is the major challenge that limits the use of these processes.

(ii) Abrasive based micromachining

In abrasive based micromachining processes such as grinding, lapping, honing, buffing and super finishing, hard abrasives are used to remove the unwanted material from work surface. The tool in the form of a wheel is used in these methods. The microgrinding tool is made of abrasive particles such as diamond and bonding material (binder) in the form of metal powder. These processes are carried out at high tool rotation speed. The material removal takes place in the form of microchips as the grinding wheel comes in contact with the work material. The mechanism of material removal includes microcutting and ploughing. The mode of material removal (ductile or brittle) depends

on the selection of input process parameters. Generally, ductile mode of material removal results in better surface finish as compared to the brittle fracture mode (Zhong, (2003)). A variety of material can be machined using these methods. Lapping and honing are also carried out in similar way as grinding. Buffing and polishing are used to provide super surface finish to the work material. The main function of these processes is to remove the machining induced damage. Both the processes use diamond abrasives and a work wheel or leather strop. The difference is that in polishing abrasives are glued to the wheel, whereas in buffing loose abrasive are used with wheel.

2.2.3 Non-conventional micromachining processes

The non-conventional (advanced) micromachining is defined as the machining processes in which the unwanted material is removed from the work surface by the use of different forms of energy such as mechanical, thermal, chemical and electrochemical or combined form of these energies. These processes are used for the machining of complex shapes on hard and difficult-to-cut materials which are otherwise not feasible using conventional machining processes. On the basis of type of energy used for material removal these processes are broadly classified into four categories as under:

- **A.** Mechanical energy based non-conventional processes
- **B.** Thermal energy based non-conventional processes
- **C.** Chemical energy based non-conventional processes
- **D.** Electrochemical energy based non-conventional processes

A brief description of all the above mentioned non-conventional micromachining processes is given below:

A. Mechanical energy based non-conventional processes

(i) Abrasive Jet Machining (AJM) Process

In AJM process, abrasive particles driven by high velocity (150-300 m/sec) air or inert gases such as N_2, CO_2 and argon are impacted on the brittle work surface through a nozzle made of high corrosion resistant materials like Tungsten carbide and sapphire. As the abrasive impacts on the workpiece surface, brittle fracture takes place and the material is chipped-off from the work

surface. The commonly used abrasive material in AJM process are silicon carbide, aluminum oxide, glass beads and sodium bi-carbonate etc. This process is relatively cheaper than the other non-conventional machining processes. But, AJM process has low MRR and aspect ratio (Jackson and Davim, (2011)). Hot air is also used as carrier media to enhance the machining rate in AJM process. The process is known as abrasive hot jet air machining process (Jagannatha et al., (2012)). It is mainly used for drilling, finishing, cutting and debarring of hard and brittle materials such as glass, quartz, ceramics, silicon etc.

(ii) Abrasive Water Jet Machining (AWJM) Process

The AWJM process is a process variant of AJM process, in which water is used as a carrier medium for abrasive particles in place of gases (Gudimetla and Yarlagadda, (2007)). The working principal of AWJM process is similar to AJM process. It is also used for the machining of both ductile and brittle materials. The major applications of AWJM process are in linear and profile cutting and drilling (Gudimetla and Yarlagadda, (2007)). One of the major application of AWJM process is dismantling of nuclear plant. The material which can be machined using AWJM process are steels, non-ferrous alloys, Ti-alloys and Ni-alloys, polymers, metal matrix composites, ceramic matrix composites wood, stone etc.

(iii) Water Jet Machining (WJM) Process

The WJM process comes under the category of mechanical type non-conventional machining processes. In WJM process, the material is removed from workpiece surface by the impact of water stream at very high speed (Benedict, (1987)). During the impact of water jet on work surface, kinetic energy is converted to pressure energy. This induces a high compressive stress on the work surface. When this stress is cross the strength of the work material, material removal takes place in the form of microchips. WJM process is used to machine soft and easy-to-cut materials such as thin sheets and foils, non-ferrous metallic alloys, wood, textiles, polymers etc. The application domain of WJM process includes paint removal, peening, drilling, milling and cleaning etc.

(iv) Ultrasonic Machining (USM) Process

The USM process is a promising mechanical type non-conventional machining process. The basic principal of material removal in USM process is the erosion caused by the impact action of abrasive

particles (Kumar et al., (2018)). In USM process, the abrasive particles strike on the work surface by the vibrating tool at very high frequency (between 16-25 kHz). In this process, the shape of the tool replicates on the workpiece, thus the shape of the machined cavity is dependent on the shape of the tool (Jain et al., (2012)). It can be used for die sinking, drilling and milling operation. In micro domain, it has the ability to machine a hole up to 5 μm in diameter in glass as silicon (Egashira and Masuzawa, (1999)). It has low MRR and low aspect ratio. Moreover, USM process is limited to machine soft materials. The application area of USM process includes automobiles, electronics, optical, aerospace etc.

B. Thermal energy based non-conventional processes

(i) Electric Discharge Machining (EDM) Process

The EDM process involves discharge of the spark between electrically conductive workpiece and electrode to erode the work material (Jain, (2009); Singh et al., (2017)). It is used to machine high strength materials such as titanium, inconel, high speed steel and metal matrix composites (Koo et al., (2008)). The basic principal of material removal in EDM process is melting and evaporation which takes place by the high frequency (10^3-10^6 Hz) discharge action in between the tool and workpiece which are submerged into a dielectric medium (Algodi et al., (2016)). The discharge action takes place in pulsating form when a potential difference is created between the tool and workpiece (Pandey and Shan, (1980)). EDM process has several variants such as die sinking EDM process, wire EDM process, ED drilling process and ED milling process, micro-EDM process, powder mixed EDM process and Dry EDM process (Garg et al., (2010); Alba-Beans et al., (2007); Pham et al., (2004); Singh et al., (2017)). It has high MRR and good surface finish. But, at the same time it suffers the problem of recast layer which deteriorates the quality of machined cavity. EDM is also used to make dies, punches, molds, wire drawing which require through holes. (Aggarwal et al., (2015); Gudimetla, (2007)). It is also utilized for micro holes, orifices, injector nozzle, texturing and fragile features (Alba-Beana, (2007)). Some researchers have utilized EDM for the generation of nano particles (Sahu et al., (2014)). The major limitation of EDM process is that it can machine only electrically conductive materials (Jain et al., (1999); Ho and Newman, (2003)). Moreover, tool design and fabrication are the other issues that are involved in EDM process (Yarlagadda et al., (1999)).

(ii) Electron Beam Machining (EBM) Process

In this process, a high intensity beam of electrons is focused on the work surface to remove the unwanted material. The machining process is carried out in a vacuum chamber (vacuum $= 10^{-4}$ torr). The material removal takes place due to melting and evaporation caused by heat generated due to the impact of electron beam. Major application of EBM process are drilling of high aspect ratio holes, perforating, slotting and integrated circuit board fabrication (Jain, (2010)). It has some limitations such as high investment cost, long production time (Hassan, (2005)).

(iii) Laser Beam Machining (LBM) Process

The LBM process is used to machine both the conductive and non-conductive materials. The basic principle of LBM process is that material is removed due to melting and evaporation of unwanted work material by the intense heat generated as a laser beam is focused on the workpiece. No vacuum is required in LBM process. The application domain of LBM process includes drilling, milling, groove making, surface texturing and fine cutting etc. (Akhtar et al., (2016), Hassan, (2005)). LBM process also used to develop high aspect ratio 3D geometries. The main disadvantages of LBM process are the high cost of investment and heat affected zone (HAZ) (Meijer, (2004)).

(iv) Ion Beam Machining (IBM) Process

In this process, charged ions are fired from an ion source (cathode) toward the work surface by means of an accelerating voltage (Hassan, (2005); Jain, (2010)). It is carried out in a vacuum chamber like EBM process. The material removal takes place from the workpiece in the form of atoms or molecules by the bombardment of accelerated electron beam. It is generally used for cleaning and finishing operations. The focused ion beam machining is used to fabricate the micro tools made of carbides and diamond materials. The size of these tools ranges from 15-100 µm.

C. Chemical energy based non-conventional processes

(i) Electrochemical Machining (ECM) Process

The ECM process works on the principle of reverse electrolysis (i.e. electroplating in reverse direction). In ECM process, a DC voltage is supplied in between the two electrodes (i.e. cathode (tool) and anode (workpiece)). Both the electrodes are submerged into an electrolyte. Material removal takes place from the work surface due to the anodic dissolution when a potential difference is created between anode and cathode. Like other above mentioned non-conventional machining processes, the shape of the tool is replicated on the work surface in ECM process (Forster et al., (2005); Ruszaj et al., (2016)). The main advantages of ECM process are high MRR and very good surface finish. However, controlling and localizing the dissolution zone is still a complicated task in this process (Sharma et al., (2019)). Also, it is limited to the machining of conductive material only (Tyagi et al., (2019)). It is used for the machining of hard carbides, super metallic alloys and specimen for tensile and fatigue test etc. Till date, several variant of ECM process have been developed to improve its performance (Chavoshi and Luo, (2015); Smith and Clare, (2016); Wang et al., (2019); Skoczypiec et al., (2016)).

(ii) Chemical Machining (CHM) process

In CHM process, the material is removed by the controlled dissolution of work material. The dissolution of workpiece takes place as a strong reagent comes in contact with it. The area of the work material which needs to be machine is kept in contact with the reagent, while the remaining area (un-machined) of workpiece kept under mask to avoid its contact with the reagent. CHM process is used to make pockets, contours on all types of electrically conductive high strength-to-weight ratio materials (Hassan, (2005)). The major limitation of CHM process is the machining of non-conductive materials.

D. Electrochemical energy based non-conventional processes

(i) Electrochemical Discharge Machining (ECDM) Process

The ECDM process is a hybrid non-conventional micromachining process. It is a combination of ECM process and EDM process. It has the ability to machine both the electrically conductive and

non-conductive materials (Paul et al., (2014); Ruszaj, (2017)). The mechanism of material removal of ECDM process is a combination of melting and high temperature chemical etching. The limitation of ECDM process are HAZ, taper and environmental issues (generates harmful gases) (Paul and Hiremath, (2013)). Till date several variants of ECDM process have been developed including electrochemical discharge turning, milling and rotary tool ECDM process (Sreehari and Sharma, (2018)).

On the basis of aforesaid discussion on micromachining processes, it can be concluded that both the hard and soft micromachining techniques are good for fabrication of miniaturized products, but hard micromachining techniques are expensive and also require clean working environment. Soft micromachining techniques are limited to polymers (such as PDMS) only. Conventional micromachining techniques requires micro tools of complex geometries that are difficult to fabricate. The EDM, ECM and CHM processes are used for machining of electrically conductive materials. EDM and LBM processes produce thermal damage around the machined cavity.

Among the non-conventional machining process that can machine electrically non-conductive materials, the USM process can be used for fabrication of micro features on glass material in this study. The research trends in non-conventional machining processes reveal that USM process secures fourth place in popularity amongst all (Figure 2.2). Figure 2.3 depicts the research trends in both the mechanical and thermal type non-conventional machining processes (i.e. USM, AJM, WJM, AWJM and LBM processes) used for machining of non-conductive hard and brittle materials (i.e. glass, quartz and ceramics) over last four decades. It can be clearly seen from Figure 2.3 that amongst all these processes, USM process is the most popular non-conventional machining process for machining of glass.
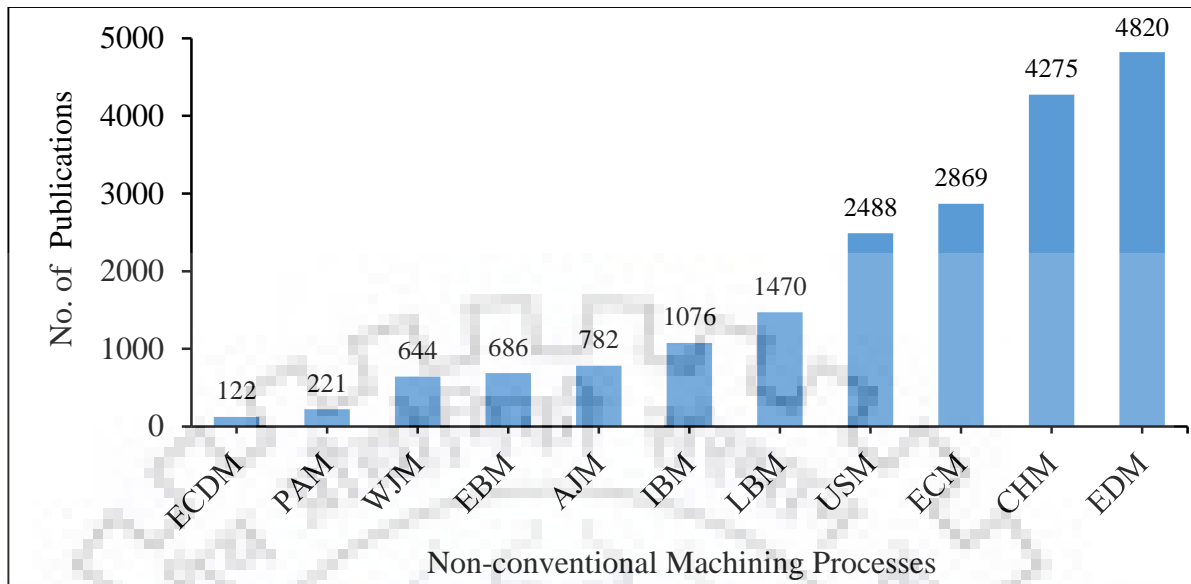
Figure 2.2 Research trends in non-conventional machining processes in last two decades [Scopus on 05/03/2019]
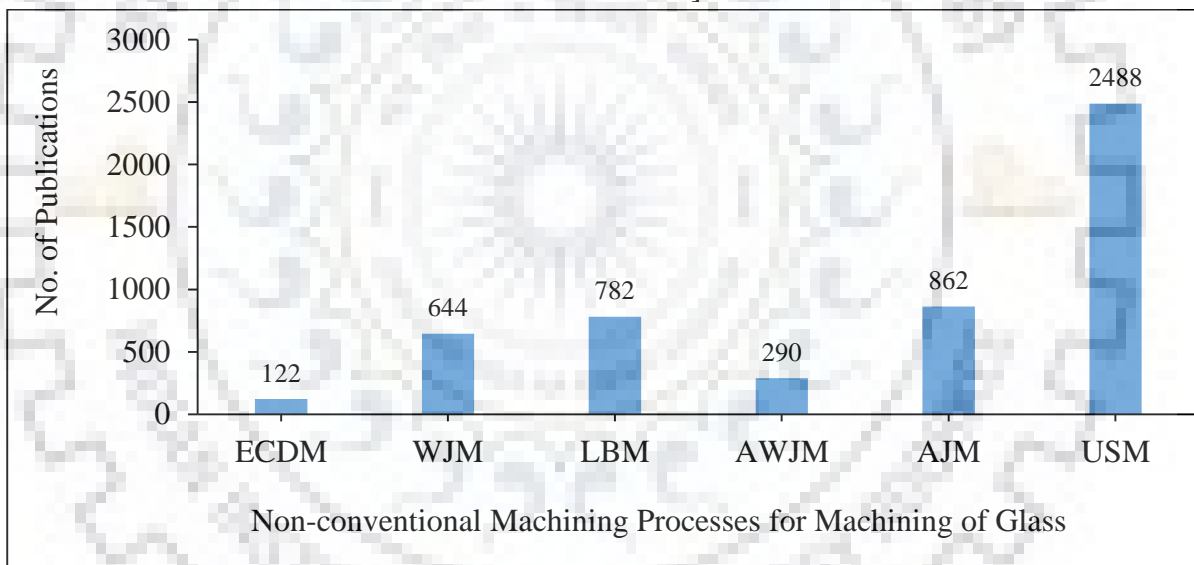
Figure 2.3 Research trends in mechanical type non-conventional machining processes in last two decades [Scopus on 05/03/2019]

2.3 Ultrasonic Machining (USM) Process

Ultrasonic energy has been used for multiple operations in different area such as machining, welding, cutting, forming, cleaning, reducing friction densification, soldering and testing of welded plastic pipes etc. (Nitoi et al., (2016); Shaw, (1956)). Among the aforesaid areas, USM process is used for machining of hard and brittle materials. This process was started in 1954 by L. Balamuth. With increase in demand of products made of hard and brittle materials, more interest

has gravitated towards the USM process. The continuous improvement in the USM process has drawn many researchers to carry out their study on this process. An overview of research trends in USM process is shown in Figure 2.4. The increase in number of publications reveal that research is continuing on USM process. The USM process comes under the category of mechanical type non-conventional machining processes and is used for the machining of both the electrically conductive and non-conductive hard (hardness $\geq$ 40 HRc) and brittle materials (Thoe et al., (1998)).
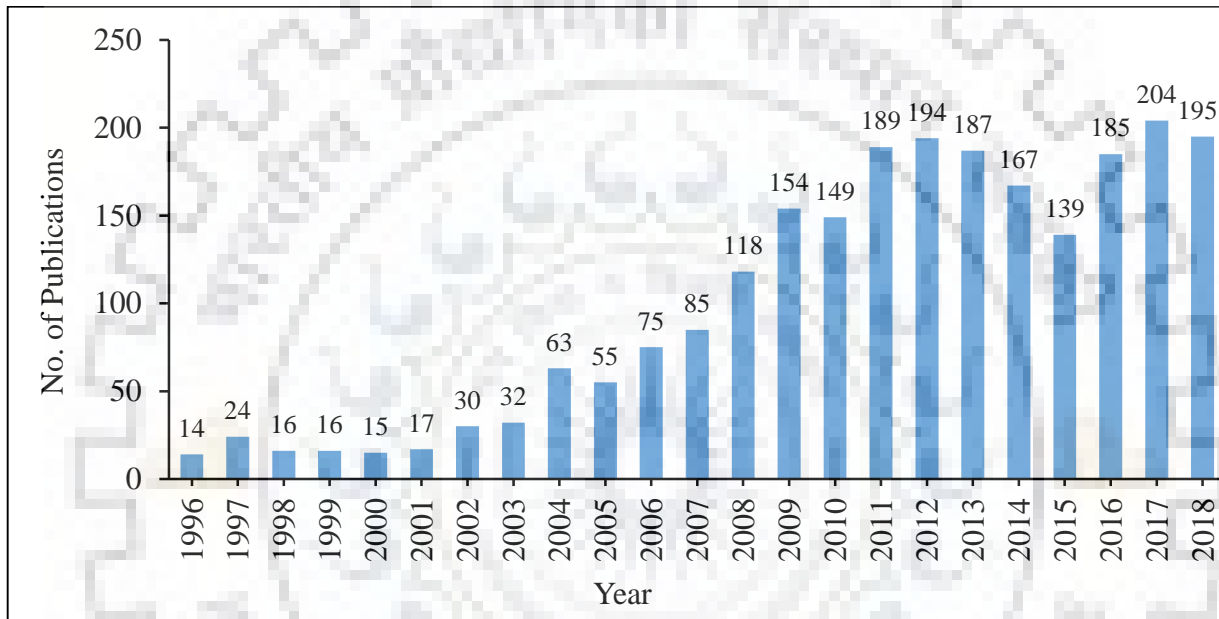
Figure 2.4 Research trends in ultrasonic machining [Scopus on 05/03/2019]

2.3.1 Working principle of USM process

In USM process, high frequency vibrational energy is provided to the tool to remove the unwanted material from work surface. In principle, abrasive slurry, a mixture of hard abrasive particles and carrier media (generally water) is supplied in between the high frequency (16-25 kHz) vibrating tool and work. During machining, the vibrating tool strikes on the abrasive particles present in between the tool and work due to which the abrasives gain kinetic energy and subsequently release the same on the work surface in the form of impact. This causes removal of work material in the form of brittle fracture. The complete mechanism of material removal involves are: (i) direct hammering/impact (ii) microchiping due to free moving abrasive particles on work surface (iii) cavitation erosion and (iv) chemical reaction between abrasive slurry and work material. Among

all the aforesaid mechanism, direct hammering/impact is the dominant mode of material removal in this process (Kumar et al., (2018)). The schematic representation of USM process setup and mechanism of material removal are shown in Figure 2.5 and Figure 2.6 respectively.
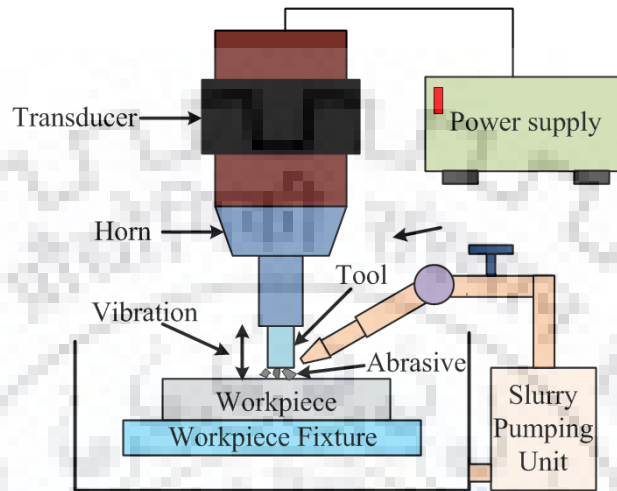
Figure 2.5 Schematic of USM process setup

(a) Hammering and impact
(b) Micro chipping
(c) Cavitation erosion
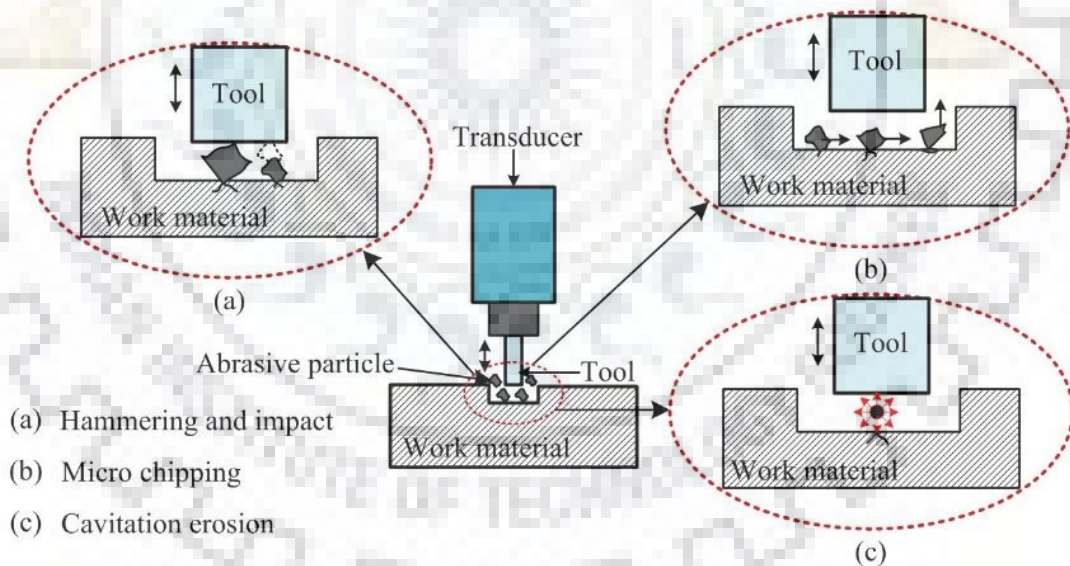
Figure 2.6 Schematics of material removal mechanism of USM process (Thoe et al., (1998))

The USM system comprises of a generator (power supply), transducer, horn or concentrator, tool and abrasive slurry. The generator converts the low frequency electrical energy (50 Hz) into high frequency electrical energy in the range of 16-25 kHz. The high frequency electrical energy is then converted into mechanical vibrations with the help of a transducer. The horn also known as

concentrator is attached to the transducer. The function of horn is to amplify the amplitude of the vibrations up to the desired level of machining. The tool is attached to the horn and vibrates in the perpendicular direction to the machine base. The slurry is pumped in between the vibrating tool and work. USM process uses several types of tool feeding system including gravity feed, counterweight gravity feed, spring loaded, pneumatic and motor driven (Pandey and Shan, (1980); Kennedy and Grieve, (1975)). Among them gravity tool feeding system is most commonly used. During entire machining period a constant flow of slurry is maintained in the machining zone (i.e. between tool and work). The continuous flow of slurry is provided to replenish the abrasives from the machining zone. The used slurry is collected back in the slurry tank and again supplied into the machining gap with the help of a pump.

2.3.2 Material removal mechanism of USM process

Several investigations were reported on the material removal mechanism of USM process. The first report was proposed by Shaw, (1956) which stated that the hammering and impact/throwing action of abrasive particles is responsible for material removal from the work surface. The cavitation erosion and chemical reaction were not taken into account for material removal in the proposed model. It was reported that the hammering takes place while using large size abrasive particles i.e. in case of small machining gap (equal to the abrasive particle size). Whereas, impact occurs when small size abrasive particles were used i.e. when machining gap is larger than the abrasive particle size. Thereafter, Miller, (1957) proposed another model to calculate the volumetric removal of material. In this model, plastic deformation of work material per blow, work hardening per unit of plastic deformation, number of blows per second, material removed per blow, rate of chipping blow and rate of tool tip area covered by the abrasive particles were considered as the parameters. It was concluded that vacuum exists on the tool tip area for some period of time. However, the developed model was limited to ductile material only. Later, Kazantsev and Rosenberg, (1965) investigated the mechanism of material removal in USM process using high speed imaging. The movement of abrasive particles in the machining gap was visualized during machining at very high frame rate (i.e. 50,000 frame per second). It was found that as the high frequency vibrating tool hits the abrasive particles, these particles penetrate into the tool machining face and also embed on the work surface. A mathematical relation was developed to describe the cutting process. The proposed model established the relationship between the quantity of work

material removed per unit time and material removed by single abrasive particle, depth of penetration and force acting on abrasive particle. In this model, the shape of abrasive particle was assumed to be a sphere, whereas abrasive particles are more or less similar to polygon (i.e. octahedron or tetrahedron). This resulted in some inaccuracies in the developed model. Subsequently, Kainth et al., (1979) also proposed a mathematical model of material removal rate for USM process. In this study, they established a relationship between material removal rate and other factors such as frequency, machining gap, number of abrasive particles, abrasive size and hardness ratio. Machining gap was determined by the contact force. The quantity of abrasive particles was found to be dependent on average diameter of abrasive particle, slurry concentration and density of liquid being used. In this model also, the shape of the abrasive particle was considered as a sphere. Initially, hemi spherical portion of work material was removed when the spherical shape abrasive impacted on the flat work surface, but in later stage, the same particle impacted on the uneven work surface. Consequently, some inaccuracies were observed.

On the basis of the work done by Shaw, Miller, Kazantsev and Rosenberg, it was concluded that in USM process, the material removal is primarily due to the hammering and impact action of free moving abrasive particles on the work surface. Kremer et al., (1981) reported that cavitation also takes a part in removing some material from work surface. But, it takes part in machining of porous work materials such as graphite. Later, Soundararajan and Radhakrishnan, (1986) investigated the material removal mechanism while machining of glass, WC and high speed steel. It was found that the soft and elastic material undergone through elastic deformation and exhibited in very low material removal rate. On the other hand, in case of hard and brittle work material like WC, no plastic deformation was observed. Thus, USM process was recommended for machining of hard and brittle work materials only.

2.4 Micro-ultrasonic Machining (Micro-USM) Process

Micro-USM process is a downscale of macro-USM process which is used to fabricate microfeatures such as microholes and microchannels with dimension less than 1 mm. Micro-USM process was introduced by Sun et al., (1996[a]) by incorporating some modifications in the conventional USM process setup. The basic difference between macro-USM and micro-USM process is in frequency, amplitude of vibration, abrasive size and tool size. Micro-USM process has been extensively used as a drilling process for various hard and brittle materials including

glass, ceramics, quartz, silicon etc. Some, investigations have also been reported on the fabrication of microchannels on hard and brittle materials.

2.4.1 Advantages and limitations of micro-USM process

The major advantage of micro-USM process is that it can machined both the conductive and non-conductive hard and brittle materials without producing any thermal damage. Moreover, it does not alter the physical, chemical and metallurgical properties of work material. The limitations of this process are low MRR, high tool wear, low penetration depth and poor form accuracy (Jain and Pandey, (2017); Yu et al., (2006).

2.4.2 Applications of micro-USM process

The applications of micro-USM process include machining of bearing used in watches, cutting of semiconductor materials and wafers, engraving of precious stones and diamond. Micro-USM process combined with self-aligned multilayer machining and assembly is used to develop 3-dimensional micro air turbine (Sun et al., (1996[a])). Another application of micro-USM process with tool rotation include fabrication of high aspect ratio microholes (diameter less than 100 μm) in silicon wafers, glass, ceramics that has specific applications such as pressure sensors and spacecraft propulsion (Sarwade, (2010); Jain and Pandey, (2016)). One more potential application of micro-USM process includes drilling of microholes in power transmission shaft and gears used in helicopter (Jain et al., (2011)).

Nowadays, micro-USM process is being used for the fabrication of microfeatures such as microholes and microchannels on glass, silicon and bones for microfluidic and biomedical applications (Cheema et al., (2015); Gupta and Pandey, (2016); Jadoun et al., (2006)). Microfluidic application requires microchannels for transfer and storage of fluids. However, fabrication of geometrically accurate high aspect ratio microstructures is a complex task in USM process. The reason behind this is the difficulty of tool handling at micro level. Moreover, the slurry replenishment also becomes difficult after reaching a particular depth of cavity. To solve these problems, several modifications were done in the conventional USM system. These modifications include vibratory motion to the workpiece, rotary motion to the tool and planetary movement of tool etc. The work done by different researchers in the area of micro-USM process is presented below.

2.5 Investigations on Development of Micro-USM Process Variants

As mentioned above, the first micro-USM system was introduced by Sun et al., (1996[a]). The objective of this research work was to resolve the problems of micro tool fabrication and handling. The setup consisted of three units such namely: wire electrical discharge grinding (WEDG) process, electric discharge machining (EDM) process and micro-USM process. In this system, rotary motion was provided to the tool and vibratory motion was provided to the workpiece. The major advantage of this system was that it eliminated the need of a separate wire electrical discharge grinding setup to fabricate the tool for micro-USM process. The WEDM and EDM processes were utilized to develop various desired size co-axial tools on the same machining system. This also eliminated the problem of tool eccentricity at high rotation speed. By utilizing this tool in-build fabrication machining system, microhole as small as 5 μm in diameter were successfully drilled in glass and silicon work materials Sun et al., (1996[b]). To encounter the problem of tool eccentricity, another variant of micro-USM process was developed by Egashira et al., (1997). In this setup, the rotary motion was provided to the workpiece instead of the tool. Further, in order to overcome the problem of tool eccentricity, a new setup of micro-USM process was developed by Kuriyagawa et al., (2001 and 2002) in which an aerostatic ultrasonic spindle was used. The spindle provided simultaneous vibratory and rotary motion to the tool. This system had a resolution (run out) of 0.7 μm at 1000 rpm. Additionally, the developed system was equipped with a numerically controlled axis work feeding unit and a dynamometer to measure machining force generated during machining. The same setup was also used to fabricate the tool using diamond abrasive wheel. Egashira et al., (2004) further developed a special cemented carbide tool for USM process using die sinking EDM process. This tool was used for gang drilling operation. In order to fabricate cemented carbide tool, a copper foil having pattern of 4×4 array of holes was fixed beneath the cemented carbide material. The EDM of cemented was carried out by applying reverse polarity due to which, a series of micro-pins were developed in the same array. This methodology was used to save the tool fabrication time. However, fabrication cost of such type of tool was high. Also, during machining tool suffers from high static load and thereby, tool breakage. Thus, in order to eliminate these issues, some researchers provided vibratory motion to the workpiece and rotary motion to the tool (Egashira et al., (1999); Yu et al., (2006).

Another variant of micro-USM process was developed by Zhang et al., (2005 and 2006) to maintain a constant/fixed machining gap. An acoustic emission technique was introduced in the existing setup of micro-USM process. This variant was termed as ultrasonic assisted lapping (USAL) process. In this process, the tool was monitored during machining through scanning process and compensated simultaneously while breakage and machining. Micro-USAL process was used for the fabrication of high aspect ratio structures. Other variants of micro-USM process were developed by changing the frequency range from 20-70 kHz, by changing the tool feeding system from gravity feed to precise fixed or continuous motion tool feeding system and by changing amplitude of tool vibration up to less than 5 µm Cheema et al., (2015). In these systems, the feed to the tool was provided in the form of step feed (in µm). Some of these tool feeding systems were controlled manually while some of them were numerically controlled.

Rotary tool micro-USM process is also a process variant of micro-USM process in which the tool vibrates as well as rotates simultaneously. This variant was developed in order to overcome the problem of debris accumulation in the machining zone. An abrasive slurry is supplied in between the tool and workpiece. The rotary motion of tool assists the abrasive particles to replenish from the machining zone. The productivity and efficiency of rotary tool micro-USM process is higher than stationary tool micro-USM process. The feasibility of rotary tool micro-USM process to fabricate different type of microfeatures has been verified by some researchers (Yu et al., (2006); Egashira et al., (1998).

On the basis of the above mentioned discussion, the process variants of micro-USM process can be classified into three categories as: (i) micro-USM process with tool vibration, (ii) micro-USM process with tool rotation and workpiece vibration and (iii) micro-USM process with vibrating and rotating tool. In the first type micro-USM system, the tool has vibratory motion and the workpiece is kept stationary. The advantages of this system are easy setup, useful for die sinking operations and multiple geometries can be fabricate at the time. The main limitations of this system are low MRR, low aspect ratio and poor form and dimensional accuracy of microfeatures. In the second type micro-USM system the vibratory motion is provided to the workpiece and the tool has rotary motion. This system has the limitations such as complex setup tool eccentricity, size of work material and multiple geometries cannot be made. In third type of micro-USM system, the tool is provided simultaneous vibratory and rotary motion. This systems has several advantages such as

higher MRR, low tool wear, high aspect ratio and flexibility in machining. The limitation of this system is tool eccentricity.

2.6 Investigations on Mechanism of Micro-USM Process

The process mechanism of micro-USM process was investigated in several studies. In most of the reported work the machined surface were examined microscopically and it was found that the micro machined surface is developed thorough hammering action of abrasive particles. Zarepour and Yeo, (2012[a] and 2012[b]) made an attempt to reveal the process mechanism of micro-USM process through single particle impingement. The morphology of work surface by single particle impingement was observed. Further, a mathematical model was developed for predicting the MRR in micro-USM process. In this model ultrasonic characteristics, abrasive size, abrasive quantity and work material were considered as input parameters. Two types of work materials were considered in this study. The developed model was verified through single particle impingement. The experimental results were in good agreement with the predictive results. The experimental results revealed that the material removal occurred in three modes namely pure ductile mode, partially ductile and partially brittle mode and pure brittle mode. The material removal modes depend on the impact energy of abrasive particles. The impact energy depends on the vibration amplitude and shape of abrasive particles.

The single particle impingement approach was also used by Cheema et al., (2015) to investigate the material removal mechanism in micro-USM process. The machined surface was analyzed on the basis of field emission electron microscopic images. Lateral cracks, radial cracks and median cracks were observed on the work surface. Also a ductile cutting mode was observed in the form of plastically deformed material. This confirmed that the material was removed from work surface in a mix mode of partially ductile and partially brittle.

Klopfstein et al., (2008) analyzed the change in microstructure of silicon work material during micro-USM process. They used confocal Raman microscopy to examine the crystallographic change in silicon structure. The results revealed the presence of two different phases namely amorphous and diamond cubic. A variation in the average surface roughness (from 5-15 nm) of the machined work material was observed at different depth of cuts. The surface roughness of

diamond cubic phase was found to be lesser for small size abrasives (0.1 µm) than that of coarser abrasives (0.25 µm).

Yu, (2006) experimentally investigated the material removal mechanism of micro-USM process by analyzing the machined surface topography with the help of optical microscopic and SEM images. Both the brittle mode and ductile mode of machining were observed on machined surface of silicon. It was explained that both the modes influenced by the abrasive particle size. The ductile mode was initiated by small size abrasive particles, whereas the brittle mode was due to the impact of large size abrasive particles.

Sarwade, (2010) also investigated the material removal mechanism of ultrasonic drilling process during machining of silicon. The machined surface morphology revealed the existence of brittle as well as ductile mode of machining. Stick slips were observed around the periphery of hole which evidenced the presence of ductile mode of machining.

Jain, (2012) studied the material removal mechanism in micro-USM process during machining of silicon and glass work materials. It was reported that basic material removal mechanism of micro-USM process comprises of (i) direct hammering (ii) solid particle erosion (iii) mechanical abrasion (iv) cavitation erosion and (v) chemical pitting. Further experimental results revealed that the ductile mode of machining exists during micro-USM of brittle material such as glass and silicon. The mode of material removal depends on the selection of input process parameters such as abrasive particle size, static load, power rating.

2.7 Investigations on Tool Behavior

Tool behavior in terms of tool wear plays a vital role in micro-USM process. The shape of the machined micro feature is decided by the shape of the tool. In other words, form accuracy of machined feture is largely dependent on the shape of the tool used. Tool wear is an unavoidable phenomenon in micro-USM process. It cannot be eliminated completely, however it can be minimized up to certain extent to achieve desired dimensional and form accuracy of the micro feature.

Adithan, (1981) studied the characteristics of tool wear in ultrasonic drilling process. It was observed that the tool wear in WC tool was greater than SS tool while machining of WC. Wear in

the tool after some time resulted in tapered holes. Tool wear resulted in insufficient circulation of abrasives which lead to reduced machining efficiency. Only longitudinal wear was observed in machining of glass, but in case of WC, lateral wear was also observed. It was concluded that higher material hardness resulted in more tool wear.

Sun et al., (1996ᵃ) reported that in micro-USM process, WC tool material performed better than SS tool material. However, while machining in macro domain SS tool was found to be superior to WC tool. Egashira et al., (1997) discussed that tool rotation enhanced the machining rate without increasing the tool wear. They also reported that on increasing the static load and vibration amplitude tool wear was found to be increased.

Egashira et al., (2002) developed a micro tool to drill a microhole of 10 μm. The tool was fabricated using the WEDG process. The drilling was performed by providing rotation to the tool. The vibratory motion was provided to the workpiece. The cutting force was found to be significantly reduced by providing vibration to the workpiece. In another study, Egashira et al., (2004) compared to the performance of different tool material during micro-ultrasonic drilling process. It was concluded that polycrystalline diamond tool proved to be a better tool material as compared to cemented carbide tool material owing to its higher wear resistance.

Choi et al., (2003) performed a comparative study on the effect of tool materials on tool wear during micro-ultrasonic drilling of Al_2O_3 ceramics. Pure tungsten and tungsten carbide were used as tool material. The mechanism of material removal of ceramics was also investigated in this study. It was observed that the longitudinal tool wear (i.e. reduction in length of tool) increased significantly by decreasing the diameter of tool. Tool wear was affected by other parameters of micro-USM process such as working load and amplitude of tool vibration. The performance of tungsten carbide was found to be superior over pure tungsten. The MRR was increased by increasing grit size.

Shinozuka, (2009) fabricated a special laminated tool for machining of multiple grooves at a time. This tool was prepared by laminating the hard material (stainless steel) and soft material (polymer) alternatively in the form of straight projections. The soft material was used as adhesive in between the layers of hard layers. The objective behind this was to reduce the machining time and to

improve the accuracy of machined grooves. The straight micro grooves of dimension 10×100 µm (depth × width) were successfully fabricated using the developed tool.

Cheema et al., (2015) studied effect of SS-304 and WC tool materials on the form accuracy of the microchannels fabricated using micro-USM process. In this study the mechanism of tool wear was also investigated. They reported that in micro-USM process, tool suffers from three types of wears namely, longitudinal wear, lateral wear and edge rounding wear. It was found the longitudinal wear occurs due to hammering action of abrasive particles, edge rounding is caused due to the hammering and abrasion by abrasive particles and lateral wear is caused due to the abrasion and rolling action of abrasive particles in the gap between tool surface and machined wall cavity. The microchannels machined by using WC tool material had better form accuracy as compared SS-304.

Wang et al., (2018) reported that SS-304 is a better tool material for USM process as compared to WC and carbon steel-1045 tools owing to its higher flexibility. They concluded that SS-304 tool had maximum material removal capability as compared to both the WC and carbon steel-1045 tool materials.

Tool wear properties are also responsible for tool wear in micro-USM process. The effect of tool material properties on tool wear was also investigated by researchers. Komaraiah and Reddy, (1993) in their comparative study on tool materials reported that tool material hardness influenced both the longitudinal and lateral wear, whereas impact strength influenced the lateral wear.

Tool wear measurement methods were also reported in some studies. A novel method to measure the tool wear in micro-USM process was proposed by Jain et al., (2012). This method is called as 'reference point method'. In this method, the tool was set to a reference point also called origin just before starting the machining process. After machining, the tool was again positioned to the reference point. The retraction of the tool was recorded in the dial indicator attached with the setup which showed the length of tool wear. In this investigation, two type of tool geometries i.e. hollow and solid were used during machining. It was revealed that the hollow tool worn out at faster rate as compared to the solid tool due to work hardening followed by micro cracking and high stresses owing to lesser surface area.

Yu et al., (2012) proposed a mathematical model to predict the tool wear in micro-USM process. They also proposed the mechanism of tool wear and reported that low cycle fatigue is the main contributing factor responsible for tool wear in this process. In this study, rotary motion was provided to the tool, however the effect of tool rotation was found to be insignificant on tool wear. They conclude that the tool wear occurs micro-ultrasonic drilling when simultaneous existence of abrasive particle and tool takes place. The tool wear was more in SS tool material as compared to the tungsten tool material. The developed model of tool wear was experimentally verified and found to be in good agreement.

Cheema et al., (2015) also proposed a mathematical model to calculate volumetric wear of tool in micro-USM process during the fabrication of microchannels. The developed model was used to describe the form accuracy of the machined microchannels. They revealed that longitudinal wear affect the depth of channel, edge rounding wear cause roundness in the bottom surface of microchannel and lateral wear causes the taper formation on the side wall of machined microchannels. It was also observed that the longitudinal wear followed by lateral and edge rounding wear has maximum contribution tool wear in total volumetric tool wear. The form accuracy was found to be mostly dependent on the size of abrasive particles. Higher power rating and higher slurry concentration caused the higher tool wear.

2.8 Investigations on Form Accuracy

The main objective of any of the micromachining process is to maintain the form accuracy of the developed features. By considering this fact in mind, Sun et al., (1996ᵃ) developed the flexible setup of micro-USM process. This setup was known as self-aligned multilayer machining and assembly (SAMMA). This SAMMA was tested by fabricating micro center pin turbine and micro force balance air turbine with better form accuracy. Egashira et al., (1997) developed a flexible setup which had an additional facility to fabricate micro tools of desired diameter which were used for drilling operation. The form accuracy of the drilled microholes was better but the machining rate was low. In order to enhance the machining rate, rotary motion was provided to the tool.

Egashira et al., (1998) again proposed a constant wear methods to improve the form accuracy of the developed microfeatures. In this method, they developed inclined cavities using square cross-section tool electrodes. Micro cavities with sharp edges were successfully developed using this

method. Additionally, a mathematical relationship was also established between depth of cut, depth of machined cavity and tool wear length.

Yu et al. (2004), developed a uniform wear method (UWM) to compensate tool wear in micro-USM process. 3D micro cavity with dimensions 231×231×69 μm (length × width × height) was developed by integrating the electrical discharge machining with CAD/CAM to micro-USM process. By applying the UWM, wear compensation was provide to the tool. As a result of that the shape of the tool remained unchanged throughout the machining process. A layer-by-layer machining approach was used and a stair like surface was achieved with a depth difference of 14μm between the designed and measured depth. It took almost 10.2 hr of machining time to fabricate this cavity.

Tool rotation also helped to improve form accuracy of the developed microfeatures. It was observed that when stationary tool micro-ultrasonic drilling were used for machining of microholes. The profile of the microhole was observed to be varying in the form of protruded surface (Kuriyagawa et al., (2001)). On increasing the depth of hole this protruded portion was found to be increased. By providing rotary motion to the tool, this problem significantly decreased. The machining rate was also increased by providing rotation to the tool.

Yu et al., (2006) reported that the accumulation of debris in the machine gap during stationary tool micro-USM process affects the surface roughness and form accuracy of the holes. A concave and convex bottom profiles of microholes were observed. The machining speed decreased due to the accumulation of debris by increasing the static load beyond a certain value. This phenomena was explained with the help of a mathematical model. It was revealed that the surface roughness was found to be dependent of the size of abrasive particles. To overcome the problem of debris accumulation rotation was provide to the tool which improved the machining rate by replenishing the debris from machining gap.

Pei et al., (2013) also observed the similar concave and convex profile of microhole in their study. They found that the concave shape was observed when small size tool (diameter less than 200 μm) coarse abrasive particles were used. In case of small size tool, abrasive can easily reach below the tool. On the other hand, convex shape was observed when fine abrasive particles were used. This was due to the accumulation of abrasive at the center of the machined hole which blocked further

movement of abrasive at the center of hole and led to the formation of convex shape of the bottom of hole.

Medis and Henderson, (2005) used the layer-by-layer approach to fabricate serpentine microchannels on silicon wafer for MEMS applications. Ultrasonic impact grinding was used to develop the microchannels with dimension 630×340 µm (depth × width) with a tool of size 320 µm in diameter. The layer-by-layer approach in micro ultrasonic impact grinding is very useful as it is capable to generate any shape. The walls of the developed microchannels were found to be tapered.

Boy et al., (2010) developed high aspect ratio microstructures using micro-USM process. These microstructures were in the shape of micro pillars with dimensions 280×6000 µm (dia. × depth) in quartz crystal. They also developed a trench of dimensions 300×1900 µm (width × depth) with the help of SS tool. The finite element modeling was applied to measure the amplitude of tool vibration and resonant frequency of the acoustic system. The acoustic system was developed by studying several PZT materials through finite element modeling.

Visvanathan et al., (2011) developed mushroom shaped structure and concave spherical structure on NBK7 glass work material using self-aligned process combining batch mode USM process, Lapping and batch mode micro-EDM (3D SOULE) process. Initially, a tool holder made of SS-440 was developed using micro-EDM process. After that, micro-USM process was used to mark the alignment area for the glass balls on silicon. Thereafter, the glass balls of diameter 1 mm were kept in silicon mask. The excess spheres were undergone through lapping process and at last micro-USM process was used to form the shell. As a result, the mushroom shape and concave shape were replicated on the glass balls. A machining rate of 24 µm/sec was achieved in this process. The resonant frequency for the developed structure was determined by perming the finite element modelling.

Viswanath et al., (2014) utilized high resolution micro-ultrasonic machining for trimming of hemispherical 3D shells. These shells were made of fused silica and used for micro birdbath resonator gyroscope. The fluid modelling was carried out to study the interaction phenomena between tool, workpiece and abrasive slurry used. The SS-304 tool with diameter 50 µm was used in this study. The surface roughness was obtained in the order of 30 nm when 10 nm diamond

abrasive particles were used. The low amplitude and small size of abrasive particles generates smoother surface, but facilitates low machining rate. The machining rate and profiles of machined workpiece were explained with the help of analytical and numerical modeling.

2.9 Investigations on Surface Finish

Surface finish is an important response characteristic of micro-USM process. It decides the use of micro feature developed for a specific application. In case of microchannels, both rough and finish bottom surfaces have their specific applications. Therefore, it needs to be taken care while development of micro features. Surface roughness is controlled by proper selection of micro-USM process parameters. Neppiras, (1964) reported that the use of fine abrasive particles (higher mesh size) in ultrasonic drilling process improved the surface finish. Smith, (1974) presented first study on the effect of slurry concentration on surface roughness of the holes drilled using USM process. Taper tool was used for drilling operation. It was concluded that the surface roughness of the holes walls found to be higher due to "furrowing effect". This effect is caused when large size abrasive particles created obstacle in the path of small size abrasive particles during exit from the hole. As a result of this machining rate decreased and tool wear increased.

Komaraiah et al., (1988) investigated the surface roughness of different work materials such as glass, ferrite, porcelain and alumina by conducting a comparative study between stationary tool and rotary USM processes. They revealed that least surface roughness was observed in alumina work material using fine abrasive particles. On the other hand, highest surface roughness was observed in porcelain work material. It was also reported that the tool having higher hardness provided better surface finish. Rotary USM process resulted in higher material removal rate, better surface finish and accuracy as compared to USM process.

Adithan and Krishnamurthi, (1978) stated that out of roundness decreased by decreasing the static load. The out of roundness decreased at hole entry and increased at exit on increasing the static load. Higher static load with mid-range of vibration amplitude in ultrasonic drilling led to finer machined surface.

Yu et al., (2006) investigated the influence of debris accumulation on the performance of micro-USM process. A mathematical model was also developed to analyze the debris accumulation

phenomena. It was observed that after a specific value of static load machining rate started to decrease. The accumulation of debris in the machining gap was found the reason for the same. The accumulated abrasive particles repetitively hit themselves in the machining zone. Due to which the abrasives took longer time to come out of the machining gap and thereby reduced the machining rate. The abrasive particle size significantly affected the surface roughness. The large size abrasive particles generated the convex surface, whereas small size abrasives formed concave surface. The theoretical results obtained on the basis of developed mathematical model were also verified experimentally.

Cherku et al., (2008) analyzed the influence of oil based abrasive and water based slurry on micro-USM process performance. It was concluded that water based slurry resulted in better surface finish when small size abrasive particles and higher slurry concentration were used. The oil based slurry was found to be suitable for all sizes of abrasive particles with low slurry concentration. As compare to water based slurry, oil based slurry provided better surface finish owing to more viscosity due to which it act as a lubricant. In case of water based slurry, the abrasive particles got penetrated in the work material creating indents on the work surface and thereby increased the roughness of machined surface.

Fan et al., (2009) proposed a multi-stage micro-USM process and studied the surface integrity of the micro-USMed surface of glass and ceramic work materials. The effects of abrasive type, slurry concentration and feed rate were systematically analyzed on the quality of machined surface in terms of depth of sub surface cracks. It was revealed that the large size abrasive particles generated a rough surface with deep penetrated cracks and scattered chipping marks. Higher slurry concentration resulted in poor quality of machined surface. A good quality machined surface was obtained in multi-stage micro-USM process when large size abrasive particles with higher feed rate followed by small size abrasive particles with small feed rate and small abrasive particles with dwelling were used step-by-step.

Jain et al., (2011) studied the machinability aspects of silicon, glass and titanium during micro-ultrasonic drilling (USD) process. They reported that surface roughness up to 2.03 μm was obtained using micro-USD process. The maximum tool wear was observed during machining of titanium.

Cheema et al., (2015) investigated the effect of feed rate, slurry concentration and power rating on surface finish of micro channels using micro-USM process. It was reported that surface roughness of microchannels prominently depends on power rating. At high feed rate, surface roughness was found to be decreased. Low power rating provided good surface finish. Slurry concentration of 20% weight by volume yielded best surface finish.

Sreehari and Sharma, (2018) conducted an investigation on improvement of surface quality of microchannels. The influence of viscosity of different liquid mediums of slurry (palm oil, transformer oil and water) was analyzed on surface finish. It was reported that the liquid medium with lesser viscosity provided better surface finish as compared to higher viscosity liquid medium. The overcut and stray cutting was observed lesser when higher viscosity liquid medium was used. It was also concluded that higher feed rate provided better surface finish and accuracy owing lesser interaction time between tool, abrasive and work at all percentage of slurry concentration taken under study.

2.10 Investigations on Additional Parameters

Choi et al., (2007) introduced chemical-assisted ultrasonic machining (CUSM) process to improve the machining rate and surface integrity. Chemical based slurry by mixing hydrofluidic (HF) acid to the alumina based abrasive slurry was used and the chemical effects were examined. Further the superiority of CUSM process was verified by comparing it with the conventional USM process. It was found that as compared to conventional USM process, the performance of CUSM process was improved by 40% and 200% in terms of surface roughness and MRR respectively. However, the diameter of hole was found to be increased when machining using CUSM process. In order to overcome this problem, HF acid concentration less than 5% was recommended for CUSM process.

Ichida et al., (2005) proposed a novel non-contact ultrasonic abrasive machining (NUAM) method for application in precision machining. In NUAM method, loose abrasive particles were excited in a liquid with the application of ultrasonic vibrations. The frequency and amplitude of vibration was kept 28 kHz and 20 μm respectively. The machining modes were investigated by varying the machining time and clearance between the horn and workpiece and changing the liquid medium used in slurry. Five types of liquid mediums i.e. water, methyl alcohol, water mixed with 6wt.% Al_2O_3 abrasive grains and methyl alcohol with 6wt.% Al_2O_3 abrasive grains were used in this

study. Three modes of material removal were observed during experimentation (Mode A) cavitation erosion (Mode B) colliding and sliding of abrasive particles on workpiece surface due to cavitation and (Mode C) small scale removal caused by the excited abrasive particles by ultrasonic energy. The scale of material removal mode was in the order of Mode A-C. In case of methyl alcohol with 6wt% Al_2O_3, Mode B was decreased by increasing the clearance. It was also revealed that the by machining in Mode C, a nanoscale finished surface can be obtained by NUAM method with generation of cavitation.

Zhang et al., (2006) proposed micro ultrasonic assisted lapping (micro-USAL) process for the generation of high surface quality microstructures. In micro-USAL process, a chemical active slurry (CAS) was used for finishing of silicon work material. A mirror like surface finish of the order of 10 nm or less was obtained using the CAS. It was reported that the surface roughness was mainly affected by the abrasive type and their size. No significant effect of other parameters like amplitude and feed speed was observed on the surface roughness.

Tateishi et al., (2009) presented electrorheological fluid assisted micro-USM process for the machining of high aspect ratio microholes on hard and brittle materials. An auxiliary electrode was positioned below the workpiece which provided strong electric field around the abrasive slurry even at higher machining depth. Due to the effect of electric field, abrasive grains were concentrated around the tool (WC with diameter = 80, 90 μm) tip throughout machining. As a result, high aspect ratio (up to 10) precise microholes were machined in quartz glass. The machining quality was increased (in terms of reduction in edge chipping of holes) by increasing the applied voltage. It was reported that by applying a voltage of 1700 V, the edge chipping of holes completely eliminated.

Lian et al., (2014) used another variant of micro-USM process which is termed as electrophoretically assisted micro-ultrasonic machining (EPAMUSM) process. In EPAMUSM process, electric field induced abrasive slurry was used to increase the machining performance of micro-USM process. Due to the applied electric field, abrasive particles could not move away from the machining area. In this process vibratory motion of frequency 60 kHz was provided to the workpiece. A potential difference was created between the rotating tool and an auxiliary electrode to generate the electric field. Ultra-fine abrasive particles absorbed the negative charges from

abrasive fluid due to high surface energy. This resulted in abrasive particle attraction towards the micro tool. As a result of that the edge chipping significantly decreased. A comparison was also carried out between EPAMUSM and conventional micro-USM processes. It was found the EPAMUSM process resulted in higher MRR than that of conventional micro-USM process.

Zeropour et al., (2010) proposed a new method for work holding and force measurement for precision micro-USM process. A vacuum chuck was used for holding and vibrating the workpiece. A force sensor was used to measure and control the machining force during machining. The machining was carried out using a micro tool of 150 μm diameter. The vacuum chuck provided a maximum lateral displacement of 1.59 μm of workpiece from its initial position which ensured the effective transfer of ultrasonic energy on the work surface. In this study, microholes with machining depth of 350 μm was achieved in 25 min.

Jain, (2014) investigated the influence of micro-USM process parameters on its performance characteristics (MRR and TWR) during machining of borosilicate glass. Taguchi's L9 orthogonal array was selected as experimental design. ANOVA was carried out to determine the main effects and significant parameters affecting the performance characteristics. It was revealed that MRR was most significantly affected by static load, whereas TWR was most significantly affected by size of the abrasive particles.

Kuriakose et al., (2016) performed an experimental investigation on micro-USM process while machining of microholes in $Zr_{60}Cu_{30}Ti_{10}$ metallic glass work material. The performance of micro-USM process was measured in terms of hole overcut, edge deviation, MRR, taper angle and TWR by the variation in the process parameters such as feed rate, concentration and abrasive grain size. It was concluded that micro-USM process can be used as better solution for drilling of microhole with lesser hole overcut, minimum edge deviation and lesser burr in all the amorphous alloys without any heat generation and microstructural change. Micro-USM process also resulted in higher MRR and low TWR. The best quality micro hole was obtained at higher feed rate and higher abrasive grain size

James and Sonate, (2017) explored micro-USM process for machining of CFRP/Ti stacks. The effect of process parameters of micro-USM process (i.e. tool material, tool type (hollow and solid) and abrasive grain size on MRR and machined surface quality was investigated. Further, the

performance of micro-USM process was compared with conventional micromachining performance during drilling of microholes on CFRP/Ti. The results revealed that micro-USM process is capable of drilling microhole on CFRP/Ti without delamination at the entrance of the hole. The large size abrasives resulted in higher MRR. Copper tool material worn out at faster rate as compared to tungsten carbide tool. Hollow tool produced higher MRR than solid tool. As compared to conventional micromachining, micro-USM process resulted in negligible (almost zero) delamination in CFRP/Ti, minimum variation in CRFP/Ti and Ti cavity size and higher tool life.

Lin et al., (2017) abricated microfluidic structures on quartz glass using different micromachining techniques such as ultra-precision machining, micro laser machining and micro-ultrasonic machining. The cross junction of microfluidic channels were manufactured using ultra-precision machining. The microstructure was controlled by adjusting the process parameters of ultra-precision machining. Laser micromachining was utilized to manufacture U-shape microchannels. But, the surface roughness was found to be poor. The high quality finish with R_a value less than 0.27 µm was achieved by ultra-precision machining. Micro-USM process successfully utilized in drilling of deep microholes (aspect ratio = 25). Edge chipping was deceased by increasing the rotation speed of tool and abrasive grain size.

Qu et al., (2018) employed micro-USM process for fabrication of micro dimples on polyamide composite material for the first time. A surface texture in the form of simple micro dimples of depths 150 µm and side lengths from 22-425 µm were developed in the area ratio from 10-30%. It was reported that the depth of micro dimples increased by increasing the abrasive particle size, static load and slurry concentration. The side length of micro dimples increased by increasing the abrasive particle size. The effect of concentration of slurry and static load on side length of micro dimples was observed to be mild. The friction coefficient of micro dimples with side length 325 or 425 µm was increased by 100% under a load of 60 N. The surface texture increased the friction coefficient and reduced the wear of micro dimples. These dual benefits resulted in a large output torque.

Wang et al., (2018) analyzed the effect of abrasive particle materials and its shape on micro-USM process performance with the help of simulation models based on smoothed particles hydrodynamics (SPH) and finite element method (FEM). Two type of abrasive particles i.e. SiC

and Al_2O_3 with cubical and spherical shapes were considered in this study. The simulated results were verified by conducting the drilling experiments using micro-USM process. From the simulation results obtained it was inferred that harder spherical shape abrasive provided higher wear resistance of abrasive particles and thereby resulted in higher MRR as compared to the conical shape abrasive particles. However, the surface quality was poor when using spherical shape abrasive particles owing to the large size cracks. The lowest tool wear was observed at a tool feed rate of 40 μm/sec. Spherical shape Al_2O_3 particles resulted in best machining performance.

Li et al., (2018) [115] utilized micro-USM process as a finishing process to removed recast layer from the micro-EDMed surface of ZrB2-SiC-grephite composite. A micro EDM process and micro USM process combined milling was performed to fabricate 3D micro cavity. Initially, micro EDM process was used to machine a 3D cavity in ZrB2-SiC-grephite composite. Subsequently, micro-USM process was used to machine the recast layer deposited on the EDMed machined surface with changing the tool. It was observed that on increasing the amplitude of tool vibration and abrasive grain size and decreasing the tool feed rate up to 13 μm/sec, more thickness of recast layer was removed. The recast layer in the form of micro pores, micro cracks and droplets were efficiently removed and the surface roughness of the order of 1.18 μm was achieved using the combination of micro-EDM and micro-USM processes.

He et al., (2019) presented electrophoresis-assisted micro-ultrasonic machining (EPAMUSM) process for drilling of microholes in hard and brittle materials. In EPAMUSM process, an electric field is created around the machining area to attract the abrasive particles so that sufficient quantity of abrasive particles are available in the machining zone throughout the machining process. The distribution of abrasive particles in the machining area during EPAMUSM process and micro-USM process were compared by conducting numerical simulation. The results showed that during entire period of machining the distribution of abrasive particles was higher in EPAMUSM process as compared to micro-USM process. As a result of that edge chipping caused by the direct interaction of tool and workpiece significantly reduced from 0.22 to 0.03 and MRR marginally improved from 1.718×10^{-4} mm^3/min to 1.916×10^{-4} mm^3/min using EPAMUSM process. The optimal parametric combination of applied voltage 7.5 V, ultrasonic power 22.5 W, spindle speed 300 rpm and a mass fraction 10% resulted in high quality microhole.

Lei et al., (2019) provided planetary movement to the tool to drill high aspect ratio micro holes in quartz crystal using micro ultrasonic drilling process. The influence of planetary parameters on process efficiency and tool wear was analyzed. It was revealed that the planetary movement of tool improved the efficiency of micro-USM process. Microholes of diameter 92 μm with aspect ratio more than ten was achieved by providing planetary movement to the tool. However, tool wear was found to be increased owing to more interaction with abrasives due to planetary movement.

The summary of the major work done and the inferences drawn from literature review of micro USM are shown in Table 2.1.

Table 2.1 Summary of work done in area of micro-USM process

Author	Workpiece material	Tool material	Abrasive used	Parameters studied	Conclusion	Inference
Yu et al. (2004)	Silicon	Tungsten	Polycrystalline diamond powder	Tool diameter and static load	3-D complex cavities can be manufactured by controlling the tool path.	Manipulator is required to develop 3D intricate geometries.
Zhang et al. (2005, 2006)	BK7 glass	High speed steel	Boron carbide	-	Single point tool can be used to machine complex profiles with good surface finish.	
Medis and Henderson (2005)	Silicon, Borosilicate glass	Steel	Silicon carbide	-		
Yu et al. (2006)	Silicon	Tungsten	Polycrystalline diamond	Abrasive particle size, Amplitude amd Static load	Debris accumulation leads to low MRR and surface finish.	Effective flushing is essential.
Pei et al. (2013)	Silicon	Tungsten	Polycrystalline diamond	Abrasive particle size and amplitude of vibration	Debris accumulation provides low MRR and also produces uneven machined surface.	

Author	Workpiece material	Tool material	Abrasive used	Parameters studied	Conclusion	Inference
Sun et al. (1996[a,b])	Silicon	SS-316, thoriated tungsten and WC	WC	Abrasive size, vibration amplitude, static load and rotation speed		
Egashira et al. (1997, 1998)	Silicon, soda glass and SS	WC	Diamond powder	Amplitude and static load		Machining cost is high.
Kuriyagawa et al. (2001, 2002)	Glass	WC	Green silicon carbide	Rotation speed	Tool rotation in micro-USM process resulted in uniform machined surface as compared to stationary tool	
Schorderet et al.(2013)	Glass, Ruby	WC wire, HSS twist drills	Boron carbide	Tool geometry	Twist drill increases the material removal rate.	
Ichida et al. (2005)	Aluminum alloy	Aluminum alloy	Alumina	Machining fluid, machining time and clearance	Material is removed due to (i) impact force, (ii) sliding of abrasive particles and (iii) due to excited abrasive particle by ultrasonic energy.	Non-contact ultrasonic abrasive machining (NUAM) process can be utilized for fine finishing of both hard and soft materials.

Author	Workpiece material	Tool material	Abrasive used	Parameters studied	Conclusion	Inference
Klopfstein et al. (2008)	Silicon	Cemented carbide	Diamond abrasives	Depth of cut, Size of abrasive	The crystallographic structure of the machined layer changes after machining.	Surface finish can be improved using smaller size abrasives.
Cherku et al. (2008)	Silicon wafer	Tungsten	Polycrystalline diamond	Abrasive particle size and slurry concentration	Oil based abrasive slurry shows better surface finish.	Better machined surface quality can be achieved.
Zarepour and Yeo (2012[a,b])	Silicon	Tungsten	Polycrystalline diamond	Particle size and slurry concentration	Ductile machining mode is achieved using single particle impacts.	
Fan et al. (2009)	Zerodur	-	Silicon carbide and alumina	Abrasive grit size, feed rate and abrasive concentration	Multi-stage micro-USM process improves the surface finish when coarse abrasive with large feed rate, fine abrasive with small feed rate are used step-by-step.	Machining rate is low as compared to conventional micro-USM process.
Visvanathan et al. (2011)	Glass	SS440 and SS316	WC	-	Micro-USM process was utilized to develop mushroom shaped & concave spherical structure	

Author	Workpiece material	Tool material	Abrasive used	Parameters studied	Conclusion	Inference
Choi et al. (2003)	Alumina and SUS-304	Tungsten and tungsten carbide	Silicon carbide and diamond	Abrasive particle size, frequency and rotation speed	Tool wear increased by reducing the tool diameter, higher grit size leads to increased diameter of hole.	Tungsten carbide is a better tool material for micro-USM process.
Cheema et al. (2015[a])	Borosilicate glass	WC and SS-304	Silicon carbide	Abrasive particle size and step feed	SS-3054 wears out at faster rate than WC. Better form accuracy ban be obtained using WC tool.	
Yu et al. (2012)	Silicon	Tungsten and SS-316	Polycrystalline diamond	Amplitude, static load, rotation speed, machining time and feed rate	Low cycle fatigue stress is mainly responsible for tool wear in micro-USM process.	Mathematical modelling of tool wear can be done.
Cheema et al. (2015[b])	Borosilicate glass	WC	Silicon carbide	Slurry concentration, abrasive particle size, power rating and workpiece feed	Longitudinal tool wear affect the depth, lateral wear causes taper formation and edge rounding wear yields rounded corners of micro-channels.	

Author	Workpiece material	Tool material	Abrasive used	Parameters studied	Conclusion	Inference
Choi et al. (2007)	Glass	WC	Alumina	Machining time and tool diameter	The chemical effect of chemical assisted-ultrasonic machining (CUSM) process overcome the problems of convention micro-USM process such as low MRR and poor surface roughness.	The CUSM process improves the machined surface quality but use of chemical as liquid medium in USM process is environmentally unfriendly.
Li and Gyanchandani (2005, 2006)	Ceramics	WC/Co and SS	WC	Amplitude of vibration	The desired geometric pattern can be easily transferred from tool to workpiece using USM process.	The shape of tool plays a vital role in micro-USM process.
Jain et al. (2012)	Silicon	Austenitic steel	Silicon carbide	Static load and tool geometry	Hollow tool wears out at faster rate than solid tool.	Solid tool can be used in micro-USM process for drilling operations.
James and Sonate (2017)	CFRP/Ti stacks	WC and Cu	Silicon carbide	Abrasive grain size	Solid tool with coarse abrasive provides higher MRR. WC wears out lesser than Cu.	

Author	Workpiece material	Tool material	Abrasive used	Parameters studied	Conclusion	Inference
Tateishi et al. (2009)	Quartz glass	WC	GC	Tool feed rate	The placement of auxiliary electrode below the workpiece provides proper distribution of abrasive particle in machining zone even at higher depth.	Machining efficiency and productivity increase by the hybridization of process.
Lian et al. (2014)	Monocrystalline silicon	WC	Silicon carbide	Abrasive size, spindle speed, DC voltage, ultrasonic power, mass fraction and feed rate	Electrophoretically induced micro-USM process enhances the MRR and reduces the stray cutting.	
He et al. (2019)	Monocrystalline silicon	WC-Co	Diamond	Ultrasonic power, spindle speed and voltage	Machining efficiency increases by the hybridization of process.	
Shinozuka (2009)	Alumina ceramics	Sandwich tool of hard (SUS 304) and soft material	Silicon carbide	Abrasive particle size	Multiple grooves can be manufactured by laminated tools.	Cost and time saving. But, complicated tool geometries are involved.

Author	Workpiece material	Tool material	Abrasive used	Parameters studied	Conclusion	Inference
Qu et al. (2018)	Polyamide composite	Mild steel	Boron carbide	Abrasive particle size, slurry concentration and static load	Surface texturing increases friction coefficient and reduce wear.	Surface texturing can be done using micro-USM process.
Li et al. (2018)	ZrB2-SiC-graphite composite	Tungsten	Boron carbide	Abrasive grain size, amplitude of vibration and feed rate	The combination of micro-EDM and micro-USM processes provides better control and accuracy.	Micro-EDM process and micro-USM process combined machining can be used for precise machining of composites.
Viswanath et al. (2014)	Fused Silica	SS-304	Diamond particles	-	The low amplitude and small size of abrasive particles generates smoother surface.	Micro-USM process can be used for the fabrication of 3D intricate shapes.
Lin et al. (2017)	Quartz	-	-	-	Micro-USM process can be utilized for drilling of high aspect ratio microholes.	
Kuriakose et al. (2016)	Metallic glass	SS	Boron carbide	Feed rate, abrasive particle size and slurry concentration	Higher feed rate and higher abrasive grain size provides higher MRR and low tool wear.	

Author	Workpiece material	Tool material	Abrasive used	Parameters studied	Conclusion	Inference
Jain et al. (2014)	Borosilicate glass	Austenitic steel	Silicon carbide	Power rating, slurry concentration, static load and abrasive particle size.	MRR is mostly affected by static load.	Tool wear needs to be controlled to achieve higher machining rate and good geometrical accuracy in micro-USM process.
Cheema et al. (2015[c])	Borosilicate glass	WC	Silicon carbide	Slurry concentration, power rating and workpiece feed	Tool wear decreases and surface finish improves while machining at lower power ratings, feed rates.	
Wang et al. (2018)	Glass	SS-304	Silicon carbide and alumina	Abrasive particle shape and abrasive type	Spherical shape abrasive provides higher machining efficiency.	
Sreehari and Sharma (2018)	Silicon wafer	WC	Silicon carbide	Slurry medium, slurry concentration and feed rate	Feature plot representation is an effective way to represent interaction effect among process parameters.	Liquid medium of slurry has great effect on quality of machined surface.
Lei et al. (2019)	Quartz crystal	Tungsten	PCD	Tool diameter, planetary movement speed and eccentric radius	Machining efficiency, aspect ratio of hole and tool wear increase by providing planetary motion to the tool in micro-USM process.	Planetary movement of tool is helpful to produce high aspect ratio micro features using micro-USM process

2.11 Gaps and Opportunities

Based upon the above mentioned comprehensive literature review following gaps and opportunities have been identified and tabulated in Table 2.2.

Table 2.2 Gaps and opportunities

S. No.	Gaps	Opportunities
1	The researchers have developed several techniques for machining of microfeatures on hard and brittle materials. But, all the existing techniques are costly, material dependent and difficult to operate. Thus, there is a need to develop a simple and cost effective micromachining technique.	Micro-USM process is a simple, cost effective and easy to operate machining process. It can be utilized for machining of complex microfeatures on hard and brittle materials irrespective of their electrical conductivity.
2	Debris accumulation is a major problem associated with micro-USM process that results in low MRR, low depth of penetration, high tool wear and poor form accuracy of microfeatures.	There is an opportunity to modify micro-USM system by providing rotary motion to the vibrating tool. Because, the rotary motion of the tool will exert centrifugal force in outward direction which will help to evacuate the debris from machining zone.
3	In rotary ultrasonic machining (RUM), diamond coated tool is used which is not only expensive but also difficult to fabricate specifically in micro domain. The use of uncoated tool in rotary tool micro-USM process has been rarely used for micromachining.	Rotary tool micro-USM process with uncoated tools is a potential area of research to augment the performance of micro-USM process. Also, the use of uncoated tool will reduce the operational cost as well as negate the requirement of coating the tool material.

4	The researchers have proposed several tool materials for micro-USM process on the basis of their properties such as hardness and wear resistance. But, using the same materials contradicting results are reported. Moreover, the literature does not reveal any information about the acoustic property of the tool material.	Extensive investigations (considering acoustic property) are required to select the suitable tool material for micro-USM process to fabricate microfeatures with desired dimensional accuracy.
5	Past research on micro-USM process had a focus on volumetric material removal and surface finish. Moreover, the quality of microfeatures in terms of form accuracy has been rarely reported in the literature.	A comprehensive investigation on form accuracy is required for rotary tool micro-USM process. This investigation will also require alternative characterization approaches. The image processing techniques can be viable solutions for characterization of machined geometries. Further, in order to get desired shape of the microfeatures, form accuracy should be considered as one of the quality characteristics in micro-USM process.
6	Form machining using micro-USM process has been performed for simple geometries (i.e. microhole and straight microchannel) with low aspect ratio.	High aspect ratio micro-holes, complex shaped microchannels can be machined by controlling the tool-abrasive-workpiece interaction and associated motions.
7	As per the published literature, the accuracy of developed microfeatures was improved by reducing the tool wear by controlling the process parameters only. Also the tool wear mechanism of rotary tool micro-USM	Tool wear mechanism of rotary tool micro-USM process needs to be explored with evidence and theoretical supports. This will help in better understanding of the process. Further, geometrical modelling is required to quantify different types of tool wear that occur

	process has not been revealed in the published literature.	during machining. This will help to provide wear compensation to the tool to get desired accuracy.
8	Theoretical modeling of material removal rate using brittle fracture theory in rotary tool micro-USM process has not been reported in literature.	Theoretical modeling of material removal rate is desirable to develop scientific theory and to predict the performance of rotary tool micro-USM process.

2.12 Problem Formulation

The present study is focused on an experimental investigation on rotary tool micro-USM process during fabrication of microfeatures such as microholes and microchannels on hard and brittle materials. This involves the design and development of rotary tool micro-USM process setup, experimentation and subsequent performance analysis, in order to develop understanding of rotary tool micro-USM process and to obtain optimal values of process parameters.

2.12.1 Objectives of the present research work

The focus of the present investigation is on the development of rotary tool micro-USM process to enhance its industrial applicability in microfluidic applications. The major objectives of the investigation are as follows:

- To develop a rotary tool micro-USM process setup for machining of microfeatures in hard and brittle materials.
- To investigate and analyze the effect of tool materials and their properties on performance of rotary tool micro-USM process.
- To evaluate the performance of rotary tool micro-USM process during machining of microholes and microchannels on borosilicate glass.
- To investigate and analyze the influence of various process parameters of rotary tool micro-USM process during drilling of microholes on hard and brittle materials.
- To investigate the tool wear phenomenon and its effect on form accuracy of microchannels during rotary tool micro-USM process.

- To develop a predictive model of material removal rate for rotary tool micro-USM process.

2.12.2 Scope of the present research work

The scope of the proposed work in terms of response characteristics and process parameters during micro fabrication of glass by using rotary tool micro-USM process is as under:

1. Design and development of rotary tool micro-USM process facility with capability to machine various microfeatures (i.e. microholes and microchannels) on hard and brittle materials.
2. Comparative analysis of stationary tool and rotary tool micro-USM processes during machining of microholes and microchannels.
3. Fabrication of microholes and microchannels on hard and brittle materials using the developed facility of rotary tool micro-USM process.
4. Characterization of fabricated microfeatures in terms of material removal rate, tool wear, dimensional and form accuracies.
5. Development of predictive models of material removal rate for rotary tool micro-USM process.

The scope of the present investigation in terms of material, response characteristics and process parameters is presented below:

- **Work material**: The investigation is planned to perform experimentation on hard and brittle materials i.e. glass, silicon and zirconia.

- **Response characteristics for machining of microholes and microchannels during rotary tool micro-USM process**

  - Material removal rate
  - Tool wear rate
  - Form accuracy
  - Depth of microhole
  - Depth of microchannel
  - Hole overcut

▷ Width overcut

▷ Edge chipping

- **Process parameters**

▷ Tool rotation speed

▷ Power rating

▷ Feed rate

▷ Abrasive size

▷ Slurry concentration

▷ Static load

2.13 Plan of the Present Research Work

The concise work plan of the present research work is presented in Figure 2.7. This plan details the flow of work to achieve the objectives of present research work.

```
┌─────────────────────────────────────────────────────────────────────────┐
│   Investigations on Rotary Tool Micro-USM and Analysis of  Process Performance │
└─────────────────────────────────────────────────────────────────────────┘
                                    │
                                    ▼
        ┌───────────────────────────────────────────────────────┐
        │        Development of rotary tool micro-USM facility      │
        └───────────────────────────────────────────────────────┘
                    │                              │
                    ▼                              ▼
        ┌─────────────────────┐      ┌─────────────────────────┐
        │ For microhole drilling │      │ For microchannel fabrication │
        └─────────────────────┘      └─────────────────────────┘
                    │                              │
                    ▼                              ▼
        ┌───────────────────────────────────────────────────────┐
        │                 Plan of experimentation                    │
        └───────────────────────────────────────────────────────┘
                                    │
                                    ▼
┌─────────────────────────────────────────────────────────────────────────┐
│              Workpiece material: Borosilicate glass                        │
│         Tool material: Tungsten carbide, Stainless steel-304               │
│ Process parameters: Tool rotation speed, feed rate, power rating, abrasive size, slurry │
│                         concentration, static load                         │
│ Response characteristics: MRR, tool wear, hole overcut, width overcut, depth of │
│           hole, depth of channel, width of channel, stray cutting          │
│ Characterization techniques: Optical microscope, stereo microscope, Tool maker's │
│       microscope, dial gauge, SEM, FESEM, image processing etc.            │
└─────────────────────────────────────────────────────────────────────────┘
                                    │
                                    ▼
                    ┌───────────────────────────┐
                    │      Pilot experimentation     │
                    └───────────────────────────┘
                                    │
                                    ▼
        ┌───────────────────────────────────────────────────────┐
        │    Selection of range of tool rotation speed and tool material │
        └───────────────────────────────────────────────────────┘
                                    │
                                    ▼
        ┌───────────────────────────────────────────────────────┐
        │    Comparison of stationary tool and rotary tool micro-USM   │
        └───────────────────────────────────────────────────────┘
                                    │
                                    ▼
┌─────────────────────────────────────────────────────────────────────────┐
│ Parametric study, mathematical modeling of MRR, tool wear analysis and optimization │
└─────────────────────────────────────────────────────────────────────────┘
            │                      │                         │
            ▼                      ▼                         ▼
    ┌──────────────┐    ┌──────────────┐    ┌───────────────────────┐
    │ For microhole  │    │ For microchannel │    │ Fabrication of complex shape │
    │    drilling    │    │   fabrication    │    │       microchannels       │
    └──────────────┘    └──────────────┘    └───────────────────────┘
            │                      │                         │
            └──────────┐          ▼          ┌──────────────┘
                       ▼  ┌────────────────────────┐  ▼
                          │ Analysis of results and discussion │
                          └────────────────────────┘
                                    │
                                    ▼
                          ┌────────────────┐
                          │   Conclusions   │
                          └────────────────┘
```

Figure 2.7 Flow chart showing plan of present experimental work

58

2.14 Summary

The chapter includes the literature review and problem formulation. The research problem was derived from the inferences of the gaps and opportunities. The objectives, scope of work and the methodology adopted to perform this investigation are presented. The research plan of present experimental work is also described in the form of flow chart.

CHAPTER 3

DEVELOPMENT OF EXPERIMENTAL FACILITY

This chapter discusses the details of pilot experimentation on rotary tool micro-USM process viz. experimental facility development, process parameters selection, methods for measuring the response characteristics. The experimental facility of rotary tool micro-USM process was developed in-house to enhance the performance of micro-USM process. Subsequently, pilot experiments were conducted using the developed facility of rotary tool micro-USM process. The objective of pilot experimentation was to select the range of tool rotation speed and tool material for rotary tool micro-USM process for subsequent experimentation on machining of microholes and microchannels on hard and brittle materials. The one-factor-at-time (OFAT) approach was used to conduct the pilot experiments.

3.1 Development of Experimental Facility

The experimental facility of rotary tool micro-USM process was developed in-house. The schematic representation of rotary tool micro-USM facility is shown in Figure 3.1. The objective for the development of rotary tool micro-USM facility was to overcome the problems (i.e. debris accumulation of abrasives in the machining zone) of stationary tool micro-USM. The developed facility of rotary tool micro-USM process is shown in Figure 3.2. It comprises of high frequency ultrasonic generator with max power supply 250 W, rotary piezoelectric transducer, micro-tool, counter weight workpiece feed unit and slurry circulation system. The main function of the power supply was to convert the low frequency electrical energy (50 Hz) into high frequency electrical energy in the range of 21 ± 1 kHz. The ultrasonic generator had the function to control the power rating with a resolution of 5 W. The high frequency electrical energy is converted into mechanical vibrations with the help of the piezoelectric transducer. In rotary tool micro-USM facility, the transducer unit was designed and fabricated such that it can rotate at variable speeds while vibrating at high frequency. The transducer can rotate up to the maximum rotation speed of 3000 rpm. A control panel was attached with the facility to control the rotation speed (Figure 3.2). A stepped shape horn/booster was attached to the transducer to amplify the amplitude of the

vibrations up to the desired level of machined. The tool holder was attached to the output end face of the horn. A micro tool was silver brazed to the tool holder.

The feed was given to the workpiece in Z-direction with the help of counter weight gravity feed mechanism as shown in Figure 3.2. This mechanism automatically maintains a constant working gap between tool and workpiece throughout the machining period. The linear motion to the workpiece was provided with the help of XY-axis table (control resolution = 0.1 µm) attached with the facility. The motion of XY-axis table was controlled numerically by using a CNC controller (Make: Sherline 5400-CNC). The controller was attached with the developed facility of rotary tool micro-USM process.
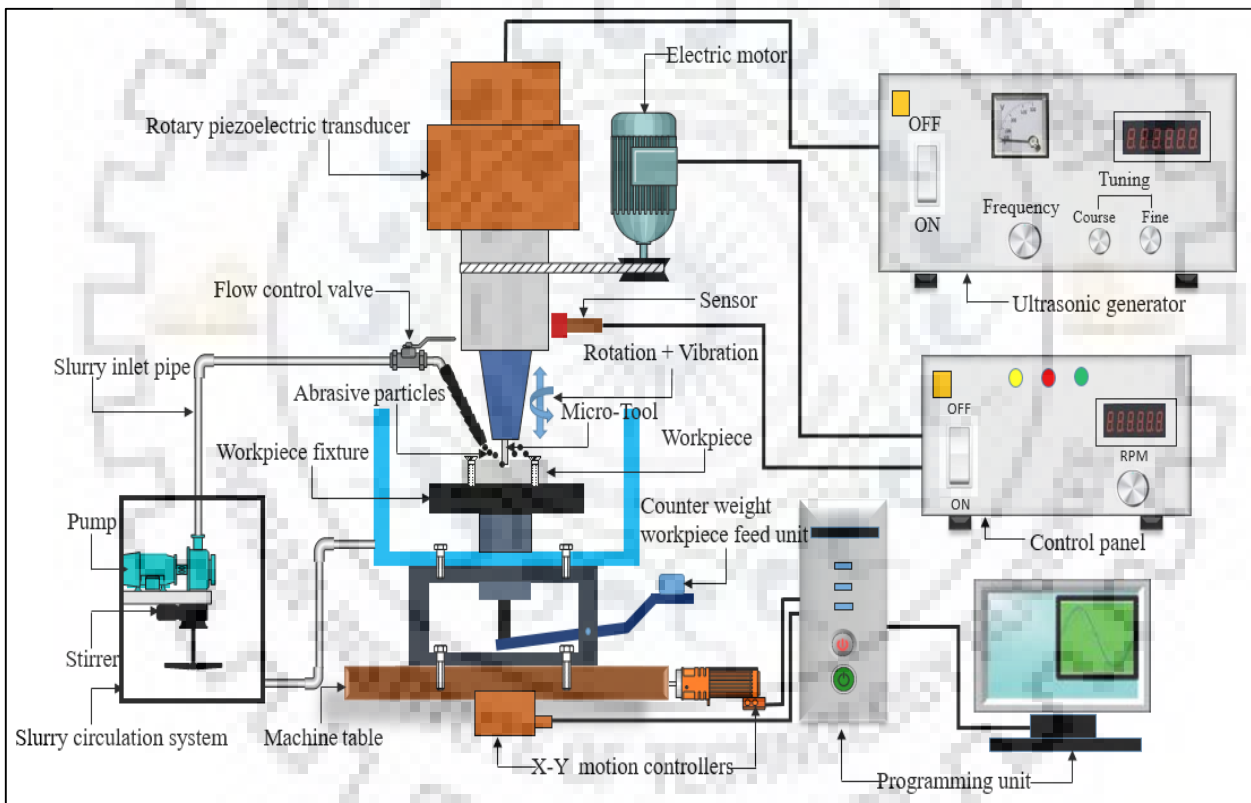
Figure 3.1 Schematic representation of rotary tool micro-USM process facility
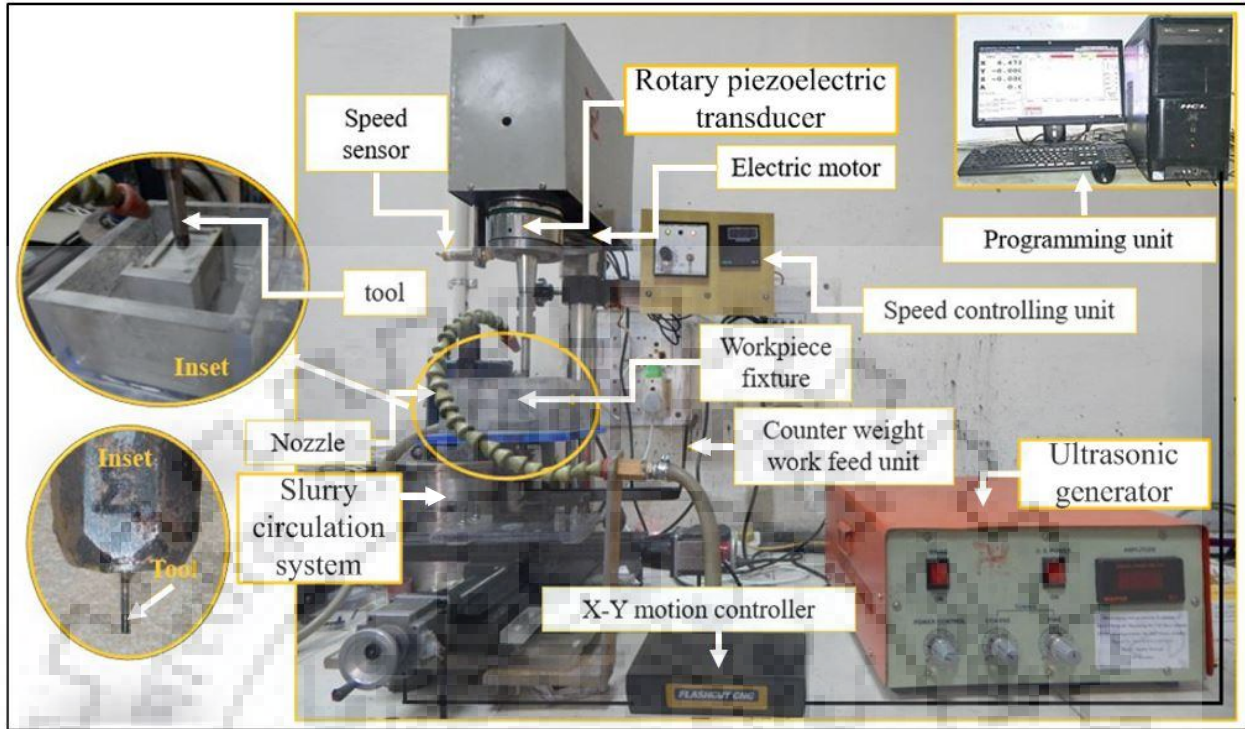
Figure 3.2 Developed facility of rotary tool micro-USM process

The workpiece was clamped on a specially designed and fabricated fixture as shown in inset of Figure 3.2. A flexible pipe was connected to the bottom portion of the fixture. This pipe was used to drain the abrasive slurry from the fixture to the slurry pumping unit. The slurry pumping unit comprised of a tank to maintain a slurry head, a stirrer to mix the abrasive and water and a pump to recirculate and transfer of the abrasive slurry in between the tool and workpiece. The bottom shape of the slurry tank was made as dome in order to avoid settling of abrasives during machining process.

The developed facility of rotary tool micro-USM process can be used to fabricate microfeatures such microholes, microchannels and other complex features on a variety of hard and brittle materials such as glass, ceramics, quartz, silicon, zirconia etc. In micro-USM process, the shape of the tool replicates on the workpiece, therefore in order to make a complex microfeatures, fabrication of complex shape tool is always a costly and challenging task. In order to overcome this problem, smooth solid cylindrical tool can be used in rotary tool micro-USM process. In micromachining, the tool should be provided a controlled path to fabricate the microfeatures

63

accurately. This necessitates the requirement of manipulator and layer-by-layer machining approach.

In layer-by-layer machining approach, several number of layers are removed one after another. In the current experimental investigation, layer-by-layer machining approach was used to fabricate microchannels. During microchannel fabrication, the tool was kept fixed and desired feed was provided to the workpiece in Y-direction and the uppermost layer of workpiece was machined. Thereafter, gravity controlled feed was given to the workpiece in Z-direction to remove the subsequent layer from the work surface. This process was continued throughout the machining period. The major advantage of layer-by-layer machining approach is that it can be used to machine both simple and complex shape microfeatures with the help of a simple cylindrical tool.

3.2 Selection of Process Parameters

Rotary tool micro-USM process involves several input process parameters which affects its performance both in direct and indirect way. The classification of these parameters is carried out in following categories:

- Abrasive based parameters
- Workpiece based parameters
- Tool based parameters
- Acoustic parameters
- Slurry based parameters
- Miscellaneous

The interrelationship between the input and output parameters of rotary tool micro-USM process is shown with the help of Ishikawa's cause and effect diagram (Figure 3.3).
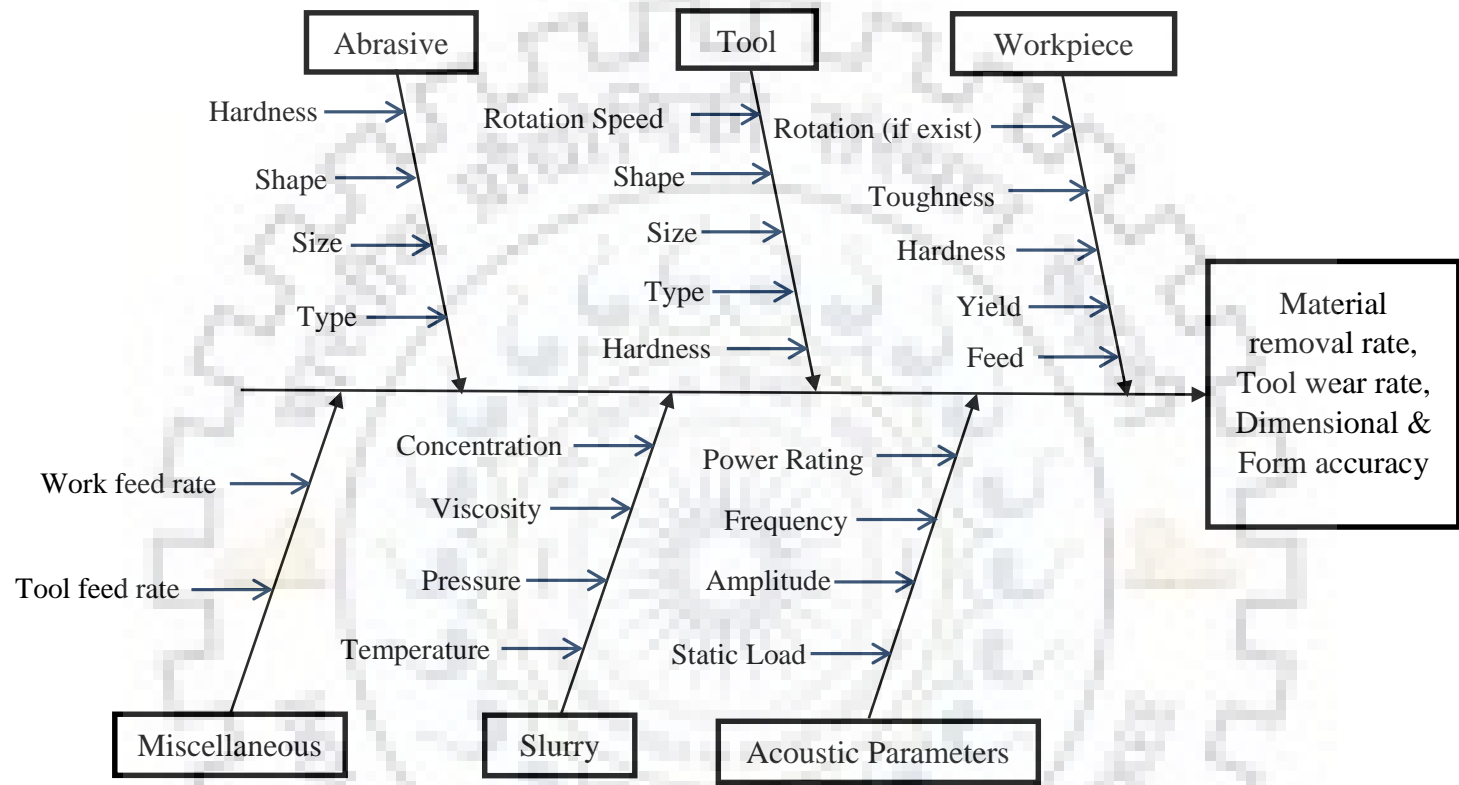
Figure 3.3 Ishikawa cause and effect diagram showing rotary tool micro-USM process parameters

3.2.1 Abrasive based parameters

In micro-USM process, the selection of type of abrasive is based on hardness of work material, usable life time of abrasive particles and process economics etc. The abrasive is selected such that it should have hardness greater than the hardness of work material. silicon carbide (SiC), boron carbide (B$_4$C), aluminum oxide (Al$_2$O$_3$), polycrystalline diamond, tungsten carbide (WC) and diamond power (diamond dust) are commonly used abrasive materials for micro-USM process. Among all the above mentioned abrasive materials boron carbide has longer usable life time as compared to silicon carbide, but, its cost is approximately five times higher than the cost of silicon carbide (Benedict, (1987)). Due to this reason silicon carbide is most preferred abrasive material among all. In USM process, the abrasive size ranges in between #200 mesh to #2000 mesh (Pandey and Shan, (1980)). While machining in micro domain, the size of abrasives greatly affect the quality (topography) of machined surface (Pei et al., (2013); Yu et al, (2006)).

As mentioned above, silicon carbide is generally used as an abrasive material in micro-USM process because it is economical and has appreciable life time. Silicon carbide is a hard and brittle crystalline material. In this experimental investigation, silicon carbide was used as abrasive material. The morphology of silicon carbide is shown in Figure 3.4 respectively.
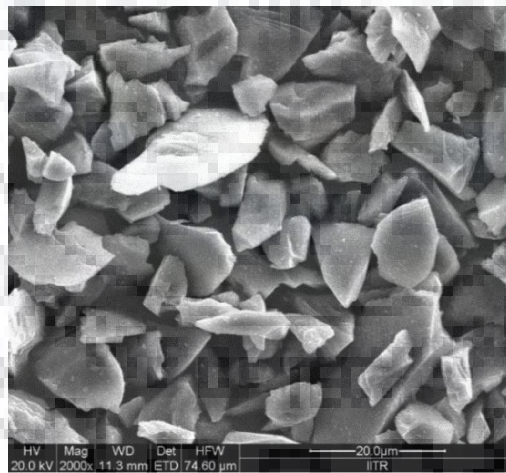
Figure 3.4 Morphology of silicon carbide abrasive particles (#1000 mesh)

3.2.2 Workpiece based parameters

In the micro-USM process, the work material is considered as a candidate work material if it is hard and brittle and it has hardness greater than equal to 40 HRc (Benedicts, (1987)). Glass, silicon

and ceramics are the candidate work materials favorable for machining by micro-USM process as they possess hardness greater than 40 HRc. These materials have superior properties like high strength, wear resistance, corrosion resistance, thermal resistance, hardness etc. (Malek et al., (2007)). Owing to such properties, these materials are commonly used in bio-medical science and engineering applications (Ji et al., (2014); Arif et al., (2011); Xiao et al., (2014); Lian et al., (2016)). Due to these reasons, borosilicate glass, silicon and zirconia were selected as work material in this investigation.

3.2.3 Tool based parameters

The tool material based parameter are very important in micro-USM process. The reason for this is that the properties of tool material greatly affect the tool wear in micro-USM process. Tool wear further affect the performance of micro-USM process in terms of form accuracy of machined micro features. Literature revealed that tungsten carbide, tungsten, SS-304 and cemented carbide are the commonly used tool materials in micro-USM (as mentioned in chapter 2). It was revealed that the performance of SS tool was better than that of WC (Adithan, (1974); Kimaraiah and Reddy, (1993)). In another investigation, conflicting opinions were reported (Egashira et al., (1997), Sun et al., (1996[a])). Due to the differences among the selection of suitable tool material, two type of tool materials (i.e. ductile and brittle) were selected in this investigation. Tool rotation speed also affect the performance of micro-USM, thus it was also included as an input parameter in this investigation.

3.2.4 Acoustic parameters

Selection of acoustic parameters is also important in both macro and micro-USM process. Acoustic parameters include frequency of ultrasonic system, amplitude and power rating of ultrasonic system. In USM system, frequency decides the number of cycles by which the tool reciprocates to and fro per unit of time (second). The frequency range from 16-25 kHz is most commonly used in USM process (Pandey and Shan, (1980)). In this investigation 21 kHz system was selected.

Power rating is defined as the amount of energy imparted by the tool to the abrasive particles present in the machining gap in the form of impact force. Subsequently, the same energy is transferred by the abrasive particles on the work surface when abrasives hit the workpiece. It is expressed in terms of percentage (%) which implies percentage of total power used in the

ultrasonic system adopted. Amplitude of tool vibration is controlled by the power rating. Higher power rating leads to higher amplitude of tool vibration and vice-versa.

3.2.5 Slurry based parameters

Slurry is a mixture of hard abrasive particles (i.e. SiC, B_4C, Al_2O_3 etc.) and a liquid medium generally water. Water is preferred because it is easily available, non-toxic and chemically non-reactive. Slurry medium is a vital parameter in USM process. It plays a dominant role in carrying the abrasive particles from slurry tank to the machining gap. It also act as a cooling medium for tool and workpiece (Thoe et al., (1998)). Moreover, it replenishes the machined debris from the machine gap during machining. Concentration of abrasive slurry is another important parameters affecting the efficiency (MRR), accuracy and quality of machined feature in USM process (Jain, (2012)). Therefore, it was selected as an input parameter in this investigation.

3.2.6 Miscellaneous parameters

Miscellaneous parameters includes feed rate of workpiece in case microchannels fabrication, feed rate of tool/workpiece in Z-direction (step feed rate) in case of layer-by-layer machining. The feed rate of workpiece in X and Y-direction governs the interaction time between tool, abrasive particle and workpiece at a particular time. The interaction time further decides the machining rate and accuracy of machined micro feature. In case of micro hole machining, tool feed rate in Z-direction decides the machining performance. In order to make precise micro features (i.e. microhole and microchannel) with optimum machining rate, proper synchronization of work and tool is necessary. Thus, in order to synchronize the work and tool work feed rate was selected as input parameter in this investigation.

3.3 Output Characteristics

The output response characteristics and their measuring characterization methods are as follows:

3.3.1 Material removal rate

Material removal rate (MRR) is defined as the amount of material removed from the workpiece surface per unit of machining time. It is expressed either by weight or by volume (Guo et al., (2017); Yadav and Yadava, (2017); (Dhakar, (2016)). The MRR is one of the most important performance measure of any of the machining process. In the present work it was calculated by

dividing the weight difference of work material before and after machining by machining time (Eq. (3.1)). The weight of the workpiece was measured with the help of a precision electronic weighing balance (Shimadzu: AUW-220D (Figure A.2 of Appendix A)). Machining time was recorded using a digital stop watch.

$$MRR \text{ (mg/min)} = \frac{(W_i - W_f)}{T_m}$$ (3.1)

where, MRR, W_i, W_f and T_m are the material removal rate, initial weight, final weight of workpiece and machining time respectively.

3.3.2 Form accuracy

Form accuracy is the degree of straightness and flatness of a machined product (Badar et al., (2005[a]); Badar et al., (2005[b])). It defines the accuracy of machined feature on the work material (Kohno et al., (1989)). It is an essential machining performance characteristics of all machining processes. The form accuracy of the machined feature entirely depends on stability of shape of the tool. Form accuracy of microchannel was calculated by measuring the dimensions (width and depth of microchannel) of the machined microchannel with the help of optical microscope (Model: Dewinter DMI Premium (Figure A.1 of Appendix A)). Subsequently, form accuracy was calculated by using following formula:

Form accuracy (%) = (100 – Form inaccuracy) (3.2)

where, form inaccuracy is expressed as:

Form inaccuracy (%) = (DV – AV)*100/DV (3.3)

where, DV is desired volume of microchannel, i.e. cuboid, AV is actual volume of machined microchannel.

The dimensional accuracy were measured in terms of depth and width of machined micro features (both microhole and microchannel). The dimensional and form accuracies were measured and analyzed by using image analysis toolbox of MATLAB v.2016b.

3.3.3 Tool wear

Tool wear is defined as the amount of material removed from the tool surface during machining. The tool wear measured in this experimental work was categorized in three distinct regions as under:

1. Longitudinal wear

2. Lateral wear

3. Edge rounding wear

Longitudinal wear is defined as the reduction in length of the tool. It is schematically shown in Figure 3.5b. Longitudinal wear occurs due to the repetitive hammering/impacts of tool on abrasive particles and also due to the cavitation action occurs on machining face of tool. The length of the tool before and after machining was measured using tool maker's microscope (Make: Nikon MM 400, resolution- 0.1 μm (Figure A.5 of Appendix A)).
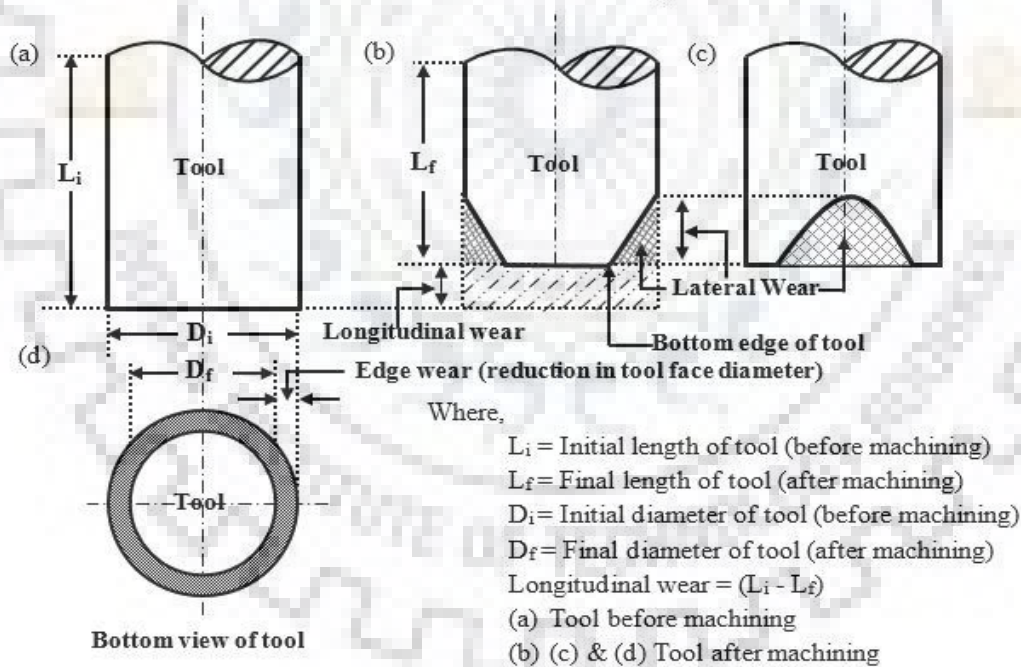
Figure 3.5 Schematic representation of (a) longitudinal wear (b and c) lateral wear (d) edge wear

As the abrasive particles enter into the lateral gap from machining gap, a 3-body abrasive wear takes place in between the abrasive particles, tool vertical surface and wall of the machined cavity. Consequently, the vertical surface of the tool gets wear out and it becomes taper. This taper on the

70

vertical surface of the tool is termed as lateral wear (Figure 3.5(b) and (c)). It was measured in 2D using stereo zoom optical microscope equipped with image analysis and measurement facility (Figure A.4 Appendix A). Field emission scanning electron microscope (FE-SEM) (Make: FEI Quanta 200 (Figure A.6 of Appendix A)) was used to capture the images of the tool. Subsequently these images were used to analyze the lateral wear of the tool.

Edge rounding wear is defined as the reduction in diameter of machining face of the tool. Schematic representation of edge rounding wear is illustrated in Figure 3.5(d). During machining, as the abrasive particles exit from the machining gap towards the lateral gap, a 3-body abrasion takes place between tool bottom edge, abrasive particles and bottom edge of machined workpiece. Consequently, bottom face diameter of tool gets reduced which is termed as edge rounding wear. The edge rounding wear was measured with the help of stereo zoom optical microscope (Make: Nikon SMZ 745, resolution- 1 µm (Figure A.4 of Appendix A)) equipped with image analysis and measurement facility.

3.3.4 Width overcut and hole overcut

Width overcut is defined as the difference between the actual width of machined microchannel and diameter of tool (i.e. desired width) in case of microchannel fabrication. Whereas, in case of microhole machining, hole overcut is defined as the difference between the actual diameter of machined microhole and the diameter of the tool (i.e. desired diameter). Width overcut and hole overcut were calculated as per Eq. (3.4) and Eq. (3.5) respectively. The schematic representation of overcut in microchannel as well as in microhole is illustrated in Figure 3.6(a) and (b) respectively. Stereo zoom optical microscope with image analysis and measurement facility (Figure A.4 of Appendix A).

Width overcut (WOC) = Actual width of microchannel (W_c) – Tool diameter (D_t)   (3.4)

Hole overcut (HOC) = Actual diameter of microhole (D_h) - Tool diameter (D_t)   (3.5)
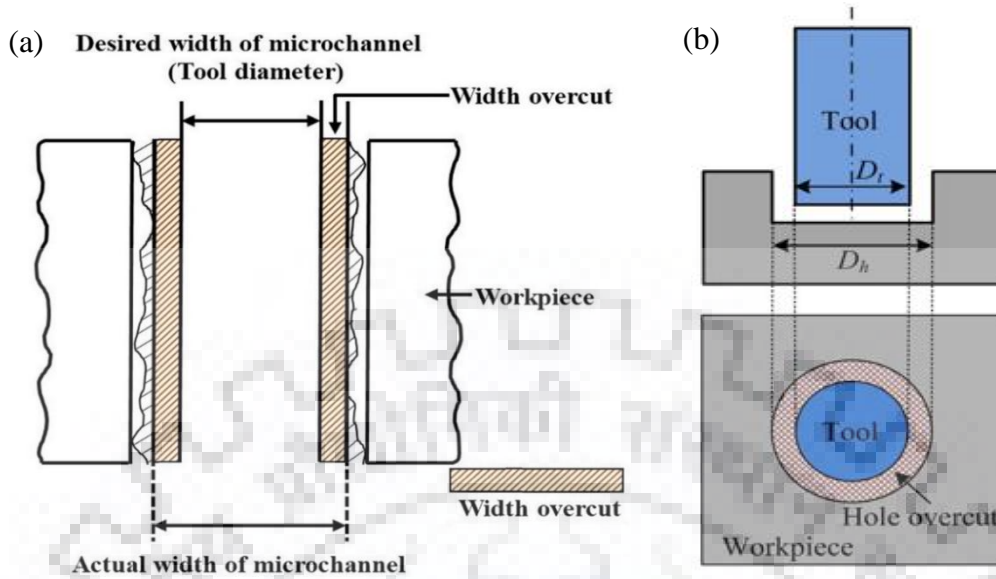
Figure 3.6 Schematic representation of (a) width overcut (b) hole overcut

3.3.5 Edge chipping/Damage

Edge chipping is defined as the unwanted damage around edges of the machined microchannels in case of microchannels fabrication. Whereas, in case of microholes, it is the unwanted damage around the periphery of the machined microhole. Schematic representation of edge chipping in microchannel and microhole is shown in Figure 3.7(a) and (b) respectively. It was measured with the help of optical microscope (Model: Dewinter DMI Premium and associated Material Plus Version 4.2 software (Figure A.1 of Appendix A)). In case of microchannels, it was measured by tracing the damaged edges of microchannel as shown in Figure 3.7(a). Whereas, in case of microhole, the damage periphery of hole was traced to determine the edge chipping (Figure 3.7). The size of edge chipping in microchannel (EC_c) was calculated as the difference of the average of inner edge width (W_{ie}) and outer edge width (W_{oe}). In case of microhole, edge chipping EC_h was calculated as the difference of average diameter of inner circle (D_i) and outer circles (D_o).

The mathematical expression used to calculate the edge chipping in microchannel and microhole are expressed in Eq. (3.6) and Eq. (3.7) respectively (Goel and Pandey, (2017); Guo et al., (2017); Gupta, (2015)).

In case of microchannels:

$$\text{Edge chipping } (EC_c) = \frac{(W_{oe} - W_{ie})}{2} \tag{3.6}$$

72

In case of microholes:

Edge chipping $(EC_h) = \frac{(D_{max} - D_{min})}{2}$ (3.7)

where, D_{max} and D_{min} are the maximum and minimum diameter of machined microhole.
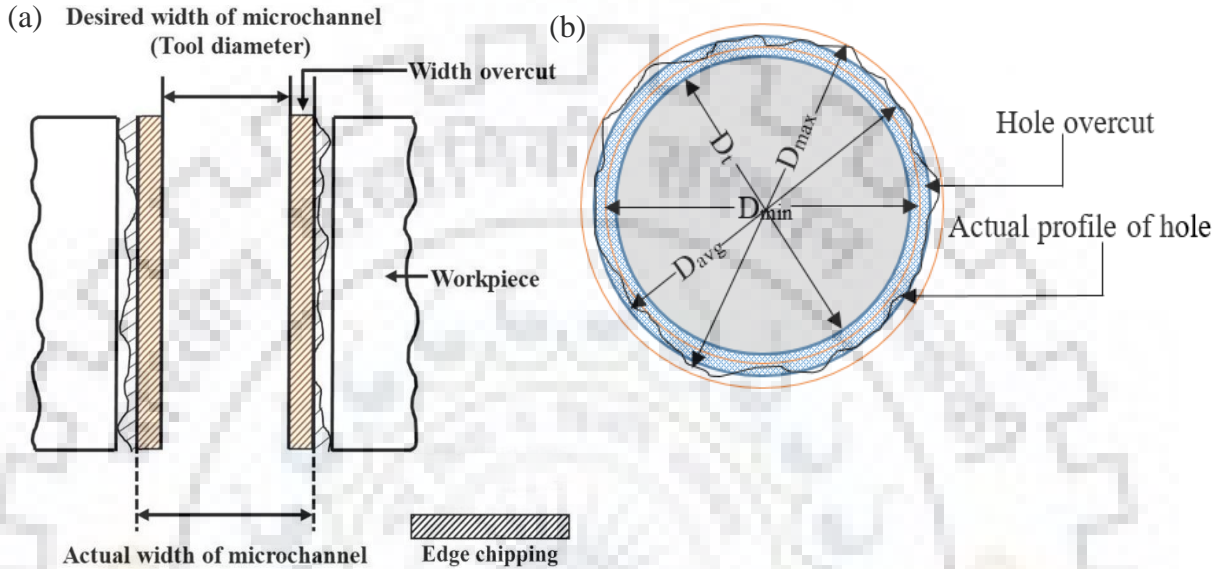
Figure 3.7 Schematic representation of (a) width of edge chipping (b) diameter of edge chipping

3.3.6 Taper angle

Taper is defined as the deviation of the machined hole wall from the axis of tool. It is schematically represented in Figure 3.8. In case of through microhole, a half taper angle was calculated in terms of degree using Eq. (3.8). The schematic representation of taper is shown in Figure 3.8. During the calculation of taper, the diameter of the microhole at entry and exit side were measured with the help of stereo zoom optical microscope (Make: Nikon SMZ 745, resolution- 1 µm (Figure A.4 of Appendix A)). The thickness of work material was measured using digital vernier caliper (Make: Mitutoyo absolute digimatic).

Taper angle (degree) $= \text{Tan}^{-1}\frac{(D_{Entry} - D_{exit})}{2T_w}$ (3.8)

where, D_{Entry} is the entrance diameter of hole, D_{Exit} is the exit diameter of hole and T_w is the thickness of the work material.
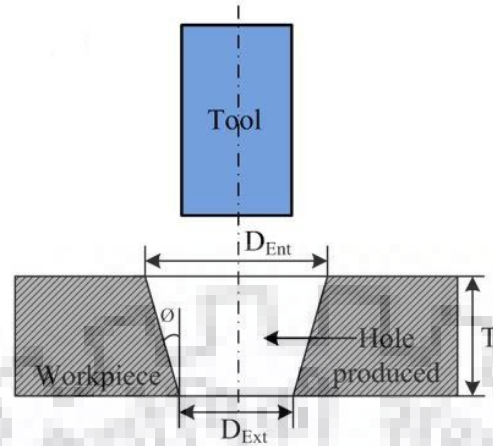
Figure 3.8 Schematic representation of taper angle

3.4 Pilot Experimentation

In this research work, the pilot experimentation was performed using One-Factor-at-a-Time (OFAT) approach. The OFAT approach is frequently used for designing the experiments. In this approach, only single input parameter is varied at a time and rest of the input parameters are kept at constant level (fixed value). This approach tells about the process behavior in terms of response characteristics with respect to change in input variables. It is also used to determine important levels of input parameters out of a large set levels of input parameters taken under study. The pilot experimentation was performed in three sets. The first and second sets were performed to select the range of tool rotation speed for machining of microholes and microchannels. The third set was performed to select the tool material for the same.

3.4.1 Selection of tool rotation speed for microholes drilling

Rotary tool micro-USM process is a newly developed process variant of micro-USM process. A limited research work is conducted on micro-USM process with tool rotation. However, micro-USM process with workpiece rotation has been investigated by some researchers. But, when the rotary motion is provided to the vibrating tool, the process mechanism may change which in turn will affect the process performance. Therefore, selection of tool rotation speed range becomes imperative for subsequent investigation as what value of tool rotation speed has to be selected. By considering the abovementioned aspect, the pilot experimentation was carried out to select the tool rotation speed of the tool for drilling of microholes.

The pilot experiments were conducted using the in-house developed rotary tool micro-USM facility shown in Figure 3.2 by adopting OFAT approach. The process parameters setting used for this experimentation is presented in Table 3.1. The effect of tool rotation speed was investigated on the performance of rotary tool micro-USM process. The depth of hole (DOH), hole overcut (HOC) and edge chipping were selected as performance measures of rotary tool micro-USM process. During experiments, rotation speed was varied from 0-700 rpm. After each experiment, the work sample was cleaned in ultrasonic cleaner (Model No. YJ5120-1 (Figure A.3 of Appendix A)) at 45 °C for 30 min and subsequently, dried in hot air. The DOH and HOC were measured with the help of optical microscope (Dewinter Material Plus: DMI Premium (Figure A.1 of Appendix A)) as per the procedure discussed in section 3.3. Edge chipping was analyzed qualitatively with the help of microscopic images. The images were captured using stereo microscope (Make: NIKON SMZ- 745T (Figure A.4 of Appendix A).

Table 3.1 Process parameters settings for tool rotation speed selection

Variable process parameters	
Rotation speed (RS)	0, 100, 200, 300, 400, 500, 600, 700 rpm
Constant process parameters	
Frequency	21 ± 1 kHz
Power rating (PR)	30%
Abrasive size (AS)	1200 mesh
Slurry concentration (SC)	10%
Static load	45 g
Tool diameter (Ø)	600 μm
Tool material & geometry	WC, Cylindrical

Analysis and discussion of results

In this set, the pilot experiments were conducted by varying the tool rotation speed in eight levels (i.e. 0, 100, 200, 300, 400, 500, 600 and 700 rpm) by keeping rest of the parameters at constant value (i.e. power rating = 30%, abrasive size = #1200 mesh, slurry concentration = 10% and static load = 45 g). The DOH, HOC and edge chipping were considered as response characteristics. The results obtained from this experimentation are given in Table 3.2. The results of experiments are

explained with the help of a model furnished in Figure 3.9. From Figure 3.9, it can be clearly seen that the proposed model is divided into three distinct zones namely zone 1, zone-2 and zone 3 according to the output responses by the variation in the rotation speed of the tool. The zone 1 and zone 3 shown by red color in Figure 3.9 indicates that the machining with stationary tool (i.e. with no tool rotation speed) and rotation speed beyond 500 rpm exhibited in low DOH, high HOC with severe edge chipping around the machined hole periphery. This was due to the reason that in case of stationary tool (i.e. with no tool rotation), as the machining proceeds up to a certain depth, abrasives start to accumulate into the machining gap (i.e. gap between tool and workpiece) by forming the multiple layers of abrasives (Figure 3.10(a)). As the tool hits the uppermost layer of abrasives, these abrasives in turn hit the abrasives of the subsequent layer and lose their energy. As a result of that low ultrasonic energy transferred from the tool to the work surface via abrasives. Consequently, machining rate decreased and low DOH was obtained. In this case, a 3-body abrasion between tool-abrasive and work material takes place in the machining zone (Figure 3.10 (a) and (b)). This results in high tool wear, HOC and poor form accuracy (taper formation) of machined micro-hole. Moreover, accumulation of abrasives hampered the circulation of abrasive slurry in the machining zone and consequently abrasives started to hit the periphery of the hole while entering into the machining zone. This caused edge chipping at the machined hole periphery.

On the other hand, as the rotary motion is provided to the tool, a centrifugal force generates on the abrasives present in the lateral gap (Fig. 3.10(c)). The lateral gap is defined as the gap between machined hole wall and tool surface (Fig. 3.10(a)). During machining, the downward motion of the tool (Figure 3.11) compresses the abrasive slurry and creates a high pressure zone beneath the tool. At the same time, the pressure around the tool vertical surface (i.e. in lateral gap) is lesser than the pressure beneath the tool (i.e. in machining gap) (Fig. 3.12(a)). Due to the mutual effect of centrifugal force and pressure difference, the abrasives move from the machining gap towards the lateral gap. Alternatively, the upward movement of the tool (Figure 3.11) creates low pressure zone beneath the tool as compared to the pressure in the lateral gap (Fig. 3.12(b)). This facilitates the easy supply of abrasives into the machining gap. Thus, the abrasives keep on replenishing from the machining zone during entire machining period. Further, due to centrifugal force, the abrasives present in the lateral gap come in contact with the wall of the machined hole without making contact with the tool surface. This result in a 2-body abrasion between the abrasives and wall of the machined hole (Fig. 3.10(c) and Fig. 3.10(d)). The 2-body abrasion occurs in the form of

sliding and rolling contacts as well as indentation of abrasives with hole wall (Komariah and reddy, (1993)). This results in negligible tool wear at the vertical face of the tool and thereby enhances the machining rate and form accuracy of machined micro-hole. But, as the rotation speed increased beyond 500 rpm, lateral vibration may induce in the tool due to which complete ultrasonic energy could not transferred on the work surface leading to shallow depth of machined hole. Moreover, lateral vibration at high rpm (beyond 500 rpm) may also damage the periphery as well as wall of machined hole. Consequently, higher edge chipping and hole overcut were observed. Another reason for severe edge chipping and high hole overcut may be the excessive centrifugal force caused by tool rotation in outward direction from the axis of tool which exerted on the abrasive particles during machining. While exiting from the lateral gap, the abrasives abraded the wall and periphery of the hole. The zone 2, (rotation speed of tool from 100 to 500 rpm) shown by green color resulted in higher depth of hole, lesser hole overcut and lesser edge chipping at hole periphery (Fig. 3.13). As mentioned above, owing to rotary motion to tool, the abrasives replenished from the machining area, thereby increased the depth of hole and reduced the hole overcut and edge chipping (Fig. 3.13). The tool rotation speed in the range of 100-500 rpm provided relatively smoother edge of the machined holes (as evidenced in Fig. 3.13). Thus, the upper and lower bounds of rotation speed of tool were fixed at 500 and 100 rpm for successive experiments.

Table 3.2 Process parameters and responses

Rotation speed (rpm)	Avg. DOH (μm)	Avg. HOC (μm)	Avg. Edge chipping (μm)
0	310	113	65
100	375	79	45
200	435	64	38
300	530	45	25
400	490	57	32
500	445	78	53
600	395	104	60
700	340	172	85
Constant parameters: Power rating = 30%, abrasive size = 1200 mesh, concentration = 10%, static load 45 g			
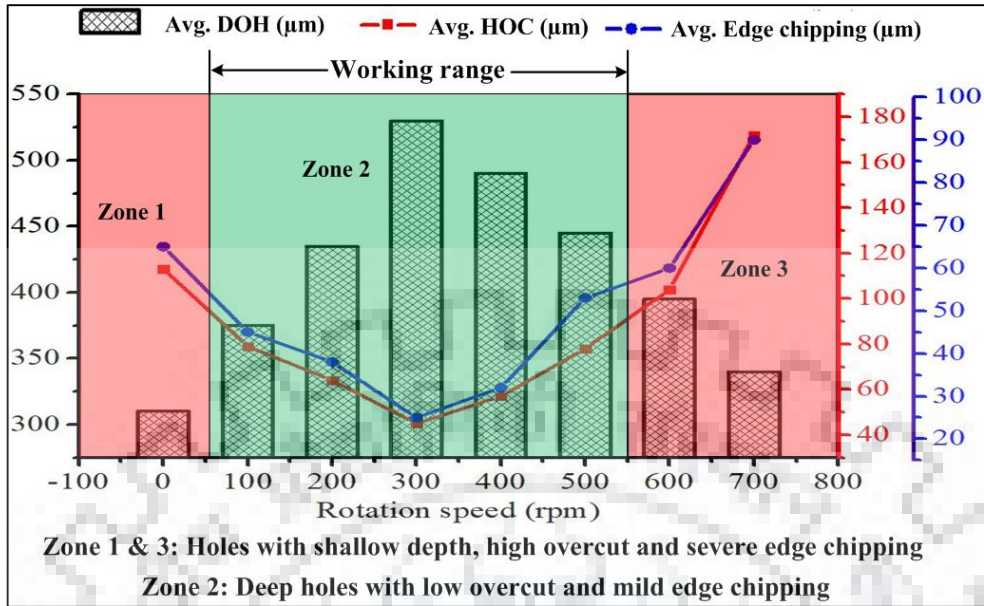
Figure 3.9 Tool rotation speed effect on DOH and HOC
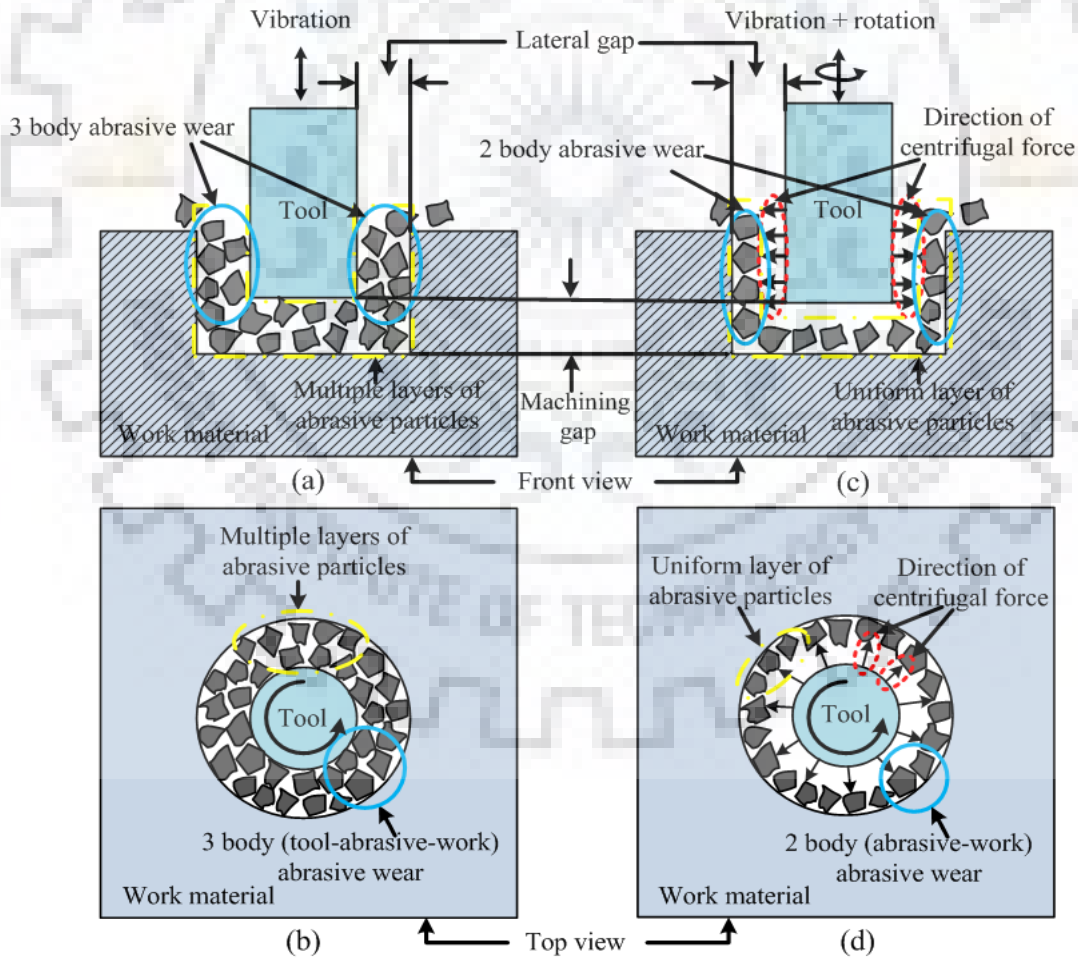
Figure 3.10 Schematic representation showing movement of abrasives in the machining zone
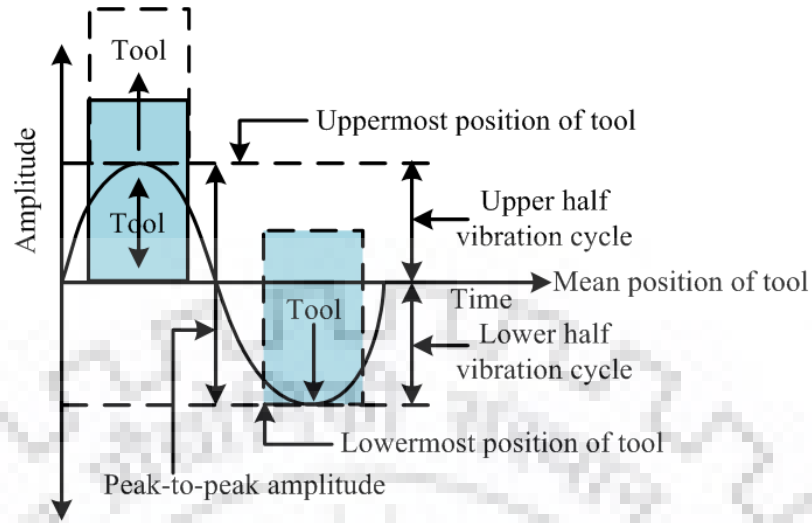
Figure 3.11 Schematic representation of vibration cycle during ultrasonic machining
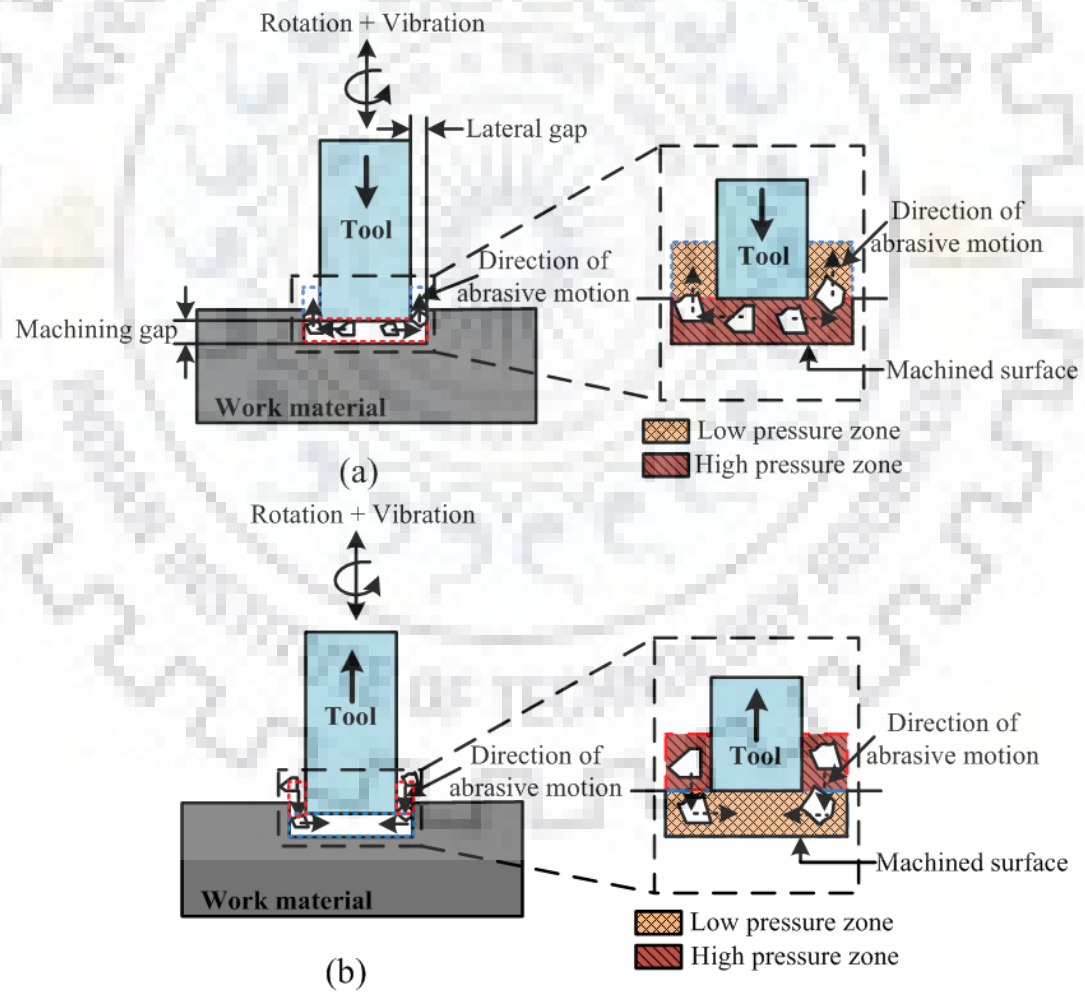
Figure 3.12 Schematic representation showing tool movement in (a) downward tool movement and (c) upward tool movement
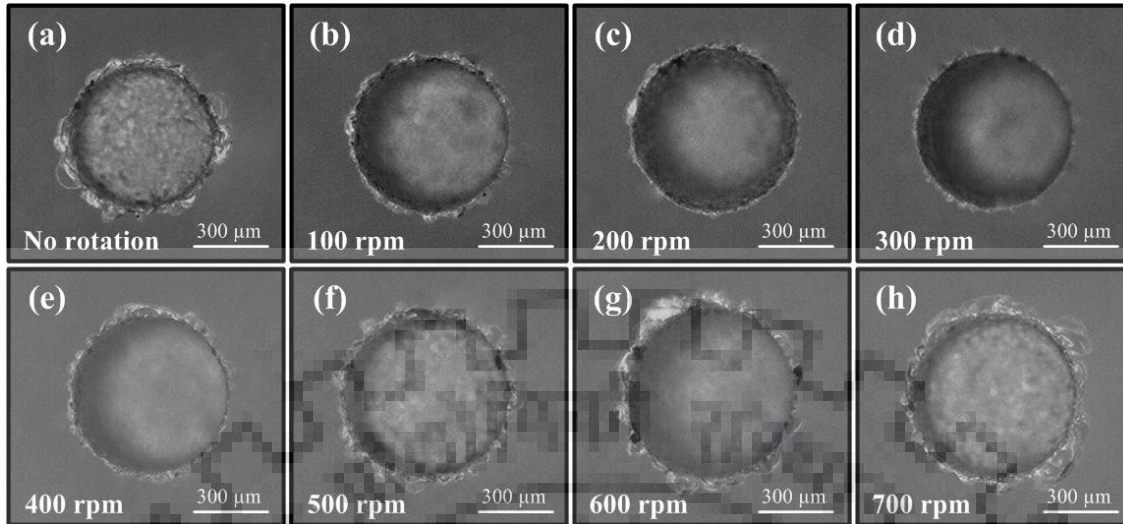
Figure 3.13 Microscopic view of micro-holes drilled at various tool rotation speed

3.4.2 Selection of tool rotation speed for fabrication of microchannels

The objective of this set of pilot experiment was to select the range of tool rotation speed for subsequent experimentation on fabrication of microchannels.

The experiments of this set were conducted using the in-house developed rotary tool micro-USM facility shown in Figure 3.2. The OFAT approach was used to perform experiments. The effect of tool rotation speed was investigated on response characteristics of microchannels such as depth of channel (DOC) and form accuracy (FA). The process parameters setting is given in Table 3.3. During trial experiments, the tool rotation speed was varied from 0 to 700 rpm with rest of the process parameters maintained at their constant level as tabulated in Table 3.3. The machining time for each experiment was kept constant. Post machining, the microchannels were sectioned along the axis A-A' (as shown in Figure 3.14). The sectioned micro channels were measured using stereo zoom microscope. The dimensional and form accuracies of microchannels were measured and analyzed by using image analysis toolbox of MALAB v.2016b. The dimensional accuracies were measured in terms of width of microchannel (WOMC) and DOC. The form accuracy of microchannel were measured as per the procedure discussed in section 3.3.
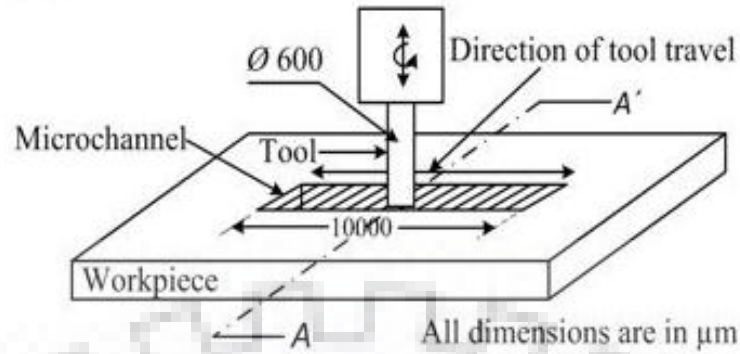
Figure 3.14 Isometric view of tool and work

Table 3.3 Process parameters settings

Variable process parameters	
Rotation speed (RS)	100, 200, 300, 400, 500, 600, 700 rpm
Constant process parameters	
Frequency	21 ± 1 kHz
Power rating (PR)	30%
Feed rate (FR)	15 mm/min
Abrasive size (AS)	1200 mesh
Slurry concentration (SC)	10%
Static load	45 g
Tool diameter (Ø)	600 μm
Tool material & geometry	WC, Cylindrical

Analysis and discussion of results

In order to select the range of tool rotation for microchannel fabrication trial experiments were conducted. The OFAT approach was used for trial experimentation. During pilot experiments, the tool rotation speed was varied from 0 to 700 rpm with rest of the process parameters maintained at their constant level (i.e. work feed rate = 15 mm/min, power rating = 30%, slurry concentration = 10%, abrasive particle size = 1200 mesh). The machining time for each experiment was kept constant. A representation of actual machined microchannel with work feed direction is shown in Figure 3.15.
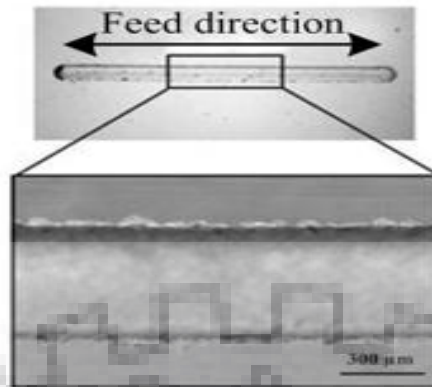
Figure 3.15 Microscopic image of machined microchannel

The results obtained from the pilot experiments are given in Table 3.4 and graphically presented with the help of a model shown in Figure 3.16. The Figure 3.16 represents the effect of tool rotation speed on form accuracy and DOC with the help of a model. The model shown in Figure 3.16 is divided into three distinct zones (i.e. zone 1, zone 2 and zone 3) according to the machining characteristics by the variation in the input parameters. The zone 1 (with no tool rotation) and zone 3 (tool rotation speed beyond 600 rpm) are denoted by red color in Figure 3.16 resulted in poor form accuracy and low depth of machined microchannels and high edge chipping. The reason attributed was that in zone 1 (when no rotation was provided to the tool), the abrasive particles accumulated (multiple layers of abrasive particles) into the machining gap as the depth of microchannel increased. Consequently, low energy was transferred on the work surface leading to high tool wear and low DOC. High tool wear caused poor form accuracy of microchannel. On the other hand at tool rotation speed beyond 600 rpm resulted in very high centrifugal force on the abrasive particles present into the machining zone. Due to this very limited quantity of abrasives particles entered and participated into the machining resulting in low tool wear and low DOC (Figure 3.16). Moreover, due to very high centrifugal force the abrasive particles impacted on the microchannel wall leading to the abrasion of microchannel wall and hence high edge chipping. This also resulted in deviation of the profile of microchannel from the desired accuracy. Another reason of poor form accuracy and low DOC at 700 rpm may be the direct interaction of tool and work material. The zone 2 (tool rotation speed from 100 rpm to 600 rpm) represented by the green color provided satisfactory results i.e. low tool wear and better dimensional and form accuracy of the microchannels (Figure 3.16). The centrifugal force generated by providing rotary motion to the tool replenished the abrasive particles into the machining zone effectively leading to better form

accuracy, DOC and lesser edge chipping. Within the range of 200-500 rpm of tool, relatively flattened bottom surfaces were obtained (as evidenced in Figure 3.16). Therefore, to cover this range, the lower and upper limits of tool rotation speed were set to 100 rpm and 600 rpm respectively for subsequent experimentation.

Table 3.4 Process parameters and responses

Rotation speed (rpm)	Avg. DOC (μm)	Avg. Form accuracy (%)	Avg. Edge chipping (μm)
0	320	55	72
100	315	68	52
200	330	78	44
300	380	86	33
400	350	82	40
500	340	79	55
600	320	75	64
700	260	61	98

Constant parameters: Power rating = 30%, feed rate = 15 mm/min, abrasive size = 1200 mesh, concentration = 10%, static load 45 g
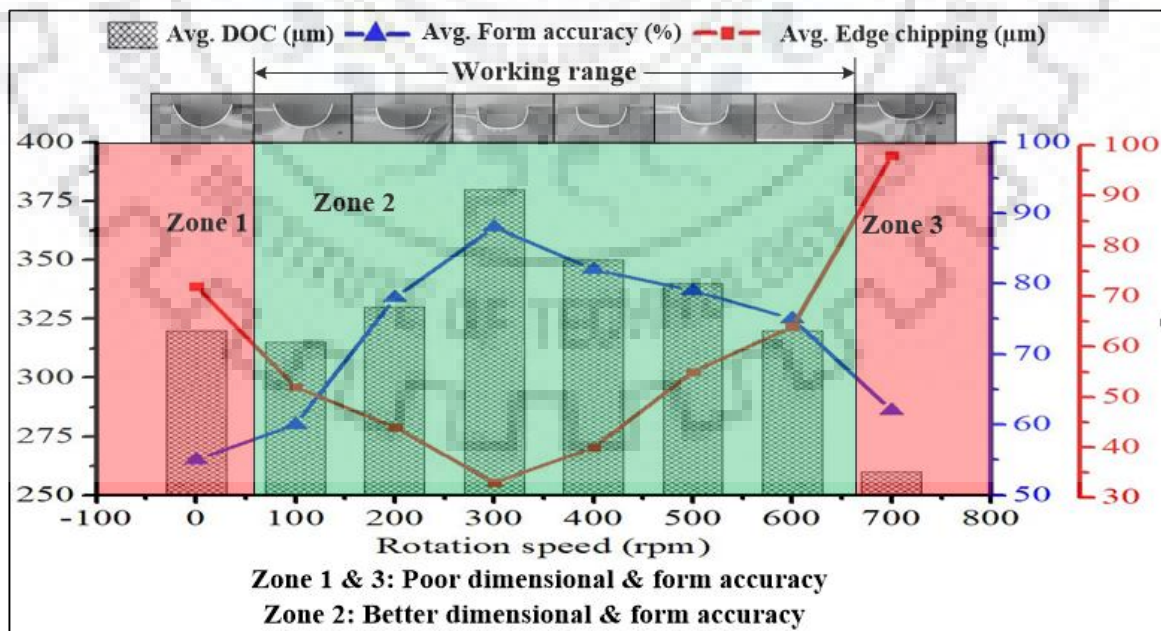
Figure 3.16 Effect of rotation speed on DOC, form accuracy and edge chipping

3.4.3 Selection of tool material

In micro-USM process, the shape of the tool replicates on the work surface (Jain, (2010)). The geometry of the machined micro feature is governed by the shape of tool. Therefore, in order to obtain dimensionally accurate microfeatures, tool should maintain its shape throughout the machining process. However, tool wear is an unavoidable phenomena of this process. It cannot by eliminated completely. Though, it can be minimized up to a certain extent by selecting proper tool material and controlling the process parameters of micro-USM process. Therefore, selection of suitable tool material is very important in this process as far as efficiency and accuracy of machined micro feature is concerned. As per the published literature, there are conflicting opinions on the selection of tool material (soft/ductile or hard/brittle) in micro-USM process (Komaraiah and Reddy, (1993); Cheema et al., (2015); Wang et al., (2018)). When rotation of the tool comes into picture, the process mechanism may change due to the centrifugal force generated by the tool rotation. This requires investigations on tool wear mechanism and the effect of tool material properties on tool wear. By considering the abovementioned aspects, two types of tool materials (i.e. Stainless steel-304 (SS-304) and tungsten carbide (WC)) were selected for rotary tool micro-USM process. The wear mechanism of both the tool materials were investigated. Subsequently, the effect of tool material properties on tool wear, MRR and surface roughness was analyzed. Also, the effects of rotary tool micro-USM parameters were investigated on tool wear and performance of rotary tool micro-USM process.

The experiments of this set were performed using the in-house developed facility of rotary tool micro-USM facility shown in Figure 3.2. Microchannels having the dimensions of 10 mm length and 600 µm width were fabricated on borosilicate glass. The experiments were carried out using OFAT approach. The experimental settings are tabulated in Table 3.5. The tool materials selected were SS-304 and WC. During experimentation, the effect of tool material properties and rotary tool micro-USM process parameters viz. rotation speed, feed rate, power rating and slurry concentration was investigated on MRR, DOC and WOC. The MRR was calculated as per the procedure mentioned in section 3.3. The DOC, WOC and machined profile of fabricated microchannel was measured with the help of an optical microscope (Dewinter Material Plus: DMI Premium (Figure A.1 of Appendix A)). Subsequently, an image processing software was used for tracing the profile of machined microchannels (Davim, (2007)). During experimentation each

experiment was repeated thrice and the average value of output parameter was considered as final response.

Table 3.5 Process parameters setting for tool material selection

Variable process parameters	
Rotation speed (RS)	100, 200, 300, 400, 500, 600 rpm
Power rating (PR)	20, 30, 40, 50, 60%
Feed rate (FR)	10, 15, 20, 25, 30 mm/min
Slurry concentration (SC)	10, 15, 20, 25, 30%
Tool material	WC, SS-304
Constant process parameters	
Frequency	21 ± 1 kHz
Abrasive size	1200 mesh
Static load	45 g
Tool diameter (Ø)	600 µm
Tool geometry	Cylindrical

Wear mechanism of SS-304 and WC tool materials

In order to investigate the wear mechanism of SS-304 and WC tool materials, experiments were conducted by using both the tool materials. During the experiments, machining time was varied from 1-5 minutes and other parameters were kept at constant level (i.e. tool rotation speed = 300 rpm, work feed rate = 20 mm/min, power rating = 40%, concentration = 15%). After each experiment, tool images (front and bottom view) were captured using stereo zoom microscope. The microscopic images of the tools after machining are presented in Figure 3.17. On the basis of the microscopic images, the wear mechanism of SS-304 and WC tool material was explained. From the microscopic images of the tool shown in Figure 3.17(a-2) and (a-3), plastic deformation can be clearly seen on the bottom face of SS-304 tool. Whereas, no such effect was observed on the bottom face of WC tool (Figure 3.17(b-2) and (b-3)). This can be attributed with the fact that in rotary tool micro-USM process, when the tool strikes on the abrasive particles, the abrasive particles get kinetic energy and release this energy on the work surface in the form of impact. As

a result of that micro cracks generate, propagate and finally micro chipping takes place by the continuous hitting of abrasives on the work surface. During machining with rotary tool micro-USM process, the tool also suffers the same impacts as the work material. Due to which compressive stresses generate on the tool bottom surface. By the continuous impact of abrasives, compression of tool bottom face takes place. Consequently, plastic deformation starts to take place in the tool bottom surface (Figure 3.18(a)). This deformation results in the flow of tool material in upward direction around the periphery of the tool leading to an increase in tool bottom face diameter (Figure 3.17(a-3)). The plastic deformation and increased diameter of tool bottom face are evidenced in Figure 3.17(p-2) and (p-3). The increased tool bottom face diameter in turn results in the increased width of microchannel (Figure 3.19(b)). As the machining continues, this deformation keeps on increasing and as a result of that more and more material accumulates around the periphery of the tool bottom face. Finally, a mushroom type shape of the tool (as evidenced in Figure 3.17(a-3)) was formed. Similar phenomenon occurred in the study conducted by Cheema et al. [21]. The mushroom shape of tool restricted the movement of abrasives from the machining gap (Figure 3.18(b)) due to which machining rate decreased. Moreover, due to the accumulated unwanted material on the periphery of tool, complete energy could not transferred on the work surface. Consequently, machining rate decreased. On further machining, shearing of accumulated unwanted material on the tool periphery and microchannel wall takes place. The shearing action is schematically shown in Figure 3.18(b). The shearing of tool and work material takes place due to the abrasion caused by abrasive particles present in the lateral gap. Consequently, a pointed edge of the tool was obtained (Figure 3.17(b-4)). Whereas, in case of WC tool material, no compression of tool bottom face was observed (Figure 3.17(b-2)). This was attributed to high compressive stress of WC tool. The hardness of WC tool is much higher than SS-304 tool material which is soft and tough in nature. Due to high hardness, WC tool was not deform by the impact of abrasive particles during entire machining. In case of WC tool, no diametric expansion was observed at tool bottom face (Figure 3.17(q-2) and (q-3)). As the machining continued, slightly rounded edges of WC tool (i.e. edge rounding wear) were observed after 3 minutes of machining. Consequently, diameter of the tool bottom face marginally reduced leading to the reduction in WOC of machined microchannel (as evidenced in Figure 3.19(a)). The increased edge rounding wear was observed when the machining was increased up to 5 minutes. The top view of microscopic images of the microchannel machined by using both the material are shown in Figure 3.19(a) and (b)

respectively. From Figure 3.19(a) and (b), it can be clearly observed that, WC tool resulted in the formation of microchannels with lesser WOC (i.e. 48 μm) as well as higher DOC (i.e. 442 μm) as compared to SS-304 tool (WOC = 82 μm and DOC = 370 μm). Further, lesser micro chipping was observed in the machined microchannel when WC tool was used.
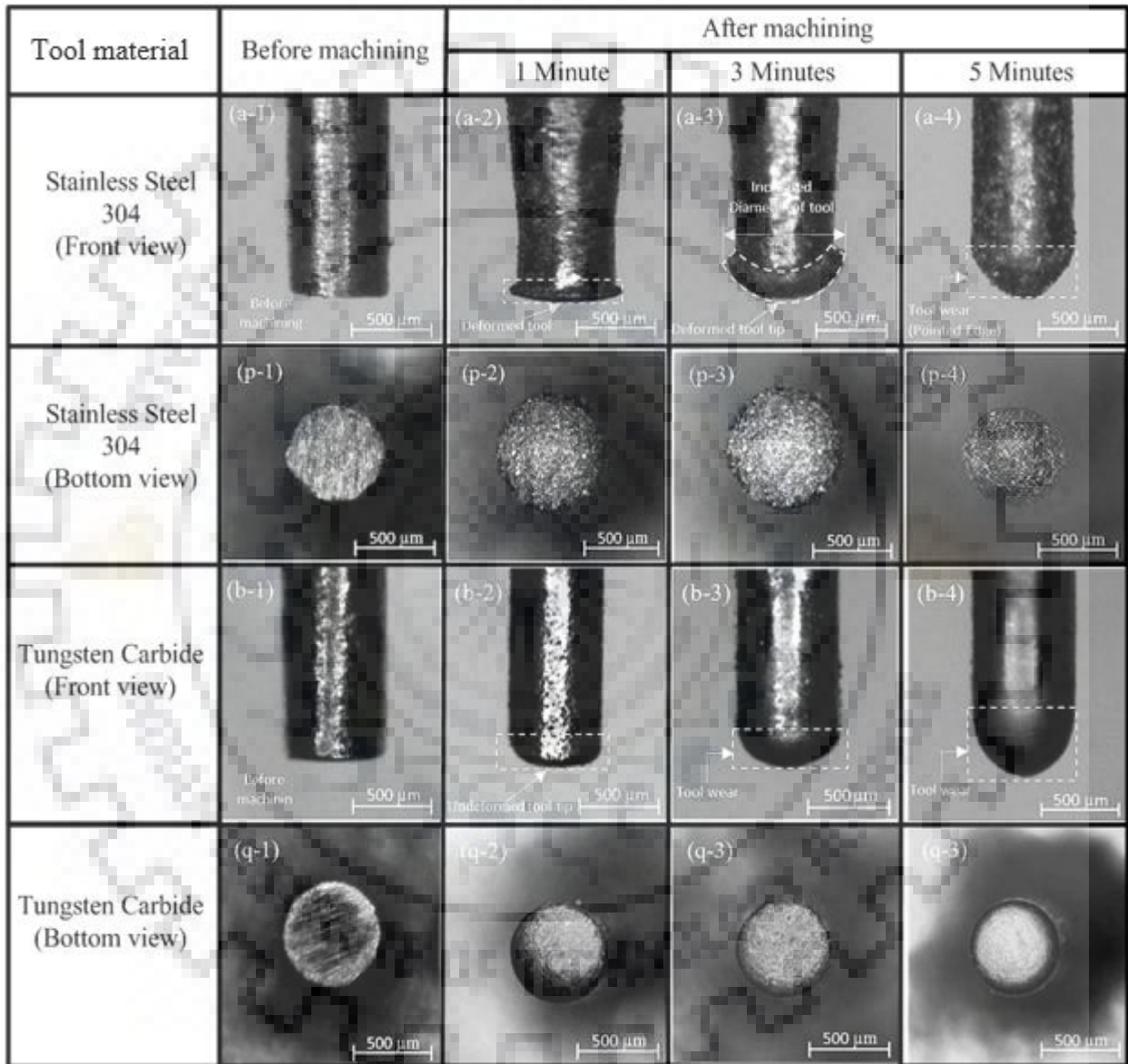
Figure 3.17 Tool images before and after machining [experimental conditions: rotation speed = 300 rpm, feed rate = 15 mm/min, power rating = 40%, concentration = 20%]
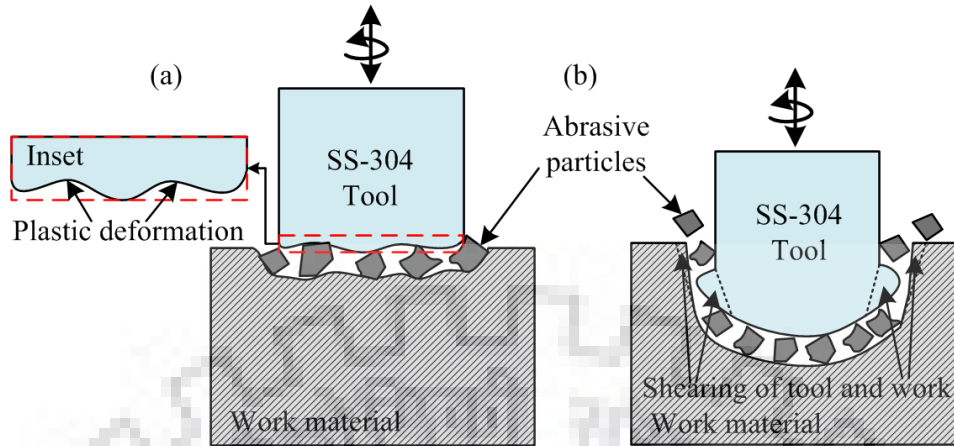
Figure 3.18 Schematic representation showing (a) plastic deformation (b) shearing of SS-304 tool material
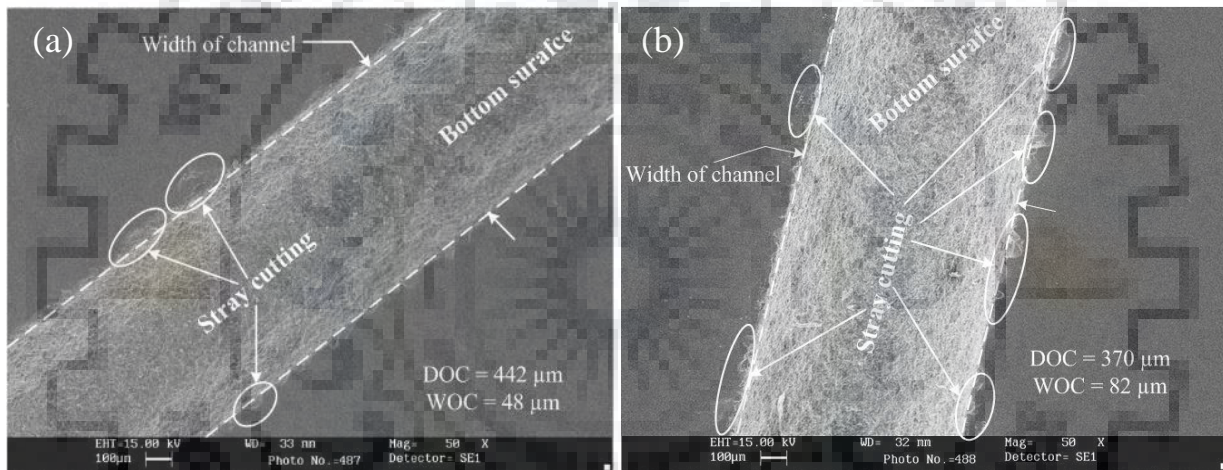
Figure 3.19 Machined microchannel using (a) WC tool (b) SS-304 tool [experimental conditions: rotation speed = 400 rpm, feed rate = 15 mm/min, power rating = 40%, concentration = 15% and machining time = 3 minutes]

From Figure 3.17(a-2), (a-3) and (a-4) and Figure 3.17(b-2), (b-3) and (b-4), it can be clearly seen that in case of rotary tool micro-USM process, no lateral wear was observed on the vertical surface of the tool which indicates that in this process, the tool suffers from longitudinal wear and edge wear only (Figure 3.20). However, in case of stationary tool micro-USM process, the tool suffers from three types of tool wear. This is due to the fact that in stationary tool micro-USM process, a 3-body abrasion takes place between tool, abrasive particles and wall of machined cavity (Figure 3.21(a)) when the abrasive particles exit from the machining gap via the lateral gap. This causes lateral wear of the tool which in turn reduces the form accuracy (i.e. taper formation) of machined

micro feature. Whereas, in case of rotary tool micro-USM process, during exit of the abrasive particles from the machining gap, the centrifugal force generated by the rotating tool pushes the abrasive particles towards the wall of machined cavity. Subsequently, these abrasive particles abraded the side wall of the machined cavity only without abrading the vertical surface of the tool (Figure 3.21(b)). This implies that a 2-body abrasion occurs between the abrasive particles and side wall of the machined cavity.
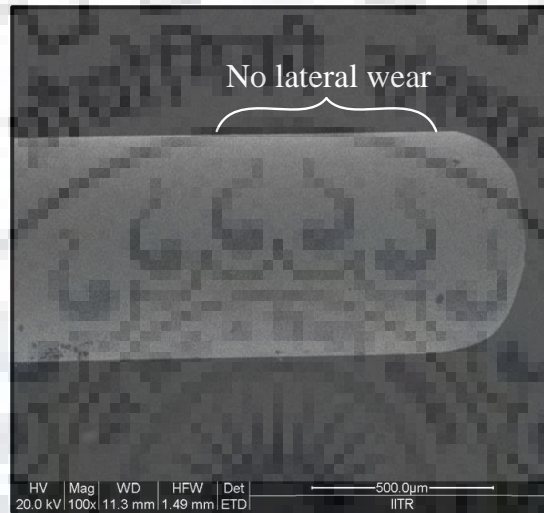
Figure 3.20 SEM micrograph of lateral face of worn out tool
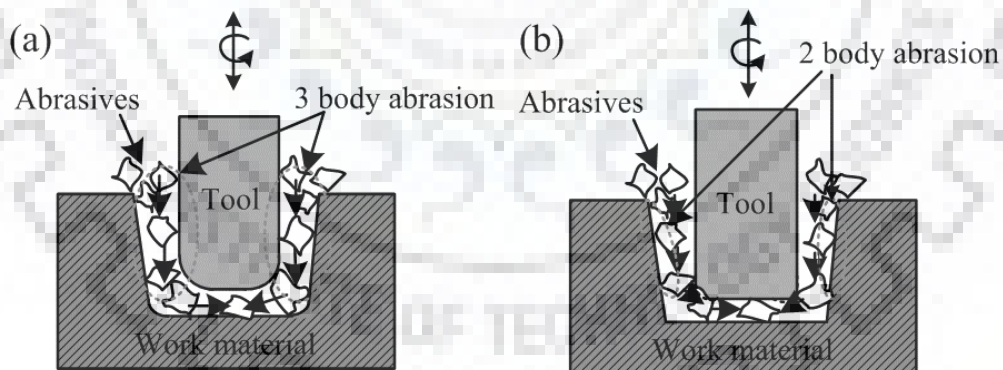
Figure 3.21 Schematic representation showing (a) 3 body abrasion (b) 2 body abrasion

Analysis and discussion of results

All the experiments were conducted as per the experimental settings given in Table 3.5. The experimental results are tabulated in Table 3.6.

Table 3.6 Process parameters and responses

Process parameters				Responses					
				WC tool			SS-304 tool		
RS (rpm)	FR (mm/min)	PR (%)	SC (%)	Avg. MRR (mg/min)	Avg. DOC (μm)	Avg. WOC (μm)	Avg. MRR (mg/min)	Avg. DOC (μm)	Avg. WOC (μm)
100	20	40	15	1.25	290	115	1.18	380	125
200	20	40	15	1.56	350	100	1.50	330	110
300	20	40	15	1.61	390	90	1.54	375	95
400	20	40	15	1.64	415	83	1.59	410	105
500	20	40	15	1.38	540	103	1.28	500	112
600	20	40	15	1.32	530	120	1.22	470	128
400	10	40	15	1.32	315	85	1.28	305	110
400	15	40	15	1.52	430	80	1.42	400	95
400	20	40	15	1.58	360	70	1.48	440	80
400	25	40	15	1.42	390	95	1.39	460	85
400	30	40	15	1.38	400	115	1.29	490	125
400	20	20	15	1.15	420	70	0.98	315	110
400	20	30	15	1.34	450	90	1.19	345	120
400	20	40	15	1.55	470	105	1.23	370	130
400	20	50	15	1.59	530	90	1.29	380	125
400	20	60	15	1.49	540	75	1.21	440	120
400	20	40	10	1.52	130	55	1.41	120	70
400	20	40	15	1.71	320	60	1.59	240	85
400	20	40	20	1.85	550	75	1.65	300	95
400	20	40	25	1.62	330	80	1.54	260	85
400	20	40	30	1.52	235	90	1.35	225	75
RS- Rotation speed, FR- Feed rate, PR- Power rating, SC- Slurry concentration									

Effect of tool material properties on tool wear, MRR and surface roughness

In rotary tool micro-USM process, the tool material properties (i.e. hardness, impact strength, compressive strength, acoustic property etc.) play a significant role in tool wear, MRR and quality of machined surface. Tool wear is an intricate phenomenon of micro-USM process which arises from the impact/hammering action of abrasive particles at ultrasonic frequency. The wear phenomenon of both the tool materials was investigated on the basis of the experiments conducted using the parametric settings given in Table 3.6. During experimentation, a fresh tool was used for each experiment. After machining, the length and machining face diameter of the tool were measured using stereo microscope. The results obtained are presented in Figure 3.22. From Figure 3.22(a), it can be observed that by increasing the machining time from 1 min to 5 min, the longitudinal wear of both the tools increased almost linearly. The WC tool showed lesser tool wear as compared to the SS-304 tool. The longitudinal wear occurs due to indentation and abrasion caused by the abrasive particles. This was attributed to the fact that, WC has the higher hardness and compressive strength than the SS-304 tool. The hard surface of WC provided high resistance towards abrasion and indentation leading to lower longitudinal wear. From Figure 3.22(b), it can be clearly seen that the WC tool face diameter decreased continuously by increasing the machining time. The edge rounding of WC tool face was due to the abrasion only. On the other hand, in case of SS-304 tool, the bottom face diameter increased up to 3 min of machining and after that a sharp decreasing trend was observed. The diametric expansion (i.e. mushroom effect) of the bottom face of SS-304 tool was due to the plastic deformation caused by the repetitive impacts/hammering caused by the abrasive particles. The mushroom effect is evidenced in Figure 3.17(a-3). Subsequently, due to excessive compressive stress, strain hardening occurred in SS-304 tool leading to an increase in the hardness of the bottom face of tool. From Figure 3.23(b), it can be observed that, even after strain hardening, the hardness of SS-304 tool bottom face was lesser than the hardness of WC tool. On further machining, the hardened surface layer of the SS-304 dislodged due to abrasion and the diameter of tool suddenly reduced (Figure 3.22(b)). In case of WC tool, no strain hardening phenomenon was observed. The hardness of WC tool remains almost same. During entire machining period (i.e. 5 minutes), the overall diametric reduction in the bottom face of the tools was more when SS-304 tool was used. This was due to the lower hardness of SS-304 than WC which caused high abrasion in SS-304.

The effect of tool material on MRR is presented in Figure 3.23(a). It can be seen that WC tool resulted in higher MRR as compared to SS-304 tool throughout machining. The high hardness of WC was responsible for higher MRR. It is believed that the indentation of abrasive particles into the tool face/work surface is inversely proportional to the hardness of tool (Komaraiah and Reddy, (1993)). Harder surface of WC tool faced lower indentation depth by abrasive particles which led to higher indentation depth into the work surface and thereby increased the fractured area on the work surface. Thus, higher MRR was obtained. Further, the acoustic properties of the WC is better than SS-304 tool which led to the higher ultrasonic energy transfer from WC tool to the abrasive particles and subsequently from abrasive particles to work surface. As a result of that higher MRR and low tool wear were obtained by using WC tool material. It was also observed that the machining rate decreased by increasing the machining time using both the tools (Figure 3.24(a)). This may be attributed to the fact that as the machining depth increased, the replenishment of abrasive particles became difficult which led to an increase in the tool wear. Further, poor slurry replenishment may also lead to crushing of abrasive particles. Consequently, machining rate decreased. But, this decrease in machining rate was faster in SS-304 as compared to WC tool.

The effect of tool material properties on the machined surface quality was also investigated and presented in Figure 3.24(b) and Figure 3.25. It was observed that the harder tool material (i.e. WC tool) resulted in smooth machined surface as compared to the softer tool (i.e. SS-304 tool). This was attributed to the higher wear resistance of WC which protected the machining face of WC tool against wear which in turn resulted in finished machined surface. The wear resistance of SS-304 tool is lower than WC due to which rough machined surface was obtained.
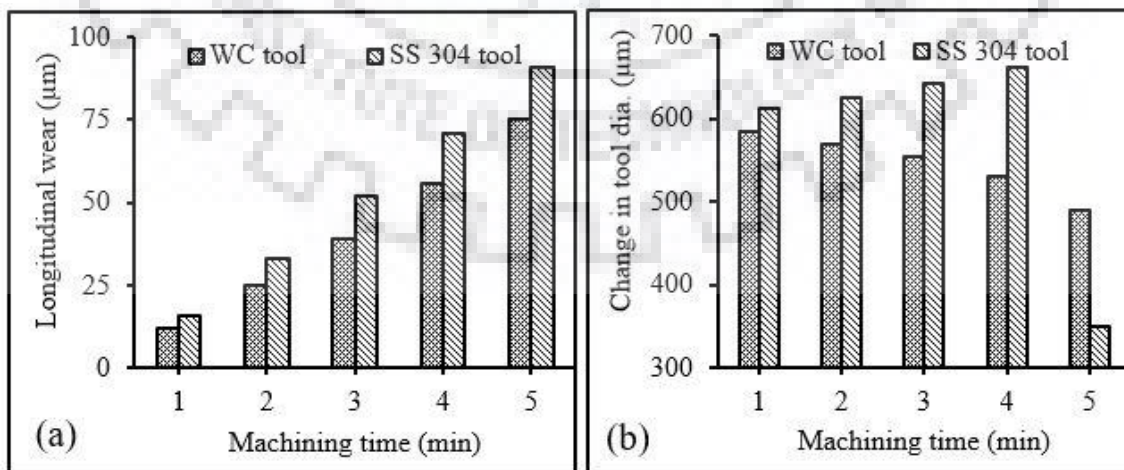
Figure 3.22 Effect of machining time on (a) longitudinal wear (b) change in tool diameter
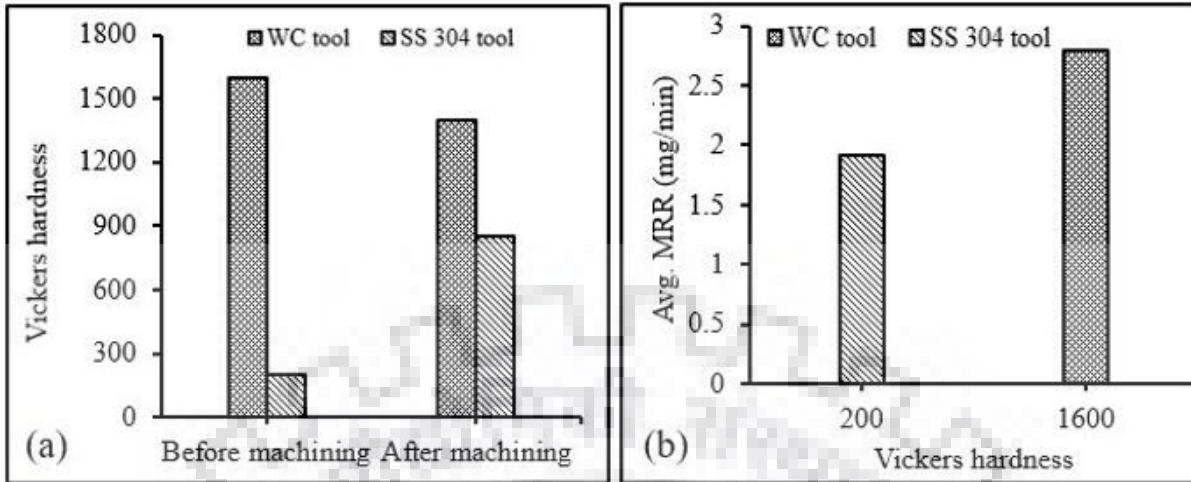
Figure 3.23 (a) Effect of hardness on Avg. MRR (b) hardness before and after machining
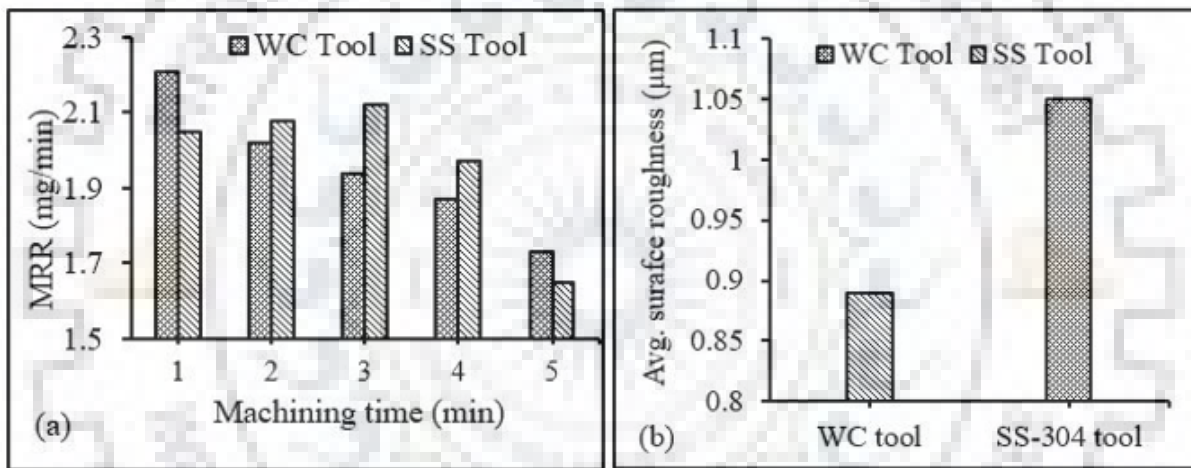
Figure 3.24 (a) Machining rate (b) effect of tool material on surface roughness
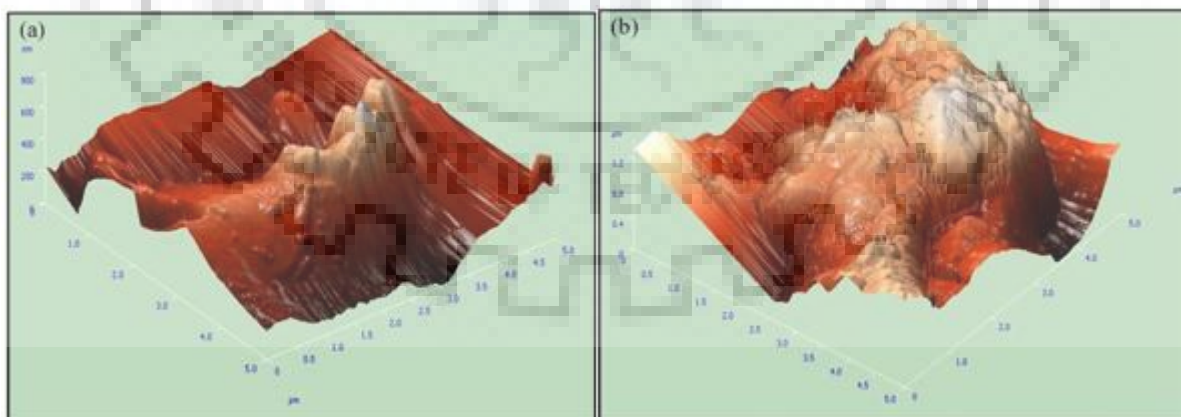
Figure 3.25 Machined surface roughness using (a) WC tool (b) SS-304 tool

93

Effect of tool rotation speed on DOC, MRR and WOC

The effect of tool rotation speed on DOC, MRR and WOC is presented in Figure 3.26(a)-(c) respectively. It can be observed from Figure 3.26(a) and (b) that by increasing the rotation speed of tool from 100 rpm to 400 rpm, the DOC and MRR increased by using both the SS-304 and WC tools. After that both started to decrease. The reason attributed was that the rotary motion of the tool exerts centrifugal force on the abrasive particles in outward direction in the machining zone. The centrifugal force facilitated the abrasive particles to move out and subsequently, new fresh sharp abrasive particles entered into the machining zone and participated into machining. This led to effective machining and as a result of that DOC and MRR increased. Beyond 400 rpm the centrifugal force increased significantly and required quantity of abrasive particles could not get sufficient time to interact with tool and subsequently on workpiece. Consequently, DOC and MRR decreased. The effect of tool rotation speed on WOC is shown in Figure 3.26(c). While using SS-304 tool, the WOC was increased by increasing the tool rotation speed. This can be inferred that by increasing tool rotation speed up to 400 rpm, more number of abrasive particles interacted with the tool. Due to which the tool bottom surface suffered by more number of impacts/hammering action which caused plastic deformation of SS-304 tool bottom face. Consequently, diameter of SS-304 tool bottom face increased due to which higher WOC was obtained. Beyond 400 rpm, the tool worn out owing to shearing of unwanted deformed material and hence WOC decreased. In case of WC tool, WOC was initially decreased up to 400 rpm of the tool due to the effective replenishment of abrasive particles from the machining zone. Thus, WOC reduced. Beyond 400 rpm, an increasing trend in WOC was observed. Also, the rotation speed of 400 rpm resulted in best possible form accuracy of the microchannels using both the tools. The cross-sectional view of microchannel obtained at 400 rpm rotation speed is shown in Figure 3.27. At higher rotation speed, due to lesser interaction time, the tool may come in direct contact with the work material leading to damage of both the tool and work material. Moreover, the lateral vibration may generate in the tool at higher rotation speed which may be responsible for higher WOC.

Figure 3.26 Effect of rotation speed on (a) DOC (b) MRR (c) WOC
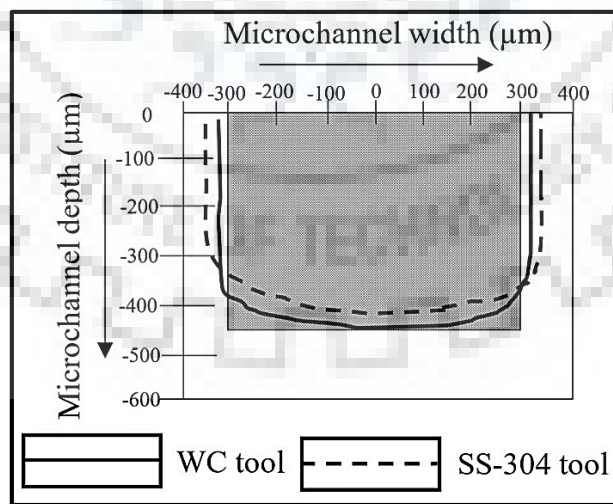
Figure 3.27 Cross-sectional profiles of microchannels obtained at 400 rpm of tool rotation

Effect of feed rate on DOC, MRR and WOC

In micro-USM, the work feed rate governs the interaction time between tool, abrasive and work material. The effect of feed rate of work on DOC, MRR and WOC of microchannels is illustrated in Figure 3.28(a)-(c) respectively. From Figure 3.28(a) and (b), it can be seen that in case of both SS-304 and WC tool, the DOC and MRR initially increased by increasing the feed rate of the work up to 20 mm/min and after that a decreasing trend was observed. This can be explained with the fact that low feed rate results in more interaction time between tool, abrasive particle and work, but at the same time more number of abrasives interacted with the tool creating more than one layer of abrasives in the machining gap leading to loss of energy. Thus, lower DOC and MRR were obtained. Whereas, at higher values of feed rate (greater than 20 mm/min), the interaction time was significantly reduced due to which low DOC and MRR was observed. At a feed rate of 20 mm/min uniform machining was observed and as a result of that maximum DOC and MRR were achieved. In case of both the SS-304 and WC tool, the WOC decreased by increasing the feed rate up to 20 mm/min and beyond that it increased (Figure 3.28(c)). At low feed rate (10 mm/min) the excessive plastic deformation increased the tool bottom face diameter which led to an increase in WOC. On increasing the feed rate lesser plastic deformation tool place and as a result of that low WOC was obtained. The workpiece feed rate of 20 mm/min also resulted in best possible form accuracy of machined microchannels. The cross-sectional view of microchannel obtained at 20 mm/min feed rate is shown in Figure 3.29.
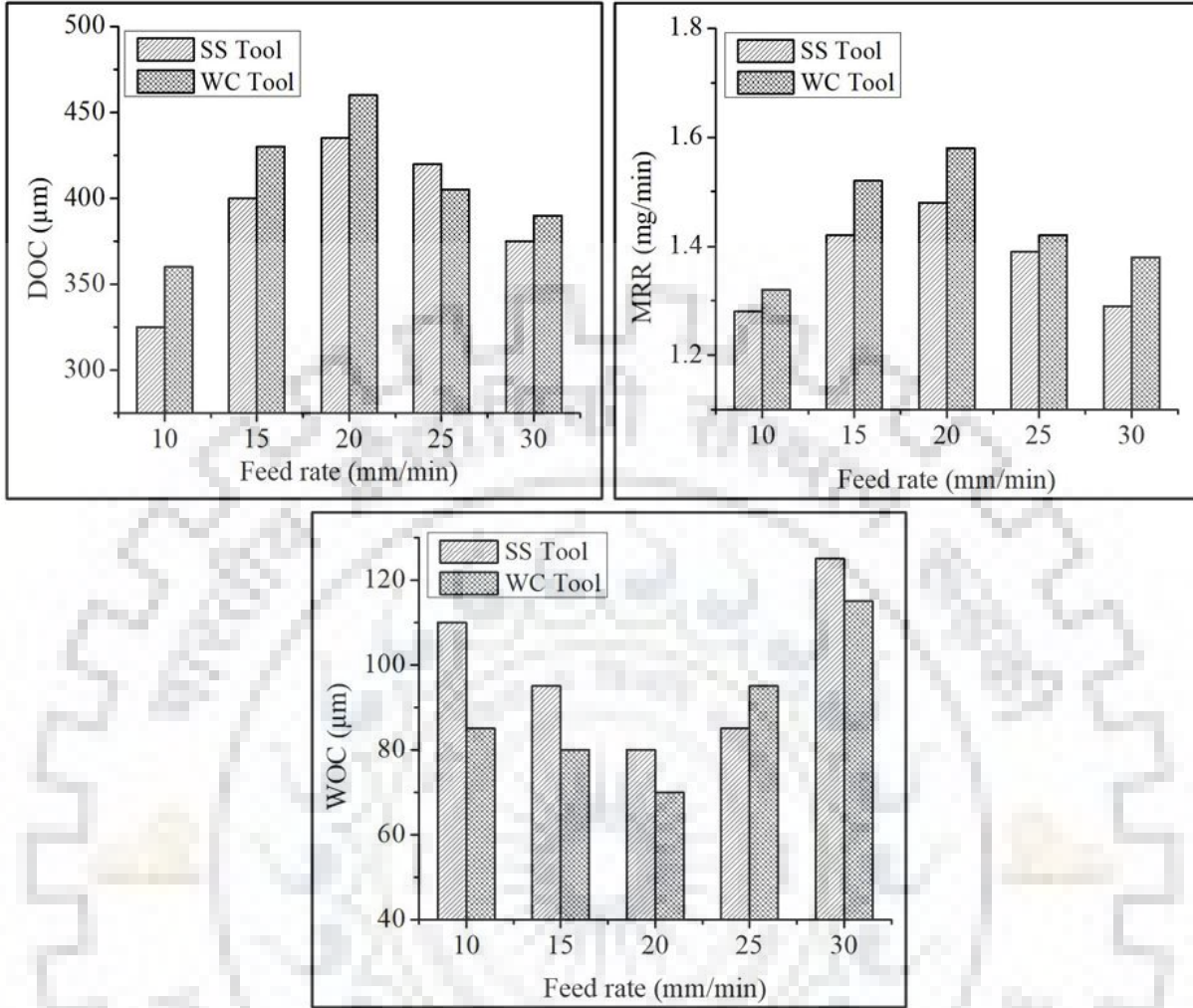
Figure 3.28 Effect of feed rate on (a) DOC (b) MRR (c) WOC
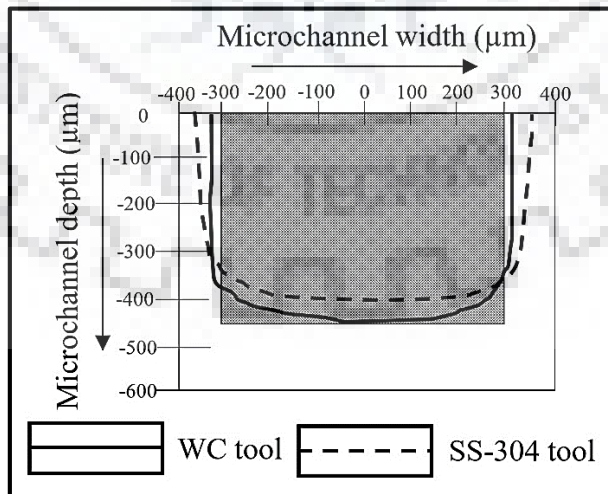
Figure 3.29 Cross-sectional profiles of microchannels obtained at 20 mm/min feed rate

Effect of power rating on DOC, MRR and WOC

The effect of power rating on DOC, MRR and WOC is presented in Figure 3.30(a)-(c) respectively. From 3.30(a) and (b) it can be clearly seen that by increasing the power rating from 20% to 60%, both the DOC and MRR increased continuously in both the SS-304 and WC tool respectively. This can be attributed to the fact that by increasing power rating, the abrasive impacts on work surface with higher force (energy). Due to which depth of crater increased leading to more material removal from work surface. Thus, DOC and MRR increased. On the other hand, the WOC initially increased by increasing the power rating up to 40% after and that a decreasing trend was observed using both the SS and WC tools (Figure 3.30(c)). The higher impact force was responsible for increased WOC up to 40% power rating. After 40% of power rating, the WOC decreased owing to the high tool wear. The best possible form accuracy of microchannel was obtained at 40% of power rating. The cross-sectional view of microchannel obtained at 40% power rating is shown in Figure 3.31. Moreover, at higher power rating, crushing of abrasive particles may be another reason responsible for low DOC, MRR and WOC.

Effect of concentration on DOC, MRR and WOC

The quantity of abrasive particles is directly proportional to the concentration of abrasive slurry. The effect of concentration on DOC, MRR and WOC is presented in Figure 3.32(a)-(c) respectively. From Figure 3.32(a) and (b) it can be observed that by increasing the concentration of slurry, the DOC and MRR were increased up to 20% of concentration and beyond that a decreasing trend was observed in both the SS-304 and WC tool. The reason can be inferred that the quantity of abrasives particles in the machining gap increased by increasing the concentration. Subsequently, the number of impacts on the work surface increased leading to more material removal from work surface. Thus, DOC and MRR increased. On further increasing the concentration beyond 20%, multiple layers of abrasives were stacked over each other. This led to loss of ultrasonic energy. Consequently, both the DOC and MRR decreased. The maximum DOC and MRR were achieved at 20% of concentration by using both the tools. The WOC was increased continuously by increasing the concentration in case of WC tool (Figure 3.32(c)). This was due to the reason that 2 body abrasion in the lateral gap increased by increasing the concentration. Due to which WOC increased. On the other hand in case of SS-304, the WOC increased up to 20% concentration and after that it started to decrease. The decreasing trend may be due to the high tool

wear caused by the shearing of the bottom face periphery. A 20% concentration exhibited in best possible form accuracy of machined microchannel. The cross-sectional view of microchannel obtained at 20% concentration is shown in Figure 3.33.

On the basis of above discussion, it can be concluded that in rotary tool micro-USM process, the performance of WC was superior over SS-304 in terms of higher DOC, MRR and lower WOC. Also, the microchannels obtained by using WC tool had better form accuracy. Therefore, WC can be suggested as a better tool material for rotary tool micro-USM process.
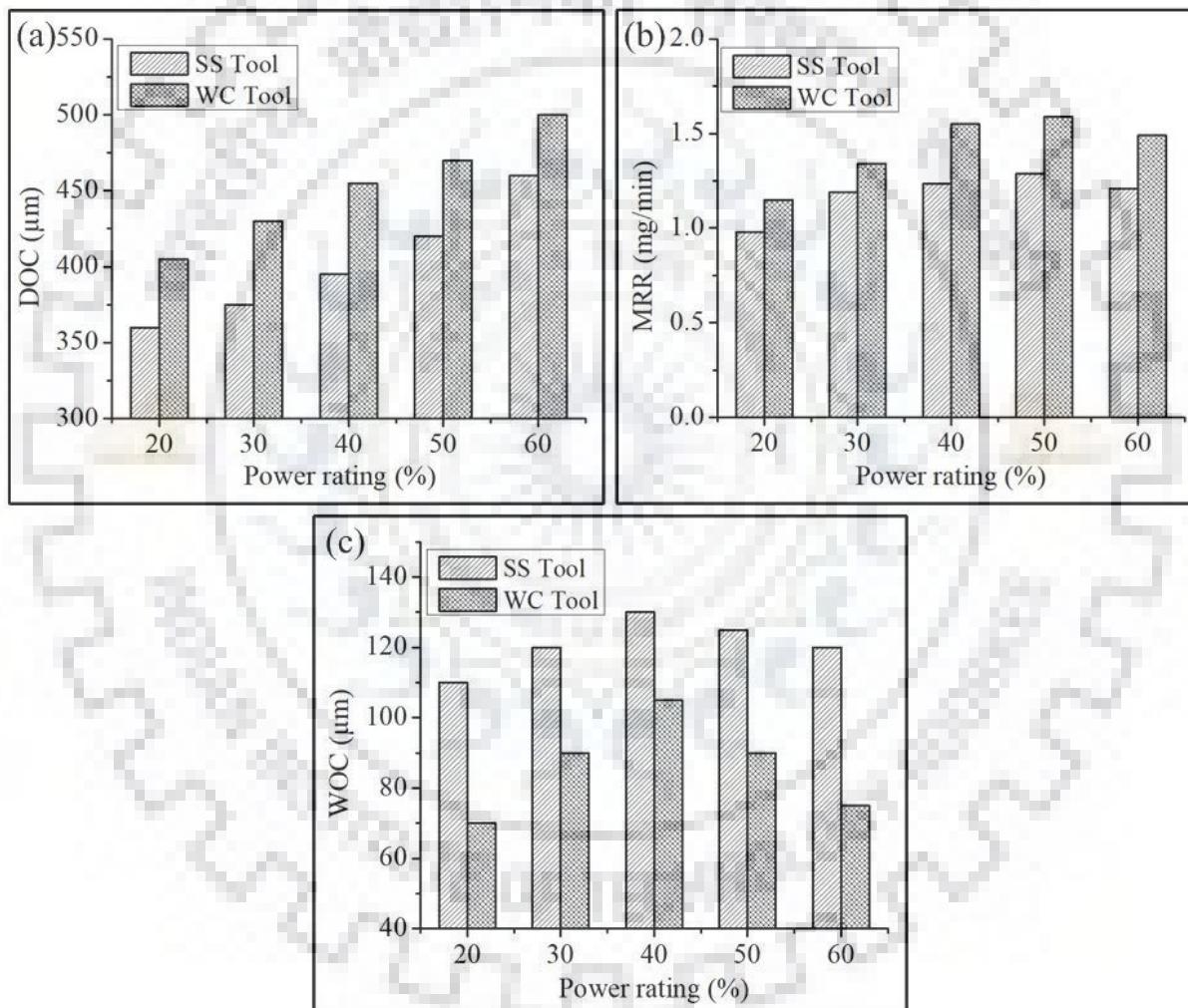
Figure 3.30 Effect of power rating on (a) DOC (b) MRR (c) WOC

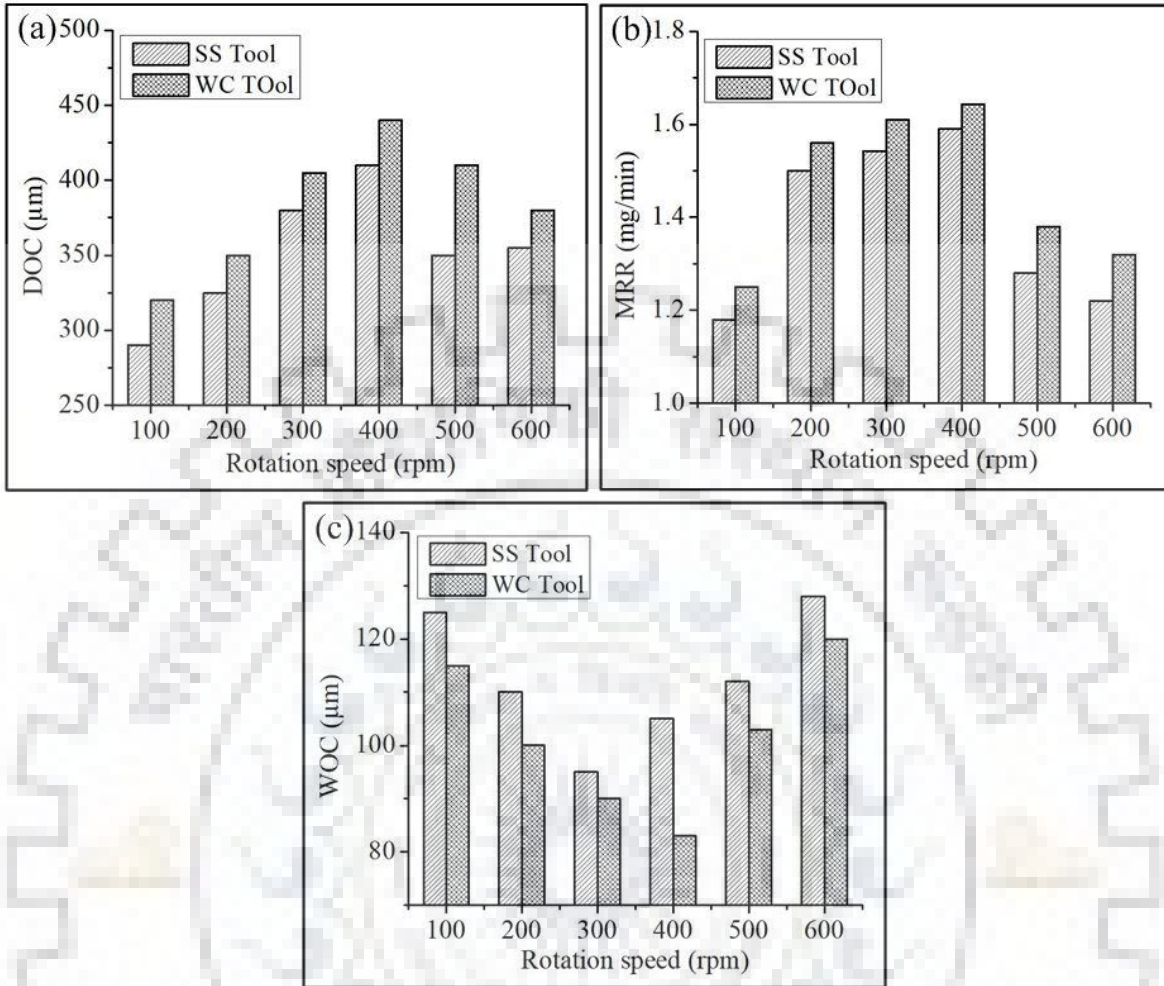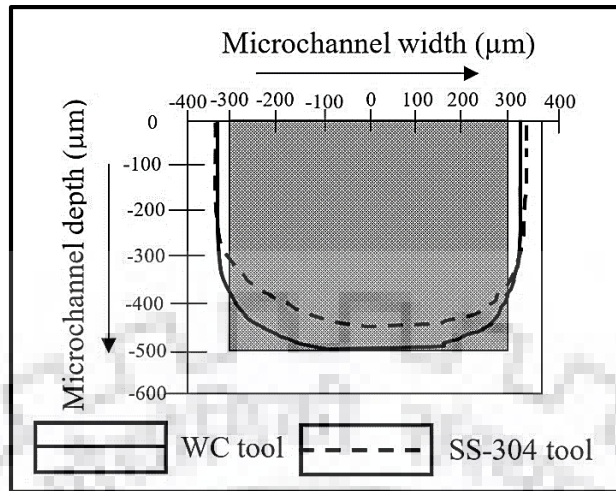Figure 3.31 Cross-sectional profiles of microchannels obtained at 60% power rating
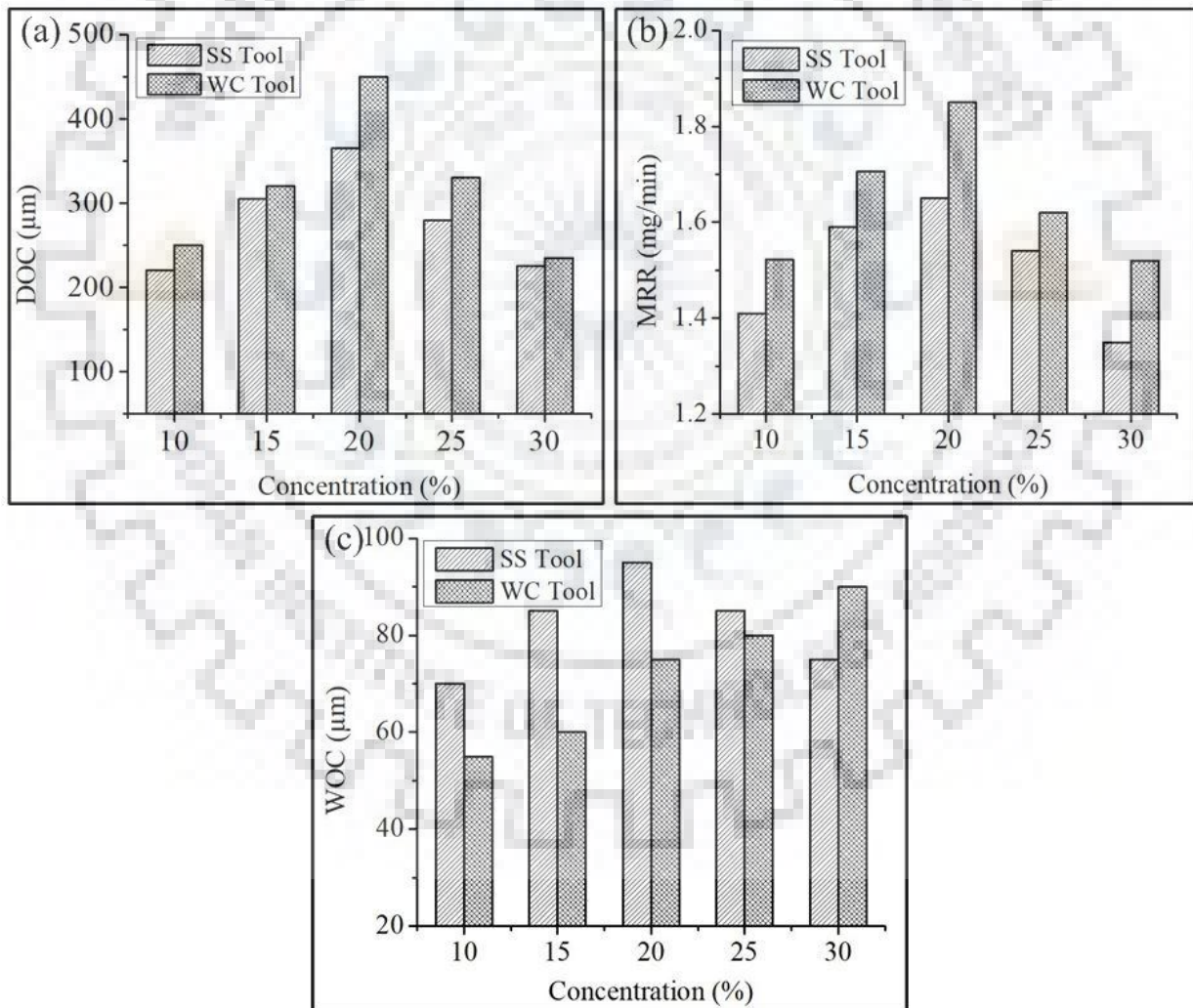
Figure 3.32 Effect of concentration on (a) DOC (b) MRR (c) WOC
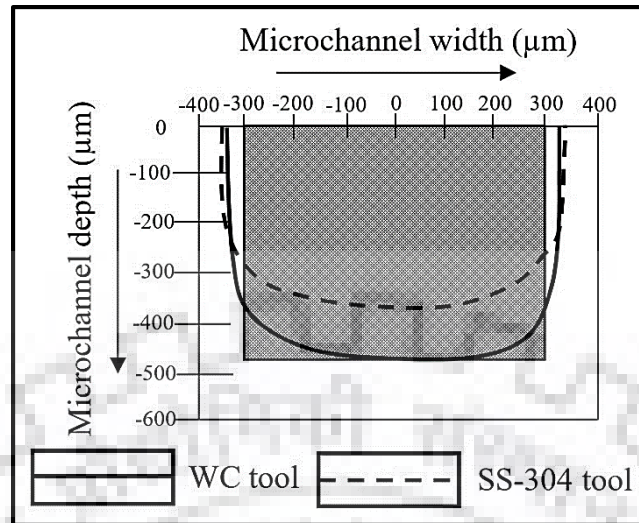
Figure 3.33 Cross-sectional profiles of microchannels obtained at 20% concentration

3.5 Summary

This chapter includes the development of rotary tool micro-USM process facility and selection of process parameters for the fabrication of microfeatures on hard and brittle materials. The parametric effect of process parameter was also discussed with the help of cause and effect diagram. Later, pilot experimentation was performed to select the range of tool rotation speed and tool material for subsequent experimentation on rotary tool micro-USM process. The pilot experimentation on microhole drilling showed that the range of tool rotation speed was from 100 rpm to 500 rpm, whereas in case of microchannel fabrication, the rotation speed of the tool was from 100 rpm to 600 rpm. The performance of WC tool was found to be superior (i.e. higher DOC, MRR and lower WOC) over SS-304 tool material owing to its higher hardness, compressive strength and good acoustic properties. Strain hardening phenomenon was observed in SS-304 owing repetitive hammering/impacts of abrasives, however no such phenomenon was observed in WC tool. The form accuracy and surface finish of microchannels machined by using WC tool was better than the form accuracy and surface finish of the microchannels machined by using SS-304.

PERFORMANCE EVALUATION OF ROTARY TOOL MICRO-USM PROCESS

This chapter reports on the performance evaluation of rotary tool micro-USM process. The objective of this chapter was to examine the effectiveness of tool rotation in micro-USM process. In order to achieve this objective, a comparative study was performed between stationary tool and rotary tool micro-USM processes. This chapter is divided into two sections. In the first section, both the rotary tool and stationary tool micro-USM processes were utilized for the machining of microholes. In the second section, microchannels were machined using both processes. The effects of various micro-USM process parameters were investigated on process responses.

4.1 Performance Analysis during Machining of Microholes

In order to analyze the performance of rotary tool micro-USM process, experimental investigation was performed on stationary tool and rotary tool micro-USM processes. Microholes were machined using both the processes. The performance of micro-USM process was measured in terms of MRR and HOC as response characteristics. The experiments were conducted using OFAT approach with four micro-USM process parameters viz. power rating, slurry concentration, static load and abrasive size. Also, a qualitative analysis of tool wear was carried out with the help of microscopic images. The experimental facility and procedures used to drill microholes are discussed in the subsequent section of this chapter.

4.1.1 Experimental facility and measurement method

The experiments were conducted on an in-house developed facility of rotary tool micro-USM process shown in Figure 3.2. The detailed description of the developed facility is provided in chapter 3. During experimentation, borosilicate glass, silicon carbide and water were selected as work material, abrasive material and liquid medium respectively. The flow rate of abrasive slurry between the tool and work was kept constant throughout the experimentation. A solid cylindrical tool of tungsten carbide material having diameter of 600 μm was used to machine microholes using both the processes.

In this investigation, the selection of input process parameters was carried out reviewing the literature followed by preliminary experiments. The power rating, slurry concentration, static load, and abrasive mesh size were selected as variable input parameters. The selected process parameters and their values were given in Table 4.1. The MRR, DOH and HOC were selected as response characteristics. The responses were measured as per the procedure discussed in section 3.3 of chapter 3. All the measurement were repeated thrice and the average value was considered as final response. The qualitative analysis of tool wear was carried out with the help of microscopic images captured by using stereo zoom microscope.

Table 4.1 Process parameters settings for comparative study on drilling of microholes

Variable process parameters	
Rotation speed (RS)	0, 300 rpm
Power rating (PR)	20, 30, 40, 50, 60%
Slurry concentration (SC)	10, 15, 20, 25%
Static load (SL)	30, 45, 60, 75 g
Abrasive size (AS)	500, 800, 1000 mesh
Constant process parameters	
Frequency	21 ± 1 kHz
Tool diameter (Ø)	600 μm
Tool material	WC
Tool geometry	Cylindrical

4.1.2 Analysis and discussion of results

In order to investigate the performance of stationary tool and rotary tool micro-USM process, the experiments were conducted as per the experimental settings given in Table 4.1. The results are tabulated in Table 4.2.

Table 4.2 Process parameters and responses of comparative study on drilling of microholes

Process parameters					Responses	
RS (rpm)	PR (%)	SL (g)	AS (mesh)	SC (%)	Avg. MRR (mg/min)	Avg. HOC (μm)
0	20	30	800	15	0.18	60
0	30	30	800	15	0.22	68
0	40	30	800	15	0.25	90
0	50	30	800	15	0.27	112
0	60	30	800	15	0.29	122
0	50	30	800	15	0.21	102
0	50	45	800	15	0.25	125
0	50	60	800	15	0.26	138
0	50	75	800	15	0.24	132
0	50	45	500	15	0.24	115
0	50	45	800	15	0.28	98
0	50	45	1000	15	0.31	81
0	50	45	1000	10	0.16	80
0	50	45	1000	15	0.23	90
0	50	45	1000	20	0.28	107
0	50	45	1000	25	0.2	120
300	20	30	800	15	0.38	65
300	30	30	800	15	0.42	73
300	40	30	800	15	0.45	82
300	50	30	800	15	0.53	95
300	60	30	800	15	0.54	107
300	50	30	800	15	0.41	90
300	50	45	800	15	0.44	108
300	50	60	800	15	0.46	113

300	50	75	800	15	0.42	120
300	50	45	500	15	0.43	105
300	50	45	800	15	0.48	80
300	50	45	1000	15	0.52	63
300	50	45	1000	10	0.46	68
300	50	45	1000	15	0.51	76
300	50	45	1000	20	0.54	91
300	50	45	1000	25	0.47	105

RS- Rotation speed, PR- Power rating, SL- Static load, AS- Abrasive size, SC- Slurry concentration

Effect of process parameters on MRR

The effects of input process parameters on MRR are shown in Figure 4.1. Figure 4.1(a) demonstrated the effect of power rating on MRR. The MRR was found to be increased with increasing the power rating both in stationary tool and rotary tool micro-USM processes. Power rating is directly associated with the vibration amplitude. As the power rating increased, abrasive particles impacted on the work surface with higher energy owing to higher amplitude of vibration. As a result of that indentation depth of abrasive particle increased and more material was removed from the work surface. Thus, increased MRR was obtained.

The effect of concentration on MRR is presented in Figure 4.1(b). The MRR increased with an increase in concentration of abrasive slurry from 10% to 20% and then it slightly decreased in both stationary tool and rotary tool micro-USM processes. The quantity of abrasives in the machining zone increased by increasing the concentration which led to increase in MRR.

With an increase in static load from 30 g to 60 g, the MRR was found to be increased (Figure 4.1(c)) and after that it slightly decreased. This can be explained with the fact that the impact force on abrasive particles increased by increasing static load. Subsequently, the same impact force transferred on the work surface by the abrasive particles which resulted in the formation of deeper craters on work surface. As a result of that higher MRR was obtained. At higher static load (here 60 g), damping of tool vibration may occur due to which lower MMR was obtained.

The MRR continuously increased by increasing the abrasive particle size 500 mesh to 1000 mesh (Figure 4.1(d)). The mesh size of abrasive is inversely proportional to the abrasive grain diameter. In case of 1000 mesh size (fine abrasives), more number of abrasives were present beneath the tool as compared when 500 mesh size abrasives (coarse) were used. More abrasives resulted in the formation of more craters on workpiece surface thereby resulting in increased MRR.

It can also be noticed from Figure 4.1(a)-(d) that rotary tool micro-USM process resulted in higher MRR as compared to stationary tool micro-USM process. The combined effect of vibration and rotation of tool was responsible for higher MRR in rotary tool micro-USM process.
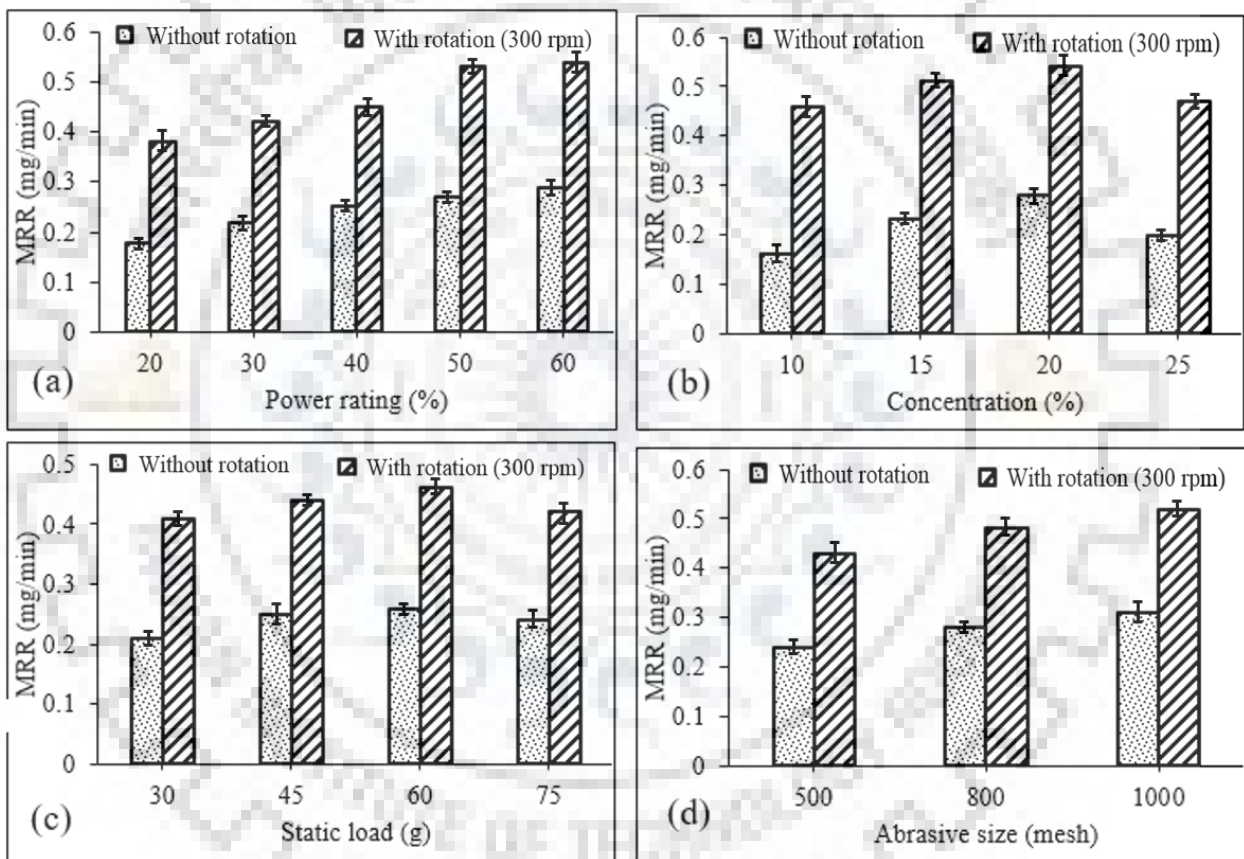
Figure 4.1 Effect of process parameters on MRR

Effect of process parameters on HOC

The effect of process parameters on HOC is shown in Figure 4.2. Figure 4.2(a) illustrated the effect of power rating on HOC. In case of stationary tool micro-USM process, the HOC was found to be increased with increase in the power rating from 20% to 60%. This was due to the fact that with

increase in the power rating the abrasive particles gained more impact energy owing to the higher amplitude of tool vibration. This led to the formation of large craters and hence increased HOC.

Figure 4.2(b) clearly indicates that HOC increased on increasing the concentration of abrasive slurry from 10% to 25%. This was due to the fact that as the concentration was increased, more number of abrasives participated in machining zone. Consequently, width of lateral gap increased which resulted in increased HOC. As compare to stationary tool micro-USM process, rotary tool micro-USM process provided lesser HOC owing to effective circulation of slurry in the machining zone.

The effect of static load on HOC is illustrated in Figure 4.2(c). The HOC initially increased on increasing the static load up to 60 g. Thereafter, a marginal reduction in HOC was noticed in both stationary tool and rotary tool micro-USM processes. Higher impact force exerted on the abrasive particle on increasing the static load till 60 g. Subsequently, same impact force transferred on work surface by the abrasive particles which led to the formation of larger craters on work surface. Due to which width of lateral gap increased and higher HOC was observed.

The effect of abrasive size on HOC is presented in Figure 4.2(d) which indicated that with an increase in abrasive mesh size from 500 mesh to 1000 mesh, HOC was found to be decreased in both stationary tool and rotary tool micro-USM processes. It can be inferred that the abrasive particle diameter decreased by increasing the mesh size of abrasive. In case of 500 mesh abrasive (coarse), higher HOC was obtained due to the higher width of lateral gap. On the other hand, in case of 1000 mesh abrasives (fine), the width of lateral gap was lowest due to which lowest HOC was obtained.

It can also be noticed from Figure 4.2(a)-(d) that rotary tool micro-USM process resulted in lesser HOC as compared to stationary tool micro-USM process.
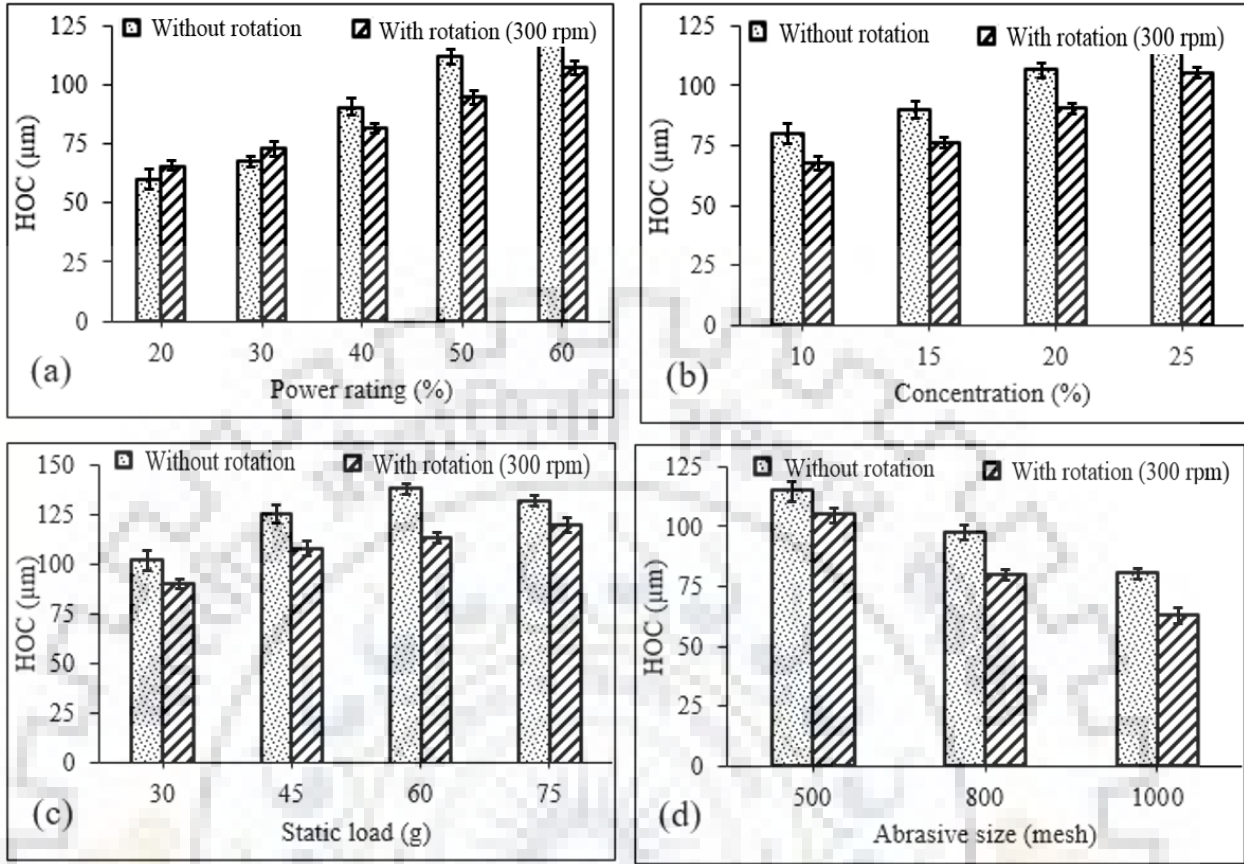
Figure 4.2 Effect of process parameters on HOC

In this comparative study, the quality of the microholes drilled by both the processes was also analyzed. The fabricated holes are shown in Figure 4.3. From Figure 4.3 it can be clearly observed that rotary tool micro-USM process resulted in damage free deep microhole as compared to stationary tool micro-USM process. Moreover, the periphery of microhole drilled by stationary tool micro-USM process was also damaged (Figure 4.3(a)) due to stray cutting caused by the deflected abrasives. Whereas, the periphery of microhole drilled by rotary tool micro-USM process was observed to be smooth (Figure 4.3(b)). The possible reason of poor quality of microhole in case of stationary tool micro-USM process was the accumulation of the debris underneath the tool owing to poor circulation of abrasive slurry. That resulted in severe tool wear (Figure 4.4(a)) and consequently microhole with taper wall and rounded bottom corner was formed (Figure 4.3(c)). The rotary motion of the tool exerted centrifugal force in outward direction (away from center) in the machining zone. As a result of that abrasives replenished from the machining area and new fresh abrasives entered into the gap. While coming outward these abrasives entered into the lateral

gap (between tool surface and wall of the hole). In the lateral gap rolling of abrasives occurred due to the rotary motion of tool which further helped the abrasives to come out from the lateral gap easily. This process was continued till the end of drilling and deeper holes were obtained. The effective circulation of abrasives resulted in less tool wear in rotary tool micro-USM process (Figure 4.4(b)) and as a result of that microhole of good dimensional accuracy (lesser taper) were obtained. The better form accuracy of machined microhole is evidenced in Figure 4.3(d).
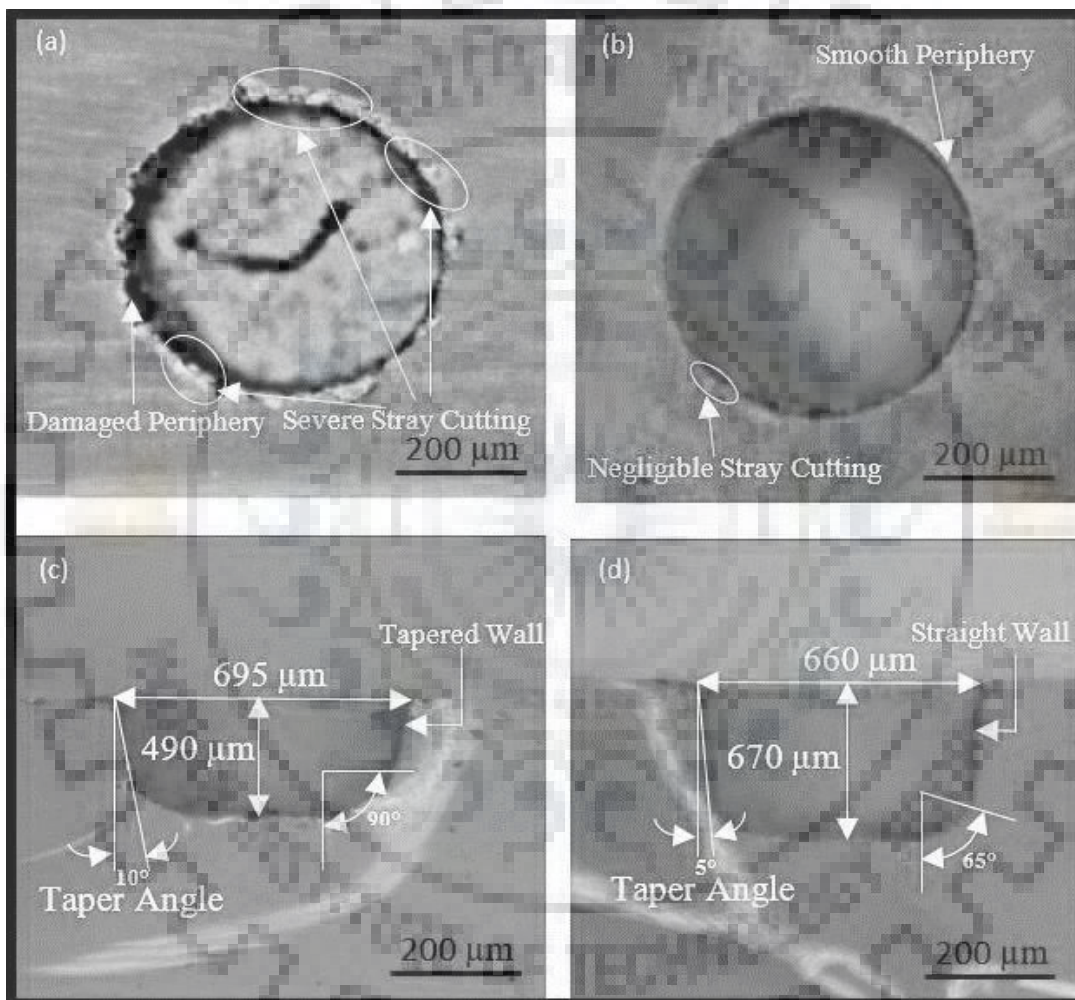
Figure 4.3 Microscopic view (top & cross-sectional view at 50X) of micro-holes drilled by (a) stationary tool micro-USM process (b) rotary tool micro-USM process
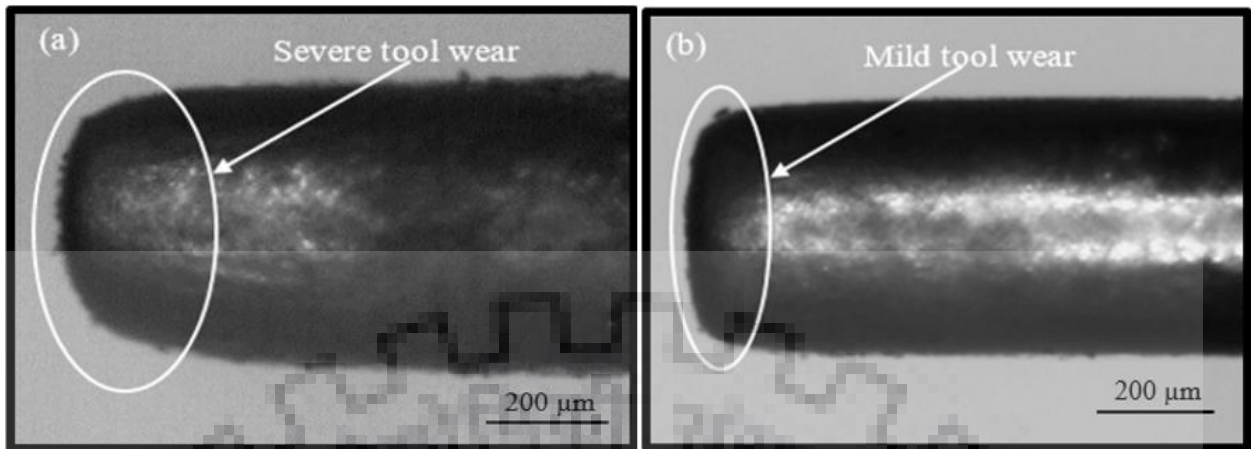
Figure 4.4 Microscopic view of tool after machining in micro-USM at 50 X (a) stationary tool micro-USM process (b) rotary tool micro-USM process

4.2 Performance Analysis during Machining of Microchannels

In order to analyze the performance of rotary tool micro-USM process, experimental investigation was performed on stationary tool and rotary tool micro-USM processes. Microchannels were machined using both the processes. The performance was measured in terms of MRR, DOC and form accuracy of microchannels as response characteristics. The experiments were conducted using OFAT approach with four micro-USM process parameters viz. power rating, slurry concentration, static load and abrasive size. Also, a qualitative analysis of tool wear was carried out with the help of microscopic images.

4.2.1 Experimental facility and measurement methods

The experiments were conducted on an in-house developed facility of rotary tool micro-USM process shown in Figure 3.2. The detailed description of the facility is provided in chapter 3. During experimentation, borosilicate glass, silicon carbide and water were selected as work material, abrasive material and liquid medium respectively. The flow rate of abrasive slurry between the tool and work was kept constant throughout the experimentation. A solid cylindrical tool of tungsten carbide material having diameter of 600 μm was used to machine microholes using both the processes.

In this investigation, the input process parameters were selected on the basis of literature review followed by preliminary experiments. The power rating, slurry concentration, static load, and abrasive mesh size were selected as variable input parameters. The selected process parameters

and their values were given in Table 4.3. MRR and DOC were selected as response characteristics. The responses were measured as per the procedure discussed in section 3.3 of chapter 3. All the measurement were repeated thrice and the average value was considered as final response. The qualitative analysis of tool wear was carried out with the help of microscopic images captured by using FESEM. The form accuracy was measured and analyzed by using image analysis toolbox of MALAB v.2016b. The complete procedure of form accuracy measurement is explained in section 3.3 of chapter 3.

Table 4.3 Process parameters settings for comparative study on machining of microchannels

Variable process parameters	
Rotation speed (RS)	0, 300 rpm
Power rating (PR)	20, 30, 40, 50, 60, 70%
Slurry concentration (SC)	10, 15, 20, 25%
Feed rate (FR)	10, 15, 20, 25 mm/min
Abrasive size (AS)	500, 800, 1000 mesh
Constant process parameters	
Frequency	21 ± 1 kHz
Tool diameter	600 μm
Tool material	WC
Static load	45 g
Tool geometry	Cylindrical

4.2.2 Analysis and discussion of results

In order to investigate the performance of stationary tool and rotary tool micro-USM process, the experiments were conducted as per the experimental settings given in Table 4.3. The results are tabulated in Table 4.4.

Table 4.4 Process parameters and responses of comparative study on machining of microchannels

Process parameters					Responses	
RS (rpm)	PR (%)	FR (mm/min)	AS (mesh)	SC (%)	Avg. MRR (mg/min)	Avg. DOC (µm)
0	20	10	1000	20	1.22	200
0	30	10	1000	20	1.51	235
0	40	10	1000	20	1.85	260
0	50	10	1000	20	2.32	290
0	60	10	1000	20	2.53	320
0	60	10	1000	20	2.18	290
0	60	15	1000	20	2.08	260
0	60	20	1000	20	1.65	225
0	60	25	1000	20	1.24	200
0	60	10	500	20	1.68	275
0	60	10	800	20	2.12	305
0	60	10	1000	20	2.19	330
0	60	10	1000	10	1.32	225
0	60	10	1000	15	1.84	285
0	60	10	1000	20	1.98	335
0	60	10	1000	25	2.21	315
300	20	10	1000	20	2.52	350
300	30	10	1000	20	2.84	385
300	40	10	1000	20	3.23	420
300	50	10	1000	20	3.51	470
300	60	10	1000	20	3.81	480
300	60	10	1000	20	2.82	305
300	60	15	1000	20	3.12	355
300	60	20	1000	20	3.29	420
300	60	25	1000	20	2.65	390

300	60	10	500	20	2.71	310
300	60	10	800	20	3.43	440
300	60	10	1000	20	3.64	495
300	60	10	1000	10	2.86	310
300	60	10	1000	15	3.12	405
300	60	10	1000	20	3.54	510
300	60	10	1000	25	3.41	430
RS- Rotation speed, PR- Power rating, FR- Feed rate, AS- Abrasive size, SC- Slurry concentration						

Effect of feed rate on MRR and DOC

In micro-USM process, the feed rate of work decides the time of interaction between tool, abrasive particles and work. The interaction time between tool, abrasive particles and work decreases by increasing the feed rate of work and vice-versa. The effect of feed rate on MRR and DOC is illustrated in Figure 4.5 and Figure 4.6. It can be clearly observed from Figure 4.5 and Figure 4.6 that in case of stationary tool micro-USM process, both the MRR and DOC decreased continuously by increasing the feed rate owing to reduction in interaction time [16]. The maximum MRR and DOC with form accuracy of 70% were obtained at 10 mm/min of feed rate and presented in Figure 4.7. On the other hand, in rotary tool micro-USM process, the MRR and DOC increased by increasing the feed rate of the work from 10 mm/min to 20 mm/min (Figure 4.5 and Figure 4.6). Beyond 20 mm/min of feed rate, a decreasing trend was observed in both the MRR and DOC. It seems that at lower value of work feed rate, the interaction time was higher due to which more abrasive particles interacted with the tool and subsequently to the work surface. Consequently, tool worn out and low MRR was obtained. At higher values of work feed rate (beyond 20 mm/min), interaction time significantly reduced leading to lesser interaction of tool, abrasive and work, Thus, low MRR and DOC were obtained. The maximum MRR and DOC were obtained at 20 mm/min of feed rate. The form accuracy of the microchannel obtained at 20 mm/min feed rate was found to be 80% (as shown in Figure 4.7(b)).
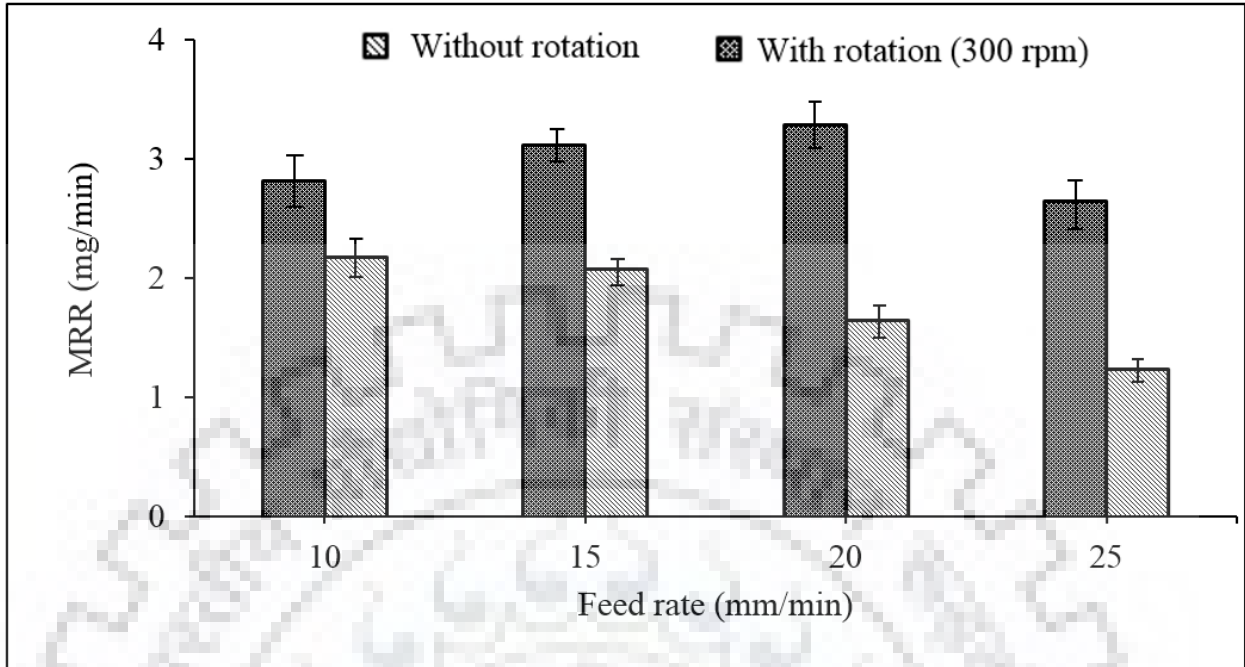
Figure 4.5 Effect of feed rate on MRR

Figure 4.6 Effect of feed rate on DOC

(a)

Depth = 420 μm
Form accuracy = 70%

300μm

(b)

Depth = 465 μm
Form accuracy = 80%

300μm

Figure 4.7 Microscopic images of cross-sectional view of microchannels machined by (a) stationary tool micro-USM process [experimental conditions: feed rate =10 mm/min, power rating = 40%, slurry concentration = 15% and abrasive size = #1000 mesh] (b) rotary tool micro-USM process [experimental conditions: rotation speed = 300 rpm, feed rate =20 mm/min, power rating = 40%, slurry concentration = 15% and abrasive size = #1000 mesh]

Effect of power on MRR and DOC

The power rating is directly proportional to the vibration amplitude (Jadoun et al., (2006)). High power rating leads to high amplitude of tool vibration and vice-versa. The effects of power rating on MRR and DOC are presented in Figure 4.8 and Figure 4.9. From Figure 4.8 and Figure 4.9, it can be observed that as the power rating increased from 20% to 60%, the MRR and DOC increased continuously in both the stationary tool and rotary tool micro-USM process. Beyond that a decreasing trend was observed in both MRR and DOC. The abrasive particles gained higher kinetic energy by the impact of tool as the power rating was increased. Subsequently, these abrasives transferred high impact energy on the work surface leading to the formation of deeper crater. As a result of that MRR and DOC increased. At higher value of power rating (i.e. 70%), the MRR may be reduced due to the formation of multiple layers of abrasives in between the tool and work due to higher amplitude of vibration at higher value of power rating which caused larger machining gap. This resulted in loss of ultrasonic energy and hence lesser MRR and DOC. The maximum MRR and DOC were obtained at 60% of power rating in both the stationary tool and rotary tool micro-USM process. The form accuracy of microchannels machined by stationary tool and rotary tool micro-USM process at 60% power rating were 73% and 82% respectively as shown in Figure 4.10.
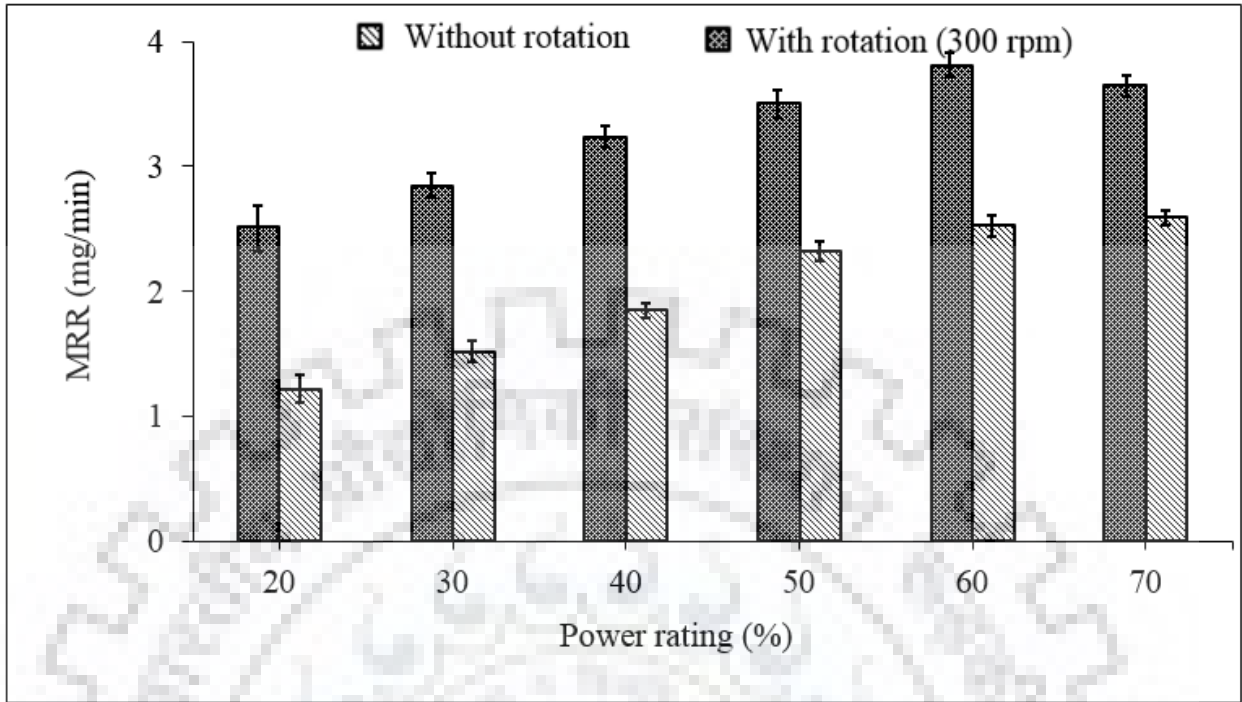
Figure 4.8 Effect of power rating on MRR

Figure 4.9 Effect of power rating on DOC

(a)

Depth = 410 μm
Form accuracy = 73%

300μm

(b)

Depth = 480 μm
Form accuracy = 82%

300μm

Figure 4.10 Microscopic images of cross-sectional view of microchannels machined by (a) stationary tool micro-USM process [experimental conditions: feed rate =10 mm/min, power rating = 60%, slurry concentration = 15% and abrasive size = #1000 mesh] (b) rotary tool micro-USM process [experimental conditions: rotation speed = 300 rpm, feed rate =20 mm/min, power rating = 60%, slurry concentration = 15% and abrasive size = #1000 mesh]

Effect of concentration on MRR and DOC

The concentration of abrasive slurry is directly related to the quantity of abrasive particles present in abrasive slurry. The effect of concentration on MRR and DOC is presented in Figure 4.11 and Figure 4.12. The MRR and DOC increased by increasing the concentration from 10% to 20%, after that both decreased marginally. The number of impact on the work surface increased by increasing slurry concentration. As a result of that MRR and DOC increased. After 20% of slurry concentration, the quantity of abrasive particles increased and excessive abrasive particles entered into the machining gap which led to the formation of multiple layers of abrasives. These abrasive particles started hitting each other before impacting on the work surface leading to loss of impact energy. Consequently, MRR, DOC and form accuracy decreased. The maximum MRR and DOC were obtained at 20% slurry concentration in both stationary tool and rotary tool micro-USM processes. At 20% of slurry concentration, the stationary tool and rotary tool micro-USM processes resulted in 65% and 87% form accuracy of machined microchannels as shown in Figure 4.13.
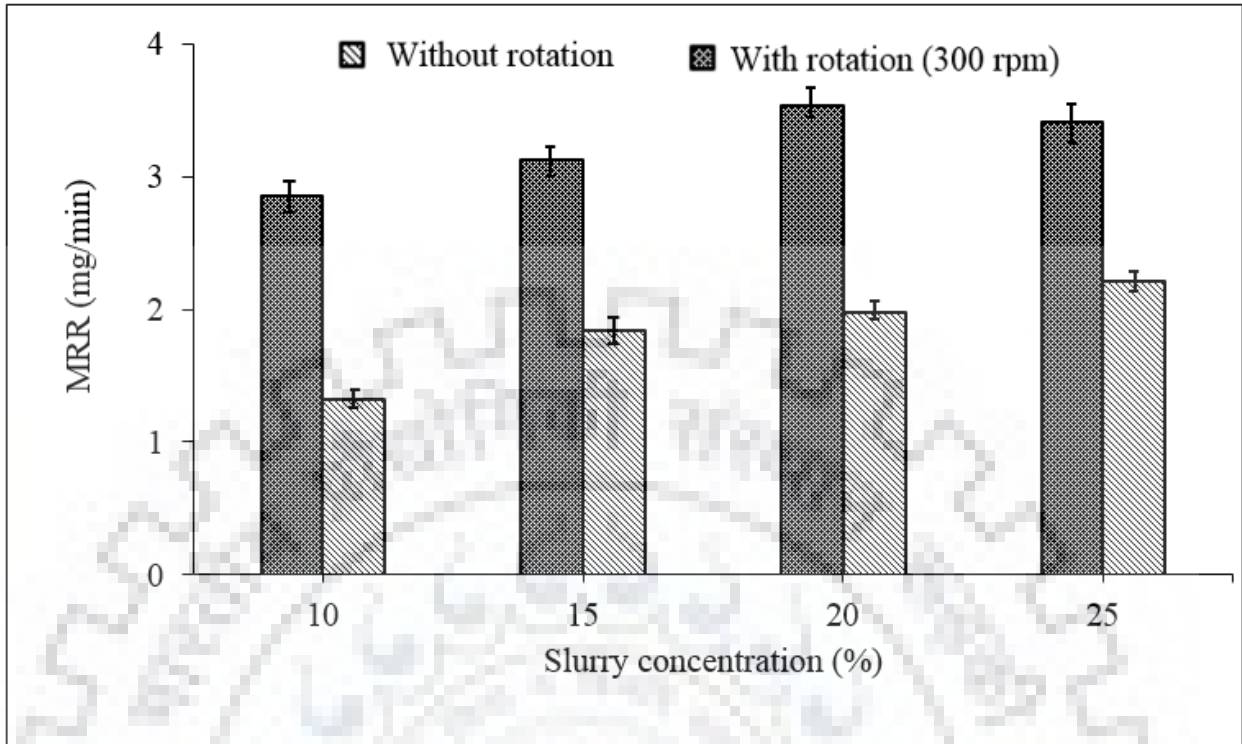
Figure 4.11 Effect of slurry concentration on MRR
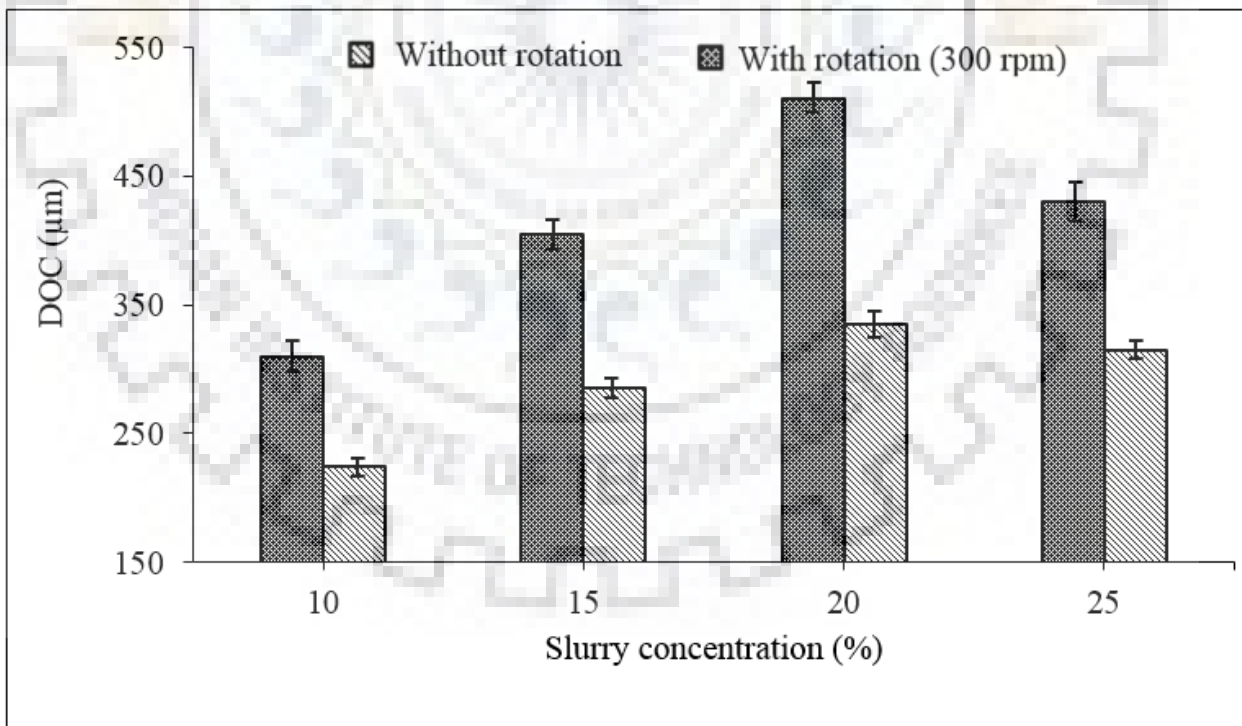
Figure 4.12 Effect of slurry concentration on DOC
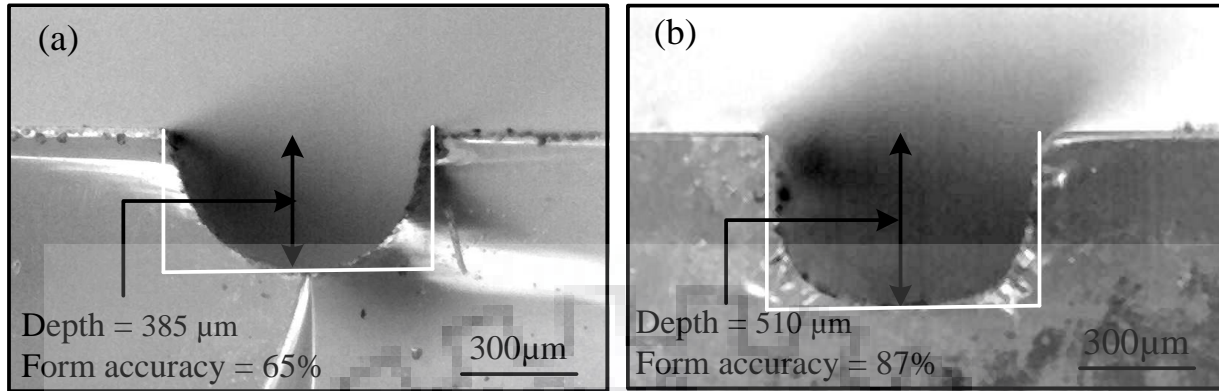
Figure 4.13 Microscopic images of cross-sectional view of microchannels machined by (a) stationary tool micro-USM process [experimental conditions: feed rate =10 mm/min, power rating = 60%, slurry concentration = 20% and abrasive size = #1000 mesh] (b) rotary tool micro-USM process [experimental conditions: rotation speed = 300 rpm, feed rate =20 mm/min, power rating = 60%, slurry concentration = 20% and abrasive size = #1000 mesh]

Effect of abrasive size on MRR and DOC

The grain size (average grain diameter) of abrasive particle is inversely proportional to the mesh number of abrasive particle. The effect of abrasive particles mesh size on MRR and DOC is illustrated in Figure 4.14 and Figure 4.15. From Figure 4.14 and Figure 4.15 it can be observed that by increasing the abrasive particle size from #500 to #1000 mesh, both the MRR and DOC increased continuously. This can be inferred that lesser number of abrasive particles participated into the machining when #500 mesh size abrasive particles were used. Due to this low value of MRR and DOC were obtained. On increasing the abrasive particle size from #500 to #800 mesh, the quantity of abrasive particles increased leading to the creation of more craters on the work surface. Thus, MRR and DOC increased. On further increasing the abrasive particle size from #800 to #1000 mesh, the average grain diameter of abrasive particles further reduced leading to more number of abrasive particles into the machining gap as compared to #800 mesh abrasive particles. Subsequently, number of impacts on the work surface were also increased. This resulted in highest value of both the MRR and DOC. The form accuracies of 67% by stationary tool micro-USM process and 86% by rotary tool micro-USM process were obtained using #1000 mesh abrasive particles (as shown in Figure 4.16).
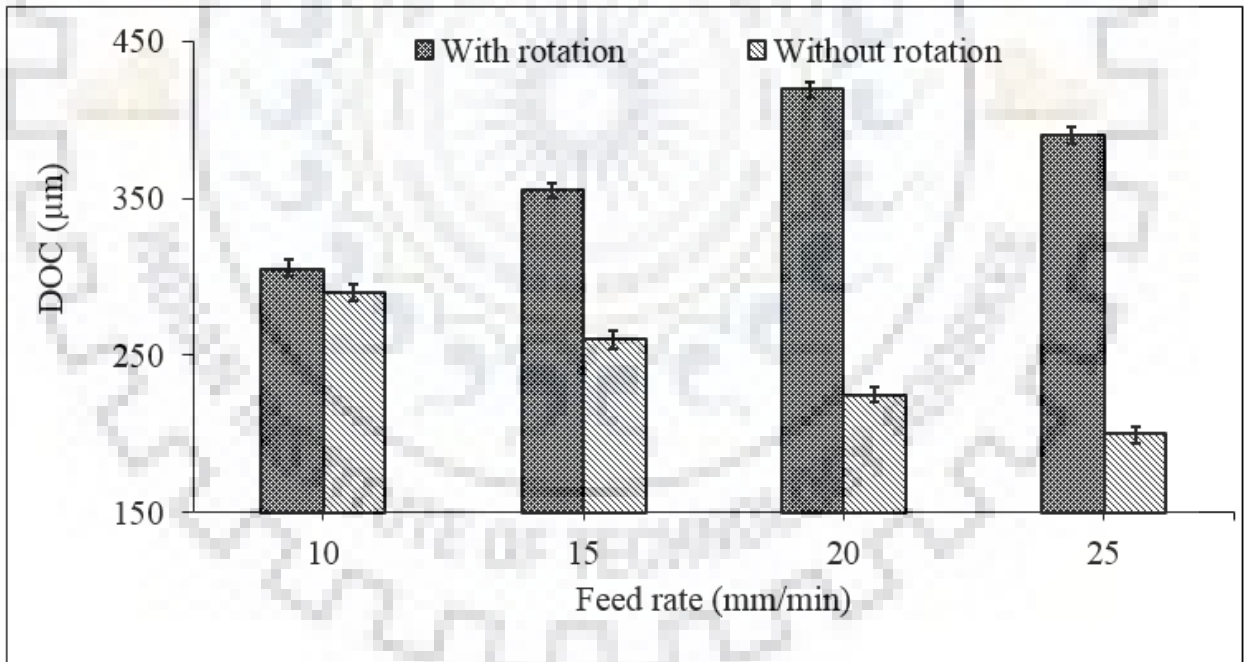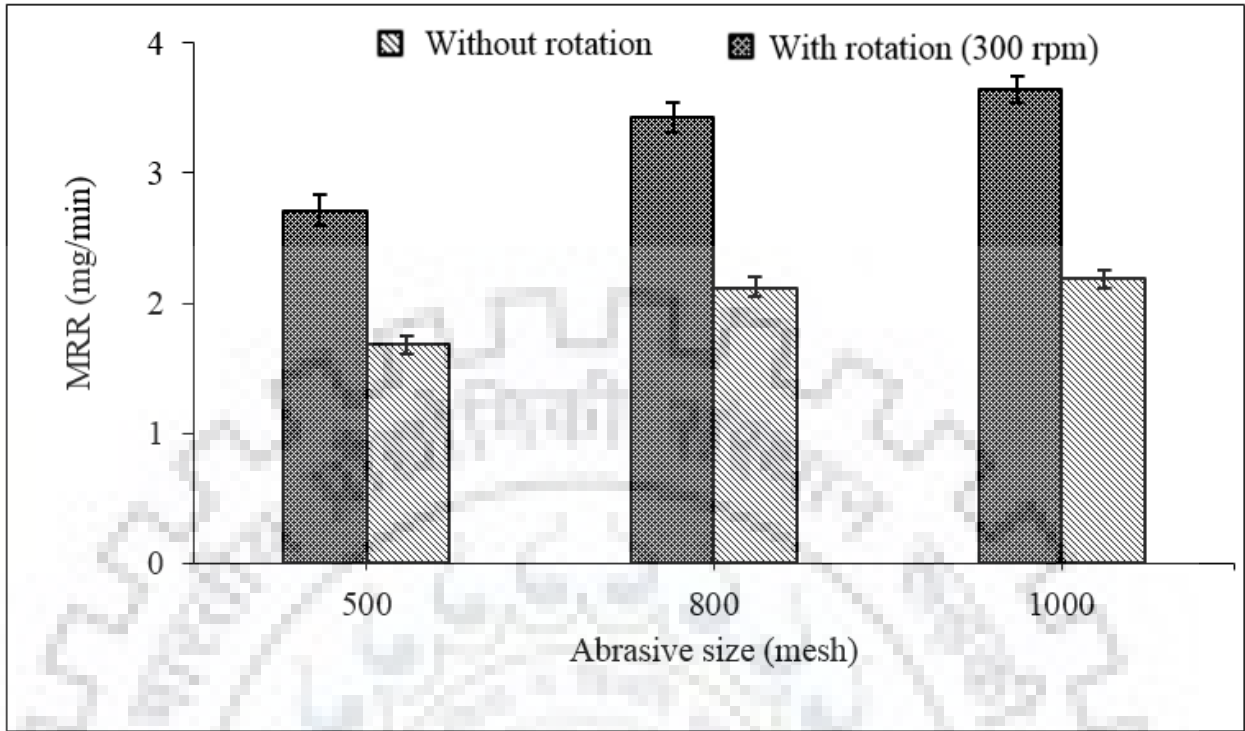
Figure 4.14 Effect of abrasive size on MRR
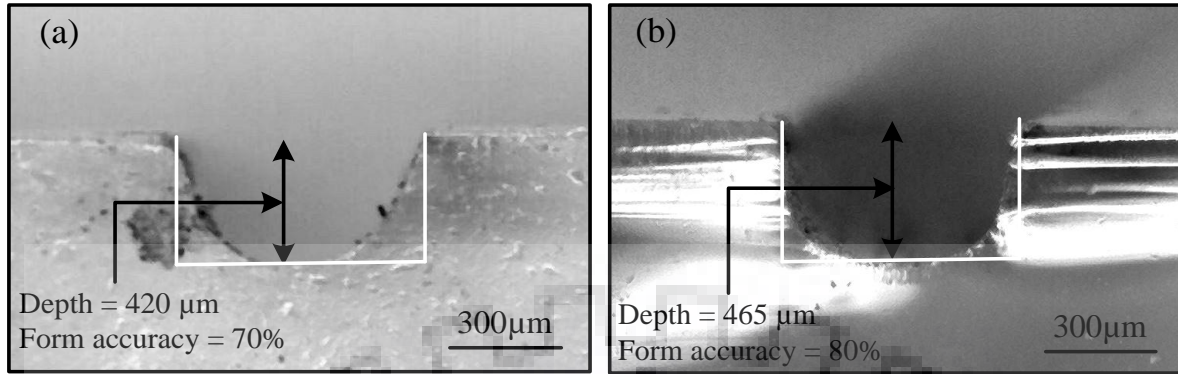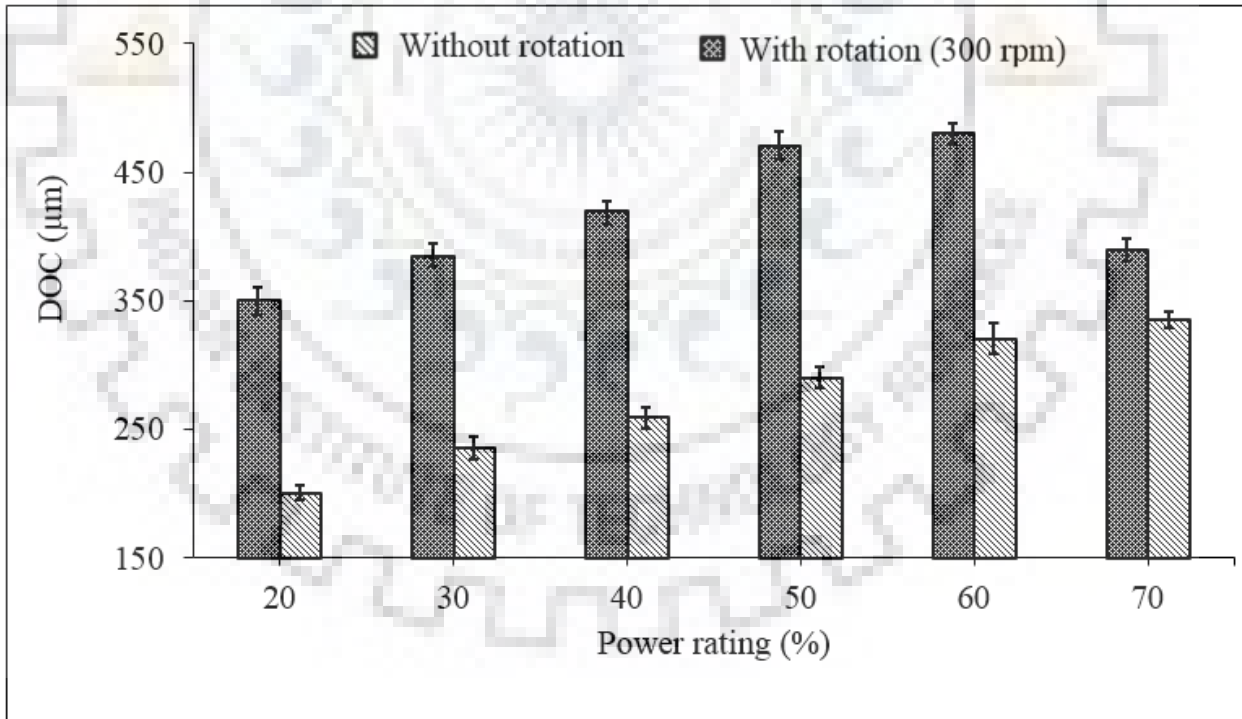

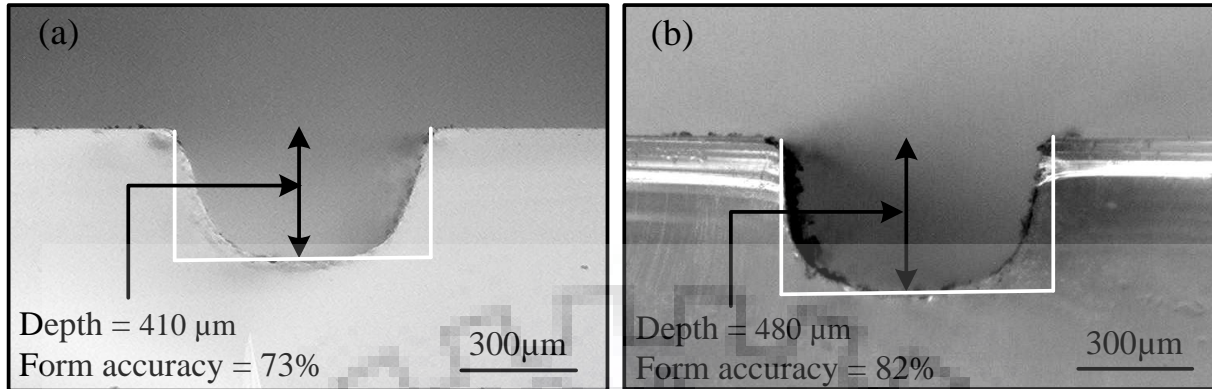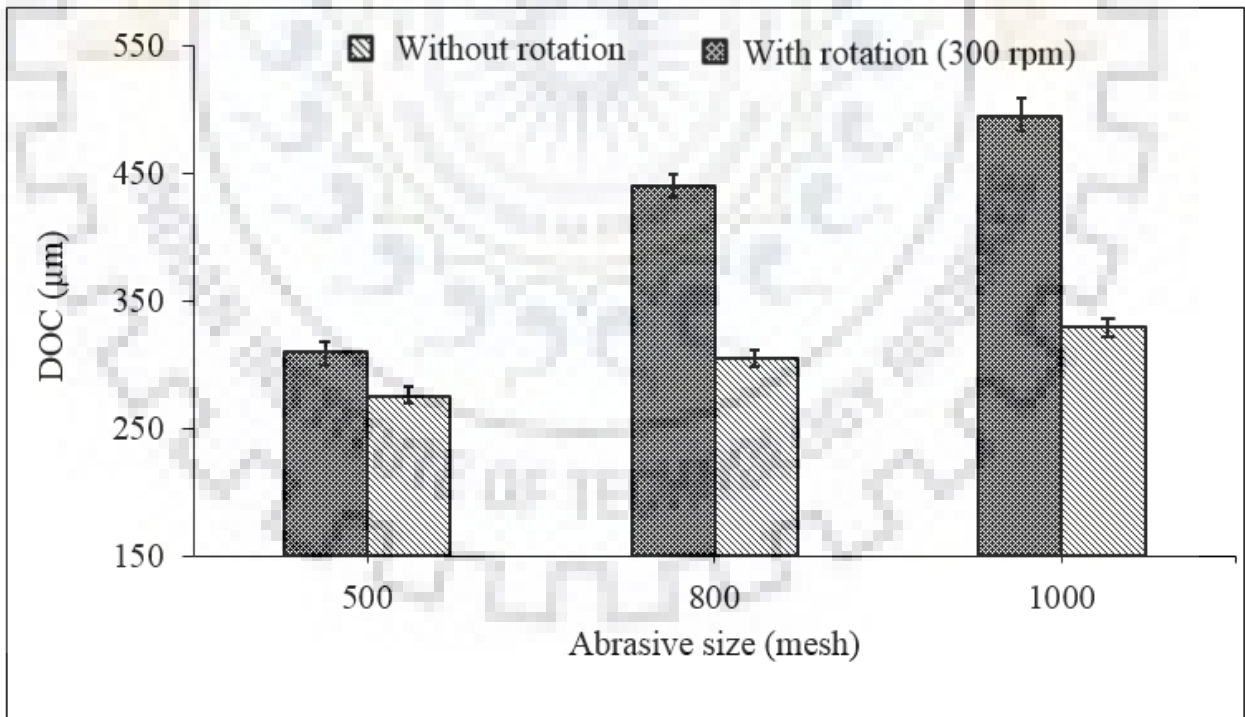Figure 4.15 Effect of abrasive size on DOC

121
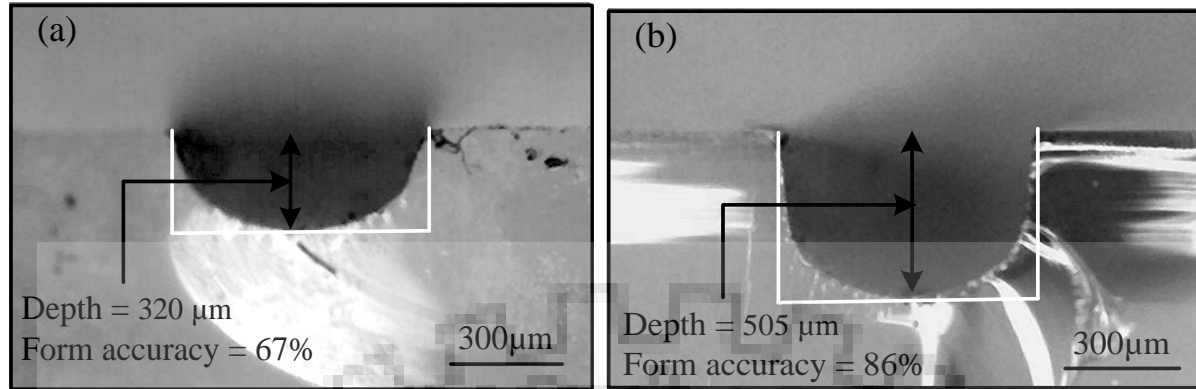
Figure 4.16 Microscopic images of cross-sectional view of microchannels machined by (a) stationary tool micro-USM process [experimental conditions: feed rate =10 mm/min, power rating = 60%, slurry concentration = 20% and abrasive size = #1000 mesh] (b) rotary tool micro-USM process [experimental conditions: rotation speed = 300 rpm, feed rate =20 mm/min, power rating = 60%, slurry concentration = 20% and abrasive size = #1000 mesh]

The results shown in Figures 4.5 to Figure 4.16 indicate that the rotary tool micro-USM process resulted in higher MRR, higher DOC and better form accuracy of microchannels as compared to stationary tool micro-USM process by varying all the input process variables. The rotary motion of the tool was the only most influencing factor responsible for this improvement in the performance of micro-USM process. This can be explained with the fact that the rotary motion of tool generates centrifugal force into the machining zone. The generated centrifugal force facilitates the abrasives motion into the machining gap. The machining gap is governed by the peak-to-peak amplitude (gap between the uppermost position and lower most position of tool) of vibration of the tool. The abrasive particles reach into the machining gap through the lateral gap (i.e. gap between the wall of machined cavity and vertical surface of tool) participate into the machining and after that come out from the machining gap through lateral gap. As a result of this the MRR, DOC and form accuracy of microchannel increased. Due to the same reason lesser stray cutting was observed in microchannels machined by using the rotary tool micro-USM process. On the other hand in case of stationary tool micro-USM process, the abrasive particles stacks (multiple abrasive layers) into the machining gap when certain depth is reached. As the machining continues, the tool continuously strikes on the abrasives. Subsequently, these abrasives hit each-other instead of striking on the work surface leading to loss of energy. Consequently, resulted in lesser MRR, DOC and poor form accuracy of machined microchannels.

After studding the effect of micro-USM process parameters on MRR and DOC, SEM analysis of form accuracy, dimensional accuracy and tool wear was carried out with the help of SEM micrographs (shown in Figure 4.17(a) and (b)). The micrographs shown in Figure 4.17(a) and (b) indicate that the profile of microchannel developed by rotary tool micro-USM process was better than stationary tool micro-USM process. In case of stationary tool micro-USM process, microchannel with tapered side wall and non-flat surface was obtained (Figure 4.17(a)). Whereas, almost flat bottom surface and straight side wall of microchannel were obtained in rotary tool micro-USM process (Figure 4.17(b)). The reason behind this was that in case of stationary tool micro-USM process, abrasive particle present in the machining gap were trapped and could not find easy path to come out from the machining gap. A 3 body abrasive wear took place in between tool vertical surface, abrasive particles and wall of machined cavity. This resulted in the side wear of tool due to relative contact between tool and abrasive particles (Figure 4.18(a)). Further this side wear replicated on the side wall of the microchannel and due to this microchannels became taper instead of straight wall and flat surface microchannel converted into tapered (V-type) microchannel which was undesired (Figure 4.17(a)). While, in case of rotary tool micro-USM process, due to centrifugal force, the abrasive particles exited from the lateral gap without abrading the vertical surface of the tool. A 2 body abrasive wear took place between abrasive particles and wall of the machined cavity (Figure 4.18(b)).
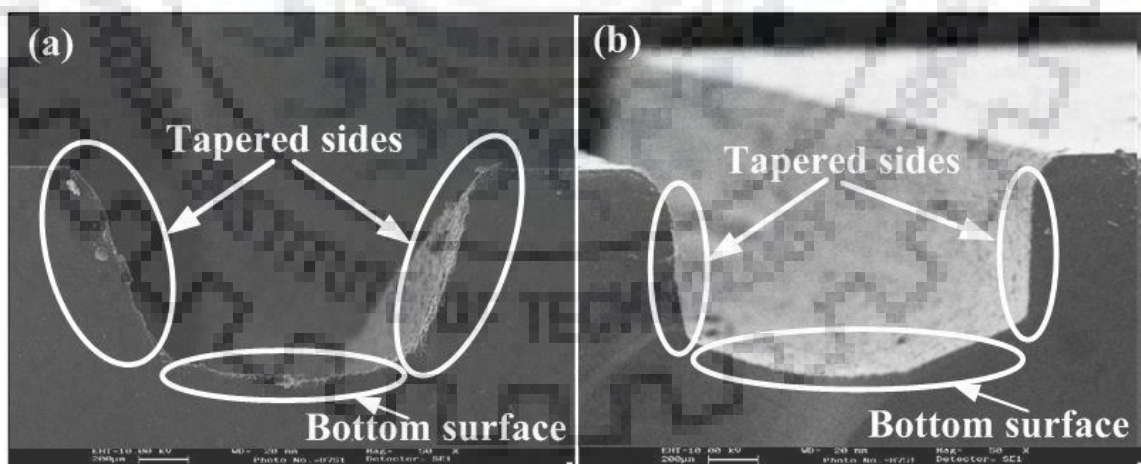
Figure 4.17 SEM micrograph of microchannel developed by (a) stationary tool micro-USM process (b) rotary tool micro-USM process [experimental condition: power rating = 60%, feed rate = 15 mm/min, slurry concentration = 20%, abrasive size = #1000 mesh]
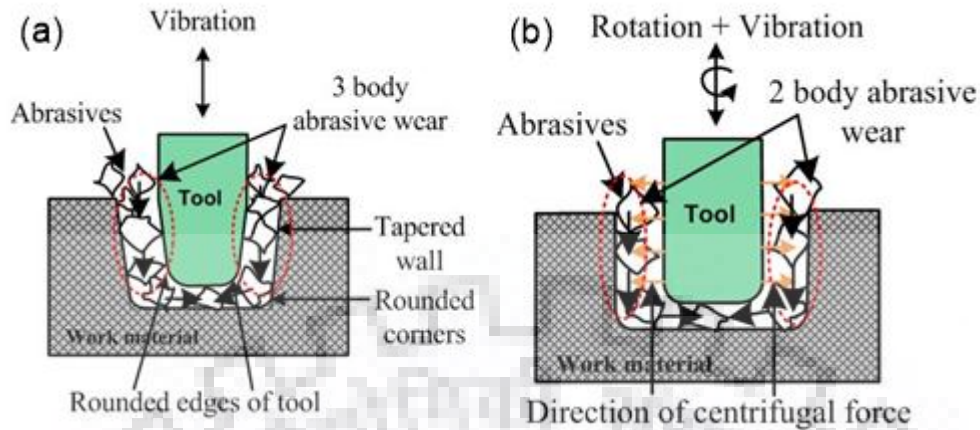
Figure 4.18 Abrasive movement in machining gap (a) stationary tool micro-USM process (b) rotary tool micro-USM process

Another cutting action which took place around the edges of microchannels and caused poor form accuracy in micro-USM process was also observed. This is known as stray cutting and it was due to the movement of deflected abrasive particles coming out of the machining gap. On the other hand in case of rotary tool micro-USM process, the rotary motion of tool provide centrifugal force to the abrasive slurry and because of that abrasive got additional assistance for easy removal from the center of working gap between rotating tool and work. Due to applied centrifugal force, the abrasives did not abrade the vertical surface of tool and a 2 body abrasive wear took place in between the abrasive particles and side wall of machined cavity. Moreover, rotation of the tool helped those abrasives which were trapped in between the rotating tool and side wall of the microchannel. Due to this negligible tool wear took place on the sides of the tool. Stray cutting as shown in Figure 4.19 was little bit more in case of rotary tool micro-USM process than stationary tool micro-USM process. The reason behind this was that due to rotary motion of tool more number of abrasives were coming out from the side gap which resulted in more relative contact between the abrasive particles and upper edge of the microchannel. In case of stationary tool micro-USM process, less number of abrasive particles were coming out of the machining gap which resulted in lower relative contact of abrasive particles and upper side edge of microchannel. Microchannels generated by rotary tool micro-USM process were better than those of generated by stationary tool micro-USM in terms of form accuracy which is desired for micro-fabrication.
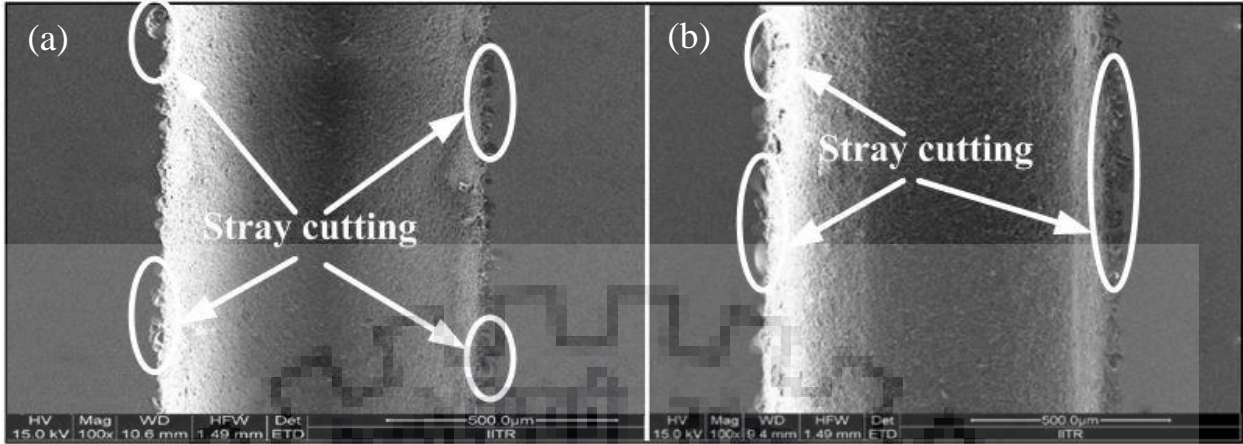
Figure 4.19 FE-SEM micrograph of microchannel developed by (a) stationary tool micro-USM process (b) rotary tool micro-USM process [experimental condition: power rating = 60%, feed rate = 15mm/min, slurry concentration = 20%, abrasive size = #1000 mesh]

The micrographs of worn out tools are shown in Figure 4.20. The tool wear was more in case of stationary tool micro-USM process (Figure 4.20(a)) as compared to rotary tool micro-USM process (Figure 4.20(b)). Three types of tool wear namely longitudinal wear, lateral wear and edge rounding wear were observed in stationary tool micro-USM process (as evidenced in Figure 4.20(a)). Longitudinal wear was due to the hammering/impact and cavitation action, edge rounding wear was due to the hammering and abrasion whereas side wear was due to the rolling and abrasion caused by abrasive particles (Cheema et al., (2005)).

Owing to the extreme wear in the vertical side of the tool, side walls of the microchannel were become tapered and due to the edge wear bottom of the microchannel became little bit rounded instead of flat. With the combining effect of lateral and edge rounding wear of tool, tapered (V-type shape) microchannel was generated by stationary tool micro-USM process (Figure 4.17(a)). On the other hand, in case of rotary tool micro-USM process, abrasive particles did not stuck in between vertical side of the tool and side wall of the work. This resulted in lesser edge rounding wear and almost negligible lateral wear of the tool and hence better form accuracy of microchannels. The negligible lateral wear in rotary tool micro-USM process is evidenced in Figure 4.17(b).
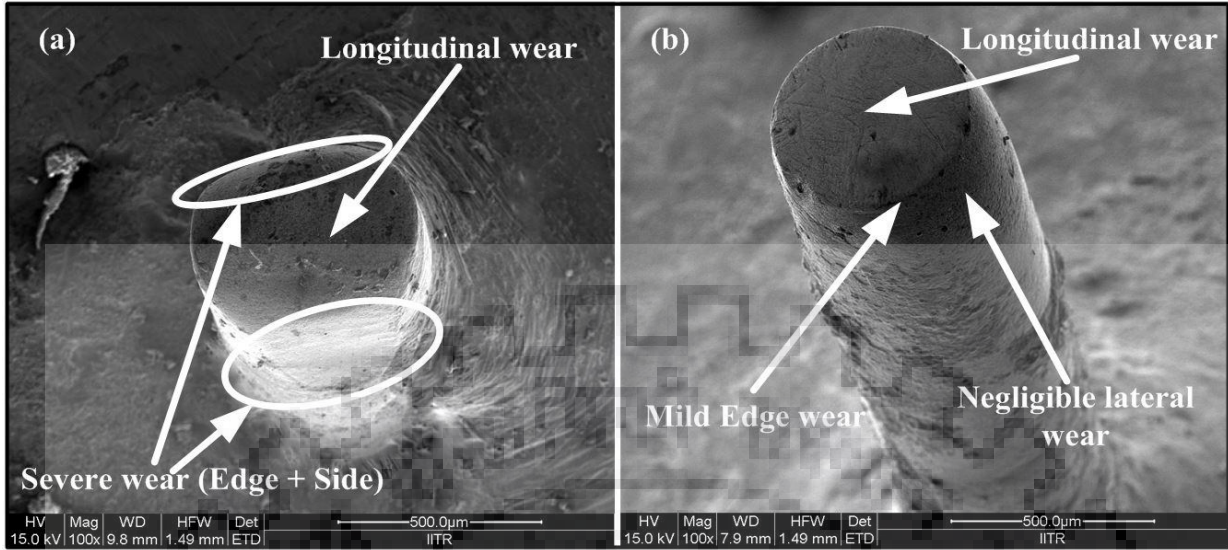
Figure 4.20 FE-SEM micrograph of tool after machining (a) stationary tool micro-USM process (b) rotary tool micro-USM process [experimental condition: power rating = 60%, feed rate = 15 mm/min, slurry concentration = 20%, abrasive size = #1000 mesh]

4.3 Summary

The present chapter reports on the performance evaluation of rotary tool micro-USM process during machining of microholes and microchannels. The performance was evaluated by comparing the performance of rotary tool micro-USM process with the performance of stationary tool micro-USM process. It was observed that the rotary motion of tool effectively replenished the abrasives from the machining zone and thereby improved the performance of micro-USM process in terms of higher machining rate, depth of microfeatures and lesser overcut. During machining of both the microholes and microchannels, the tool wear was found to be lesser in rotary tool micro-USM as compared to stationary tool micro-USM process. In case of stationary tool micro-USM process, three types of tool wear (i.e. longitudinal wear, lateral wear and edge wear) were observed. Whereas, in case of rotary tool micro-USM process, only two types of tool wear (i.e. longitudinal wear and edge wear) were observed. Owing to the lesser tool wear, better form accuracy was obtained during rotary tool micro-USM process as compared to stationary tool micro-USM process. Thus, the rotary tool micro-USM process was selected for further experimentation on fabrication of microfeatures on hard and brittle materials.

CHAPTER 5

INVESTIGATIONS ON MICROHOLE DRILLING

As discussed in previous chapter, the performance of rotary tool micro-USM was superior over stationary tool micro-USM process. Therefore, it can be preferred over stationary tool micro-USM process for machining of hard and brittle materials. The present chapter is dedicated to investigate rotary tool micro-ultrasonic drilling (USD) process for machining of microholes in hard and brittle materials. An extensive experimentation followed by parametric optimization is carried out in this chapter to prove the machining capability of rotary tool micro-USD process. The outcome of this chapter will expand the industrial applicability of micro-USM process in the area of bio-medical science, microelectronic and automotive industries.

5.1 Investigations on Microhole Drilling

5.1.1 Introduction

Hard and brittle materials such as ceramics, glass and silicon are gaining huge importance in engineering and bio-medical science applications (Ji et al., (2014); Arif et al., (2011); Xiao et al., (2014); Lian et al., (2016)). The superior properties like high strength, high wear resistance, high thermal resistance and high hardness make these materials as a better choice for above mentioned applications. However, the superior properties of these above mentioned materials make them extremely difficult to machine specifically in micro domain. Thus, in this chapter, the rotary tool micro-USD process is utilized for machining of micro-holes in zirconia, silicon and glass work materials. A comprehensive experimentation was performed to understand and investigate the effect of work material properties on rotary tool micro-USD process performance by varying the input parameters. Subsequently, the machined micro-holes and tool surface were analyzed considering stereo microscope and scanning electron microscope (SEM) images. Eventually, the parameters of rotary tool micro-USD process were optimized for machining of deep microholes.

5.1.2 Experimental facility and measurement methods

The ultrasonic drilling was performed on an in-house developed facility of rotary tool micro-USD process shown in Figure 3.2. The detailed description of the micro-USD facility is provided in chapter 3. The drilling tests were conducted on three work materials viz. zirconia, silicon and glass using tungsten carbide and silicon carbide as tool and abrasive materials. The properties of these work materials are given in Table 5.1. Tap water was selected as liquid medium for slurry owing to its low cost and easy availability. During experimentation, the abrasive slurry was fed in the machining gap at a constant rate to avoid any kind of turbulence. Tool rotation speed, power rating, slurry concentration and abrasive size were used as variable parameters in this experimentation. The process parameter and their levels are given in Table 5.2. The OFAT approach was used to conduct the experiments. The performance of rotary tool micro-USD process was evaluated in terms of MRR, DOH and HOC. The MRR and HOC were calculated as per procedure given in section 3.3 of chapter 3. Post drilling, tools were also cleaned and dried. After machining, the images of tools were captured using microscope (Make: NIKON SMZ-745T (Figure A.4 of Appendix A)). Each experiment was conducted thrice at same parametric setting and mean value was consider as final output. The profile of drilled microhole was captured and characterized using stereo zoom microscope.

Table 5.1 Properties of borosilicate glass, silicon and zirconia (Guzzo et al., (2004))

Properties	Work material		
	Glass	Silicon	Zirconia
Density (g/cm^3)	2.23	233	5.5
Fracture toughness (MPa/m$^{-1/2}$)	0.8	0.7	8-10
Hardness (GPa)	5.7	6.5	10-12
Young's modulus (GPa)	64	130-188	140-210

Table 5.2 Process parameters settings for drilling of microholes

Variable parameters	Ranges
Power rating	20 - 60%
Rotation speed	100 - 500 rpm
Abrasive size	#1000 - #1800 mesh
Concentration	10 – 25%
Constant parameters	**Value**
Frequency	21 ± 1 kHz
Static load	60 g
Tool diameter (Ø)	600 µm
Tool material & geometry	WC, cylindrical
Work material	Glass, Silicon, Zirconia

5.1.3 Analysis and discussion of results

In order to investigate rotary tool micro-USD process for machining of microholes, the experiments were conducted as per the experimental settings given in Table 5.2. The results are tabulated in Table 5.3 to Table 5.5.

Table 5.3 Process parameters and responses for drilling of microholes in glass

Process parameters				Responses		
RS (rpm)	PR (%)	AS (mesh)	SC (%)	Avg. MRR (mg/min)	Avg. DOH (µm)	Avg. HOC (µm)
100	40	1000	15	0.432	490	110
200	40	1000	15	0.478	565	95
300	40	1000	15	0.524	660	65
400	40	1000	15	0.483	615	70
500	40	1000	15	0.432	550	80
300	20	1000	15	0.318	415	62
300	30	1000	15	0.375	480	68
300	40	1000	15	0.402	495	81

300	50	1000	15	0.453	540	92
300	60	1000	15	0.487	560	105
300	40	800	15	0.374	490	60
300	40	1000	15	0.423	530	75
300	40	1200	15	0.450	550	84
300	40	1000	10	0.498	580	100
300	40	1000	15	0.465	555	92
300	40	1000	20	0.488	630	65
300	40	1000	25	0.476	590	79
RS- Rotation speed, PR- Power rating, AS- Abrasive size, SC- Slurry concentration						

Table 5.4 Process parameters and responses for drilling of microholes in silicon

Process parameters				Responses		
RS (rpm)	PR (%)	AS (mesh)	SC (%)	Avg. MRR (mg/min)	Avg. DOH (μm)	Avg. HOC (μm)
100	40	1000	15	0.463	510	120
200	40	1000	15	0.558	590	107
300	40	1000	15	0.575	680	80
400	40	1000	15	0.502	635	72
500	40	1000	15	0.448	570	70
300	20	1000	15	0.346	440	70
300	30	1000	15	0.410	510	78
300	40	1000	15	0.454	545	90
300	50	1000	15	0.505	580	105
300	60	1000	15	0.547	610	120
300	40	800	15	0.510	590	103
300	40	1000	15	0.518	650	75
300	40	1200	15	0.519	615	94
300	40	1000	10	0.405	520	67
300	40	1000	15	0.474	570	89
300	40	1000	20	0.515	600	100
300	40	1000	25	0.501	560	115
RS- Rotation speed, PR- Power rating, AS- Abrasive size, SC- Slurry concentration						

Table 5.5 Process parameters and responses for drilling of microholes in zirconia

Process parameters				Responses		
RS (rpm)	PR (%)	AS (mesh)	SC (%)	Avg. MRR (mg/min)	Avg. DOH (µm)	Avg. HOC (µm)
100	40	1000	15	0.329	400	85
200	40	1000	15	0.371	465	75
300	40	1000	15	0.391	505	65
400	40	1000	15	0.407	515	72
500	40	1000	15	0.376	460	83
300	20	1000	15	0.255	340	55
300	30	1000	15	0.319	400	75
300	40	1000	15	0.372	440	95
300	50	1000	15	0.406	460	110
300	60	1000	15	0.443	475	130
300	40	800	15	0.337	410	85
300	40	1000	15	0.366	480	60
300	40	1200	15	0.332	420	72
300	40	1000	10	0.296	410	42
300	40	1000	15	0.343	455	56
300	40	1000	20	0.387	495	68
300	40	1000	25	0.396	475	90

RS- Rotation speed, PR- Power rating, AS- Abrasive size, SC- Slurry concentration

Effect of power rating on MRR, DOH and HOC

As already discussed, in USM process, power rating/ultrasonic power is directly related to the amplitude of vibration. The effect of power rating on MRR, DOH and HOC is presented in Figure 5.1, Figure 5.2 and Figure 5.3 respectively. From Figure 5.1 to Figure 5.3, it can be clearly seen that an increase in power rating, the MRR, DOH and HOC increased continuously for zirconia, silicon and glass work materials. The reason attributed to these trends can be explained with the fact that as the power rating increased, the abrasives impacted the work

surface with higher energy owing to higher amplitude of vibration. As a result of that deep craters were formed on the work surface leading to increased MRR as well as higher depth of machined hole. It was also observed that at lower power ratings (i.e. from 20% to 40%), the machining rate as well as DOH increased at faster rate as compared to higher power ratings (i.e. from 50% to 60%). This can be inferred that the tool wear was also higher at higher power rating owing to the heavy impacts on the abrasives. Moreover, it seems that at higher power rating, multiple layers of abrasives may form beneath the tool leading to higher tool wear and increased HOC (Figure 5.3). Another reason for increased HOC may be the crushing of abrasives at higher power rating due to which multiple layers of abrasives may form in the machining area leading to increased HOC.
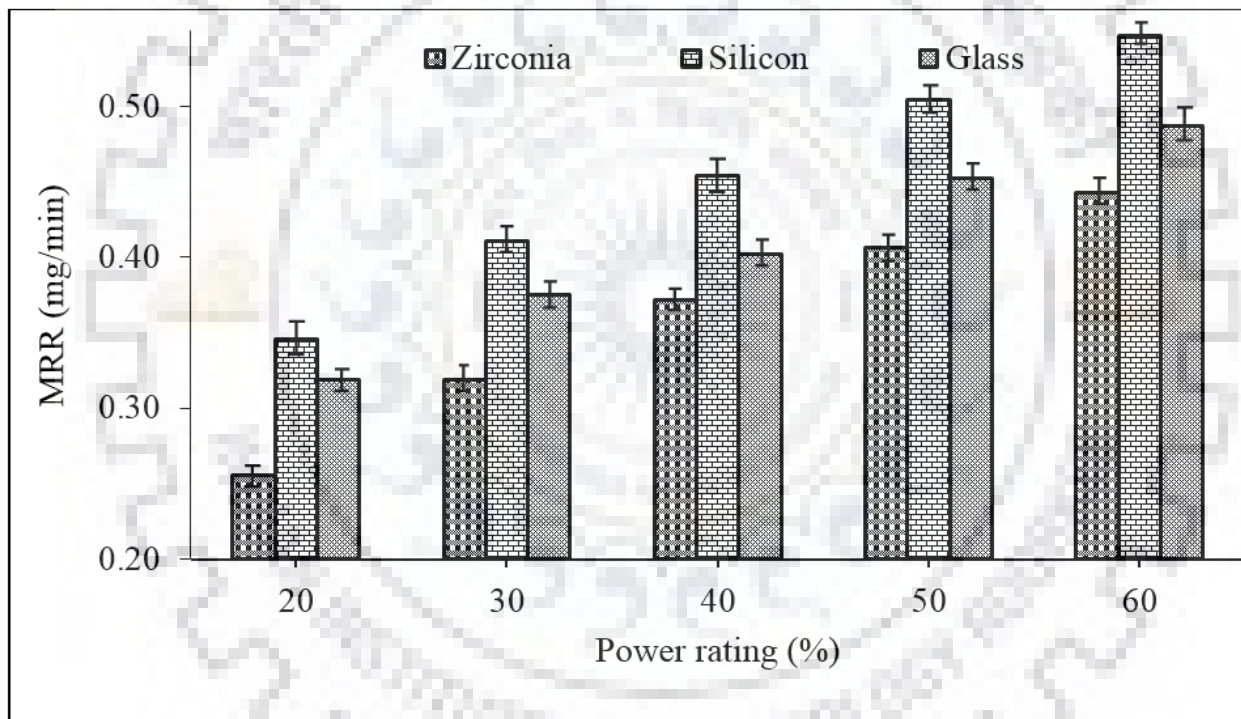
Figure 5.1 Effect of power rating on MRR
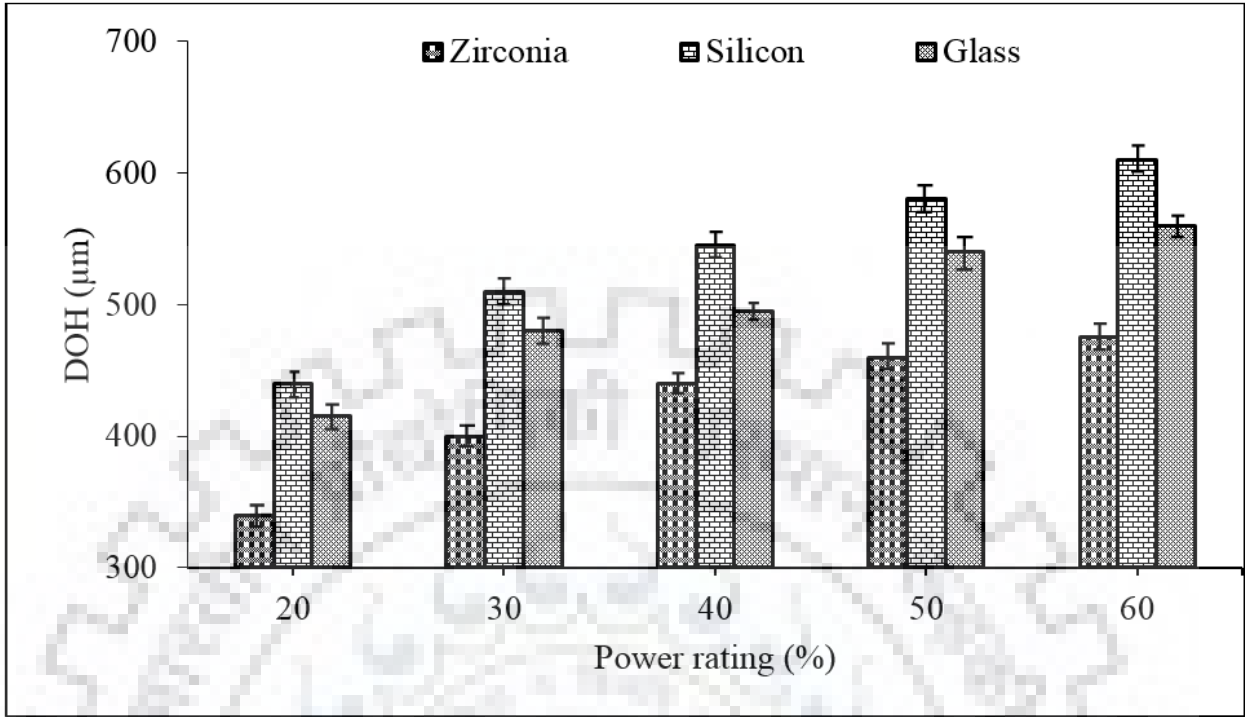
Figure 5.2 Effect of power rating on DOH
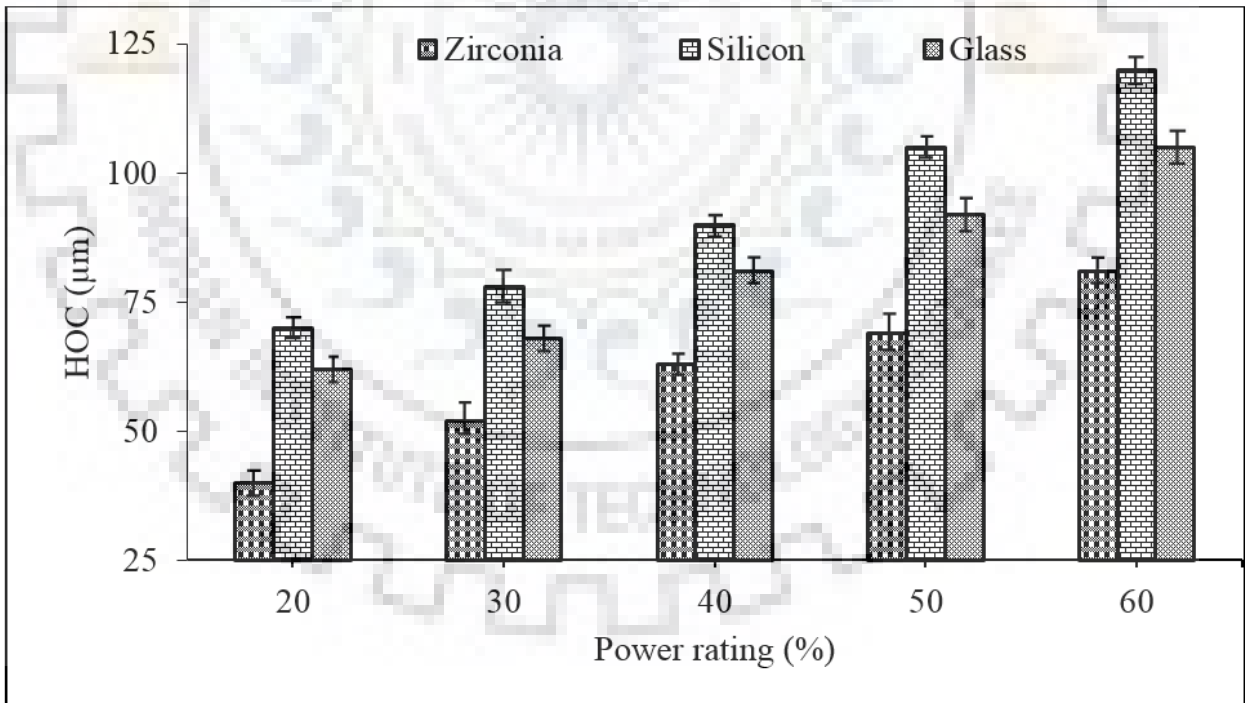
Figure 5.3 Effect of power rating on HOC

Effect of rotation speed on MRR, DOH and HOC

The effect of rotation speed on MRR, DOH and HOC is depicted in Figure 5.4, Figure 5.5 and Figure 5.6 respectively. It can be noticed that an increase in rotation speed of the tool from 100 rpm to 300 rpm, both the MRR, DOH increased continuously and beyond that a decreasing trend was observed in both (i.e. MRR and DOH). Maximum MRR, DOH and HOC for all the work material was obtained at 300 rpm of tool. This can be explained with the reason that the centrifugal force on abrasives increased as the rotation speed was increased from 100 rpm to 300 rpm. Owing to this, the abrasives replenished from the machining zone and immediately new sharp abrasives came and participated in machining leading to increased MRR and DOH. Beyond 300 rpm, centrifugal force on abrasives significantly increased and the abrasives could not get enough interaction time with the tool and work surface. Consequently, both the MRR and DOH decreased. Form Figure 5.6, it can be observed that the HOC decreased as the rotation speed increased from 100 rpm to 300 rpm. Thereafter, an increasing pattern in HOC was observed till 500 rpm. As mentioned above, the effective replenishment of abrasives was the reason for lesser HOC up to 300 rpm. However, beyond 300 rpm, the abrasives impacted on the wall of the machined hole with higher energy due to higher centrifugal force. This led to high rate of 2-body abrasion on the wall of machined hole. Thus, HOC increased.
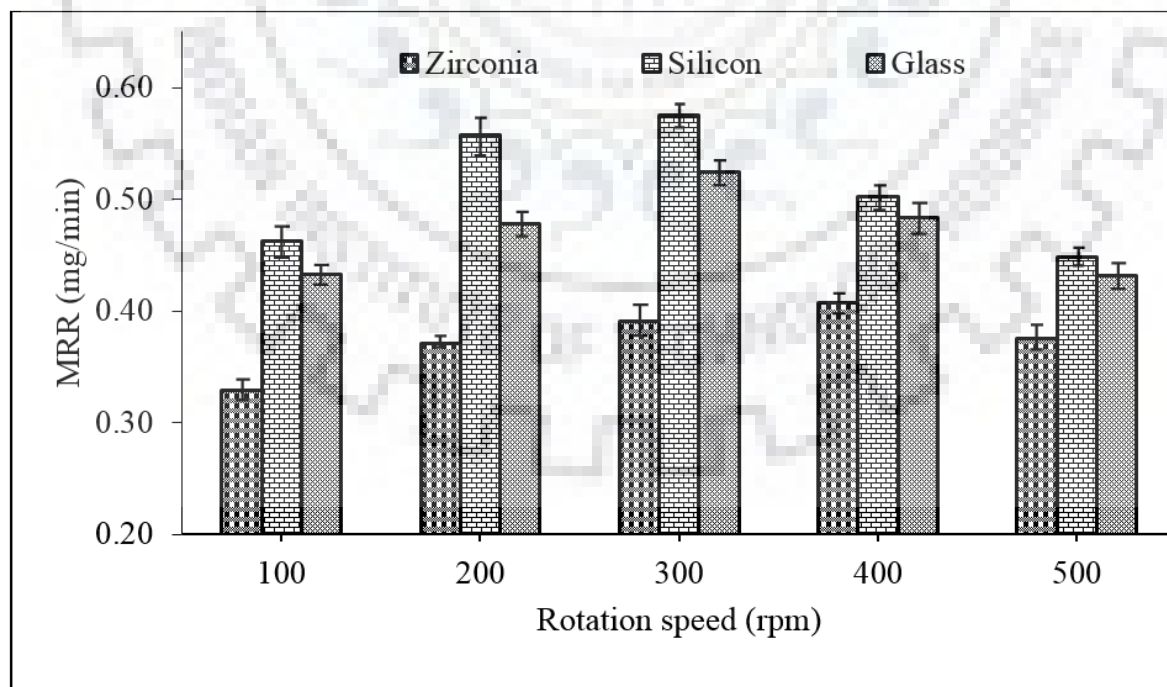
Figure 5.4 Effect of rotation speed on MRR
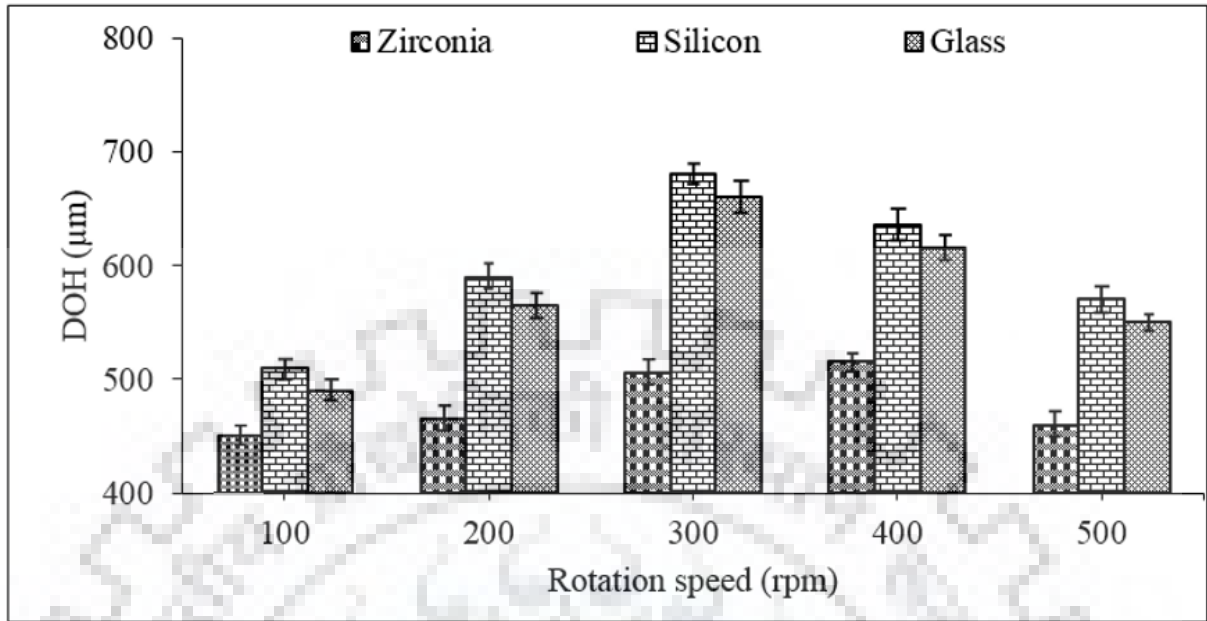
Figure 5.5 Effect of rotation speed on DOH
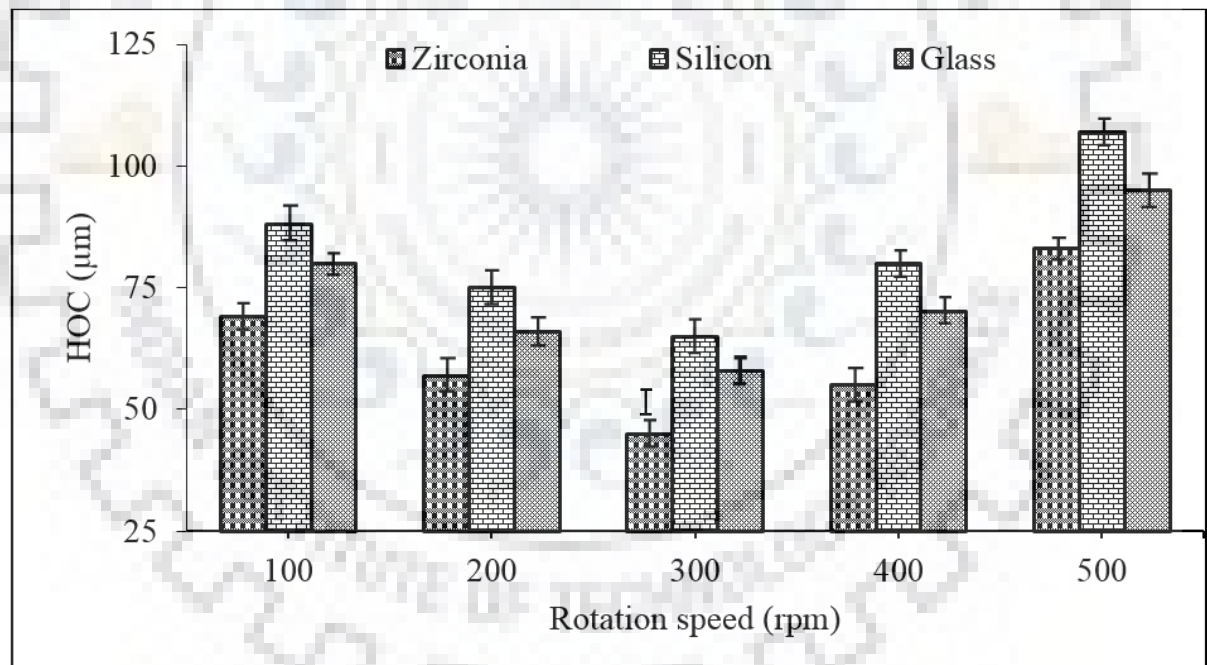
Figure 5.6 Effect of rotation speed on HOC

Effect of abrasive size on MRR, DOH and HOC

The abrasive size (average grain diameter) is expressed in terms of mesh size/number. The effect of abrasive mesh size on MRR, DOH and HOC is presented in Figure 5.7, Figure 5.8 and Figure 5.9 respectively. From Figures 5.7 and Figure 5.8, it can be depicted that by increasing the

abrasive mesh size from #1000 mesh to #1200 mesh, the MRR and DOH increased. On further increasing the mesh size of abrasive from #1200 mesh to #1800 mesh, both the MRR and DOH found to be decreased. On the other hand, by increasing the abrasive mesh size, HOC initially decreased up to #1200 mesh and after that it started to increase (Figure 5.9). This was attributed to the reason that in case of #1000 mesh abrasives, lesser number of abrasives participated into machining owing to large average grain diameter. Due to which lower MRR, and DOH were obtained. By increasing the mesh size of abrasives from #1000 mesh to #1200 mesh, the average grain size of abrasives decreased and as a result of that more number of abrasives entered into the machining area and participated into machining. Thus, higher MRR and DOH achieved. On further increasing the mesh size from #1200 mesh to #1800 mesh, the number of abrasives into the machining area increased significantly leading to the creation of multiple abrasive layer beneath the tool. As a result of that lesser ultrasonic energy transferred on the work surface via abrasives. Consequently, MRR and DOH decreased. High HOC was obtained while using coarse (#1000 mesh) and very fine (#1800 mesh) abrasives. This was due to the large lateral gap which may form by using large grain diameter (#1000 mesh) abrasives and also due to the multiple layers of abrasive in case of #1800 mesh. The abrasive size of #1200 mesh resulted in maximum MRR and DOH and minimum HOC owing to the laminar layer of abrasives present beneath the tool.
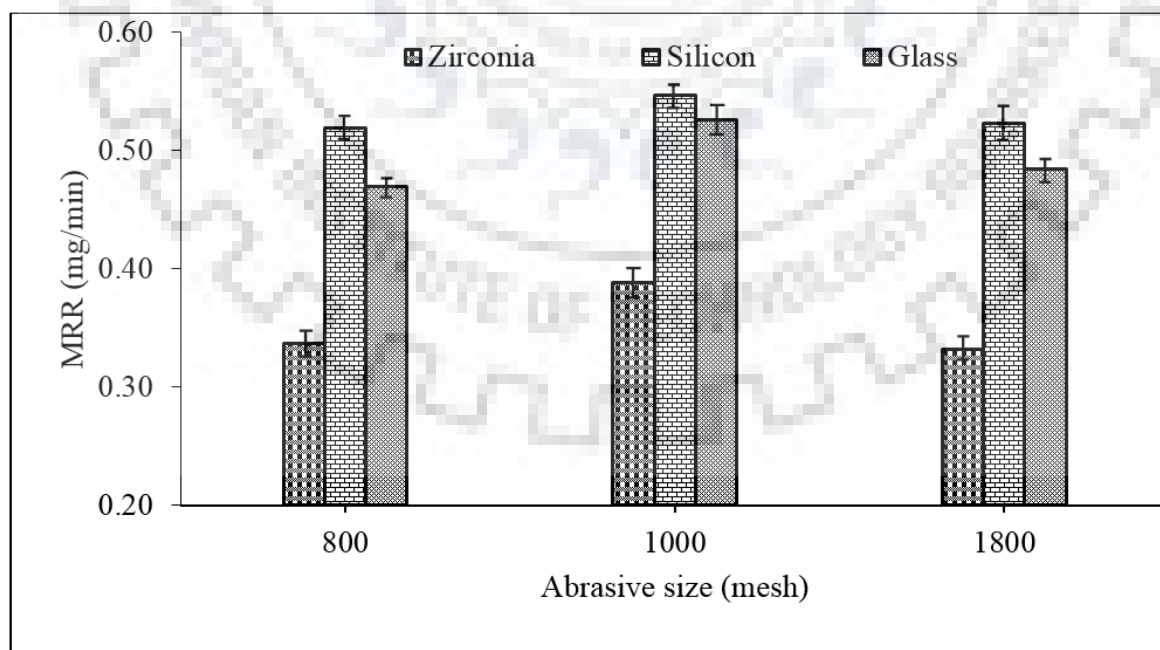
Figure 5.7 Effect of abrasive size on MRR

136
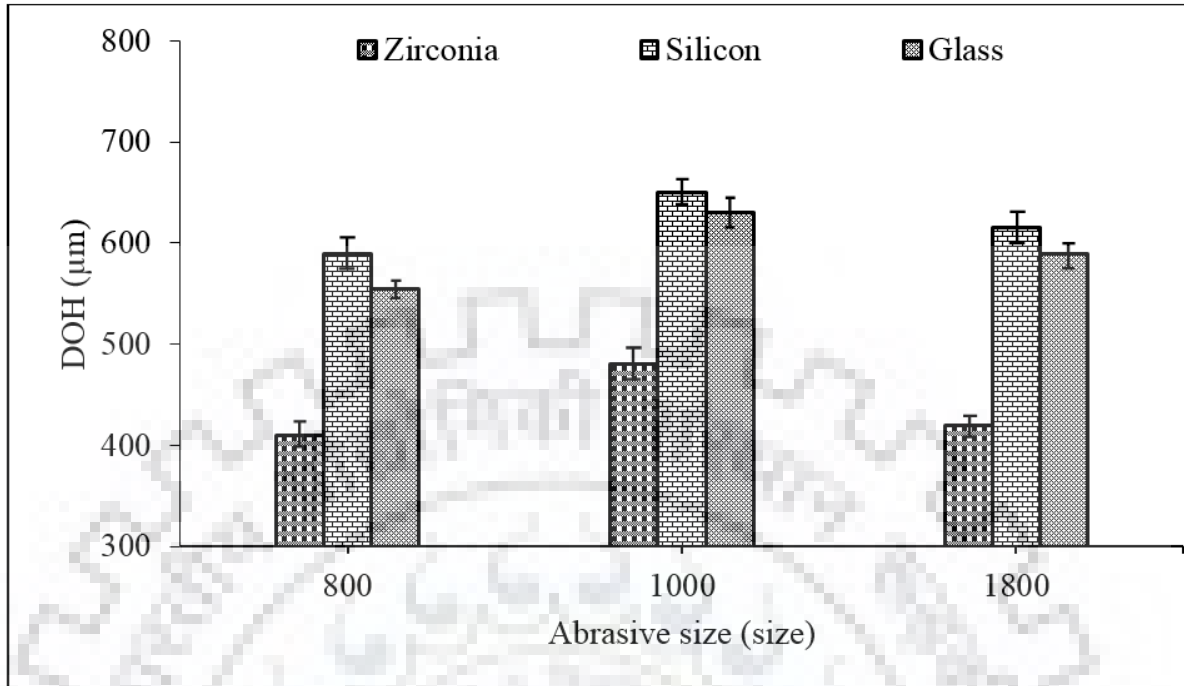
Figure 5.8 Effect of abrasive size on DOH
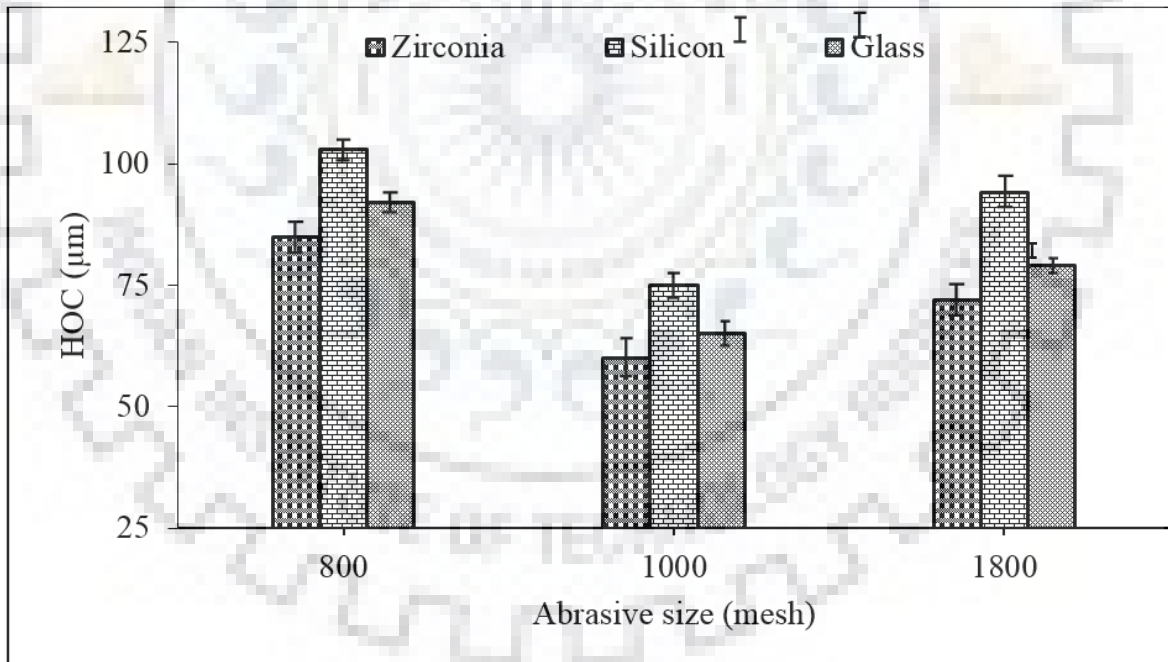
Figure 5.9 Effect of abrasive size on HOC

Effect of concentration on MRR, DOH and HOC

The effect of concentration on MRR, DOH and HOC is depicted in Figure 5.10, Figure 5.11 and Figure 5.12 respectively. From Figure 5.10 to Figure 5.12, it can be depicted that as the

concentration increased from 10% to 20%, both the MRR and DOH increased and thereafter, both found to be decreased. On the other hand, a continuous increment was observed in HOC by increasing the concentration from 10% to 25%. The quantity of abrasives increased by increasing the concentration. Due to which more abrasives participated in machining and led to the creation of more craters on workpiece. Thus, increased MRR, DOH and HOC. But beyond 20% concentration, the quantity of abrasives in the machining area became significantly higher leading to the condition of multiple layers of abrasives. In this condition, the tool strikes on the uppermost layer of abrasives after that these abrasives interact with the abrasives of the subsequent layer instead on the work material surface. This results in loss of some ultrasonic energy and leads to low MRR and high tool wear. Consequently, machining rate and DOH decreased. The maximum MRR and DOH were observed at 20% of slurry concentration, whereas minimum HOC was observed at 10% slurry concentration.
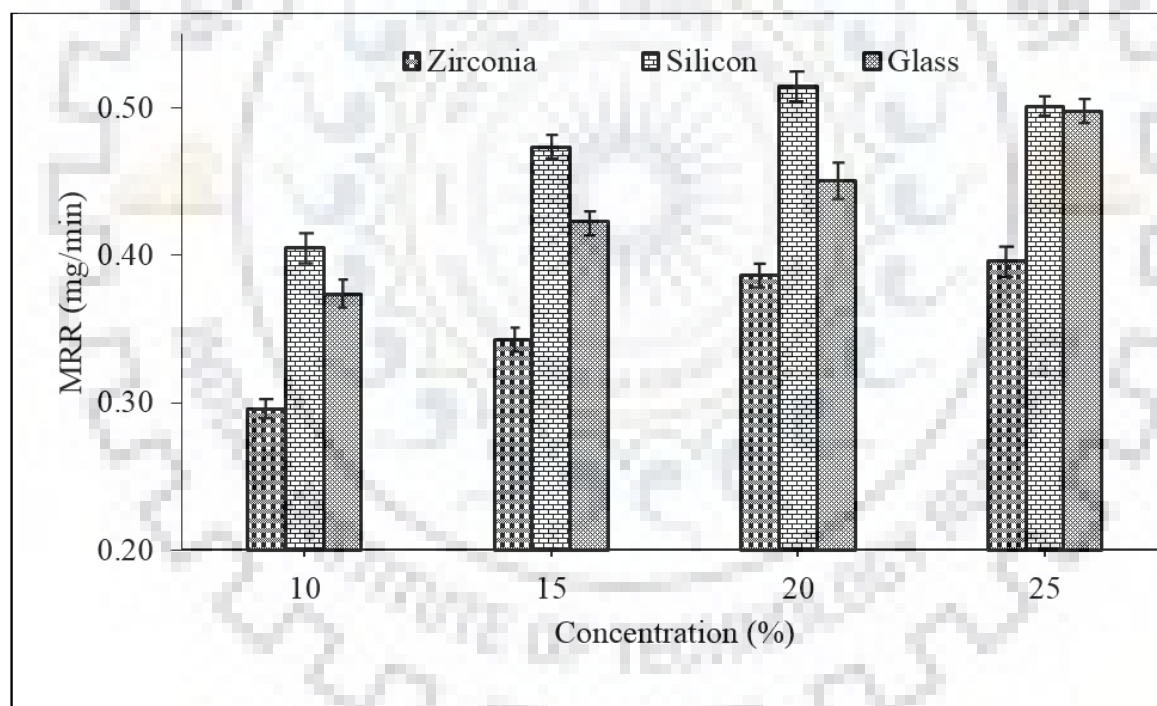
Figure 5.10 Effect of concentration on MRR
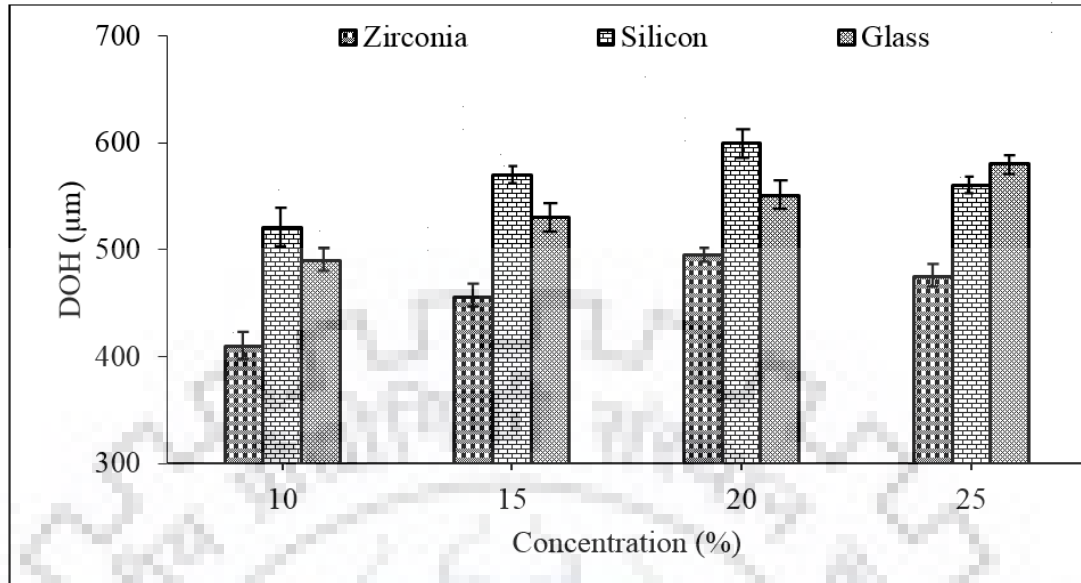
Figure 5.11 Effect of concentration on DOH
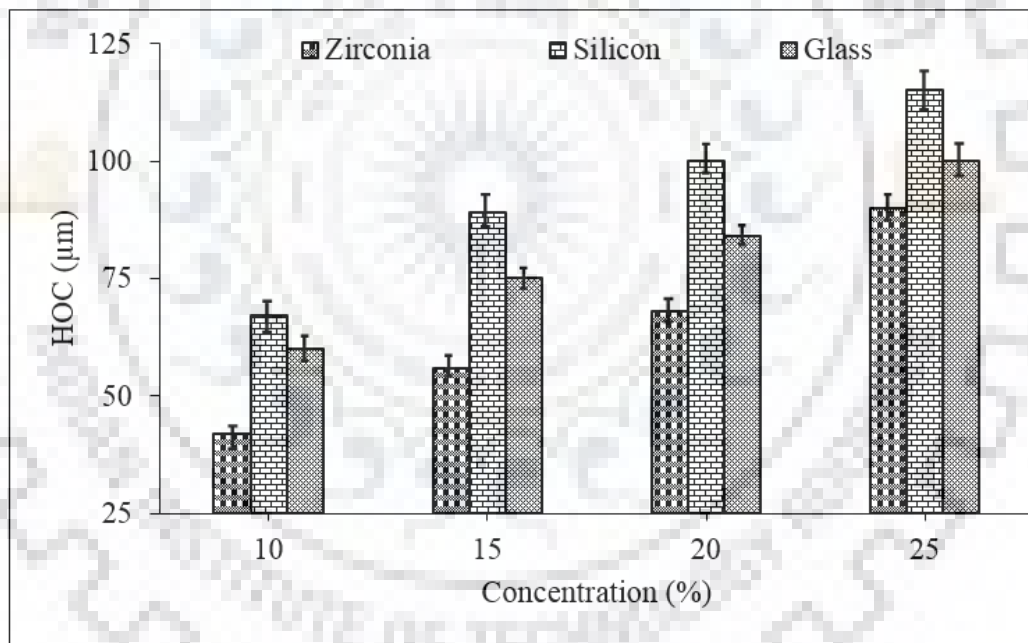
Figure 5.12 Effect of concentration on HOC

It is to be noticed that in all cases with all the parametric conditions shown in Figures 5.1 to Figure 5.12, maximum MRR and DOH were obtained in silicon followed by glass and zirconia work material. The HOC was also higher in silicon as compared to glass and zirconia. These results clearly indicate that the properties work material such as hardness and fracture toughness also effect the performance (i.e. MRR, depth of hole and hole overcut) of rotary tool micro-USD

process. As per Table 5.1, the order of the hardness for the work materials is zirconia > silicon > glass. Whereas, the order of fracture toughness of work material is zirconia > glass > silicon. The experimental results indicated that the order of MRR and HOC coincided with the order of fracture toughness of work materials. Therefore, it can be said that the fracture toughness plays more significant role than hardness in material removal during rotary tool micro-USD process. It is to be noticed that silicon is monocrystaline material and zirconia is a polycrystalline material. On the application of load, crack propagates more easily in monocrystalline materials rather than the polycrystalline materials. This is because propagation of dislocation in monocrystalline material faces very less resistance due to absence of grain boundary. On the other hand, grain boundaries present in polycrystalline material hinder the movement of dislocations which ultimately increase its fracture toughness. Low fracture toughness of silicon promoted generation and propagation of cracks and eventually material removal due to the impact by abrasives in rotary tool micro-USD process. As a result of that silicon exhibited in higher MRR, DOH as well as HOC as compared to glass and zirconia. These results concur with the findings of Komaraiah and Reddy, (1993).

From the above discussion, it can be said that the work material properties greatly affect the machining rate of rotary tool micro-USD process. By considering this fact, the effects of work material properties on the quality of machined holes were also analyzed. In order to study these effects, SEM micrographs of machined hole periphery were considered and machining induced damage/edge chipping was observed in all the three work materials. The micrographs are presented in Figure 5.13. From Figure 5.13, it can be clearly seen that the edges of the hole are smooth in case of zirconia work material (as evidenced in Figure 5.13(a) as compared to silicon and glass. The edge chipping around the hole periphery was also found to be minimum (i.e. 21 µm) in zirconia. On the other hand, maximum edge chipping (i.e. 74 µm) on the periphery of machined hole was observed in case of silicon work material as evidenced in Figure 5.13(b). The edge chipping (i.e. 44 µm) in glass was found to be lesser than silicon but higher than zirconia (as evidenced in Figure 5.13(c). It can be seen in Figure 5.13(a)-(c) that the machining damage was in the decreasing order of the fracture toughness of the work materials (i.e. silicon < glass < zirconia). Thus, it can be concluded that low fracture toughness of silicon is responsible for higher damage. Due to low fracture toughness of silicon, the edges of the hole got damaged easily while entering and exit of abrasives in the machining zone. On the other hand, higher

fracture toughness of zirconia provided resistance against cracking/damage and as a result of that relatively smooth edges of hole were obtained.
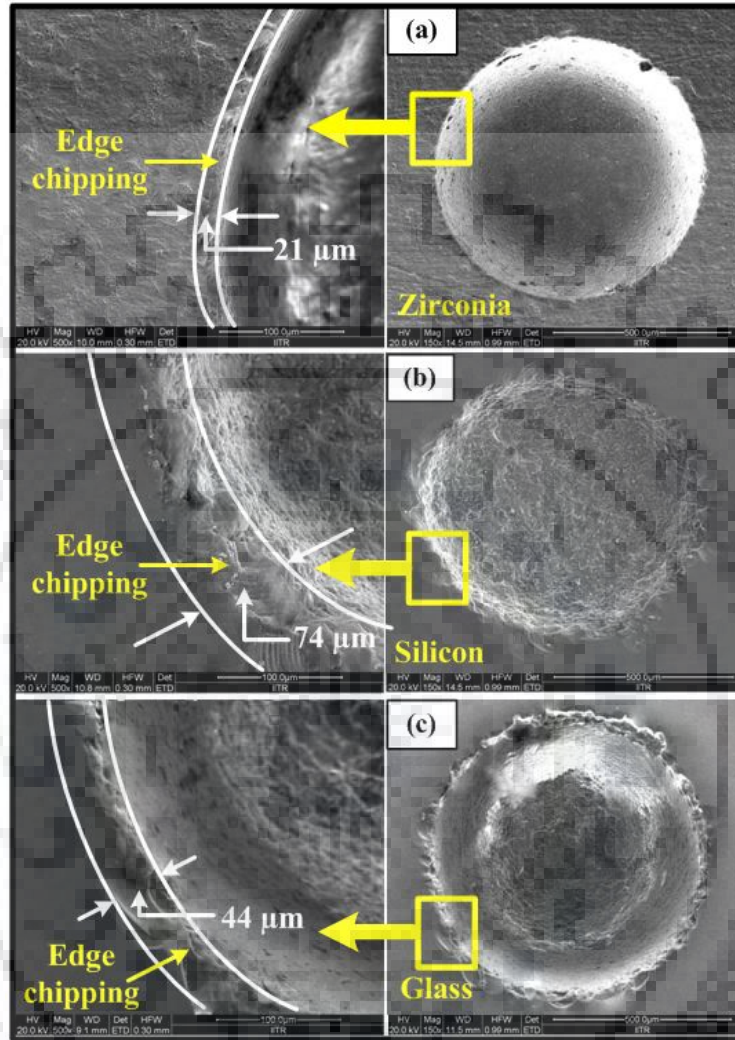
Figure 5.13 Quality of hole surface (a) zirconia, (b) silicon and (c) glass [experimental condition: rotation speed = 300 rpm, power rating = 40%, abrasive size = #1000 mesh, concentration = 20%]

After studding the effect of rotary tool micro-USD process parameters on its response characteristics, the tool wear during rotary tool micro-USD process was also analyzed. In order to analyze the tool wear, experiments were conducted on zirconia, silicon and glass work materials by varying the machining time from 60-90 sec with an interval of 15 sec. After the completion of each experiment, the tool wear was measured in terms of reduction in length of tool (i.e. longitudinal tool wear). Optical microscope was used to measure the reduction in length of tool. The results obtained are furnished in Figure 5.14. After machining, the images of the

worn out tool were also captured using stereo microscope. These images are furnished in Figure 5.15. On increasing the machining time from 60-90sec., the tool wear was found to be increased continuously (Figure 5.14). The maximum tool wear was observed during machining of zirconia (as evidenced in Figure 5.15). Whereas, minimum tool wear was observed during machining of glass. This can explained with the fact that work material hardness played a major role in tool wear. Because, the hardness of zirconia is maximum and the glass has minimum hardness among all three work materials. This implies that the tool wear in rotary tool micro-USD process is directly proportional to the hardness of the work materials. This can be inferred that in case of harder work material (i.e. zirconia), the indentation by the abrasive into the tool surface was also higher. That led to removal of more material from tool surface. Whereas in case of relatively less hard work material (i.e. silicon and glass), the indentation by the abrasives on the tool surface was lower. Due to this, lesser tool wear was observed. Further, from Figure 5.15, it is interesting to note that rotary tool micro-USD process resulted in almost negligible lateral wear (i.e. taper formation on tool vertical surface) of tool during machining of micro-holes in all the work materials. The tool was found to be suffered from longitudinal wear and edge rounding wear. Longitudinal wear is already explained and edge rounding wear is the reduction in tool machining face diameter. The edge rounding wear of tool was higher during machining of zirconia as compared to silicon and glass (as evidenced in Figure 5.15). It occurred due to the abrasion caused by moving abrasives and tool bottom edge when the abrasives exit from machining gap (Cheema, (2015)).
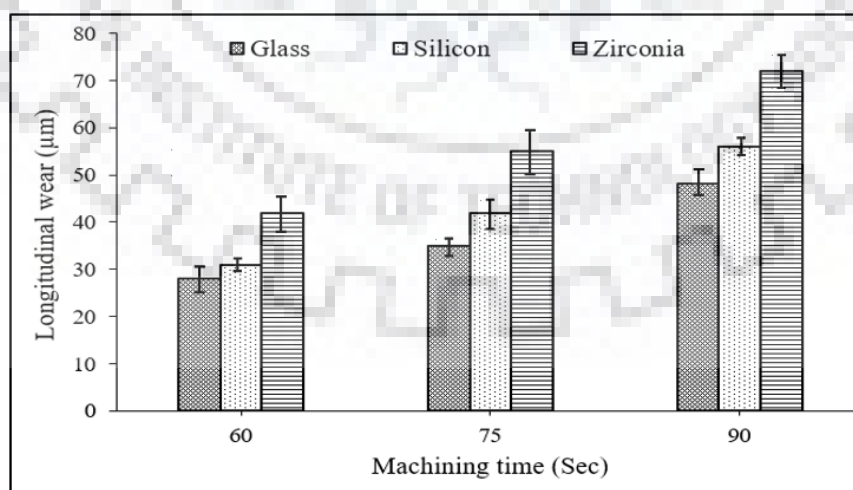
Figure 5.14 Effect of machining time on tool wear [experimental condition: rotation speed = 300 rpm, ultrasonic power = 40%, abrasive size = #1000 mesh, concentration = 20%].

Machined material	Machining time (Sec)		
	60	75	90
Borosilicate glass	(a) 500 μm	(b) 500 μm	(c) 500 μm
Silicon	(d) 500 μm	(e) 500 μm	(f) 500 μm
Zirconia	(g) 500 μm	(h) 500 μm	(i) 500 μm
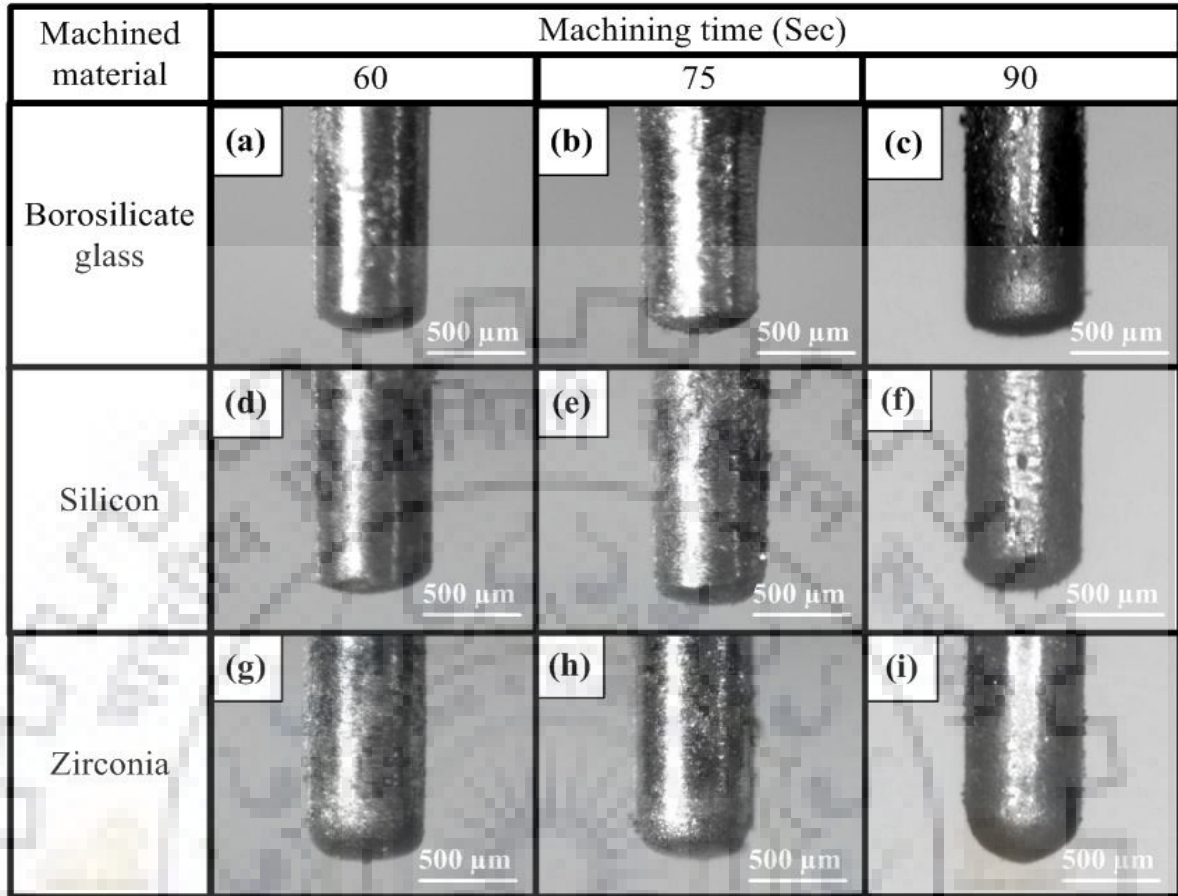
Figure 5.15 Microscopic images of tools at different time intervals after machining of (a-c) glass, (d-f) silicon and (g-i) zirconia

In order to understand any of the machining process, a clear understanding about its material removal mode is very essential. Therefore, with this objective, the mode of material removal during rotary tool micro-USD of zirconia, silicon and glass was also investigated. The machined surface topographies of work materials are shown in Figure 5.16. From Figure 5.16, it can be clearly seen that brittle fracture in the form of sharp cracks was the mode of material removal during rotary tool micro-USD process of all the three work materials. It is believed in impact machining that as the indentation depth reaches beyond the critical depth of indentation, micro cracks generate and propagate by the continuous impact of abrasives on work surface. Eventually, material is chipped off and created a crater on the work surface. The size of micro cracks was largest for silicon followed by glass and zirconia. These micro cracks are clearly evidenced in the magnified view of machined work surfaces shown in Figure 5.16(a)-(c). The large size of micro cracks for silicon work material again justifies it's higher rate of material removal and depth of hole as compared to glass and zirconia.
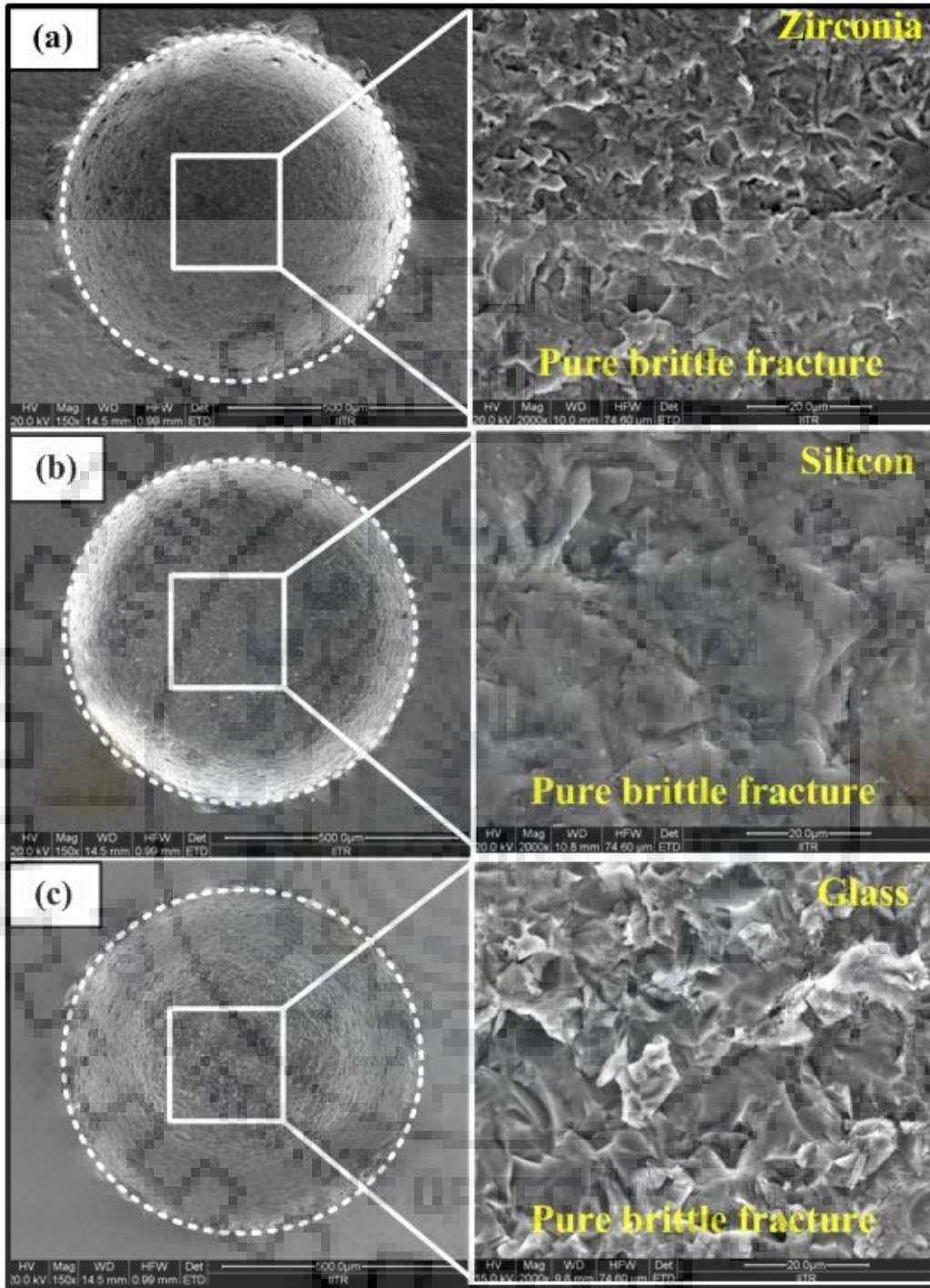
Figure 5.16 Machined hole morphology (a) zirconia, (b) silicon and (c) glass [experimental condition: rotation speed = 300 rpm, ultrasonic power = 40%, abrasive size = #1000 mesh, concentration = 20%]

5.1.4 Multi criteria optimization for microhole drilling

The experimental study is applicable to industries only if the effect of all the input parameters can be studied on its output parameters simultaneously. Also, in order to make a process industrially viable, optimization of its process parameters for desired multiple outputs is essential. Process optimization determines the maximum productivity and effectiveness of any process. It also helps the production engineer to select the input variable parameters to get a desired output. Many times multiple outputs of different nature (e.g. high material removal rate, high depth of hole and low hole overcut) are required simultaneously. In this particular case, owing to the conflicting nature of the responses, optimization becomes a complicated task. Even a slight change in the value of any input parameter may completely change the output of multiple responses. In order to resolve this problem researchers have been using several methodologies viz. desirability, grey relational analysis, genetic algorithms, utility and technique for order preference by similarity to ideal solution (TOPSIS) etc. for multi-objective optimization (Rao et al., (2010); Sharma et al., (2011); Cheema et al. (2013); Baishya et al., (2013); Sharma and Deb, (2014); Elsayed et al., (2014); Shi et al., (2015), Singh et al., (2017); Kumar and Singh, (2019); Malviya and Desai, (2019)). In the current research work, a desirability approach based on multi-response optimization was used to optimize the RTMUSD process for maximum MRR, depth of hole and minimum hole overcut. This approach was proposed by Derringer and Suich, (1980) and it is frequently used for MRO. In this approach, each of the response variable y_i is normalized to a desirability value d_i which lies in between 0-1. The value of d_i depends upon the "desirability" of corresponding response. The value of d_i increases/decreases with an increase/decrease in response's desirability. The value of $d_i = 0$ shows the undesirable response. On the other hand, if the value of $d_i = 1$, it shows completely desired response. Following equations are used to express the individual desirabilities as per the desired response (i.e. "higher the better" or "lower the better").

For "higher the better"

$$d_i = \begin{cases} 0 & y_i \leq y_{min} \\ \left[\dfrac{y_i - y_{max}}{y_{max} - y_{min}}\right]^r & y_{min} < y_i < y_{max} \\ 1 & y_i \geq y_{max} \end{cases} \tag{5.1}$$

For "lower the better"

$$d_i = \begin{cases} 1 & y_i \leq y_{min} \\ \left[\dfrac{y_{max} - y_i}{y_{max} - y_{min}}\right]^r & y_{min} < y_i < y_{max} \\ 0 & y_i \geq y_{max} \end{cases} \qquad (5.2)$$

where, y_{max} and y_{min} represents the maximum and minimum value of y_i. The value of r decides the shape of desirability function and its value ranges from 0.1-10. After determining the value of d_i, overall desirability (d) is calculated using Eq. 5 by taking the geometrical mean of all individual desirability.

$$d = (d_1 \times d_2 \times d_3 \ldots \ldots \ldots \ldots \ldots \times d_k)^{\frac{1}{k}} \qquad (5.3)$$

The Minitab-17 software was used to carry out the optimization. During optimization, the objective function (i.e. desired responses) were set to 'maximize MRR and DOH and 'minimize HOC. The input parameters values (both upper and lower) for all the responses were set to 'in range' as tabulated in Table 5.6. Each of the response was given equal weightage owing to the reason that both machining efficiency (i.e. MRR and DOH) as well accuracy (i.e. HOC) of machined feature are essential for any machining process. The optimization results and plot are presented in Table 5.7 and Figure 5.17 respectively. From Figure 5.17, it can be depicted that power rating 42.22%, rotation speed 500 rpm, abrasive size #1800 mesh and concentration 23.93% with 88.22% desirability was the optimal parametric setting for desired responses (i.e. maximum MRR of 0.513 mg/min, maximum DOH of 652.96 μm and minimum HOC of 72.76 μm).

Table 5.6 Range of process parameters for MRR, DOH and HOC

Input parameters	Goal	Constraint limits	
		Lower	Upper
Power rating (%)	In range	20	60
Rotation speed (rpm)		100	500
Abrasive size (mesh)		#1000	#1800
Slurry concentration (%)		10	25
Output parameters	Goal	Weightage	
MRR (mg/min)	To maximize	1	
Depth of hole (μm)			
Hole overcut (μm)	To minimize		

146

Table 5.7 Optimization results

Process parameters	Optimal values	Avg. MRR (mg/min)	Avg. DOH(μm)	Avg. HOC (μm)	Desirability (%)
Power rating (%)	42.22				
Rotation speed (rpm)	500	0.513	652.96	72.76	88.22
Abrasive size (mesh)	1800				
Concentration (%)	23.93				
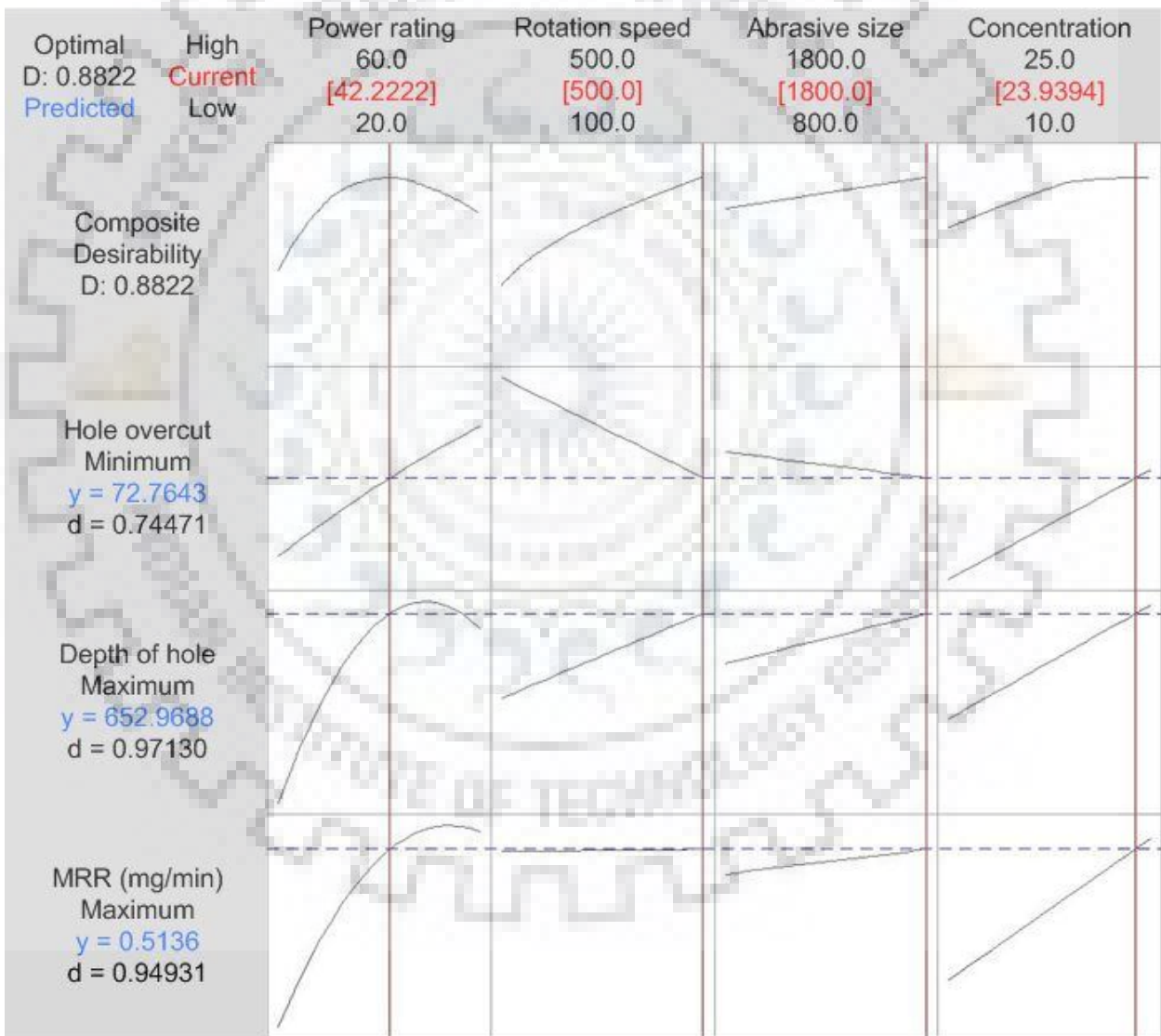
Figure 5.17 Optimization plot

After obtaining the optimal parametric setting, the rotary tool micro-ultrasonic drilling process was utilized for machining of deep micro-holes. The optimal parametric conditions of ultrasonic power = 40%, rotation speed = 500 rpm, abrasive size = #1800 mesh and concentration = 24% were used during deep micro-hole machining. During experiments, the machining was performed at 150 sec, 210 sec and 300 sec. For all the experiments same tool was used. After machining, the form accuracy of the machined micro-holes was examine and analyzed with the help of SEM micrographs presented in Figure 5.18(a)-(c). The micrographs presented in Figure 5.18(a)-(c) indicated that with an increase in machining time from 150 sec to 300 sec, the DOH significantly increased. It is evidenced in Figure 4.71(a) that the wall of the machined micro-hole was almost straight at lower depth. As the DOH increased slight taper and edge rounding was observed on the wall and corners of the bottom surface of holes (Figure 5.18(b) and (c)). The reason for this taper formation and edge rounding seems to be the poor slurry circulation or crushing of abrasives at higher depth which may results in edge rounding wear of tool. Consequently, holes with slightly rounded corners at bottom were obtained. The machining time of 300 sec resulted in micro-hole with 4355 µm depth. As far as micro hole machining of glass is concern, the depth of hole achieved in this study is higher than the depth of holes reported in the literature available.
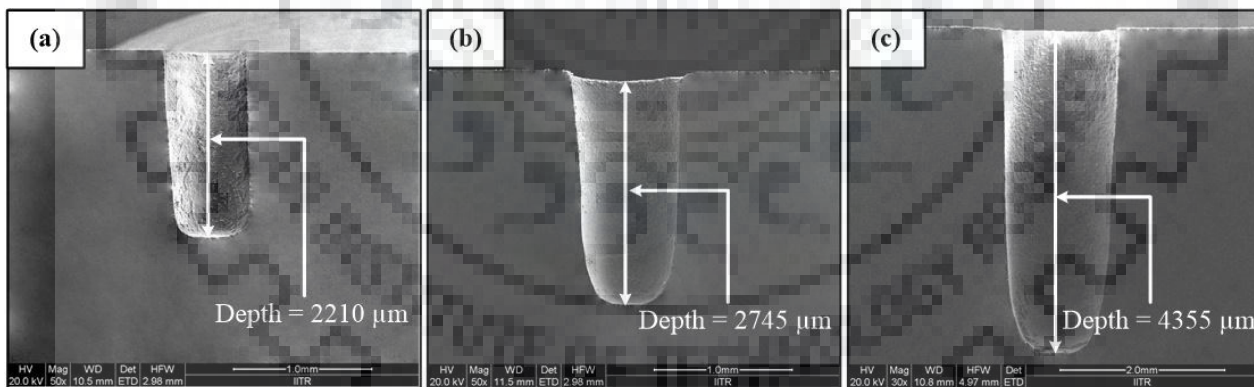
Figure 5.18 Microscopic cross-sectional views of machined micro-holes

5.2 Summary

In the present chapter, rotary tool micro-USD process is utilized for machining of microholes in hard and brittle materials. Three work materials i.e. glass, silicon and zirconia were machined and the effect of rotary tool micro-USD process parameters was investigated on its performance. It was observed that maximum machining rate and machining depth were obtained during

machining of silicon. However, the overcut was also found maximum in silicon as compared to glass and zirconia. This indicates that fracture toughness of work materials as compared to their hardness play a major role in deciding the performance of rotary tool micro-USD process. Interestingly, the tool wear was observed to be higher during machining of zirconia owing to its higher hardness as compared to glass and silicon. This indicates that tool wear is dependent on hardness of work material instead of fracture toughness. In order to investigate the mode of material removal during rotary tool micro-USD process, machined surfaces of work materials were analyzed with the help of FESEM images. Pure brittle fracture was found to be the dominant mode of material removal in all three work materials. The rotary tool micro-USD process parameters were optimized by employing desirability approach to achieve maximum MRR, DOH and minimum HOC simultaneously. At optimal parametric combination, the rotary tool micro-USD process successfully machined a microhole of 4355 μm depth in glass work material.

INVESTIGATIONS ON TOOL WEAR AND ITS EFFECT ON FORM ACCURACY OF MICROCHANNELS

Tool wear is an inevitable phenomenon and hence a prime challenge in micro-USM process. Therefore, quantification and reduction of tool wear is essential to enhance the quality of machined microchannels. The objective of present chapter was to reduce the tool wear and to improve the form accuracy of microchannels machined by rotary tool micro-USM process. In order to achieve this objective, a quantitative relationships among the tool wear, form accuracy and MRR were established. Initially, different types of tool wear that occurs in rotary tool micro-USM process were identified on the basis of tool, abrasive and workpiece interaction phenomenon. Later, a geometrical model for the quantification of tool wear in rotary tool micro-USM process was developed. Further, the contribution of different types of tool wear on the dimensional as well as form accuracies were evaluated. Further, parametric investigation and optimization was carried out during fabrication of microchannels using rotary tool micro-USM process. The last section of this chapter deals with the machining of complex shapes microchannels for microfluidic applications.

6.1 Investigations on Tool Wear and its Effect on Form Accuracy of Microchannels

6.1.1 Introduction

In micro-USM the shape of the tool decides the final shape of the machined geometry. Thus, in order to get the desired dimensional and form accuracy of the microfeatures, it is essential to retain the shape of the tool (i.e. reduction of tool wear) (Hu et al., (2007)). However, tool wear is an inevitable phenomenon and hence a challenge in micro-USM process. Accumulation of abrasives/debris inside machining gap is mainly responsible for tool wear and thereby poor accuracy of microfeatures. Tool wear can be reduced by the replenishment of abrasive slurry in the machining zone by providing rotary motion to the tool. Therefore, in this research work, rotary motion was provided to the tool to reduce the tool wear. Apart from this, wear compensation is another method to reduce/control tool wear (Yu et al., (2004)). Wear compensation can be applied only after quantifying the amount of tool wear. As mentioned in

chapter 2, some strategies were proposed by researchers to measure the tool wear (Jain et al., (2012); Yu et al., (2012); Cheema et al., (2015)), but these strategies are limited to stationary tool micro-USM process only. As far as rotary tool micro-USM process is concerned, no information about the amount of tool wear, type of tool wear and their effect on dimensional and form accuracy of machined microfeatures were revealed by the published literature. Thus, in this chapter, experiments were performed to understand the different types of tool wear in rotary tool micro-USM process. During experimentation, microchannels were machined on borosilicate glass using rotary tool micro-USM process. The effects of rotary tool micro-USM process parameters on the tool wear were investigated. A two-dimensional (2D) geometrical model for the quantification of tool wear was developed by measuring the wear dimension of the tool. This 2D model was then converted into three dimensions for evaluating the total volumetric wear (TVW) of tool. In addition, after quantifying the tool wear, the contribution of the different types of tool wear on dimensional as well as form accuracies were evaluated and rotary tool micro-USM process parameters were optimized for desired responses

6.1.2 Experimental facility and measurement methods

The ultrasonic drilling was performed on an in-house developed facility of rotary tool micro-USD process shown in Figure 3.2. The detailed description of the micro-USD facility is provided in chapter 3. In order to investigate the effect of tool wear, microchannels were machined on borosilicate glass work material. During machining, tungsten carbide and silicon carbide were selected as tool and abrasive materials. Tap water was selected as liquid medium for slurry owing to its low cost and easy availability. The abrasive slurry was fed in the machining gap at a constant rate throughout machining to avoid any kind of turbulence. Tool rotation speed, work feed rate, power rating, slurry concentration and abrasive size were used as variable parameters in this experimentation. The process parameter with their levels are given in Table 6.1. The experimentation was performed using OFAT approach. The MRR, DOC, WOMC, form accuracy and total volumetric wear (TVW) of tool were selected as response characteristics. The process parameter and their levels are given in Table 6.1. A stereo zoom microscope (Make: NIKON SMZ-745T (Figure A.4 of Appendix A)) with image analysis and measurement facility was used to measure the tool wear in 2D. The dimensional and form accuracies were measured and analyzed by using image analysis toolbox of MALAB v.2016b. MRR was measured as per

the procedure given in section 3.3 of chapter 3. The dimensional accuracies of microchannels were measured in terms of WOMC and machined DOC using stereo zoom microscope. The form accuracy of microchannels was measured as per the procedure given in section 3.3 of chapter 3. Each experiment was conducted thrice at same parametric setting and mean value was consider as final response.

Table 6.1 Process parameters settings for microchannel fabrication

Variable process parameters	
Power rating (PR)	20, 30, 40, 50, 60%
Rotation speed (RS)	100, 200, 300, 400, 500, 600 rpm
Feed rate (FR)	10, 15, 20, 25, 30 mm/min
Abrasive size (AS)	1000, 1200, 1800 mesh
Slurry concentration (SC)	10, 15, 20, 25, 30%
Constant process parameters	
Frequency	20 ± 1 kHz
Static load	45 g
Tool diameter (Ø)	600 µm
Tool material	WC
Tool geometry	Cylindrical

6.1.3 Tool wear mechanism in rotary tool micro-USM process

The different types of tool wear during rotary tool micro-USM process in fabrication of microchannels were not revealed from the published literature. However, investigation had been conducted on types of tool wear during micro-USM process (Cheema, (2015)). Thus, in order to understand the types of tool wear in rotary tool micro-USM process, it is imperative to first understand the types of tool wear that prevail in micro-USM process. In micro-USM process, the tool vibrates at ultrasonic frequency and repetitively strikes on the abrasive particles, which are present in the machining gap. The quantity of abrasive particles in the machining gap at a time instance, depends on the size of machining gap and abrasive slurry concentration. The physical reasons for tool wear are direct or indirect interactions of tool, abrasive particle and work material. Literature, suggests that three types of interactions during micro-USM process, that

results in tool wear, namely tool-abrasive, tool-abrasive particle-work and tool-work. A solid and smooth tool with longitudinally cylindrical cross-section is considered for all these interactions.

The first type of interaction is tool-abrasive particles interaction. This interaction takes place when the displacement amplitude of vibration is greater than the size of selected abrasive particles. This implies that as the tool goes to its initial equilibrium position, the machining gap. While coming to the final equilibrium position, the tool strikes on abrasive particles underneath. In turn, abrasive particles impact on the work surface (Figure 6.1(a)) and create small craters on it. Owing to very large machining gap, in this interaction, the abrasive particles may form multiple layers over each-other (Figure 6.1(a)). Consequently, these abrasive particles interact with each other and lose their energy before impacting on the work material surface. This results in lower MRR. In addition, later to impact on the work material, if abrasive particles rebound, they will abrade the machining face (bottom face) of the tool (Figure 6.1(b)). The result in loss of tool material from the machining face and reduction in length of tool. This reduction is termed as longitudinal wear (Cheema et al., (2015)). The abrasion of tool by abrasive particles also wear out the sharp edges of tool, i.e., at the intersection of cylindrical surface and bottom surface of the tool (Figure 6.1(c)). Thus, machining face will have a reduction in tool diameter on continuation of micro-USM process. This wear has been referred as edge rounding wear (Cheema et al., (2015)). Also, a 3 body abrasion takes place in the lateral gap due to which some material is removed from the vertical surface of tool and may result in taper of tool as well as machined surface. This taper formation in the tool vertical surface is termed as lateral wear (Cheema et al., (2015)).
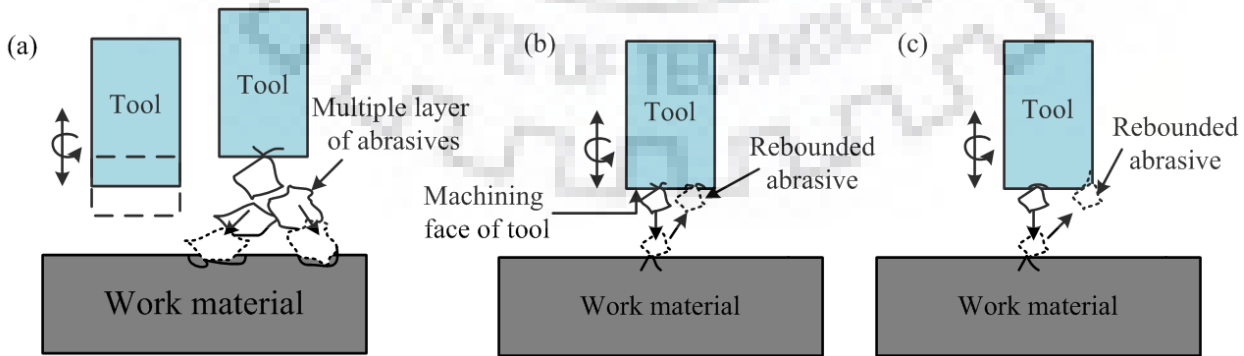
Figure 6.1 Tool-abrasive interaction (a) multiple layers of abrasives in the machining gap (b) wear of machining face of tool (c) wear of tool edge

The second type of interaction that wears tool during micro-USM process is tool-abrasive-work. It exists when the size of selected abrasive particles is approximately equal to the displacement amplitude of vibration. Here, when tool moves to its initial equilibrium position (Figure 3.12), the machining gap is just sufficient to permit entry of only single layer of abrasive particles between the tool and work material (Figure 6.2). While moving downward, the tool performs hammering action on the abrasive particles. Subsequently, these abrasive particles strike uniformly on the surface of the work material. During hammering action, the energy imparted by the tool to the abrasive particle is completely transferred to the work material and results in a theoretical maximum of MRR. Also, this localized hammering causes indentations on the machining face of tool and results in reduction in tool length, i.e., longitudinal tool wear.

Figure 6.2 Tool-abrasive particle-work interaction

The third type of interaction that wears tool during micro-USM process is tool-work interaction, i.e., a direct contact between tool and work material. Though, absolutely undesirable but it may occur when the displacement amplitude of the tool is smaller than the size of selected abrasive particles. This results in a very narrow machining gap that may restrict the entry of abrasive particles in the machining gap (Figure 6.3(a)). Thus, the tool performs a direct hammering on work surface. This results in the formation of radial/median cracks followed by the lateral cracks due to excessive loads by the direct contact of the tool to the work material (Figure 6.3(b)). These cracks cause severe damage to both, the tool as well as work.

Displacement amplitude < Abrasive size

(a)   (b)

Tool

Tool

Tool

Median crack —   Lateral crack   Radial crack

Work material

Contact surface

Work material
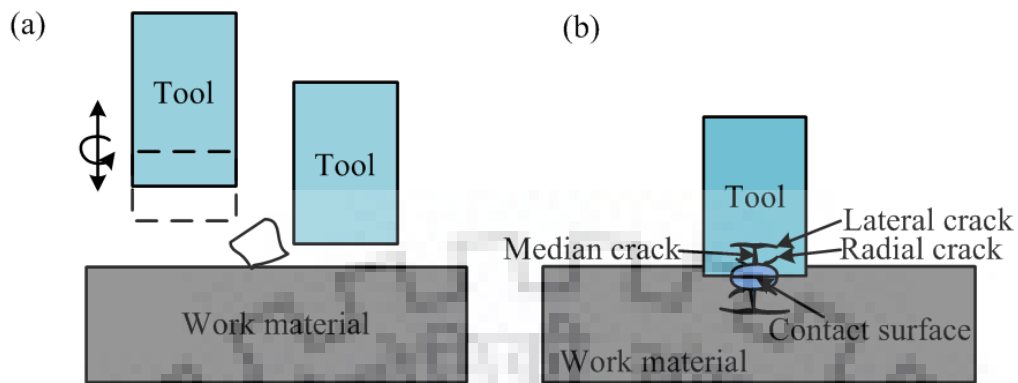
Figure 6.3 Tool-work direct interaction (a) restricted abrasive particle (b) brittle fracture

In rotary tool micro-USM process, apart from direct or indirect interactions of tool, abrasive particles and work in the machining gap, there exist centrifugal force, which provide interaction of abrasive particles and vertical wall of work material in the lateral gap. Thus, experimentation on rotary tool micro-USM process was conducted using reduced OFAT approach to investigate the types of tool wear with combination of parametric settings given in Table 6.1.

In order to investigate the mechanism of tool wear in rotary tool micro-USM process, a qualitative comparison of the tool shape was carried out with the help of microscopic and SEM images. The rotary tool micro-USM process tools before machining and worn out tools post machining revealed that all the worn out tools had similar types of tool wear. The Figure 6.4(a) shows microscopic image of one such tool. The longitudinal wear, similar to micro-USM process was observed in rotary tool micro-USM process (Figure 6.4(a-2)). It seems that continuous hammering and abrasion are responsible for this type of tool wear. This can be explained with fact that during rotary tool micro-USM process, as the tool repeatedly strikes on abrasive particles present into the machining gap, the abrasive particles in turn impact/hammer on the work surface leading to the generation of micro cracks. These micro cracks merge with each other and form craters on work surface and consequently, the material removal takes place. Similar impacts and hammering action are faced by the tool. The machining face of tool suffered by hammering/impact action is schematically shown in Figure 6.5 as zone 1. Due to continuous hammering/impact action in zone-1, as soon as the tool material exceeds its fatigue limit some material get dislodged from the machining face of the tool in the form of small craters. These

craters are clearly evidenced in Figure 6.6(a) and (b). Consequently, the length of the tool get reduced. After impacting on the work surface these abrasive particles move towards the lateral gap through zone 2 (Figure 6.5) and fresh abrasive particles enters into the machining gap. As mentioned in the earlier, the vibratory motion of tool creates high pressure into the machining zone which accelerates the movement of the existing abrasive particles in machining gap toward the exit through lateral gap. While moving towards lateral gap the abrasives particles come in contact with the vibrating as well as rotating machining face of the tool and abrade its edges in zone-2. The abraded edge of the tool is evidenced in Figure 6.6(c). The arrows shown in Figure 6.6(c) indicate the direction of abrasive particles motion during the abrasion of tool. The abrasion results in edge rounding wear on the machining face of the tool. The edge rounding wear is apparent from the front view of the microscopic image of worn out tool, shown in Figure 6.4(a-2). Further, the diameter of machining face of tool reduces. The reduced diameter on machining face of the tool is evidenced from Figure 6.4(a-3).

An interesting observation was made from Figure 6.4(a-2) that during rotary tool micro-USM process, there was negligible lateral wear. This was contrary to the types of tool wear observed with micro-USM process without any tool rotation. The tool rotation in rotary tool micro-USM process exerts centrifugal force on the abrasive particles in the outward direction from the axis of rotation. Also, due to tool rotation, the vertical surface area of tool continuously changes and the time available for interaction between abrasive particles and lateral face of tool is less. Consequently, the abrasive particles abrade vertical surface of work material far more than the lateral face of tool. Thus, the types of tool wear in rotary tool micro-USM process are only longitudinal wear and edge rounding wear. The schematic illustration of worn out tool is shown in Figure 6.4(b).
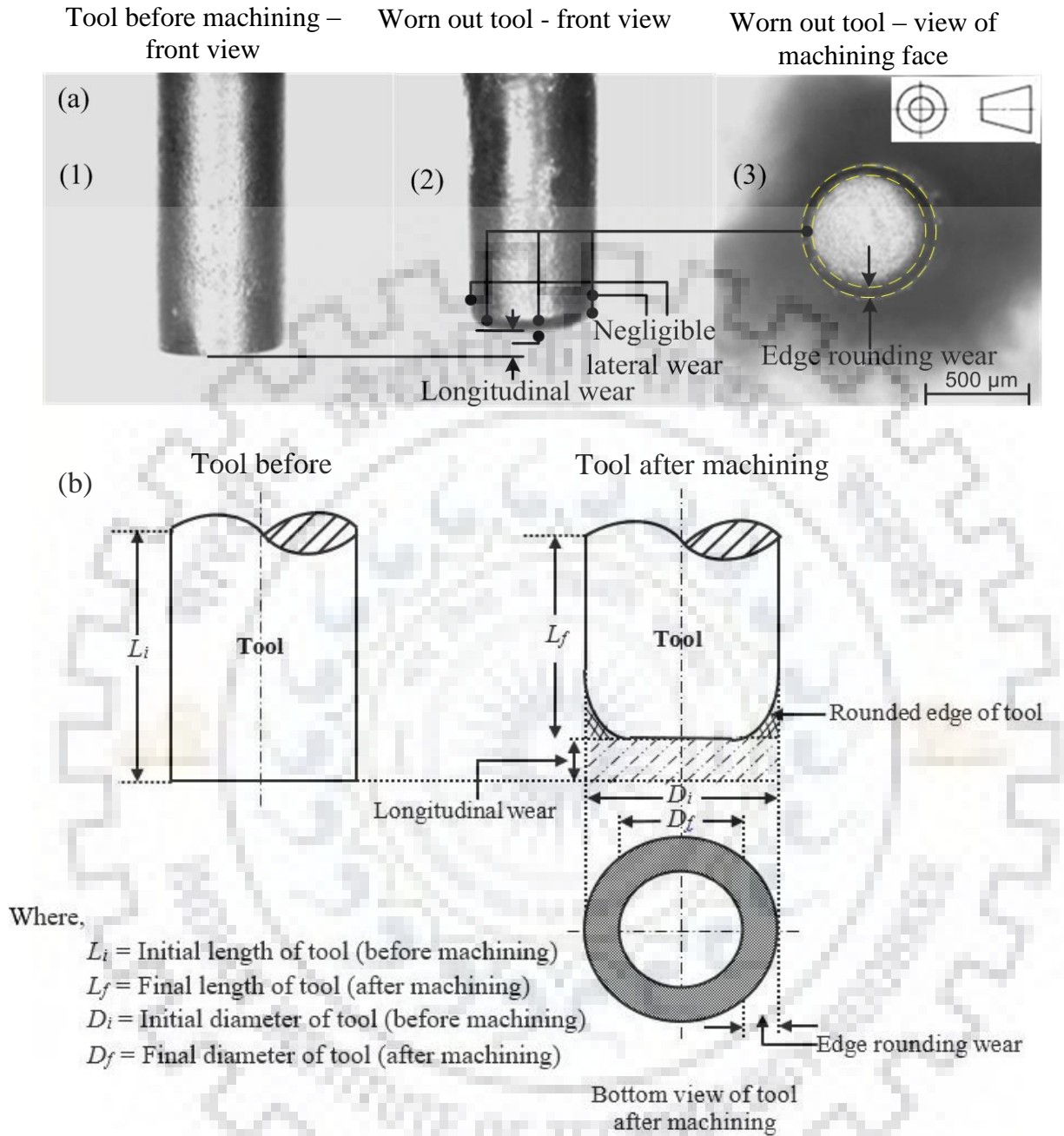
Figure 6.4 (a) Microscopic images of tool before and after machining (b) schematic illustration of tool wear in rotary tool micro-USM process
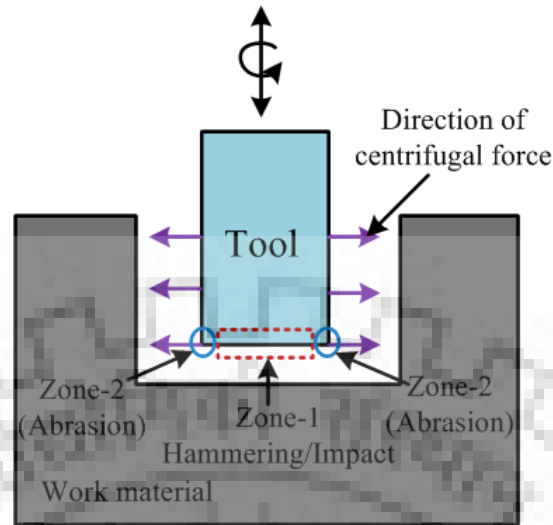
Figure 6.5 Schematic showing zones of hammering/impact and abrasion of tool
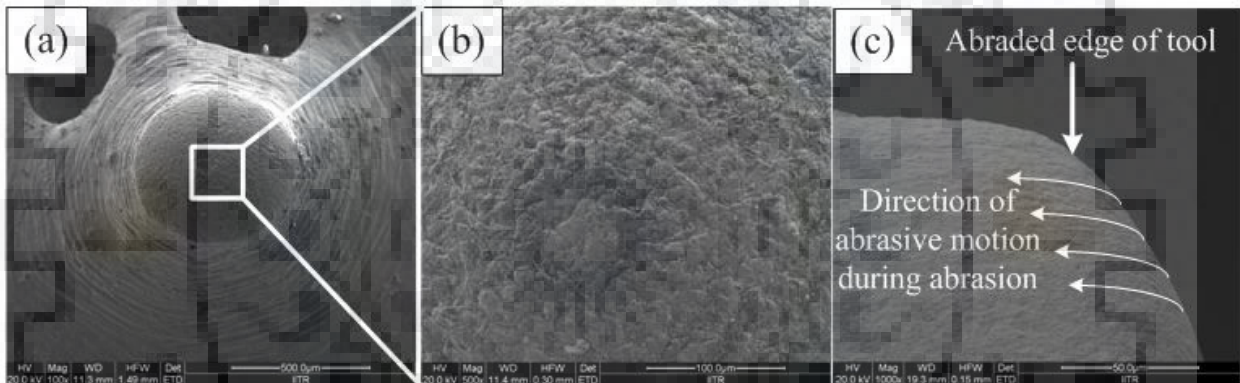
Figure 6.6 FESEM image of worn out tool showing (a) machined face of tool (b) magnified view of machined face of tool (c) abraded edge of tool

It can be suggested that predominant mechanisms of rotary tool micro-USM process that results in tool wear are hammering, impact (on machining face) and abrasion (on edges). These mechanism results in fatigue loading on tool (Yu et al., (2012); Jackson and Davim, (2011)). It seems that rotary tool micro-USM process can provide better form accuracy of the machined micro channels. However, it is imperative to note that vertical surface of work material in the lateral gap is continuously abraded by abrasives during rotary tool micro-USM process. It can be presumed that machined cavity will have certain taper (Figure 6.7(a) and (b)). If better form accuracy is desired, it is essential to quantify tool wear and later relate this tool wear with form accuracy of machined micro channels. Additionally, it is essential to identify those machining conditions which result in lowest possible tool wear (longitudinal and edge rounding) and best

159

possible form accuracy. This will also result in better understanding of the rotary tool micro-USM process. The subsequent section details the quantification of linear tool wear from 2D images of worn out tool by converting them into three dimensions for volumetric tool wear.
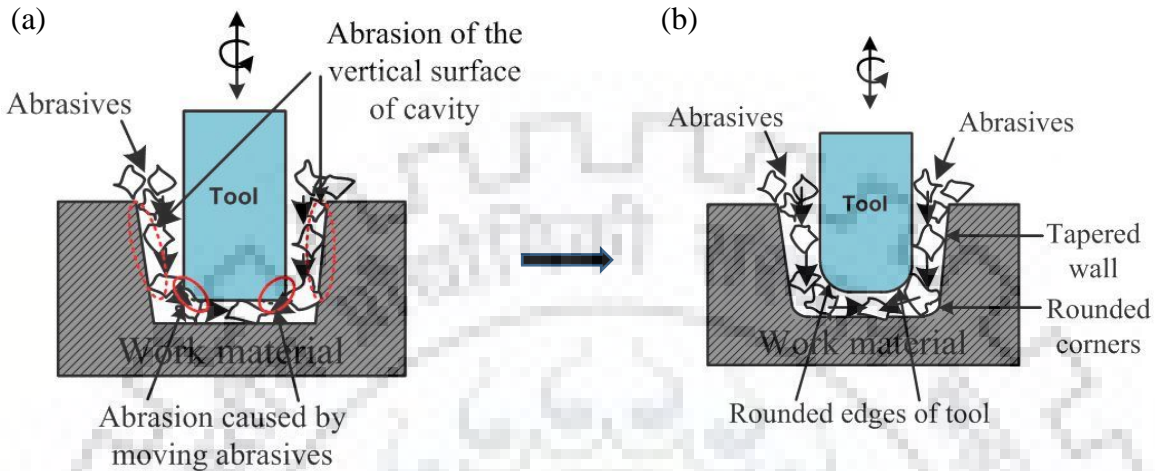
Figure 6.7 Tapered vertical surface of work material (a) during rotary tool micro-USM process (b) post rotary tool micro-USM process

6.1.4 Mathematical analysis of tool wear

Quantification of tool wear is very essential in micro-USM process to achieve desired machining accuracy. Quantification can be done in two ways i.e. by weight measurement technique and linear measurement technique. Weight measurement technique seems to be ineffective at micro-level since it requires highly precise weighing equipment. Also, it does not provide information about the wear distribution on the tool surface. Linear measurement of tool wear is a better alternative in micro-domain measurement. But, it only works when a uniform wear takes place on tool surface. In case of non-linear wear of tool surface multiple measurement are required to quantify the tool wear. In rotary tool micro-USM process, non-uniform wear takes place on the tool surface. Tool wear can be distributed into different wear zones that depend on the nature of tool, abrasive particle and workpiece interactions as discussed in previous subsection. In this section the quantification of non-linear tool wear is presented with the help of a mathematical model. Two dimensional tool wear measurements were carried out and subsequently converted into a three dimensional measurement model. The developed model helped in quantification of tool wear in rotary tool micro-USM process. Thereafter, required compensation can be provided to the tool during machining to achieve desired dimensional and form accuracy of machined

microfeatures. Primarily, tool wear in rotary tool micro-USM can be quantified considering the following two categories:

(A) Longitudinal wear

The longitudinal wear is occurs due to hammering/impact and cavitation actions in the machining gap. It affect the depth of microfeatures to be developed. Longitudinal tool wear refers to the reduction in length of the tool during machining. The longitudinal tool wear in rotary tool micro-USM process is schematically illustrated in Figure 6.8. If L_i is the tool length before machining and L_f is the tool length after machining. The volume of tool worn out by longitudinal wear ($V_{Longitudinal\ wear}$) for a solid cylindrical tool can be calculated using Eq. (6.1).
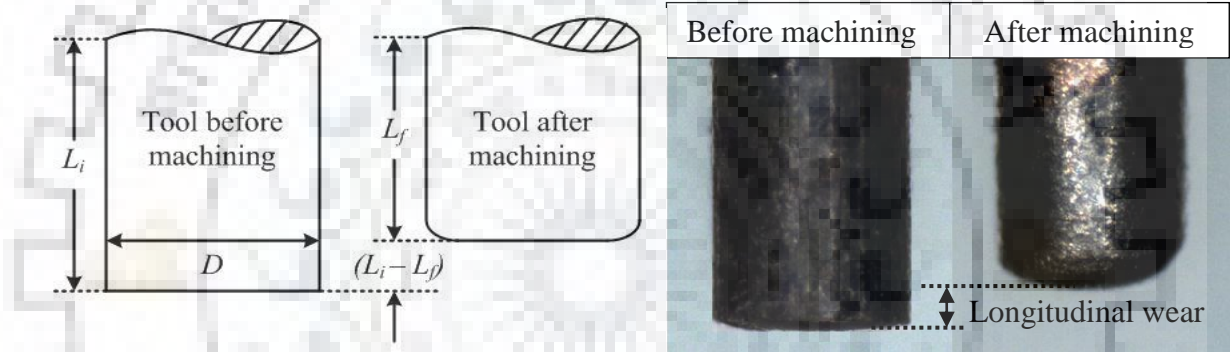
Figure 6.8 Schematic representation and actual images of tool before and after machining

$$V_{Longitudinal\ wear} = \pi r^2 (L_i - L_f) \tag{6.1}$$

where, r is the radius of the tool

(B) Edge rounding wear

During machining, the abrasive particles presents in the machining gap needs an exit that is provided by the lateral gap. During exit from machining gap towards lateral gap these abrasive particles come in contact with the vibrating as well as rotating machining face of the tool and abrade its edges as evidenced in Figure 6.9(c). The abrasion results in reduction of tool face diameter which is termed as edge rounding wear (Figure 6.9(a)).

The volumetric edge rounding wear can calculated by tracing the rotary tool micro-USM's tool edge after machining. The traced profile was assumed as a quadratic curve. This curve passes

through the rectangular surface (PQRS) as shown in Figure 6.9(a). The right section of the quadratic curve (traced profile) represents the edge rounding wear on the tool. The tool rotation results in edge rounding wear throughout the machining face (Figure 6.9(b)).
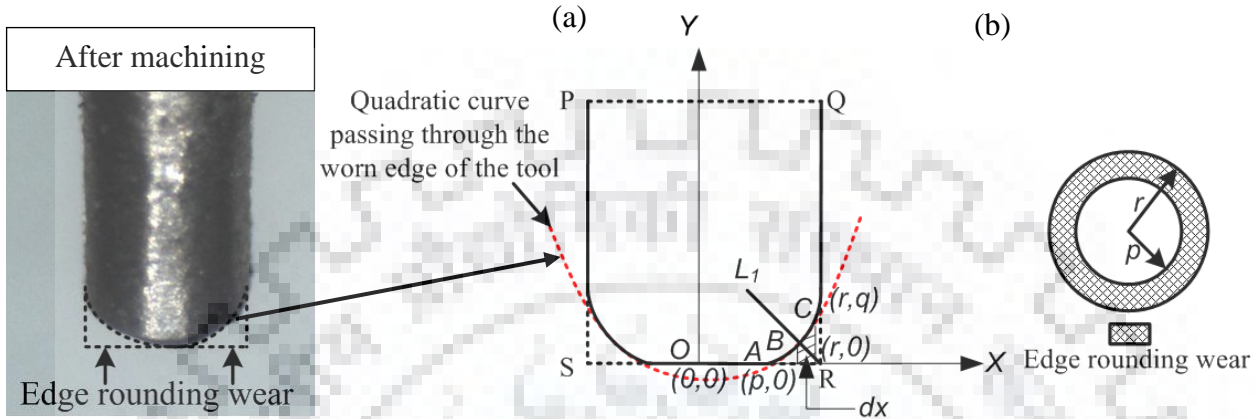
Figure 6.9 Schematic representation of (a) traced profile (b) bottom view of tool after machining

The quadratic curve passes through points A, B and C on the worn out tool (Figure 9a) with length of curve sections AB equal to BC. The co-ordinates of point A, C and R are (p, o), (r, q) and (r, 0), respectively. Where, p is the radius of machining face of the tool (reduced diameter) after machining and q is the height up to which edge rounding wear occurred. Considering, the general quadratic equation as:

$$y = mx^2 + c \tag{6.2}$$

where, m and c are the constants.

Since, both the points A and C are on the considered quadratic curve, these points will satisfy the curve's equation. Thus the equation of this curve will then be:

$$y = \frac{q(x^2 - p^2)}{(r^2 - p^2)} \tag{6.3}$$

The distance between the points A (p, 0) and R (r, q) will be equal to the distance between the points R (r, q) and C (r, 0), so $q = (r - p)$.

The volume of the edge rounding wear is given by the equation

$$V_{Edge\ rounding\ wear} = 2\pi \int_p^r x \frac{q(x^2 - p^2)}{(r^2 - p^2)} dx$$

$$= \frac{2\pi q}{(r^2 - p^2)} \int_p^r (x^3 - p^2 x) dx$$

$$= \frac{2\pi q}{(r^2 - p^2)} \left[\frac{x^4}{4} - \frac{p^2 x^2}{2} \right]_p^r$$

$$= \frac{2\pi q}{(r^2 - p^2)} \left[\frac{r^4}{4} - \frac{p^2 r^2}{2} - \frac{p^4}{4} + \frac{p^4}{2} \right]$$

$$= \frac{2\pi q}{(r^2 - p^2)} \left[\frac{r^4}{4} + \frac{p^4}{4} - \frac{p^2 r^2}{2} \right]$$

$$= \frac{2\pi q}{4(r^2 - p^2)} [r^2 - p^2]^2$$

$$V_{Edge\ rounding\ wear} = \frac{\pi q}{2} [r^2 - p^2] \tag{6.4}$$

Total volumetric wear $= V_{(Longitudinal\ wear)} + V_{(Edge\ rounding\ wear)}$

$$V_{Total\ volumetric\ wear} = \pi r^2 (L_i - L_f) + \frac{\pi q}{2} [r^2 - p^2] \tag{6.5}$$

The longitudinal wear, edge rounding wear and TVW of tool were calculated using Eqs. (6.1), (6.4) and (6.5) respectively to investigate the effect of tool wear on performance of rotary tool micro-USM process.

6.1.5 Analysis and discussion of results

In order to investigate the effect of tool wear and rotary tool micro-USM process parameters on dimensional and form accuracy of the machined microchannels, the experiments were conducted as per the experimental settings given in Table 6.1. The results are tabulated in Table 6.2.

Table 6.2 Process parameters and responses for fabrication of microchannels

Process parameters					Responses				
RS (rpm)	FR (mm/min)	PR (%)	AS (mesh)	SC (%)	Avg. WOC (µm)	Avg. DOC (µm)	Avg. FA (%)	Avg. TVW (mm³)	Avg. MRR (mg/min)
100	15	40	1200	15	690	285	84	0.028	1.69
200	15	40	1200	15	675	347	86	0.027	1.98
300	15	40	1200	15	645	389	88	0.025	2.10
400	15	40	1200	15	660	409	87	0.027	2.27
500	15	40	1200	15	670	560	86	0.031	3.19
600	15	40	1200	15	710	178	83	0.024	1.09
300	10	40	1200	15	645	280	85	0.036	1.54
300	15	40	1200	15	660	362	86	0.028	2.03
300	20	40	1200	15	690	471	86	0.026	2.74
300	25	40	1200	15	670	390	87	0.022	2.19
300	30	40	1200	15	640	380	88	0.018	2.03
300	15	20	1200	15	650	427	84	0.032	2.39
300	15	30	1200	15	680	551	85	0.034	3.21
300	15	40	1200	15	695	501	86	0.037	2.94
300	15	50	1200	15	690	485	86	0.042	2.83
300	15	60	1200	15	700	295	87	0.046	1.74
300	15	40	1000	15	665	258	87	0.038	1.45
300	15	40	1200	15	635	545	85	0.042	2.97
300	15	40	1800	15	710	298	84	0.022	1.83
300	15	40	1200	10	640	283	87	0.022	1.52
300	15	40	1200	15	665	342	86	0.031	1.92
300	15	40	1200	20	695	547	85	0.042	3.26
300	15	40	1200	25	690	335	86	0.044	1.96
300	15	40	1200	30	710	260	86	0.046	1.56
RS- Rotation speed, FR- Feed rate, PR- Power rating, AS- Abrasive size, SC- Slurry concentration									

Effect of tool rotation speed on tool wear, MRR, DOC, WOMC and form accuracy

Tool rotation speed is a dominant parameter in rotary tool micro-USM process. It plays an important role in this process as it facilitates the movement of abrasive particles in the machining gap. The dimensions of tool after machining at various tool rotation speeds were measured and subsequently used in subsection 6.1.4 to calculate longitudinal wear, edge rounding wear and total volumetric wear. The results are tabulated in Table 6.3 and plotted in Figure 6.10.

Table 6.3 Total volumetric wear of tool at different tool rotation speeds

Rotation speed (rpm)	LW	ERW	TVW	CLW	CERW
100	0.0085	0.0145	0.0230	36.87	63.13
200	0.0127	0.0049	0.0176	72.10	27.90
300	0.0141	0.0037	0.0178	79.18	20.82
400	0.0175	0.0062	0.0237	73.92	26.08
500	0.0249	0.0090	0.0339	73.36	26.64
600	0.0057	0.0069	0.0126	44.97	55.03

LW: Longitudinal wear (mm^3), ERW: Edge rounding wear (mm^3), TVW: Total volumetric wear (mm^3), CLW: Contribution of longitudinal wear (%), CERW: Contribution of edge rounding wear (%)

It can be seen from Figure 6.10 that by increasing the tool rotation speed, TVW decreased up to 300 rpm and thereafter it increased. On the other hand, the MRR increased by increasing the rotation speed up to 300 rpm and beyond that it decreased (Figure 6.11). This was attributed with the fact that rotary motion of the tool exerts centrifugal force on the abrasive particles leading to the circulation of abrasive particles into the machining zone. Due to which fresh abrasive particles enter and participate into machining and as a result of that the TVW of tool decreased and MRR increased. Moreover, it seems that at 300 rpm, the centrifugal force on the abrasive particles was enough to replenish the slurry from the machining zone without abrading the tool edge. Thus, resulted in highest MRR and lowest edge rounding wear of tool (as evidenced in Figure 6.12) and hence lowest TVW. The best possible form accuracy was also observed at 300 rpm of the tool. This is evidenced in the cross sectional image of machined microchannels shown in Figure 6.10. It seems that parametric combination of rotary tool micro-USM process parameters that result in lowest edge rounding wear and maximum MRR will provide best

possible form accuracy (88%). At these settings, if a fixed value of DOC is desired then longitudinal wear should be compensated by 0.16 µm for 1µm DOC, e.g. the compensation of longitudinal wear will be 64 µm for desired DOC of 400 µm. The decreasing trend of MRR beyond 300 rpm was due to the reduction in interaction time between tool, abrasive particles and work.

It can also be observed from the cross sectional image of microchannels shown in Figure 6.10 that the form accuracy decreased with an increase in edge rounding wear of tool. On further increasing the rotation speed beyond 300 rpm, the centrifugal force on the abrasive particles increased due to which rate of slurry replenishment increased leading to increased rate abrasion of tool edge and poor form accuracy of microchannel. The abraded edge of the tool obtained at 500 rpm is evidenced in Figure 6.12. Thus, highest TVW of tool was observed at 500 rpm. At 600 rpm, excessive centrifugal force was generated on the abrasive particles into the machining zone due to which very limited quantity of abrasive particles participated into the machining leading to limited interaction between tool, abrasive particles and work. As a result of that low TVW (as evidenced in Figure 6.12) and low DOC/MRR were obtained. Moreover, tool rotation speed beyond 300 rpm increased the rate of abrasion of vertical wall of the machined microchannel which further resulted in increased WOMC as seen from Figure 6.12.
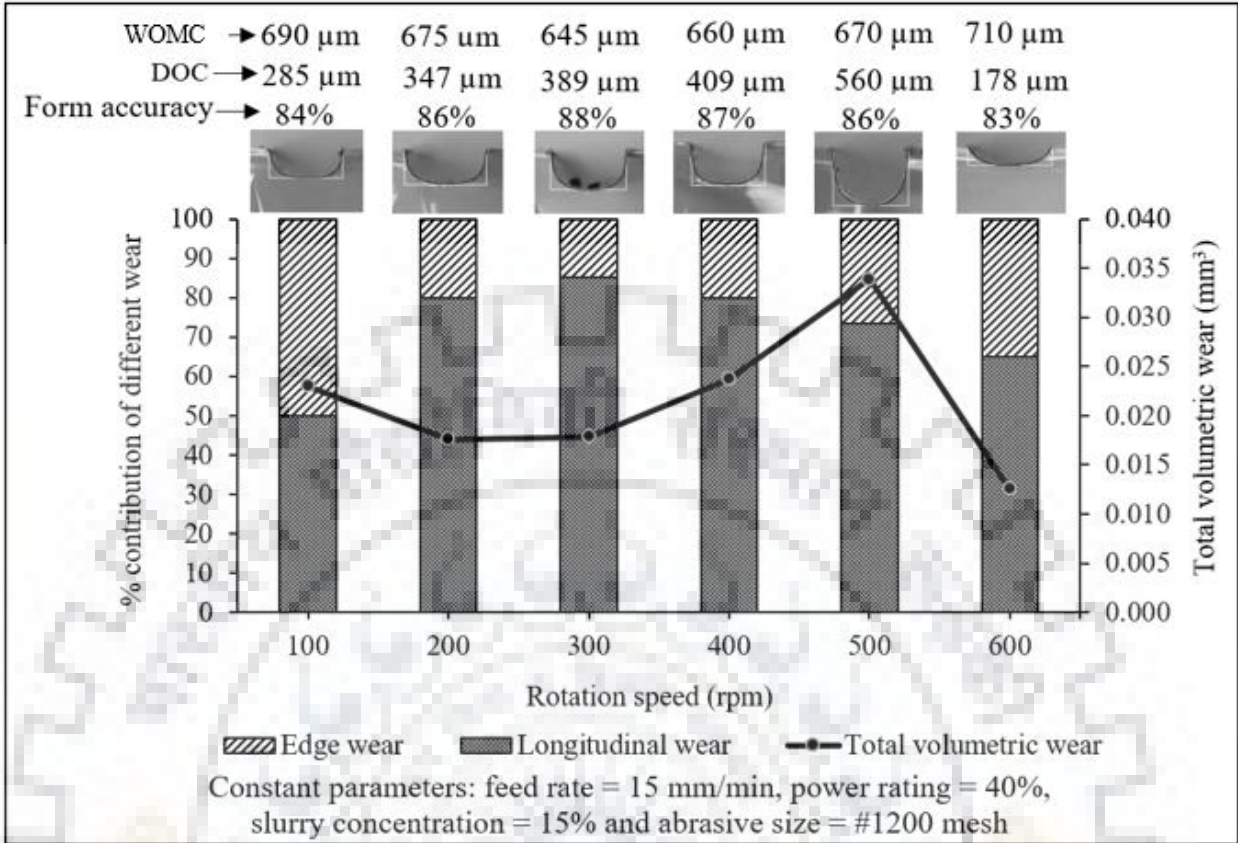
Figure 6.10 Effect of rotation speed on TVW and percentage contribution of different wear
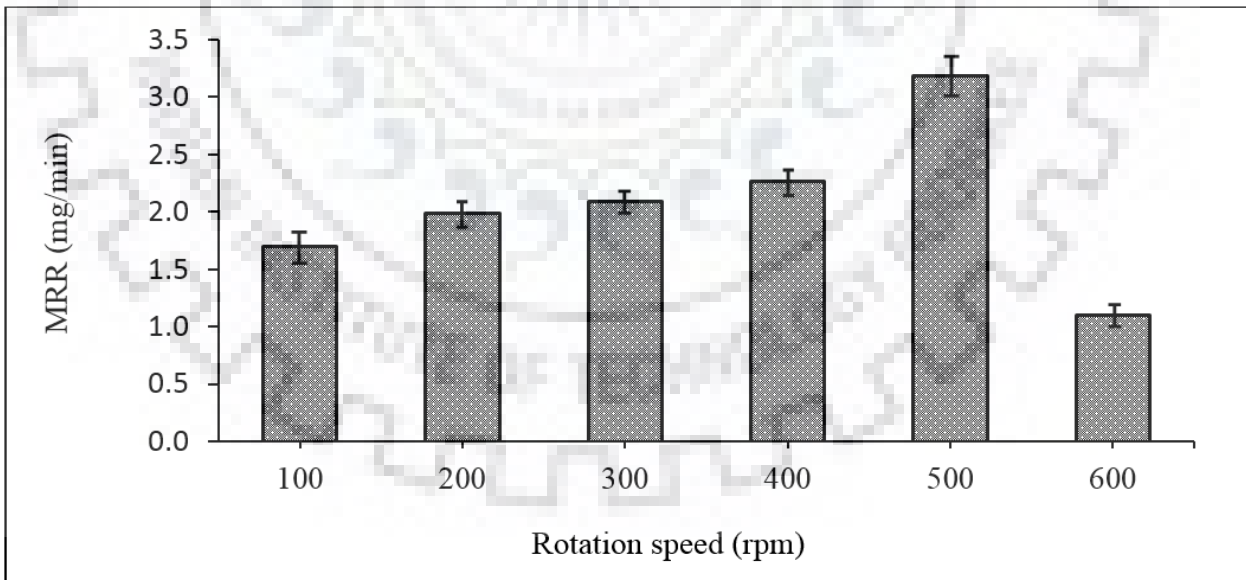
Figure 6.11 Effect of rotation speed on MRR
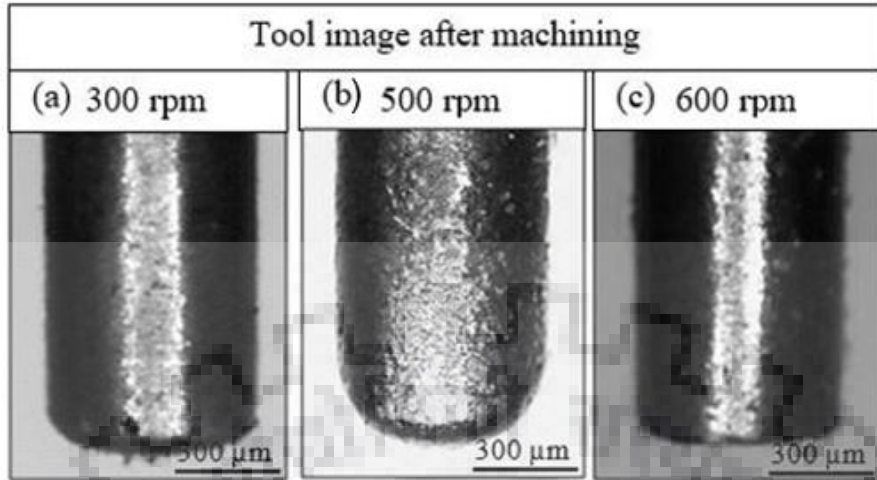
Figure 6.12 Microscopic image of tool after machining

Effect of feed rate on tool wear, MRR, DOC, WOMC and form accuracy

The work feed rate can be defined as the interaction time between the tool, abrasive particles and work simultaneously. The lower feed rate results in more interaction time of tool, abrasive particles and work at a time and vice-versa. Feed rate is an important rotary tool micro-USM process parameter which affects the MRR, tool wear as well as the form accuracy of the machined microchannel. The dimensions of tool after machining at various tool rotation speeds were measured and subsequently used in subsection 6.1.4 to calculate longitudinal wear, edge rounding wear and total volumetric wear. The results are tabulated in Table 6.4 and plotted in Figure 6.13.

Table 6.4 Total volumetric wear of tool at different feed rates

S. No.	Feed rate (rpm)	LW	ERW	TVW	CLW	CERW
1	10	0.0254	0.0110	0.0365	69.75	30.25
2	15	0.0212	0.0107	0.0319	66.45	33.55
3	20	0.0175	0.0100	0.0276	63.58	36.42
4	25	0.0138	0.0084	0.0222	62.34	37.66
5	30	0.0096	0.0050	0.0146	65.85	34.15

LW: Longitudinal wear (mm^3), ERW: Edge rounding wear (mm^3), TVW: Total volumetric wear (mm^3), CLW: Contribution of longitudinal wear (%), CERW: Contribution of edge rounding wear (%)

The effect of feed rate on tool wear and MRR are presented in Figure 6.13 and Figure 6.14. It can be observed from Figure 6.13 that the TVW decreased almost linearly by increasing the feed rate of the work. The minimum TVW was obtained at 30 mm/min of work feed rate. The reason attributed was that the interaction time between tool, abrasive particles and work was reduced by increasing the feed rate. On the other hand, the MRR increased by increasing the feed rate of work up to 20 mm/min and thereafter it decreased (Figure 6.14). This can be explained by the fact that at 20 mm/min of feed rate, the abrasive particles got sufficient time to interact with tool and subsequently transferred their energy on work material. Thus, maximum MRR was obtained. The best possible form accuracy was obtained at 30 mm/min of work feed rate. Which is evidenced in cross sectional view of microchannel shown in Figure 6.13. It is to be noticed that at 30 mm/min of work feed rate, the edge rounding wear was also minimum. The parametric settings of rotary tool micro-USM process at which the edge rounding wear was lowest resulted in best possible form accuracy of the microchannel. At these settings, if a fixed value of DOC is desired then longitudinal wear should be compensated by 0.13 µm for 1 µm DOC, e.g., the compensation of longitudinal wear will be 52 µm for desired DOC of 400 µm.

This can be seen from the cross sectional view of microchannels shown in Figure 6.13 that an increase in edge rounding wear of the tool resulted in reduction in form accuracy of the microchannels.

The DOC was significantly affected by varying the feed rate. By increasing the feed rate, DOC was initially increased up to 20 mm/min and beyond that it decreased (Figure 6.13). The maximum DOC was obtained at 25 mm/min. At 25 mm/min of feed, rate the longitudinal wear was lesser due to which higher depth was obtained.

Figure 6.13 Effect of feed rate on TVW and percentage contribution of different wear
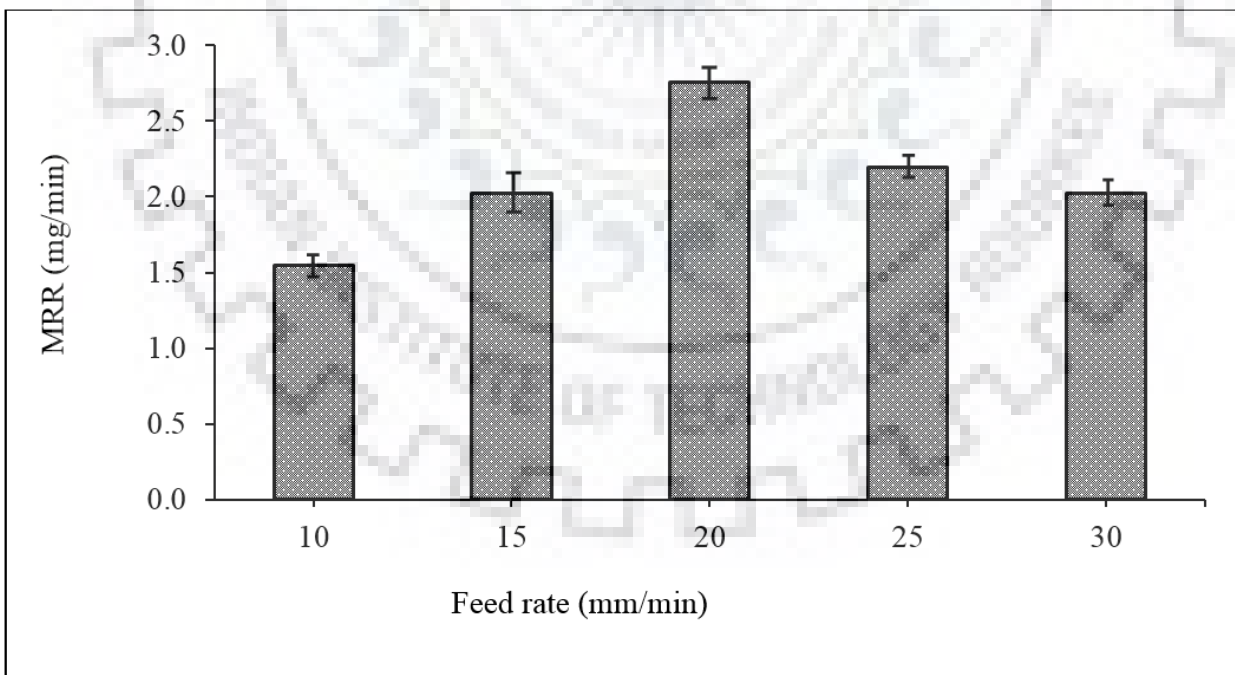
Figure 6.14 Effect of feed rate on MRR

170

Effect of power rating on tool wear, MRR, DOC, WOMC and form accuracy

The dimensions of tool after machining at various tool rotation speeds were measured and subsequently used in subsection 6.1.4 to calculate longitudinal wear, edge rounding wear and total volumetric wear. The results are tabulated in Table 6.5 and plotted in Figure 6.15.

Table 6.5 Total volumetric wear of tool at different power ratings

S. No.	Power rating (%)	LW	ERW	TVW	CLW	CERW
1	20	0.0153	0.0228	0.0381	40.09	59.91
2	30	0.0192	0.0198	0.0390	49.22	50.78
3	40	0.0209	0.0211	0.0420	49.77	50.23
4	50	0.0260	0.0182	0.0442	58.81	41.19
5	60	0.0339	0.0118	0.0457	74.24	25.76

LW: Longitudinal wear (mm^3), ERW: Edge rounding wear (mm^3), TVW: Total volumetric wear (mm^3), CLW: Contribution of longitudinal wear (%), CERW: Contribution of edge rounding wear (%)

Power rating is termed as the energy transferred by the vibrating tool to the abrasive particles during impact. Subsequently, this energy is transferred by the abrasive particles on the surface of work in the form of impact. The amplitude of vibration of the tool is directly proportional to the power rating. Higher power rating results in higher amplitude of vibration and vice versa. Subsequently, the abrasive particles hammer/impact on the work surface with higher energy leading to the formation of deeper craters on the surface of work and increase MRR. As tool hits the abrasive particles underneath, the machining face of tool also experiences the same hammering effect/impacts repeatedly. Due to these repetitive impacts some material is removed from the tool bottom face in the form of small craters. It is evidenced from Figure 6.15 that an increase in power rating resulted in increased TVW. Moreover, at high power rating multiple layers of abrasive particles may be formed in the machining gap owing to high amplitude of vibration. Consequently, TVW increased. The MRR and DOC increased with an increase in power rating up to 40% power rating and beyond that both decreased (Figure 6.16 and Figure 6.15). The reason for decreasing trend was that at higher power rating, the tool suffered from excessive hammering action due to the formation of multiple layers of abrasive particles leading to the higher longitudinal wear of tool in TVW as compared to edge rounding wear and hence

low DOC. The best possible form accuracy of microchannel was observed at 60% power rating as shown in Figure 6.15. Invariably, the best form accuracy corresponds to those parametric settings that resulted in lowest edge rounding wear of tool. At these settings, if a fixed value of DOC is desired then longitudinal wear should be compensated by 0.47 μm for 1μm DOC, e.g. the compensation of longitudinal wear will be 14 μm for desired DOC of 300 μm

It is to be noticed that at low power rating, the contribution of edge rounding wear was more as compare to longitudinal tool wear whereas at higher value of power rating, longitudinal wear of the tool was more than edge rounding wear. From Figure 6.15 it can be observed that longitudinal tool wear was increased linearly by increasing the power rating, whereas, edge rounding wear was linearly decreased (Figure 6.15).
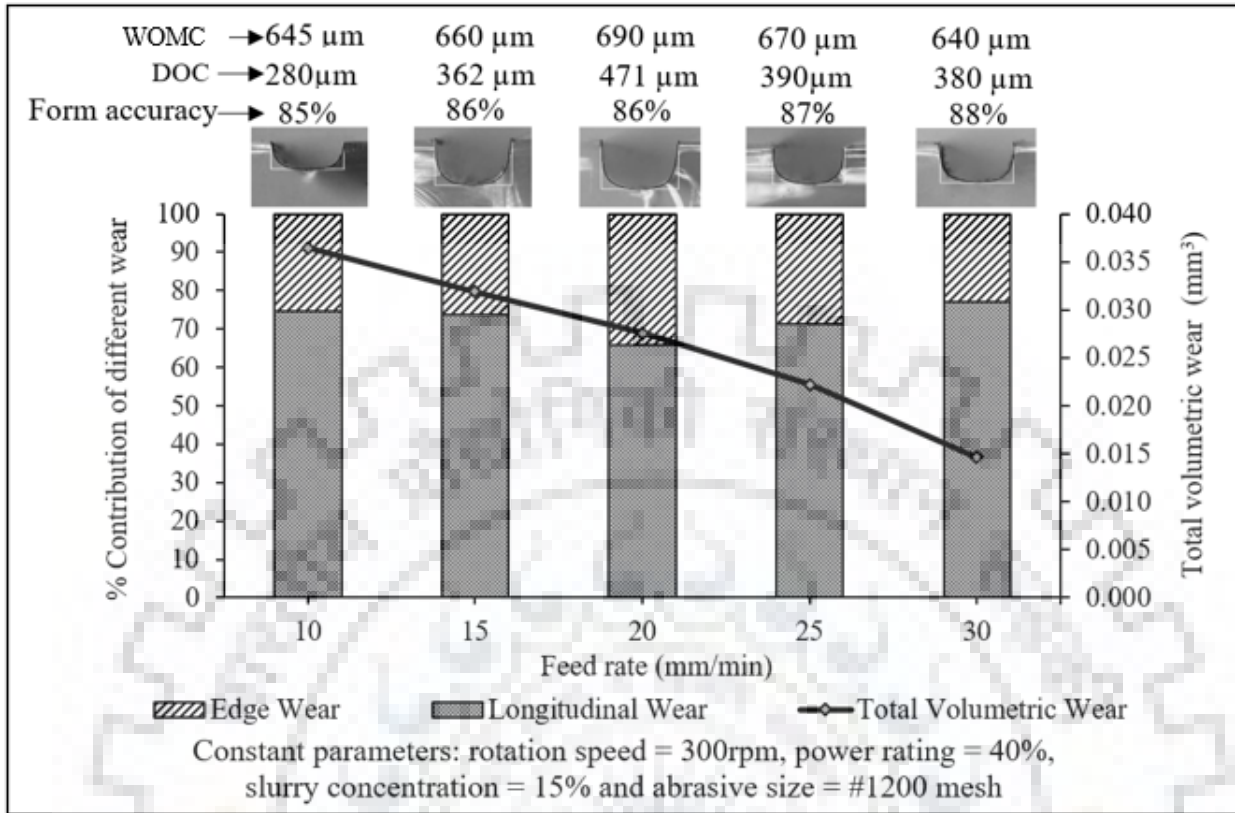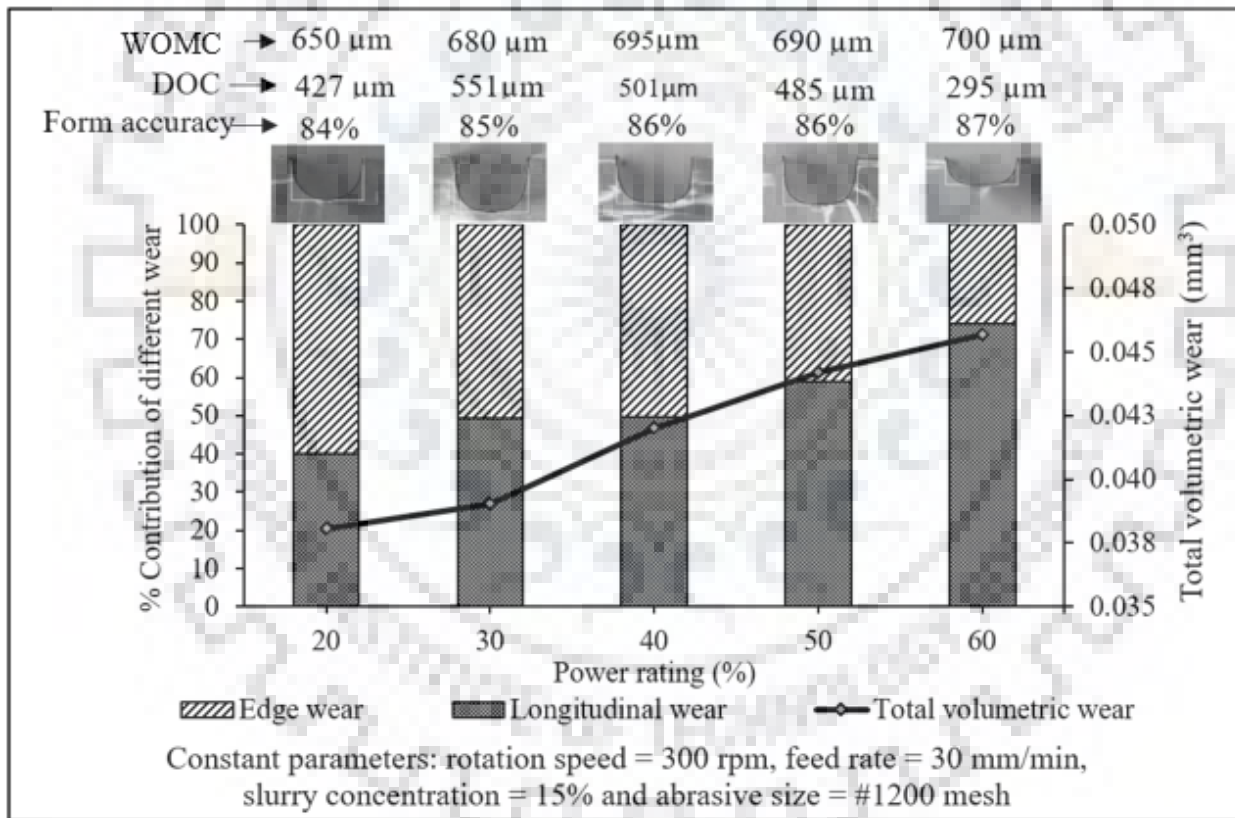

Figure 6.15 Effect of power rating on TVW and percentage contribution of different wear
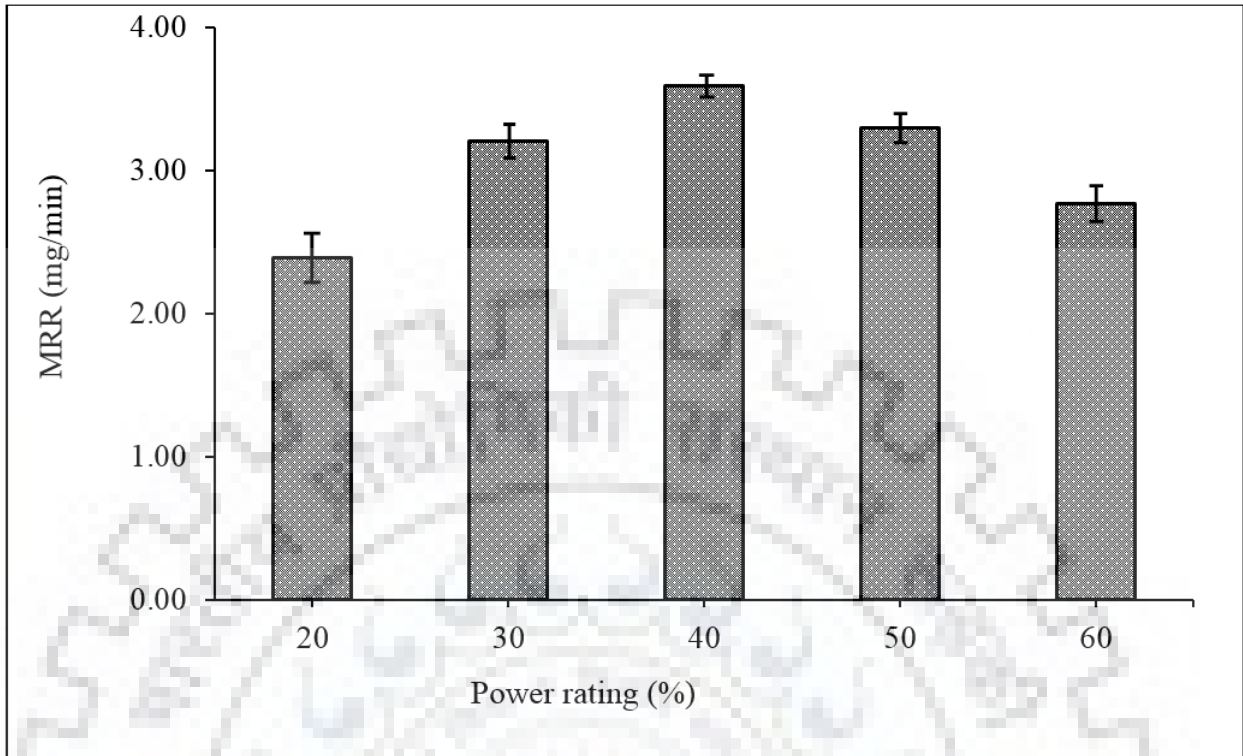
Figure 6.16 Effect of power rating on MRR

Effect of slurry concentration on tool wear, MRR, DOC, WOMC and form accuracy

The dimensions of tool after machining at various tool rotation speeds were measured and subsequently used in subsection 6.1.4 to calculate longitudinal wear, edge rounding wear and total volumetric wear. The results are tabulated in Table 6.6 and plotted in **Figure 6.17**.

Table 6.6 Total volumetric wear of tool at different concentrations

S. No.	Concentration (%)	LW	ERW	TVW	CLW	CERW
1	5	0.0136	0.0060	0.0196	69.24	30.76
2	10	0.0175	0.0177	0.0353	49.68	50.32
3	15	0.0215	0.0296	0.0511	42.07	57.93
4	20	0.0232	0.0211	0.0443	52.31	47.69
5	25	0.0297	0.0193	0.0490	60.58	39.42
LW: Longitudinal wear (mm^3), ERW: Edge rounding wear (mm^3), TVW: Total volumetric wear (mm^3), CLW: Contribution of longitudinal wear (%), CERW: Contribution of edge rounding wear (%)						

The slurry concentration defines the number of abrasive particles, available at a time, for machining on the work surface. The TVW increases with an increase in slurry concentration (as evidenced by Figure 6.17). Whereas the DOC and MRR were increased up to 20% of concentration and after that both decreased (Figures 6.17 and Figure 6.18). The reason that can be attributed for the observed trend is that by increasing the slurry concentration more number of abrasive particles participate in machining which leads to the formation of more craters on work surface as well as machining face of tool. As a result of that both TVW and MRR increased. But, higher slurry concentration (beyond 20%) may results in formation of multiple layers of abrasive particles in the machining gap. These abrasive particles interact among themselves as well as with tool and work material leading to lesser energy transferred on work surface. These interactions result in lesser MRR and DOC and high TVW as evidenced from Figures 6.17 and Figure 6.18 with 0.70 mm^3/min MRR, 260 μm DOC and 0.490 mm^3 TVW for 30% slurry concentration. The form accuracy was also reduced by increasing the concentration owing to tool wear. The best form accuracy was measured at 10% of slurry concentration. This is attributed with the fact that at 10% slurry concentration, few abrasive particles interacted with the vibrating tool leading to lowest abrasion at the tool edge and hence lowest edge rounding wear of tool. At these settings, if a fixed value of DOC is desired then longitudinal wear should be compensated by 0.24 μm for 1 μm DOC, e.g. the compensation of longitudinal wear will be 72 μm for desired DOC of 300 μm.

The parametric value of 20% slurry concentration resulted in lowest value of measured form accuracy. It is evident from Figure 6.17 that form accuracy is directly proportional to the edge rounding wear of the tool. The effect of edge rounding wear on the form accuracy was more than that of longitudinal wear.
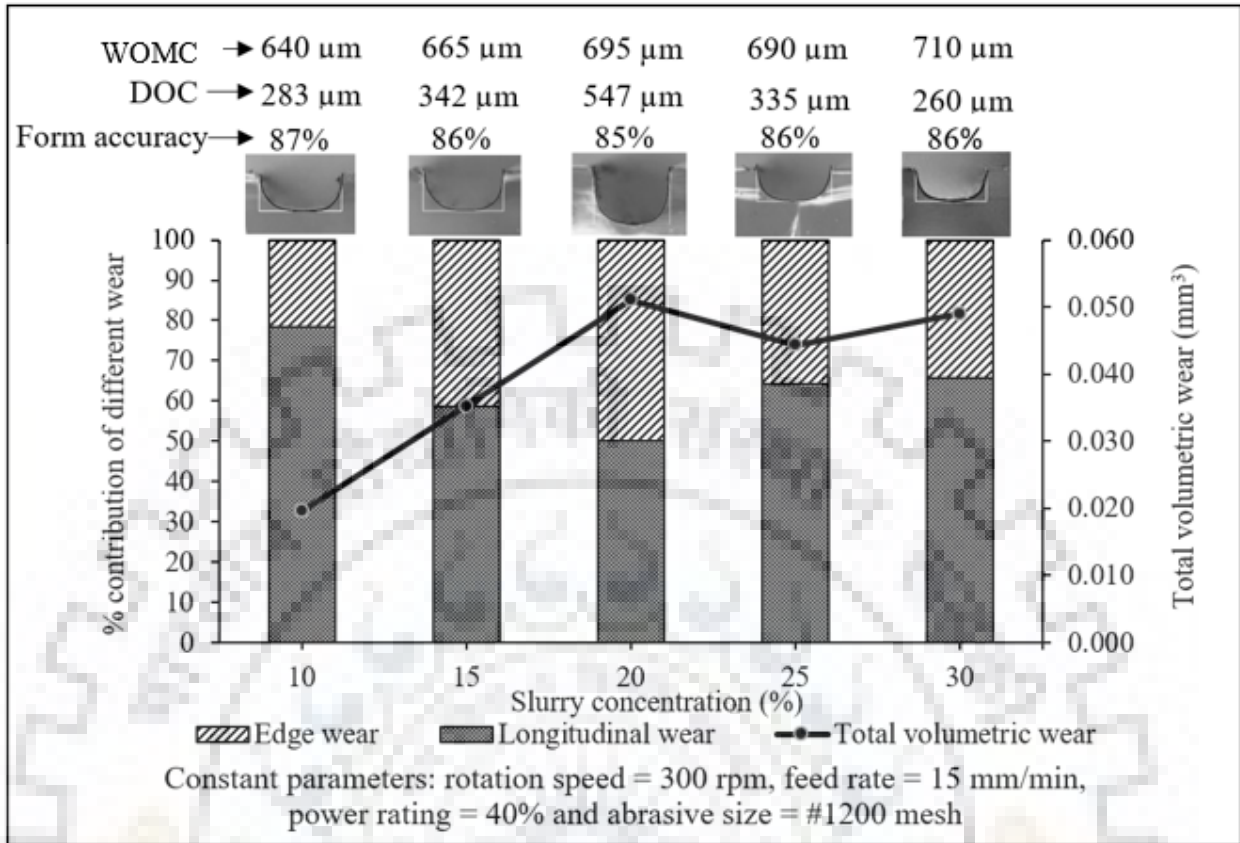
Figure 6.17 Effect of slurry concentration on TVW and percentage contribution of different wear
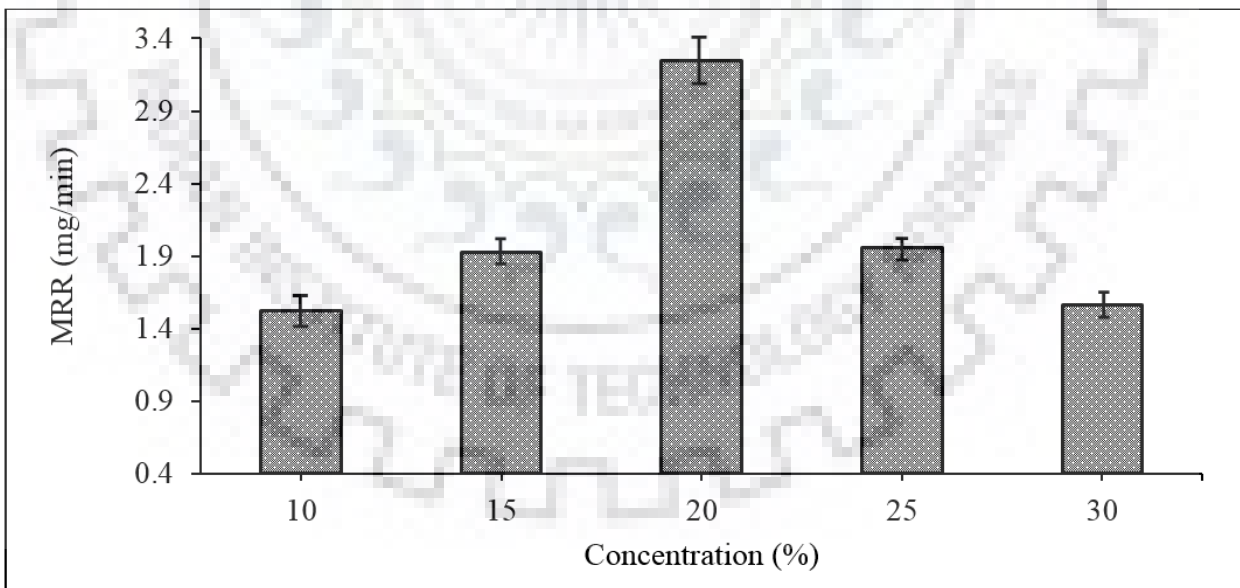
Figure 6.18 Effect of slurry concentration on MRR

Effect of abrasive particles size on tool wear, MRR, DOC, WOMC and form accuracy

The dimensions of tool after machining at various tool rotation speeds were measured and subsequently used in subsection 6.1.4 to calculate longitudinal wear, edge rounding wear and total volumetric wear. The results are tabulated in Table 6.7 and plotted in **Figure 6.19**.

Table 6.7 Total volumetric wear of tool at different abrasive sizes

S. No.	Abrasive size (mesh)	LW	ERW	TVW	CLW	CERW
1	1000	0.0305	0.0108	0.0413	73.92	26.08
2	1200	0.0229	0.0299	0.0528	43.36	56.64
3	1800	0.0203	0.0069	0.0272	74.77	25.23

LW: Longitudinal wear (mm^3), ERW: Edge rounding wear (mm^3), TVW: Total volumetric wear (mm^3), CLW: Contribution of longitudinal wear (%), CERW: Contribution of edge rounding wear (%)

The abrasive particles size affects the tool wear as well resultant crater on the work material. Thus, experiments were conducted to investigate the effect on abrasive particles size on tool wear, MRR, DOC, WOC and form accuracy during rotary tool micro-USM process. The results are plotted and shown in Figures 6.19 and Figure 6.20. Amongst the three mesh numbers of abrasive particles selected, the largest abrasive particle size (#1000 mesh) provided 87% of form accuracy with 675 µm WOC and 258 µm DOC.

Generally, larger abrasive particle size produces larger crater on work and well as tool surface and resulted in more MRR, DOC and tool wear [102]. Interestingly, the DOC achieved by #1000 mesh was substantially lower than DOC of 545 µm, which was achieved by #1200 mesh. It seems that owing to larger size of #1000 mesh, lesser number of abrasive particles enter in the machining gap. Consequently, lesser number of abrasive particles participated in machining and resulted in low MRR, DOC, TVW and wider WOMC (675 µm).

The abrasive particle size with #1200 mesh number is smaller than # 1000 mesh number. Thus, with #1200 mesh number, sufficient number of abrasive particles participated in the machining and results in tool-abrasive-work type interaction. This interaction provides complete transfer of ultrasonic energy to the work material and provides higher MRR and DOC. The abrasive particles with #1800 mesh number provided highest WOMC (710 µm). It seems that multiple

layers of abrasive particles formed in the machining gap and lateral gap when #1800 mesh number (fine grains) abrasive particles were used. Consequently, MRR and DOC decreased whereas WOMC increased. The percent contribution of longitudinal tool wear in TVW is 80%. These outcomes proves that with #1800 mesh number, the tool-abrasive particle interaction takes place.
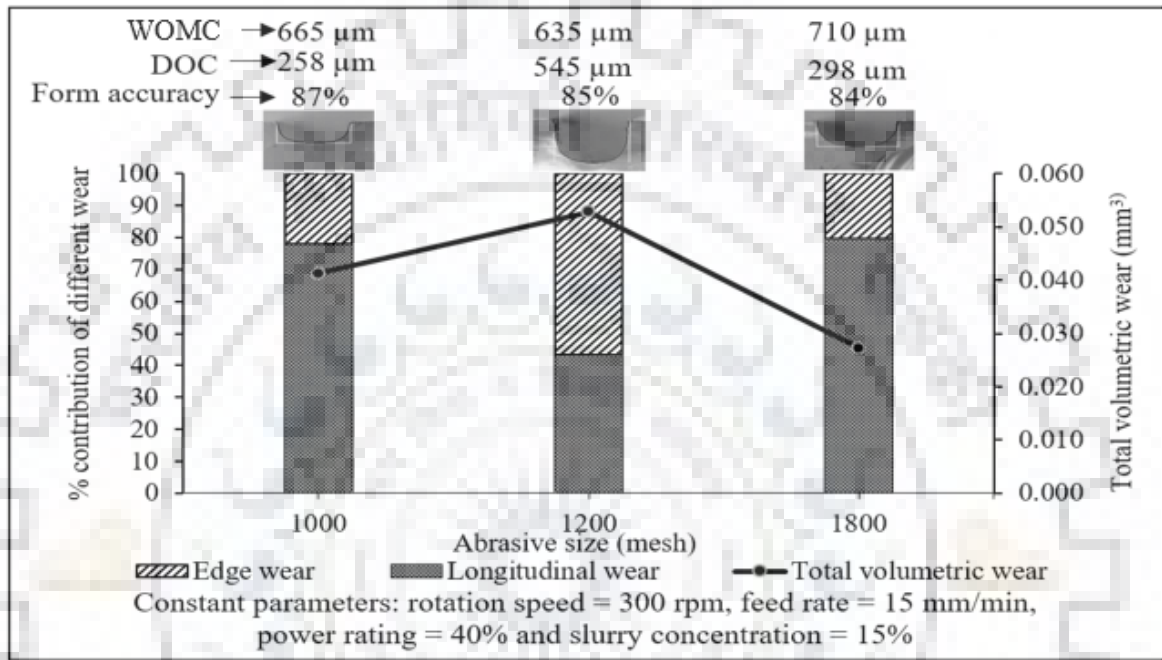
Figure 6.19 Effect of abrasive particle size on TVW and percentage contribution of different wear
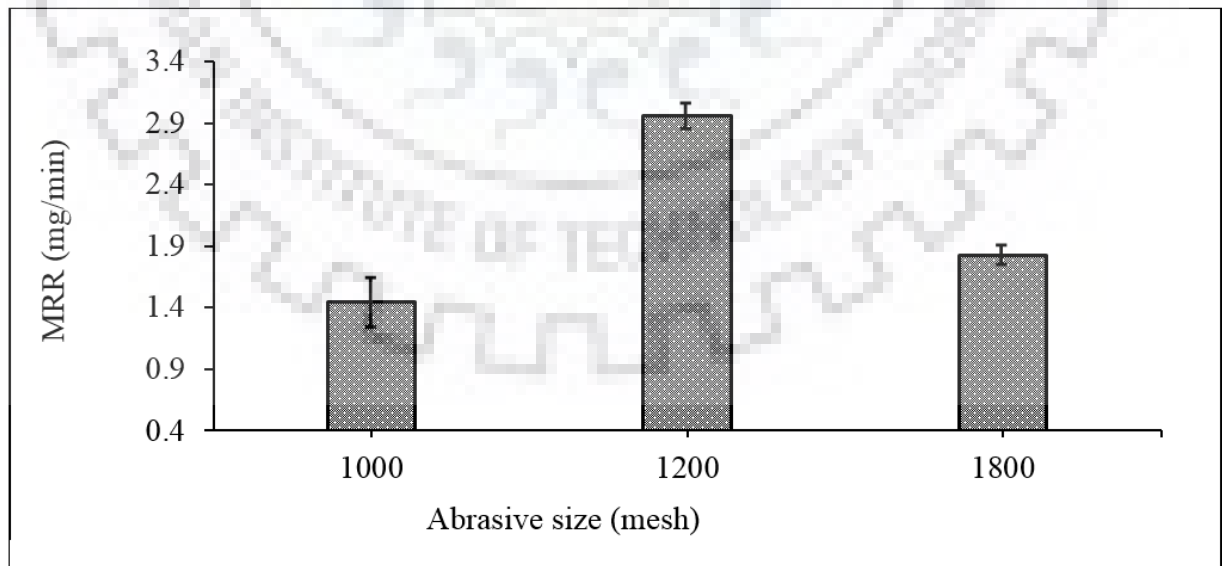
Figure 6.20 Effect of abrasive particle size on MRR

177

From the above discussion it can be conclude that all the rotary tool micro-USM process parameters affected the tool wear and form accuracy of microchannels. It was also found that the edge rounding wear of tool significantly affected the form accuracy of the machined microchannels as compared to longitudinal wear of tool. Thereby, the control over edge rounding wear of the tool is more important than longitudinal wear as far as the form accuracy of the microchannel is concerned. The tool wear can be control by controlling the input process parameters. Further, in order to improve the form accuracy of machined microchannels, experiments were conducted at the parametric combinations at which lower edge rounding wear was obtained in the previous experimental results shown in Figures 6.10 to Figure 6.20. The average % contribution of longitudinal and edge rounding wear, TVW, dimensional and form accuracy were selected as response characteristics in these experiments. The experimental settings and their results are presented in Table 6.8. From the experimental results presented in Table 6.8, it can be seen that parametric combination (rotation speed 300 rpm, feed rate 30 mm/min, power rating 60%, slurry concentration 10%, and abrasive particle mesh size #1800) resulted in 91% form accuracy. The photographic view of the cross section this microchannel and tool after machining is shown in Figure 6.21. At these settings, if a fixed value of DOC is desired then longitudinal wear should be compensated by 0.19 µm for 1 µm DOC, e.g. the compensation of longitudinal wear will be 123.5 µm for desired DOC of 650 µm. In the subsequent section of the paper, the parametric optimization of rotary tool micro-USM process was carried out to obtain the minimum TVW and WOMC and maximum MRR and DOC.

Table 6.8 Process parameters that provide low edge rounding wear and their responses

Parametric settings					Responses						
Rotation speed (rpm)	Feed rate (mm/min)	Power rating (%)	Slurry concentration (%)	Abrasive size (mesh)	Average % contribution of longitudinal wear	Avg. % contribution of edge wear	Avg. TVW (mm³)	Avg. MRR (mg/min)	Avg. DOC (µm)	Avg. WOC (µm)	Avg. form accuracy (%)
300	30	60	10	1800	75.87	24.13	0.044	2.27	630	650	91
400	15	50	30	1000	73.74	26.26	0.049	2.29	615	670	88
200	10	40	25	1000	69.46	30.54	0.053	2.27	620	660	87
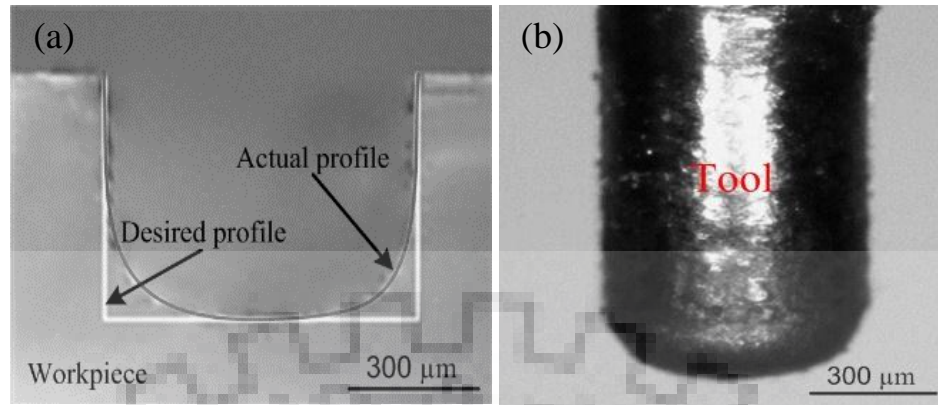
Figure 6.21 Microscopic images of microchannel cross-section and tool after machining obtained by confirmation experiment (experimental conditions: rotation speed = 300 rpm, feed rate = 30 mm/min, power rating = 60%, slurry concentration = 10% and abrasive particle size = #1800 mesh)

6.1.6 Multi criteria optimization for microchannels

The microchannel fabrication process was optimized to achieve maximum MRR, DOC, form accuracy and minimum TVW and WOMC. The input parameters values (both upper and lower) for all the responses were set to 'in range' as tabulated in Table 6.9. During optimization, equal weight was given to each response. The results of optimal setting were rotation speed = 347 rpm, feed rate = 25.35 mm/min, power rating = 34.54%, concentration = 14.44% and abrasive particle size = #1315 mesh. The aforesaid optimal setting provided maximum MRR = 2.90 mg/min, DOC = 517.48 µm, form accuracy = 86.54% and minimum TVW = 0.0170 mm^3 and WOMC = 663.18 µm. The overall desirability obtained was 0.800, which provides a compromise between MRR, DOC, form accuracy, TVW and WOMC. The optimized results obtained is shown in Figure 6.22.

Table 6.9 Range of process parameters for TVW, MRR, DOC, WOMC and form accuracy

Input parameters		Rotation speed (rpm)	Feed rate (mm/min)	Power rating (%)	Abrasive size (mesh)	Slurry concentration (%)
Goal		In range				
Constraint limit	Lower	100	10	20	#1000	10
	Upper	600	25	60	#1800	25
Output parameters		TVW (mm^3)	MRR (mg/min)	Form accuracy (%)	DOC (µm)	WOMC (µm)
Goal		To minimize			To minimize	
Weightage		1				
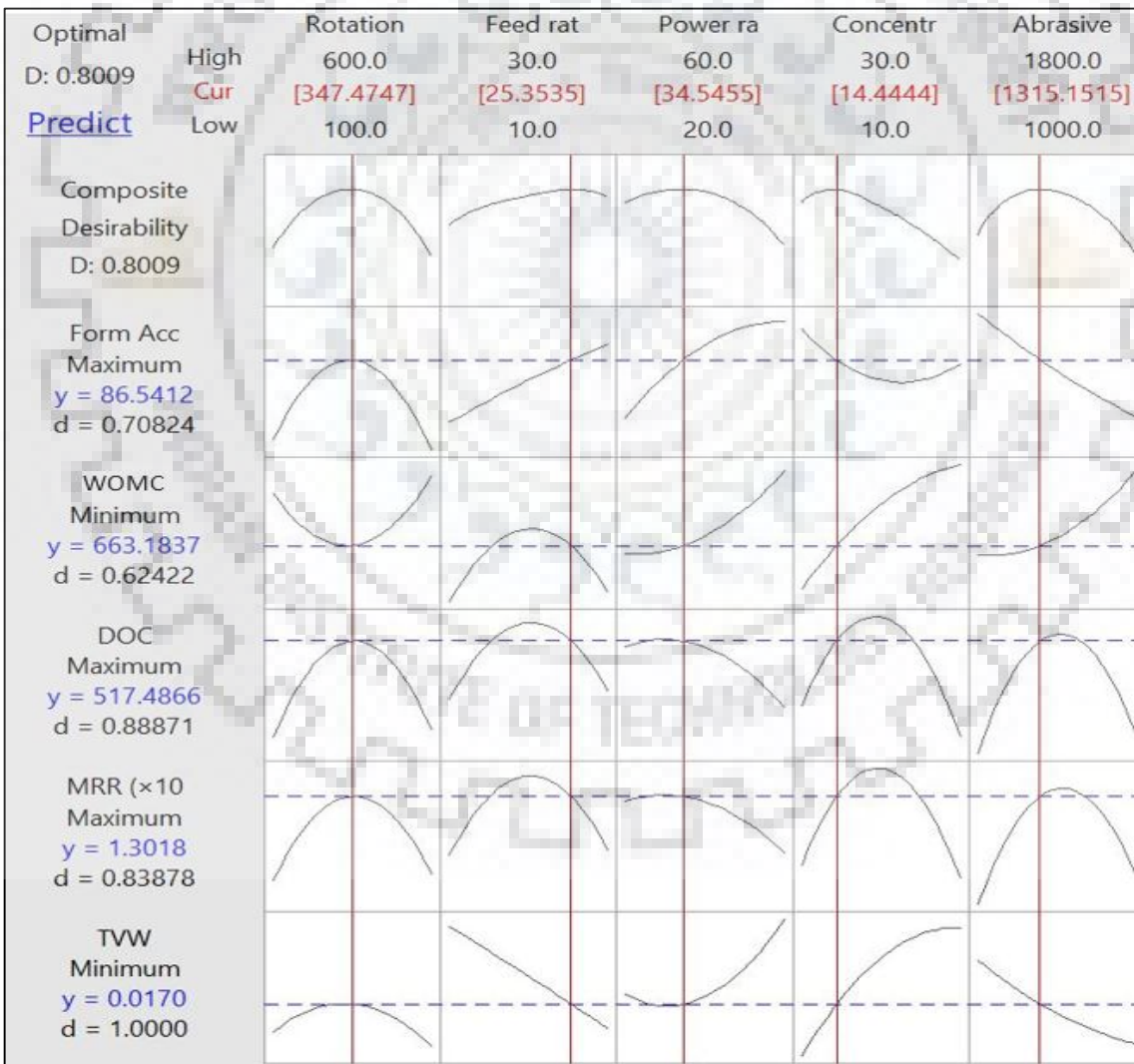
Figure 6.22 Optimization plot

180

After obtaining the optimum values of rotary tool micro-USM process parameters for maximum MRR, DOC and form accuracy and minimum TVW and WOC using desirability approach, confirmatory experiments were conducted in order to validate optimal settings and corresponding value of TVW. The closest mesh number available commercially for abrasive particles was 1500 mesh number, so it was used for confirmatory experiments. These experiments were repeated three times and the average value of the TVW was considered as final value. The confirmatory experiments resulted in an average MRR of 3.23 mg/min, DOC of 475 μm, form accuracy of 87.5%, TVW of 0.0189 mm^3 and WOC = 695 μm respectively. These results were quite close to the predicted value of all responses with an average error of 10%. The contribution of longitudinal wear in TVW was approximately 80%. At these optimal parametric setting, if a fixed value of DOC is desired then, longitudinal wear should be compensated by 0.092 μm for each 1 μm DOC, e.g. the required compensation of longitudinal wear will be 47 μm for desired DOC of 400 μm during the rotary tool micro-USM process.

6.1.7 Fabrication of complex profile micro channels

The complex profiles of micro channels were fabricated on glass slides, i.e. double Y, serpentine, single-Y + serpentine, double-Y + zig-zag, mixed shape (i.e. double-Y + zig zag + serpentine) as shown in Figure 6.23 at the optimal parametric conditions. The measured values of quality characteristics such as depth of channel, width of channel, MRR and surface roughness of these feature are tabulated in Table 6.10. The surface quality of the micro channels was evaluated using surface roughness tester. The comparative results of the DOC, WOC, MRR and SR are shown in Figure 6.24(a) and Figure 6.24(b)). It can be clearly see from Figure 6.24(a) and Figure 6.24(b) that that the values of the responses (i.e. DOC, WOC, MRR and SR) do not change significantly by changing the profile of the microchannels. These types of microchannels are widely used for micro-fluidic applications.
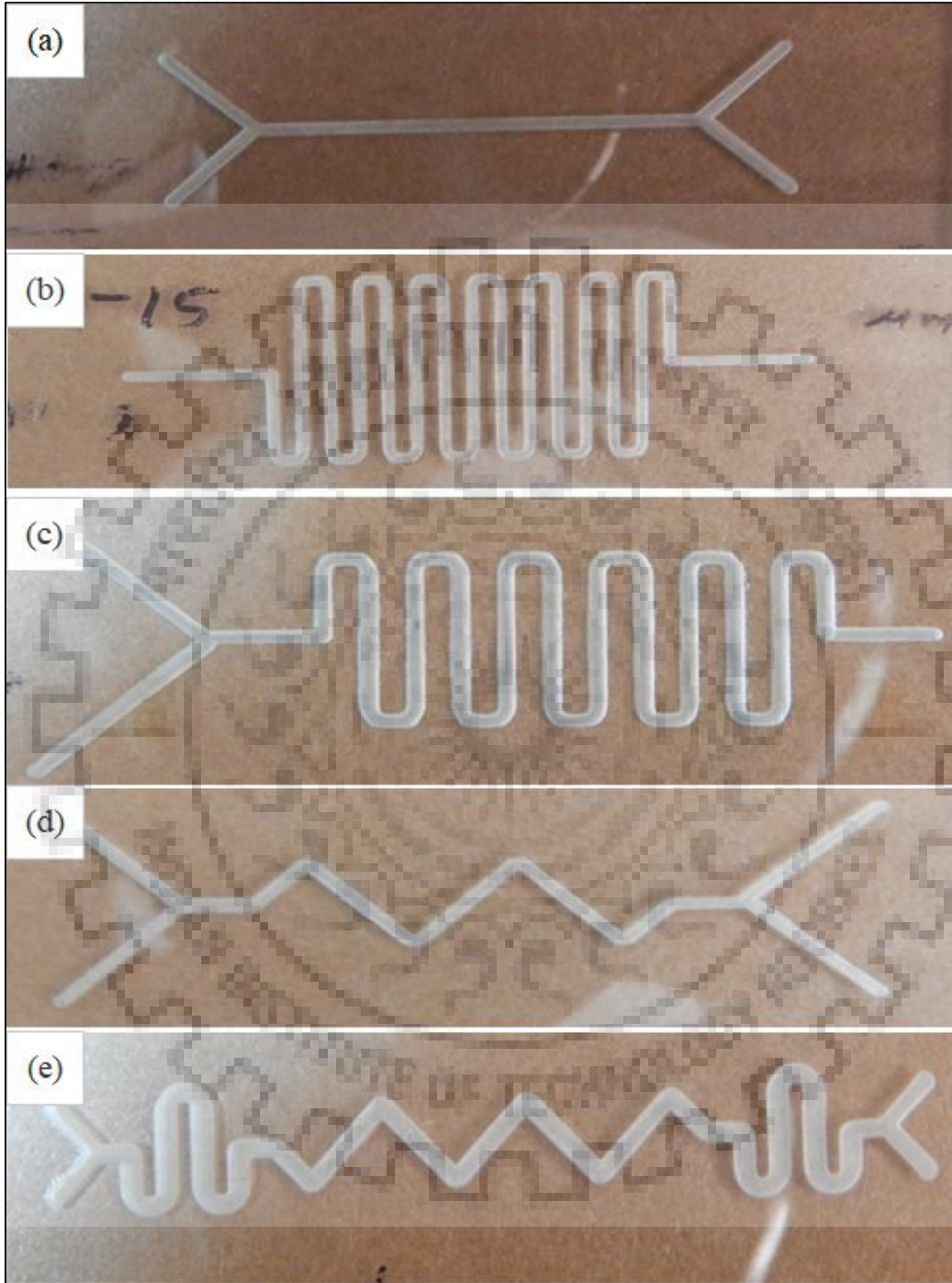
Figure 6.23 Developed microfeatures: (a) double-Y microchannel (b) serpentine microchannel (c) single-Y + serpentine microchannel (d) double-Y + zig-zag microchannel (e) double-Y + serpentine + zig-zag microchannel

Table 6.10 Values of complex shape quality characteristics

Shape type	Width (μm)	Depth (μm)	SR (μm)	MRR (mg/min)
Double-Y	690	300	1.24	1.52
Serpentine	720	270	1.08	1.49
Single-Y + serpentine	710	260	1.11	1.49
Double-Y + Zig-zag	710	250	1.15	1.45
Double-Y + Serpentine + Zig-Zag	900	200	1.23	1.36
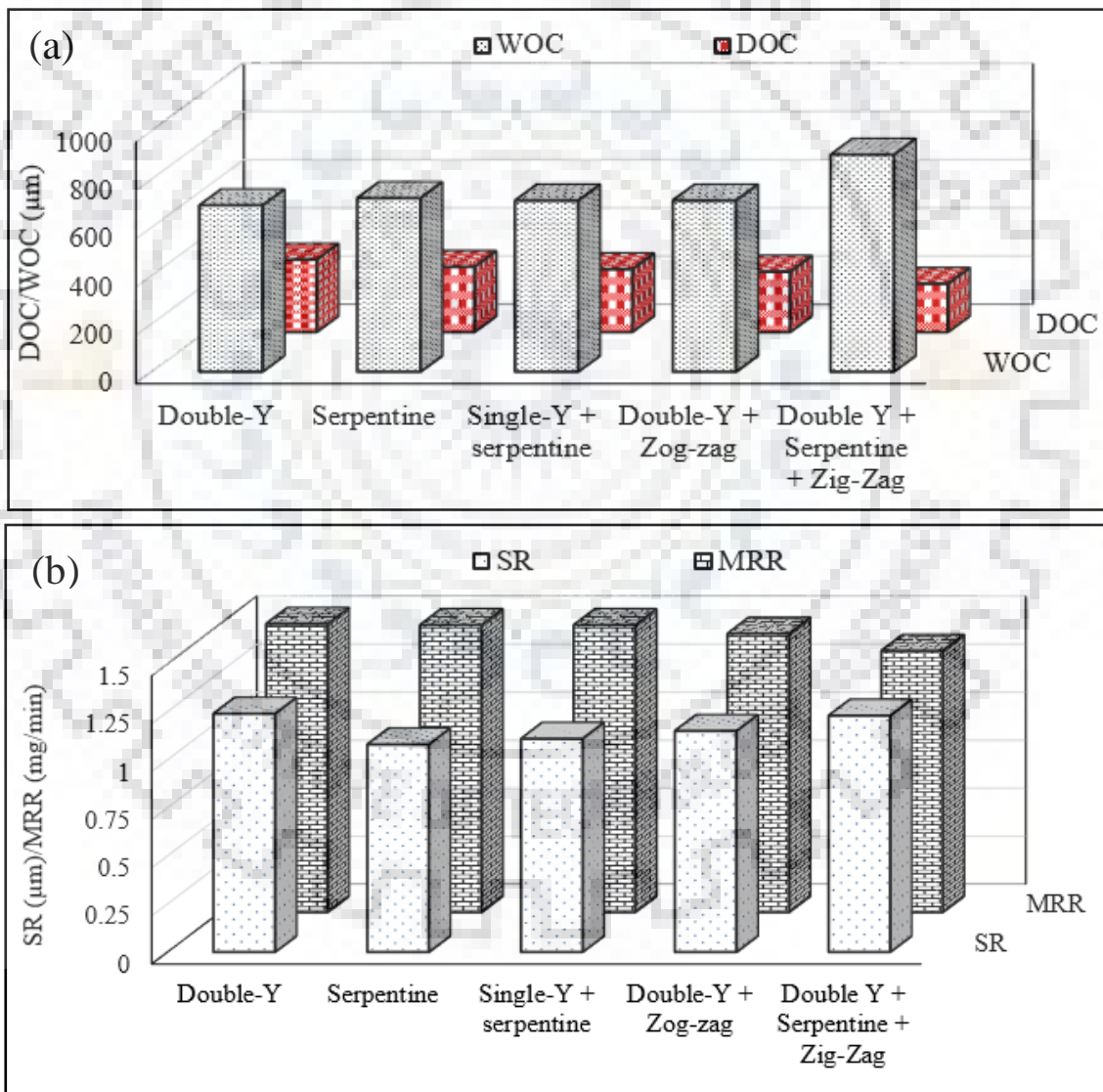
Figure 6.24 Comparative of responses of different types of microchannel profiles (a) WOC and DOC (b) SR and MRR

6.2 Summary

In this chapter, an experimental investigation was performed on tool wear and its effects on form accuracy of microchannels during rotary tool micro-USM process. Initially, the tool wear mechanism of rotary tool micro-USM process was explored with the help of microscopic images. The tool, abrasive and work interaction was taken into account while exploring the tool wear mechanism. Two types of tool wear i.e. longitudinal wear and edge wear were observed on the machining face of the tool. Lateral wear was found to be negligible in rotary tool micro-USM process. This was due to the rotary motion of tool that exerted centrifugal force on abrasives due to which abrasives replenished from the machining zone. This reduced the tool wear and improved the dimensional and form accuracy of machined microchannels. Subsequently, geometrical model of tool wear to calculate the volumetric tool wear was proposed. The developed model was used to describe the form accuracy of the machined microchannels. After that the effect of tool wear and rotary tool micro-USM process parameters were investigated on form accuracy of machined microchannels. The form accuracy of microchannels was found to be dependent on edge rounding wear as compared to the longitudinal wear. The best possible form accuracy of microchannels was obtained at the parametric settings of rotary tool micro-USM process at which edge rounding wear was minimum. The desired DOC at the best possible form accuracy (i.e. at lowest edge wear) of the microchannel can be obtained by providing longitudinal wear compensation to the tool. The rotary tool micro-USM process parameters were optimized by employing desirability approach to achieve maximum MRR, DOC and minimum WOMC and TVW of tool simultaneously. Additionally, complex shape microchannels were successfully machined using rotary tool micro-USM process.

CHAPTER 7

DEVELOPMENT OF MATHEMATICAL MODEL TO PREDICT MATERIAL REMOVAL RATE

Theoretical modeling of material removal rate using brittle fracture theory both in stationary tool and rotary tool micro-USM process is not revealed in literature. The development of material removal rate model is desirable to develop scientific theory and to predict the performance of micro-USM and optimize the input parameters for desired output. The developed model will help in establishing the relationship between input parameters of micro-USM process and its performance (i.e. MRR). With this objective, the present chapter reports on development of a theoretical model of MRR for rotary tool micro-USM process. The model was developed with the assumption that the material is removed from the workpiece as a result of pure brittle fracture. During the modeling of MRR, indentation depth, number of abrasive particles participating into machining and the indentation force on abrasive particles were also determined. The developed model of MRR was validated through experiments that were conducted on borosilicate glass work material. Additionally, the prediction accuracy of the model was checked through statistical analysis.

7.1 Development of Predictive Model of Material Removal Rate

In micro-USM process, the material removal rate depends on the mechanism of material removal. The material removal mechanism in micro-USM process has been reported in some investigations (Sarwade, (2010); Jain, (2012); Cheema, (2015). According to these investigations, the hammering and impact followed by microchiping/abrasion, cavitation erosion and chemical action between slurry and work material are the associated phenomena for material removal (Figure 2.6). Among all the above mentioned mechanisms, hammering and impact action are known to be the predominant mechanisms for material removal in micro-USM process. The mechanism of material removal in USM process has been studied by several researchers (Kazantsev and Rosenberg, (1965); Kennedy and Grieve, (1975); Kremer et al., (1981); Miller, (1957); Shaw, (1956)). In the present model, the mechanism of material removal during rotary tool micro-USM process is assumed to take place in pure brittle fracture mode according to the indentation fracture theory due to the indentation of abrasive particles on work

surface. The shape of the abrasive particle is considered as a regular tetrahedron and schematically shown in Figure 7.1.

During rotary tool micro-USM process, as a hard abrasive particle strikes on the brittle work material, a localized plastic deformation takes place at the contact surface of work material as shown in Figure 7.2. During downward motion of tool (i.e. loading cycle), the impact force by the abrasive on the workpiece increases, resulting in increase of depth of indentation. Consequently, a median crack starts to form below the plastically deform surface. The median crack is shown in Figure 7.2. During upward motion of the tool (i.e. unloading cycle), the developed median crack starts to close and subsequently a lateral crack formation takes place parallel to the work surface in outward direction from the median crack as shown in Figure 7.2 (Lawn, (1993)). During complete unloading the lateral crack propagates towards the work surface and material is peeling off from work surface in the form of a crater as shown in Figure 7.2. The penetration depth act as an intermediate which establish interrelationship between rotary tool micro-USM process input parameters and MRR. The assumption taken for the development of the MRR model are as follows:

1. The mode of material removal is pure brittle fracture caused by the impact of abrasive particles.
2. All the abrasive are of same size and shape.
3. The shape of the abrasive particle is regular tetrahedron as depicted in Figure 7.2 (Jain, (2012)).
4. A uniform layer of abrasives exists in the between the tool and workpiece.
5. All the abrasive particles hit the work surface by one of its vertices
6. All the abrasives take part into machining.
7. The indentation depth of all the abrasive particles is the same.
8. Tool deformation and stray cutting are not considered
9. The flow rate of abrasive slurry is kept constant throughout machining.
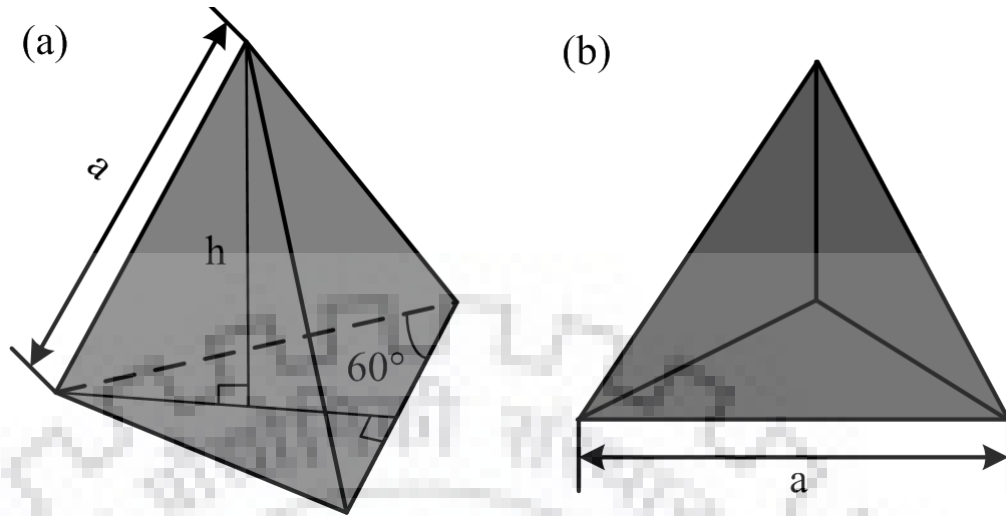
Figure 7.1 Schematic of abrasive particle showing (a) isometric view (b) top view
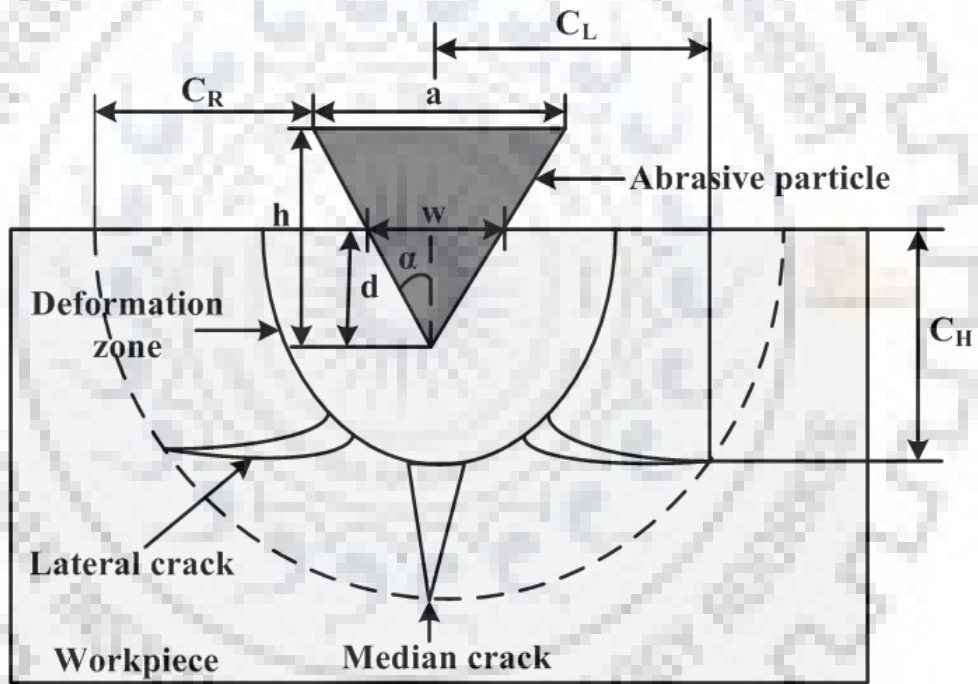
Figure 7.2 Schematic representation of crack development in brittle material

Nomenclature

a	Side length of abrasive	h	Height of abrasive
d	Indentation depth	A	Amplitude of vibration
f	Frequency of vibration	A_i	Indentation area
n	Number of abrasives	KE	Kinetic energy
σ_w	Tensile Strength of workpiece	A_i	Indentation area
N	Tool rotation speed	n	Number of passes
d_1	Indentation depth at bottom of cavity	w	Width of working gap
d_2	Indentation depth at side wall of cavity	m	Mass of abrasive
F_n	Normal load	W_a	Weight of abrasive
F_{n_1}	Normal load at bottom of cavity	b	Width of indentation
r	Tool radius	v	Velocity of tool
υ	Poisson's ratio	H_v	Vickers hardness
α	Half angle of abrasive	T_m	Machining time
F_{n_2}	Normal load at side wall of cavity	F_c	Centrifugal force
K_{ic}	Fracture toughness of workpiece	E	Elasticity
v_1	Velocity of abrasive particle at bottom	C	Slurry concentration
v_2	Velocity of abrasive particle at side wall	D_t	Tool diameter
A_{i_b}	Indentation area at bottom of cavity	C_L	Depth of lateral crack
A_{i_s}	Indentation area at side wall of cavity	ρ_a	Density of abrasive
A_{i_s}	Indentation area at bottom of cavity	C_L	Length of lateral crack

7.2 Material Removal Rate (MRR)

The material removal rate (MRR) can be calculated by determining the indentation volume. The indentation volume is the volume of the indented part of the abrasive particles in to the work surface. It is equal to the amount of work material removed by the impact of abrasives. The indentation volume was calculated by applying the indentation fracture theory. According to this theory and work done by Lawn et al., (1980); Lawn, (1993); Marshall et al. (1982), the length of lateral crack C_L and depth of lateral crack C_H (shown in Figure 7.3) developed by the indentation od abrasive into the work material can be calculated using by the following relation:

$$C_L = C_2 \left(\frac{1}{tan\alpha}\right)^{5/12} \left[\frac{E^{3/4}}{H_v K_{IC}(1-v)^{1/2}}\right]^{1/2} F_n^{5/8} \qquad (7.1)$$

$$C_H = C_2 \left(\frac{1}{tan\alpha}\right) \frac{E^{1/2}}{H_v} F_n^{1/2} \qquad (7.2)$$

where, K_{IC} is the fracture toughness of work material, E is the modulus of elasticity, v is the Poisson's ratio, F_n is the normal load and C_2 is a constant ($C_2 = 0.226$).
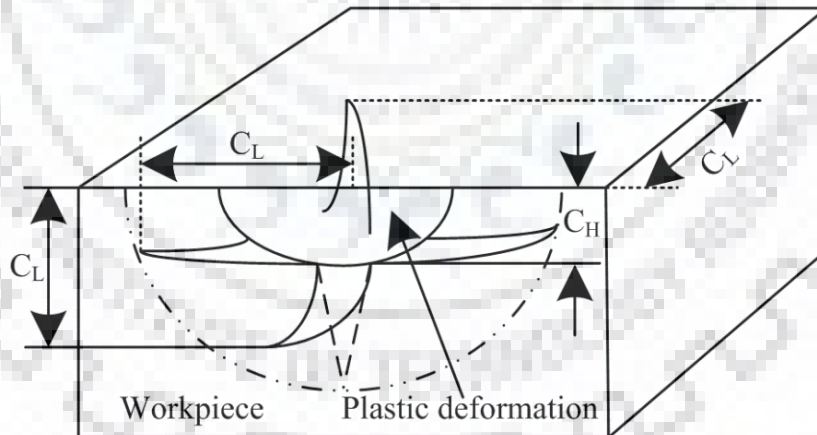
Figure 7.3 Schematic representation showing dimensions of crack

It can be clearly seen from Figure 7.3 that both the length and width of length of lateral crack developed by indentation is equal (i.e. $2C_L$). The volume of material removed (MR_a) during single penetration period is nearly equal to the volume of the regular tetrahedron. It can be given by the following expression:

$$MR_a = \frac{1}{3} \times 2C_L \times 2C_L \times C_h \tag{7.3}$$

By substituting the value of C_L and C_h from Eq. (7.1) and Eq. (7.2) into Eq. (7.3) the MR_a can be expressed as:

$$MR_a = \frac{4}{3}\left[C_2\left(\frac{1}{tan\alpha}\right)^{5/12}\left[\frac{E^{3/4}}{H_vK_{IC}(1-v)^{1/2}}\right]^{1/2}F_n^{5/8}\right]^2 C_2\left(\frac{1}{tan\alpha}\right)\frac{E^{1/2}}{H_v}F_n^{1/2} \tag{7.4}$$

If there are n number of abrasive particle participating into the machining, f is the frequency of impacts and T_m is the machining time, then the total volumetric material removal rate MRR_{Total} can be expressed as:

$$MRR_{Total} = \frac{n}{T_m} \times MRR_a \times f \tag{7.5}$$

7.2.1 Indentation depth

In rotary tool micro-USM process, during impact, the indentation force is applied due to the kinetic energy (K.E.) of the abrasive particle received by the tool. The displacement of the vibrating tool is given by Eq. (7.6):

$$x = Asin2\pi ft \tag{7.6}$$

where, A is the amplitude of tool vibration, f and t are frequency of vibration and time respectively.

The velocity of the tool is expressed as:

$$v = 2\pi fAcos2\pi ft$$

For maximum velocity of the tool, $cos2\pi ft = 1$. Accordingly,

$$v_{max} = 2\pi fA \tag{7.7}$$

where, v_{max} is the maximum velocity of the tool.

If it is assumed that the same velocity is imparted to the abrasive particle by the tool. Then, KE of the abrasive particle can be expressed as:

$$KE = \frac{1}{2}mv_1{}^2 \tag{7.8}$$

where, m and v_1 are the mass and velocity of the abrasive particle.

Using Eq. (7.7) and Eq. (7.8), KE can be expressed as:

$$KE = \frac{1}{2}m(2\pi fA)^2$$

$$KE = \frac{1}{2}(V\rho_a)(2\pi fA)^2 \tag{7.9}$$

where, V and ρ_a are the volume and density of abrasive particle. Eq. (7.9) can be simplified as:

$$KE = \frac{1}{2}\left(\frac{a^3}{6\sqrt{2}} \times \rho_a\right)(2\pi fA)^2 \tag{7.10}$$

where, a is the side length of the abrasive particle (Figure 7.2(a)).

After striking on work surface (Figure 7.4(a)), the abrasive transfer its energy to the work material and creates an indentation depth 'd_1' as shown in Figure 7.4(b). The indentation depth can be referred as the displacement of abrasive in to workpiece. The work done by the abrasive particle in this process can be equated to the KE of the abrasive particle.

Hence,

$$F_{n1} \times d_1 = \frac{1}{2}\left(\frac{a^3}{6\sqrt{2}} \times \rho_a\right)(2\pi fA)^2 \tag{7.11}$$

The value of impact force F_{n1} can be obtained by the property of work material.

By solving Eq. (7.11) indentation height (h_1) can be expressed as:

$$d_1 = \frac{8a^3\rho_a\,(\pi Af)^2}{3\sqrt{6}\,\sigma_w\,w^2} \tag{7.12}$$

where, σ_w and w are the strength of workpiece material and width of indentation at the workpiece surface.

Due to the rotation of tool, a centrifugal force F_c acts on the abrasive due to which abrasive strikes on the side wall of the cavity (Figure 7.4(a)).

191
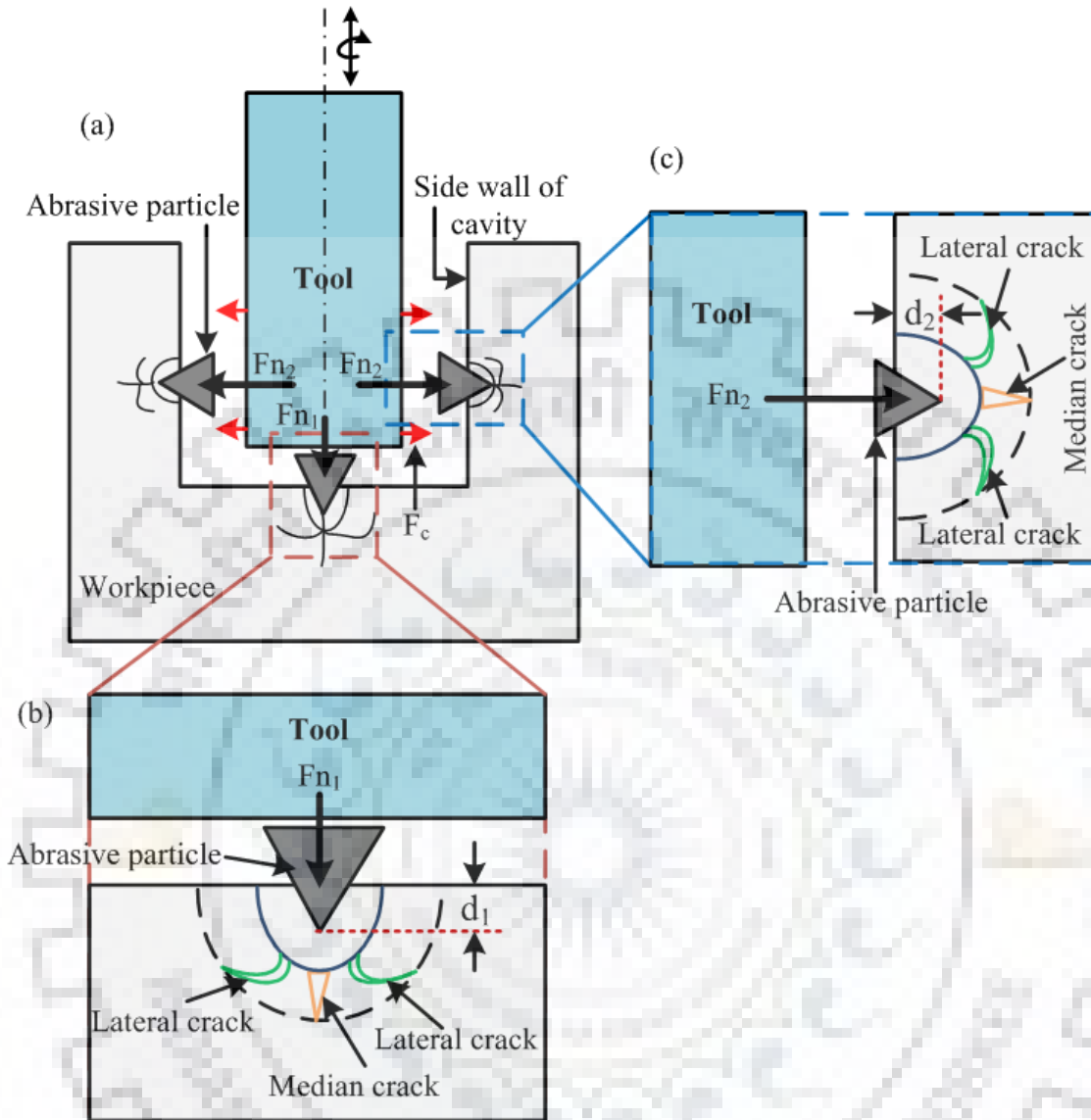
Figure 7.4 Schematic representation showing (a) tool, abrasive particle and workpiece interaction (b) impact of abrasive particle beneath the tool (c) impact of abrasive particle at side wall of cavity

In this case, if the velocity of abrasive particle due to centrifugal force F_c is v_2. It can be expressed as:

$$v_2 = \frac{2\pi r N}{60}$$

(7.13)

where, r and N are radius and rotation speed of the tool respectively.

The abrasive particle hits the side wall of the machined cavity and creates an indentation of depth d_2 (Figure 7.4(c)). Now, by substituting the value of v_2 from Eq. (7.13) into Eq. (7.8) and equating work done by abrasive and KE of abrasive particle.

$$F_{n2} \times d_2 = \frac{1}{2}\left(\frac{a^3}{6\sqrt{2}} \times \rho_a\right)\left(\frac{2\pi r N}{60}\right)^2 \tag{7.14}$$

On solving Eq. (7.14) the indentation depth (d_2) of abrasive at side wall of cavity can be obtained as:

$$d_2 = \frac{a^3 \rho_a \, (\pi r N)^2}{450\sqrt{6}\, \sigma_w \, w^2} \tag{7.15}$$

7.2.2 Number of abrasive particles

As the abrasives particle hit the workpiece with one of its vertices, the height of the machining gap (distance between tool and work) can be expressed by the height of the abrasive (h) as shown in Figure 7.5. If the tool is of solid cylindrical shape having diameter d_t (Figure 7.5). The average number of abrasive particles into the working gap can be obtained by:

$$Volume\ of\ working\ gap = (Volume\ of\ abrasive + Volume\ of\ liquid) \tag{7.16}$$
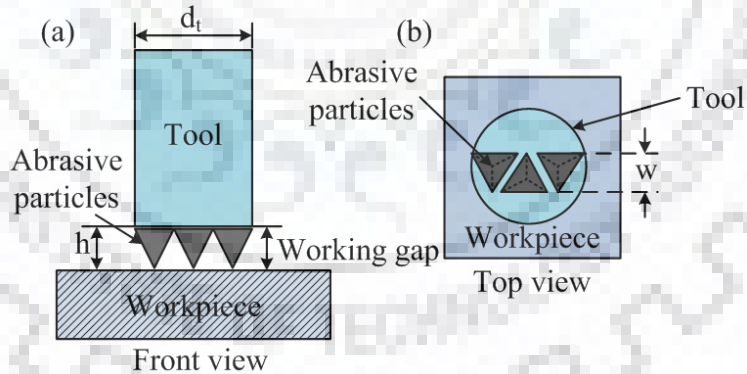
Figure 7.5 Number of abrasive particles in the machining gap (a) front view (b) top view

$$Volume\ of\ working\ gap = \frac{Weight\ of\ abrasives}{Density\ of\ abrasives} + \frac{Weight\ of\ liquid}{Density\ of\ liquid}$$

$$\frac{\pi d d_t^2 h}{4} = \frac{W_a}{\rho_a} + \frac{W_a}{C} \tag{7.17}$$

where, W_a and C are the weight of abrasives and concentration of the abrasive particles in slurry by weight (i.e. ratio of weight of abrasive to the weight of the liquid medium).

$$W_a = Volume\ of\ abrasive\ \times Density\ of\ abrasive$$

$$\frac{\pi d_t^2 h}{4} = Volume \times Density \left[\frac{1}{\rho_a} + \frac{1}{C}\right]$$

$$\frac{\pi d_t^2 h}{4} = \frac{a^3\sqrt{2}}{12} \times \rho_a \left[\frac{1}{\rho_a} + \frac{1}{C}\right] \times n \tag{7.18}$$

where, a and h are the side length and height of the regular tetrahedron abrasive particle. On simplifying the above Eq. (7.18).

$$n = \frac{\frac{3\pi}{\sqrt{2}} d_t^2 h}{a^3 \left[1 + \frac{\rho_a}{C}\right]} \tag{7.19}$$

Geometrically, the relationship between a and h can be expressed as:

$$h = \frac{a\sqrt{6}}{3} \tag{7.20}$$

From Figure 7.3, the geometrical relation between a, h, w and d can be expressed as:

$$\frac{a}{h} = \frac{w}{d} \tag{7.21}$$

By substituting the values of MR_a and N from Eq. (7.4) and Eq. (5.19) into Eq. (7.5), the MRR_{Total} can be obtained as:

$$MRR_{Total} = \frac{\frac{3\pi}{\sqrt{2}} d_t^2 h}{a^3 T_m \left[1 + \frac{\rho_a}{C}\right]} \times f \times \frac{4}{3} C_2^3 \left[\left(\frac{1}{tan\alpha}\right)^{11/6} \left[\frac{E^2}{H_v^3 K_{IC}^2 (1-\upsilon)}\right] F_n^{7/4}\right] \tag{7.22}$$

Normal load F_n can be calculated by the workpiece material properties.

$$F_n = \sigma_w A_i \tag{7.23}$$

where, σ_w and A_i are the workpiece material strength and indentation area respectively.

MRR_{Total} is the sum of the volume of work material removed at the bottom as well as the side wall of the cavity and it can be written as:

$$MRR_{Total} = MRR_{bottom} + MRR_{side\,wall} \tag{7.24}$$

$$MRR_{bottom} = \frac{\frac{3\pi}{\sqrt{2}}d_t{}^2 h}{a^3 T_m\left[1+\frac{\rho_a}{C}\right]} \times f \times \frac{4}{3}C_2^3\left[\left(\frac{1}{tan\alpha}\right)^{11/6}\left[\frac{E^2}{H_v^3 K_{IC}^2(1-v)}\right]F_{n_1}{}^{7/4}\right] \tag{7.25}$$

where, F_{n_1} is the normal load at the bottom of the cavity as shown in Figure 7.4(b).

$$MRR_{side\,wall} = \frac{\frac{3\pi}{\sqrt{2}}d_t{}^2 h}{a^3 T_m\left[1+\frac{\rho_a}{C}\right]} \times f \times \frac{4}{3}C_2^3\left[\left(\frac{1}{tan\alpha}\right)^{11/6}\left[\frac{E^2}{H_v^3 K_{IC}^2(1-v)}\right]F_{n_2}{}^{7/4}\right] \tag{7.26}$$

where, F_{n_2} is the normal load at the side wall of the cavity as shown in Figure 7.4(c).

If A_{i_b} and A_{i_s} are the indentation area at the bottom and side wall of the cavity respectively. Then the normal loads F_{n_1} and F_{n_2} can be determined as:

$$F_{n_1} = \sigma_w A_{ib} \tag{7.27}$$

Similarly,

$$F_{n_2} = \sigma_w A_{is} \tag{5.28}$$

On further simplifying Eq. (7.27) and Eq. (7.28), normal loads F_{n_1} and F_{n_2} can be expressed as:

$$F_{n_1} = \frac{K_1 a^2 \rho_a^{\frac{2}{3}}(\pi A f)^{\frac{4}{3}}}{\sigma_w^{\frac{1}{3}}} \tag{7.29}$$

$$F_{n_2} = \frac{K_2 a^2 \rho_a^{\frac{2}{3}}(\pi r N)^{\frac{4}{3}}}{\sigma_w^{\frac{1}{3}}} \tag{7.30}$$

where, $K_1 = 0.5$ and $K_2 = 0.072$ are the constants.

On substituting the values of F_{n_1} and F_{n_2} from Eq. (5729) and Eq. (7.30) into Eq. (7.25) and Eq. (7.26) and after that substituting the value of MRR_{bottom} and $MRR_{side\,wall}$ from Eq. (7.25) and Eq. (7.26) into Eq. (7.24), MRR_{Total} can be determined as:

$$MRR_{Total} = \frac{\pi^{\frac{10}{3}}a^3 \rho_a^{\frac{2}{3}}d_t{}^2 f C_2^3}{\sqrt{3}\sigma_w^{\frac{1}{3}}T_m\left(1+\frac{\rho_a}{C}\right)}\left(\frac{1}{(tan\alpha)}\right)^{\frac{11}{6}}\left(\frac{E^2}{H_v^3 K_{IC}^2(1-v)}\right)\left[K_1^{\frac{7}{4}}(Af)^{\frac{7}{3}}+K_2^{\frac{7}{4}}(rN)^{\frac{7}{3}}\right] \tag{7.31}$$

Equation (7.31) shows the developed model of MRR for rotary tool micro-USM process. According to Eq. (7.31), MRR is a function of frequency of vibration, amplitude of vibration,

tool radius, tool rotation speed, slurry concentration, abrasive size, properties of workpiece and abrasive materials such as fracture toughness, hardness, modulus of elasticity, poison's ratio and half angle of abrasive particle. The developed model of MRR was verified with the help of experiments which were conducted on glass workpiece.

The MRR was predicted using the Eq. (7.31). The value of input process parameters and properties of work and abrasive materials used for the prediction of MRR are tabulated in Table 7.1.

Table 7.1 Input parameters and their values, work and abrasive material properties

Input parameters	Values
Frequency (f)	21±1 kHz
Rotation speed (N)	100, 200, 300, 400, 500, 600, 700 rpm
Amplitude (A)	10, 12, 14 µm
Abrasive size (a)	8, 12, 14 µm
Slurry concentration (C)	5, 10, 15, 20 %
Static load	0.44 N
Tool radius (r)	300 µm
Microchannel dimensions	10 mm × 600 µm (L × W)
Work material properties	
Density (ρ_a)	2.23 kg/mm^3
Strength of workpiece (σ_w)	280 GPa
Hardness (K_{IC})	0.75 MPa.m$^{1/2}$
Poison's ratio	0.23
Abrasive material properties	
Material used	Silicon carbide (SiC)
Density (ρ_a)	2.23 kg/mm^3

During the prediction of MRR, only brittle fracture caused by impact action caused by abrasives was considered. The MRR for different values of input parameters as tabulated in Table 7.1 was predicted using Eq. (7.31). The predicted results with respect to each variable process parameter are discussed in the subsequent subsection.

7.3 Predicted Results of the Developed MRR Model

The developed model was used to predict the MRR for rotary tool micro-USM process beyond the selected range of the rotary tool micro-USM process parameters. During the prediction of MRR, only one variable parameter was varied at a time while the other variable parameters were set at constant value. This was done to investigate the effect of individual rotary tool micro-USM process parameter on MRR. The predicted results are furnished in the subsequent subsection.

7.3.1 Predictive effect of amplitude on MRR

The MRR was predicted for various values of amplitude as tabulated in Table 7.2. The amplitude was measured at different power ratings using the approach recommended by Khemelev et al., (2008) and Cheema, (2015). The predictive results are plotted in Figure 7.6. From Figure 7.6, it can be observed that the MRR increased linearly by increasing the amplitude of tool vibration from 9 μm to 15 μm. This can be inferred that as the amplitude of vibration increased, the tool impacted on the abrasives with higher energy. Subsequently, the abrasives imparted higher impact energy on the work surface leading to the formation of deeper/larger crater. As a result of that MRR found to be increased.

Table 7.2 Predicted MRR at different values of amplitude

Parameter	Value	Predicted MRR (mg/min)		
		Rotation speed (200 rpm)	Rotation speed (300 rpm)	Rotation speed (400 rpm)
Amplitude (μm)	9	1.03	1.13	1.23
	10	1.31	1.44	1.57
	11	1.63	1.79	1.96
	12	2.01	2.21	2.41
	13	2.47	2.72	2.96
	14	2.87	3.16	3.44
	15	3.35	3.69	4.02
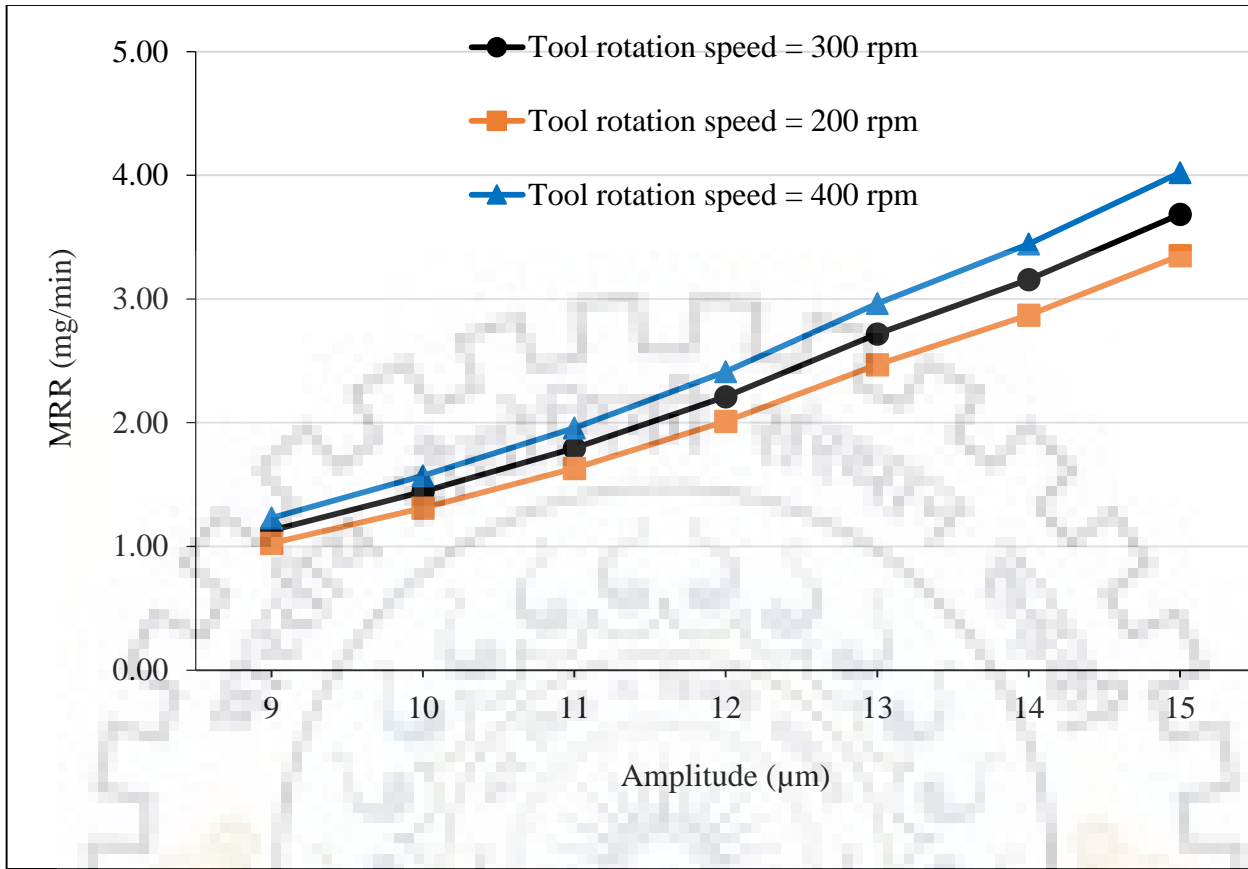
Figure 7.6 Predictive effect of amplitude on MRR

7.3.2 Predictive effect of rotation speed on MRR

The MRR was predicted for various values of tool rotation speeds as tabulated in Table 7.3. The results are plotted in Figure 7.7. From the predictive effect of tool rotation speed on MRR shown in Figure 7.7, it can be observed that with an increase in tool rotation speed from 100 rpm to 700 rpm, marginal increment was noticed in MRR. The attributed reason for this trend may be explained with the fact that the material removal in USM process is dominantly removes due to the hammering/impact action of the abrasives on work surface (Benedict, (1987)). Tool rotation did not contributed into the material removal mechanism it only assisted the abrasives to come out from the machining zone so that new fresh abrasives can enter into the machining zone. Thus, no improvement in MRR was obtained by varying the tool rotation speed. The marginal increment was due to the effective replenishment of the abrasives due to which new fresh abrasives participated into machining.

Table 7.3 Predicted MRR at different values of tool rotation speed

Parameter	Value	Predicted MRR (mg/min)		
		Amplitude (12 µm)	Amplitude (13 µm)	Amplitude (14 µm)
Rotation speed (rpm)	100	2	2.42	2.76
	200	2.03	2.45	2.79
	300	2.06	2.48	2.82
	400	2.07	2.49	2.83
	500	2.09	2.51	2.85
	600	2.1	2.53	2.86
	700	2.11	2.54	2.87
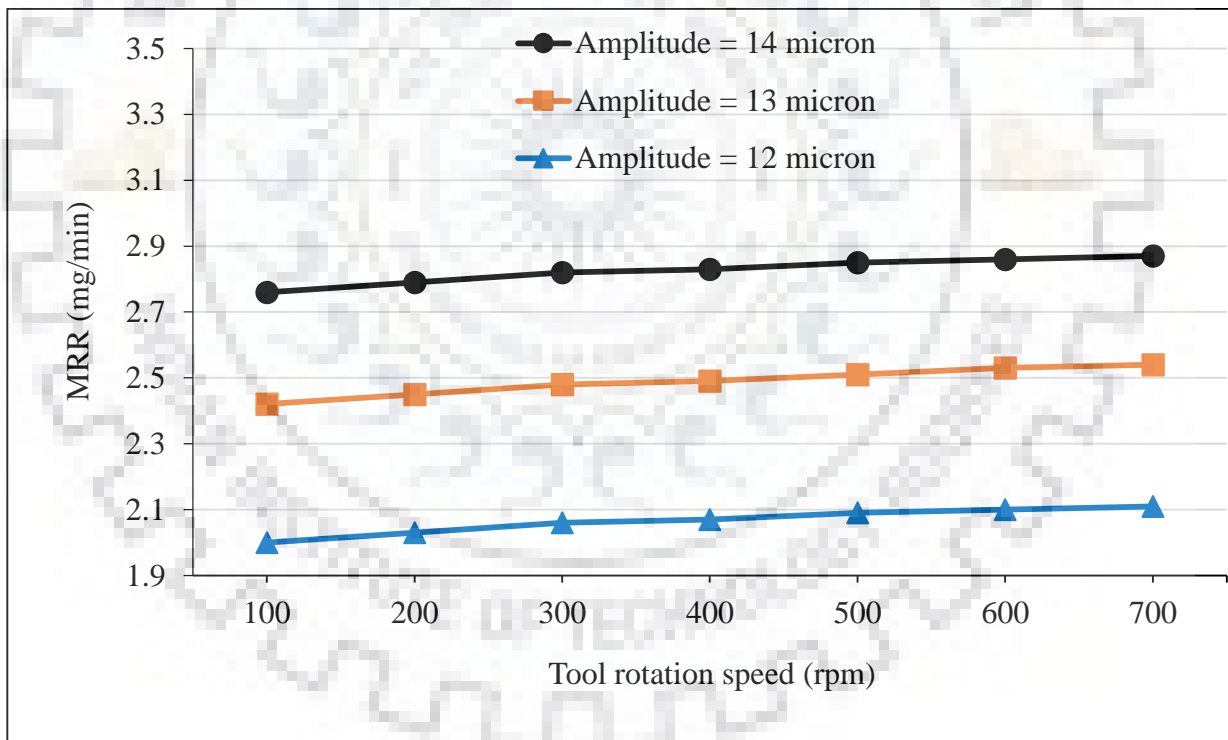
Figure 7.7 Predictive effect of tool rotation speed on MRR

7.3.3 Predictive effect of abrasive size on MRR

The MRR was predicted for various values of abrasive size as tabulated in Table 7.4. The predictive effect of abrasive grain size on MRR is depicted in Figure 7.8. It was observed that the MRR continuously increased by increasing the abrasive size. The size of the crater formed due to the impact of abrasives depends on the size of the abrasive used. Large size abrasive leads to the formation of larger crater and vice-versa. Large size craters further leads to the removal of more material from work surface. Due to the same reason, the MRR was found to be increased by increasing abrasive grain size in rotary tool micro-USM process. From Figure 7.9, it can also be noticed that rate of increase in MRR was higher when amplitude of vibration was increased as compare increase in abrasive grain size. This ensures the higher significance of amplitude over abrasive grain size in rotary tool micro-USM process.

Table 7.4 Predicted MRR at different values of abrasive size

Parameter	Value	Predicted MRR (mg/min)		
		Amplitude (12 µm)	Amplitude (13 µm)	Amplitude (14 µm)
Abrasive size (µm)	8	1.91	2.009	2.31
	9	2.15	2.26	2.60
	10	2.39	2.514	2.89
	11	2.63	2.76	3.18
	12	2.86	3.01	3.46
	13	3.12	3.28	3.77
	14	3.59	3.77	4.34
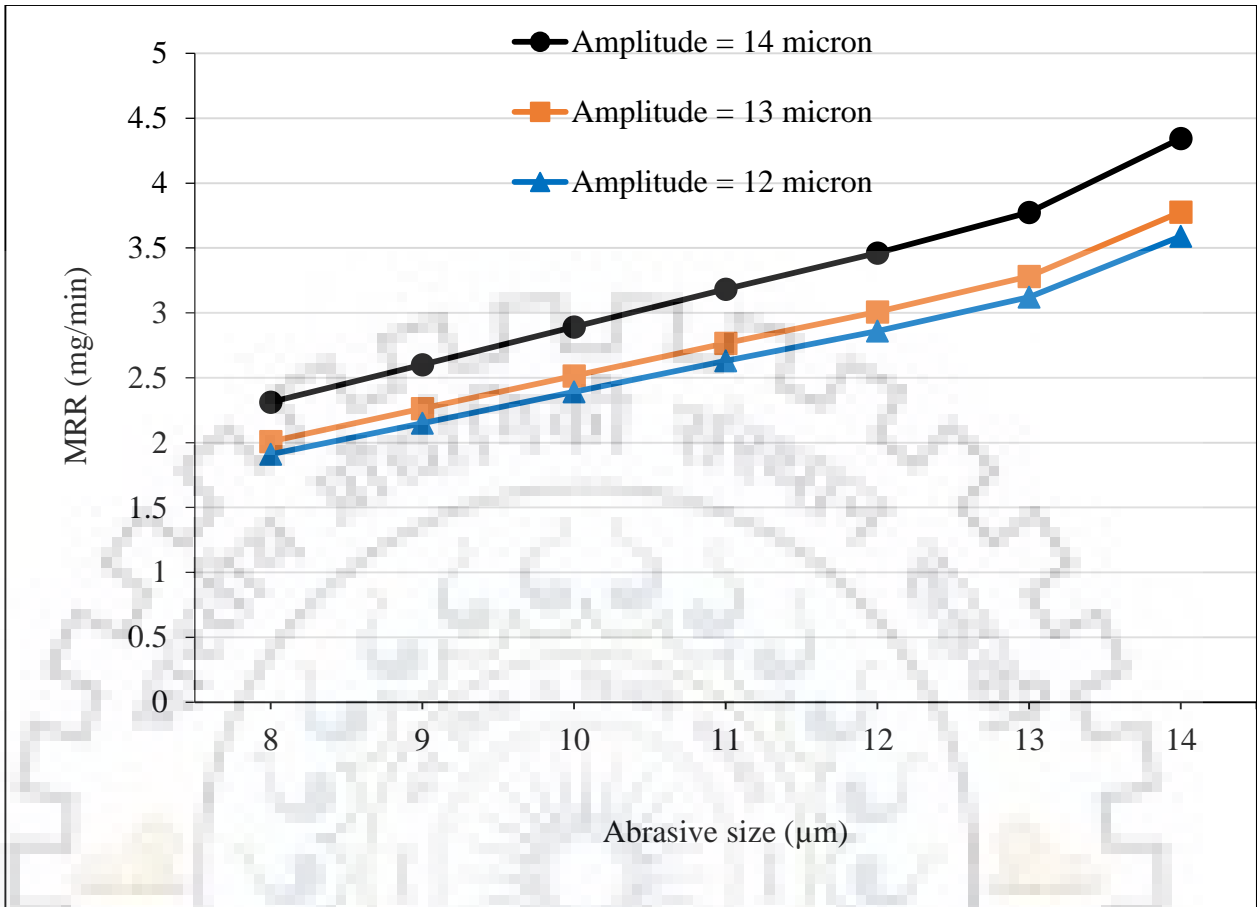
Figure 7.8 Predictive effect of abrasive size on MRR

7.3.4 Predictive effect of concentration on MRR

The MRR was predicted for various values of concentration as tabulated in Table 7.5. The predictive effect of abrasive grain size on MRR is depicted in Figure 7.9. From the predictive effect of concentration on MRR presented in Figure 7.9, it can be observed that by increasing the concentration of abrasive slurry, MRR increased. This was attributed to the reason that the number of abrasives increased on increasing the concentration. Due to which, more abrasives participated into machining. This led to the generation of more craters on the work surface and as a result of that more material was removed from the surface of workpiece.

Table 7.5 Predicted MRR at different values of concentration

Parameter	Value	Predicted MRR (mg/min)		
		Amplitude (12 μm)	Amplitude (13 μm)	14 μm Amplitude (14 μm)
Concentration (%)	5	2.09	2.50	2.98
	10	2.15	2.57	3.07
	15	2.17	2.6	3.1
	20	2.184	2.62	3.12
	25	2.219	2.66	3.17
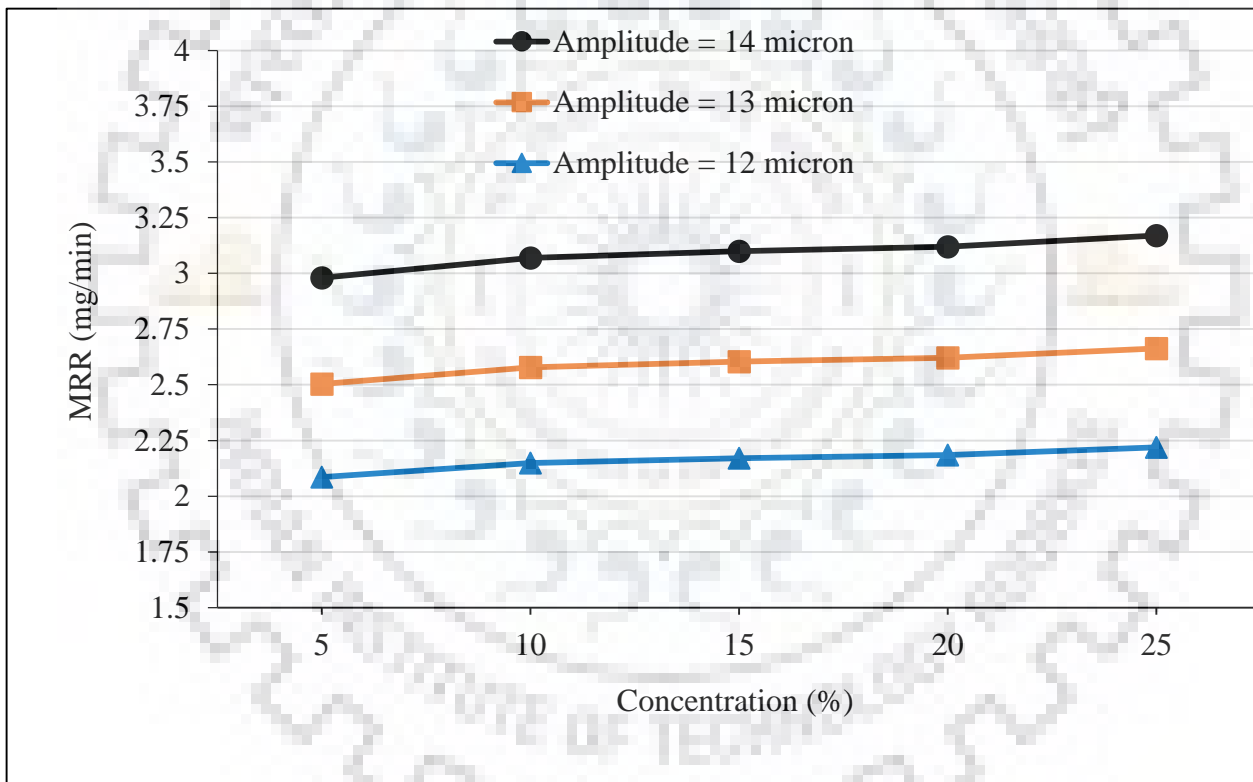
Figure 7.9 Predictive effect of concentration on MRR

7.4 Experimental Verification of Developed MRR Model

In order to verify the developed model of MRR for rotary tool micro-USM process, the experiments were conducted as per the experimental settings tabulated in Table 7.1. The results obtained from the experiments were compared with the predicted results obtained by the

developed model of MRR. The comparison of both the actual and predicted results are tabulated in Table 7.6 to Table 7.9 and the comparative plots are shown in Figures 7.10 to Figure 7.13. From Figures 7.10 to Figure 7.13, it can be noticed that all the predicted results corresponding to each input process parameter were in good agreement with the actual results obtained experimentally.

Table 7.6 Predicted and actual MRR at different values of amplitude

Parameter	Value	MRR (mg/min)	
		Predicted	Actual
Amplitude (µm)	10	1.31	1.37
	12	2.01	2.13
	14	2.87	2.79
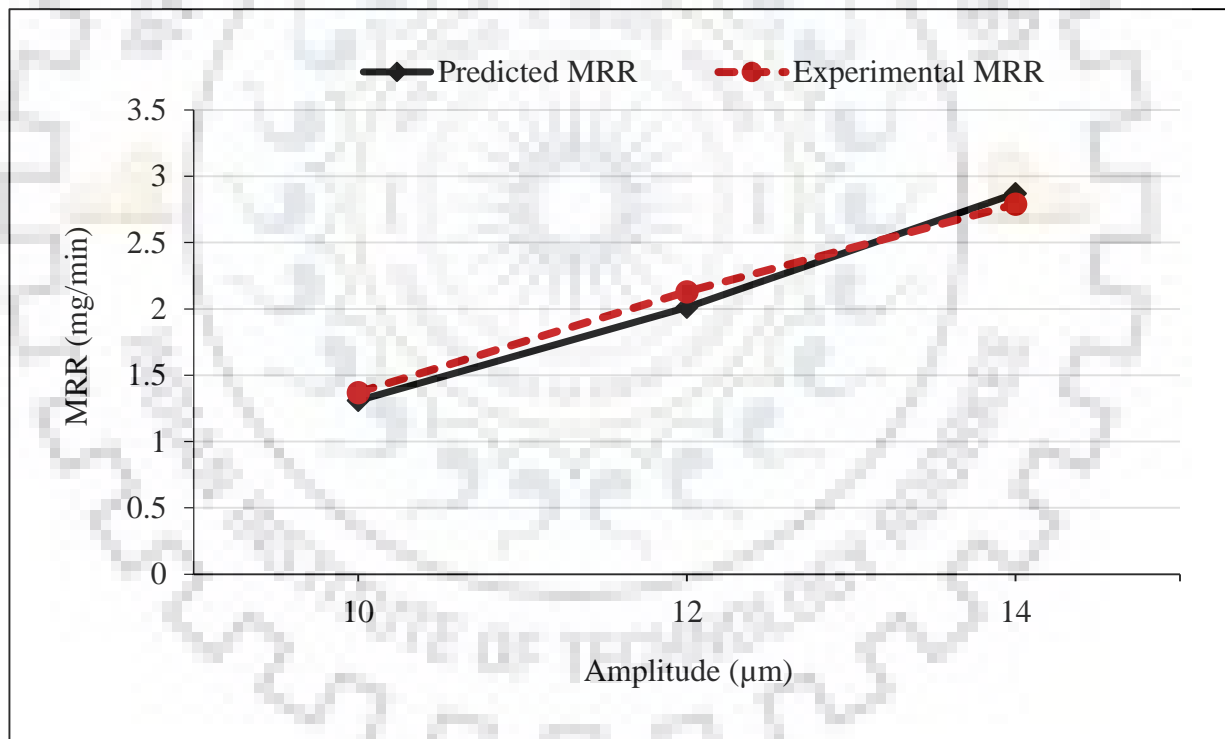
Figure 7.10 Comparative results of MRR at different amplitudes

203

Table 7.7 Predicted and actual MRR at different values of tool rotation speed

Parameter	Value	MRR (mg/min)	
		Predicted	Actual
Rotation speed (rpm)	100	2.76	2.21
	200	2.79	2.54
	300	2.82	2.96
	400	2.83	2.81
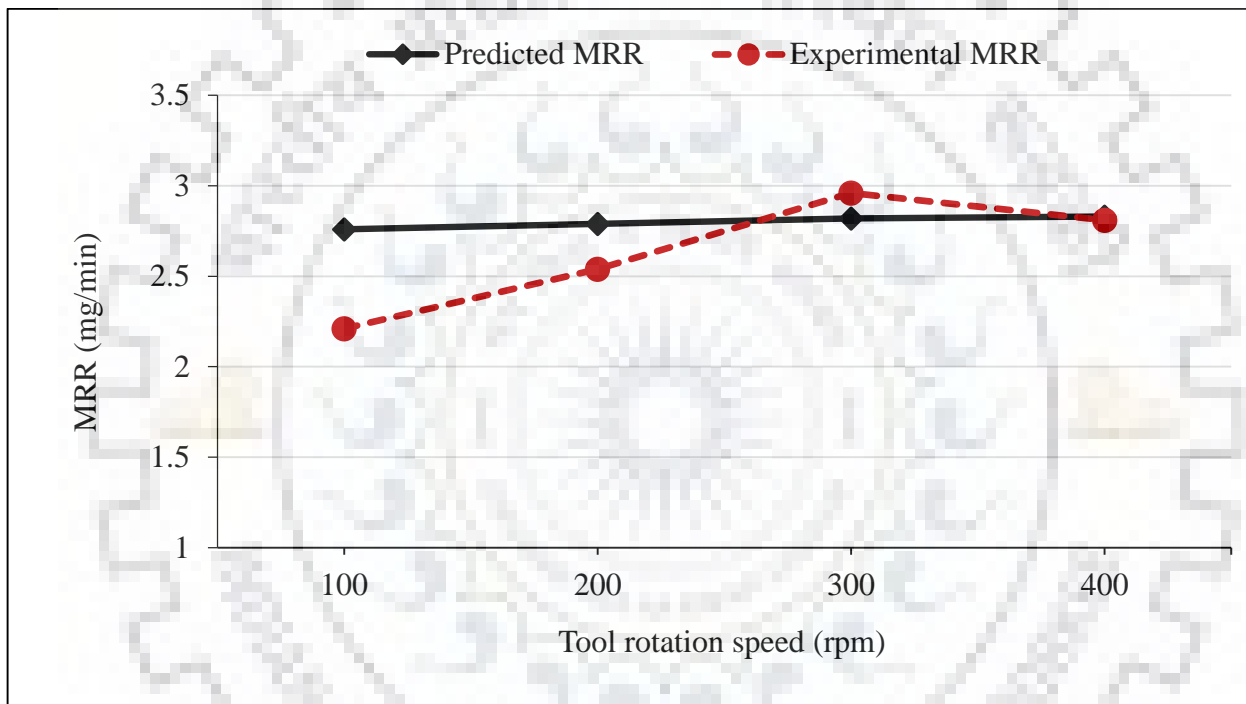
Figure 7.11 Comparative results of MRR at different rotation speeds

Table 7.8 Predicted and actual MRR at different values of abrasive size

Parameter	Value	MRR (mg/min)	
		Predicted MRR	Actual MRR
Abrasive size (µm)	8	1.91	1.84
	12	2.86	2.97
	14	3.59	2.85
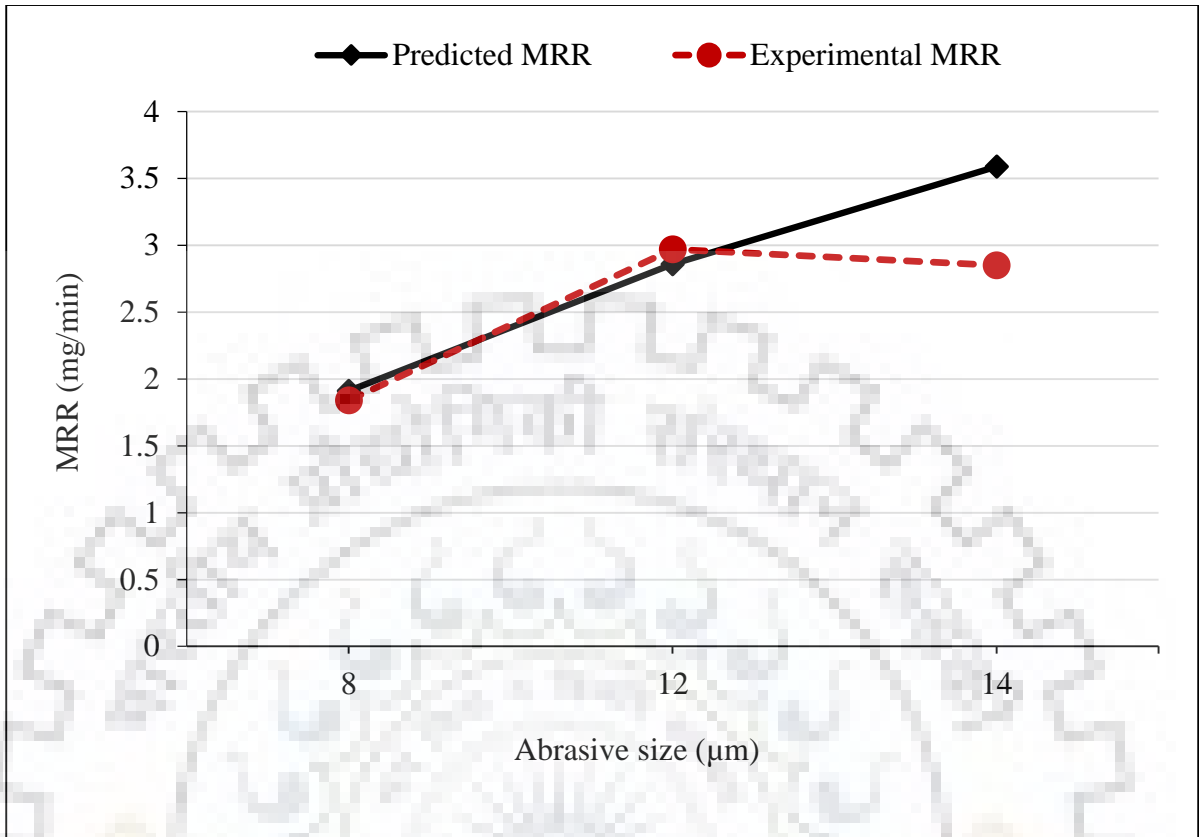
Figure 7.12 Comparative results of MRR at different abrasive grain size
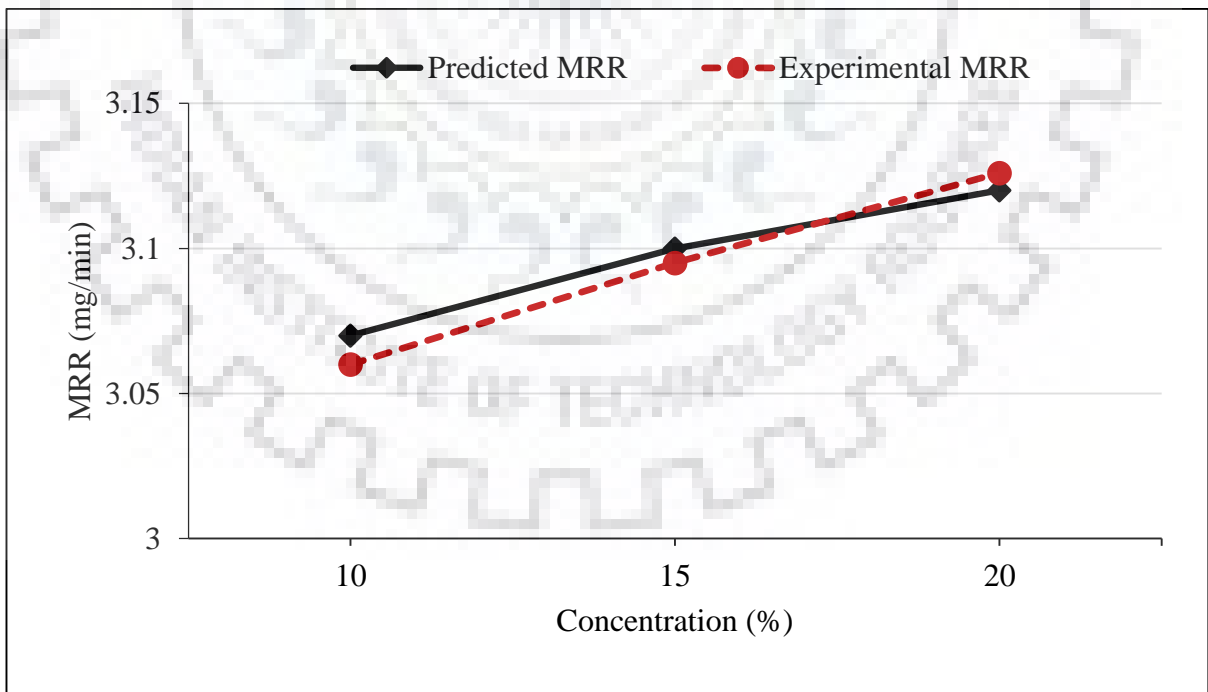
Figure 7.13 Comparative results of MRR at different concentration

Table 7.9 Predicted and actual MRR at different values of concentration

| Parameter | Value | MRR (mg/min) | |
		Predicted	Actual
Concentration (%)	10	3.07	3.06
	15	3.1	3.095
	20	3.12	3.126

Further, in order to examine the prediction accuracy of the developed MRR model for rotary tool micro-USM process, statistical analysis was also carried out. During statistical analysis, coefficient of correlation (R-value) and mean absolute percentage error (MAPE) were calculated. The coefficient of correlation (R-value) was calculated to check the degree of association between predicted and experimental values. The MAPE was calculated to predict the accuracy of the developed models. The R-value and MAPE were calculated as per the Eq. (7.32) and Eq. (7.33) (Sharma et al., (2017)).

$$R - value = \sqrt{1 - \frac{\sum_{j=1}^{n}(E_j - P_j)^2}{\sum_{j=1}^{n}(P_j)^2}} \qquad (7.32)$$

$$MAPE = \frac{1}{n}\sum_{j=1}^{n}\left(\frac{E_j - P_j}{E_j}\right) \times 100 \qquad (7.33)$$

where, E, P and n are the experimental (actual) output, predicted output and number of pattern in the data set respectively.

From the results obtained by conducting statistical analysis, it was found that the predicted MRR and experimental MRR showed R-value = 0.9976 and MAPE = 2.45%. Therefore, it can be concluded that the developed MRR model is adequate and it can be used to estimate the MRR for rotary tool micro-USM process.

7.5 Summary

In this chapter, a predictive model of MRR for rotary tool micro-USM process is developed. In order to develop the model, mechanism of material removal was assumed due to the pure brittle

fracture caused by the impact of abrasive particles on work surface. The predictive model was developed under certain assumptions. During the development of the model, a relationship between depth of indentation and input parameters of rotary tool micro-USM process is also established. The developed model was verified through experimental and statistical analysis for different values of input process parameters such as amplitude of vibration, tool rotation speed, abrasive size and concentration of slurry. Both the predicted and experimental results were found to be in good agreement. The developed model can be used to predict the MRR for rotary tool micro-USM of other hard and brittle materials.

CHAPTER 8

CONCLUSIONS AND SCOPE FOR FUTURE WORK

The present chapter summarizes the conclusions drawn from the present research endeavor and future scope of work. This chapter is divided into six sections, first section presents the generalized conclusions that have been drawn from chapter three. Section two to five present the major outcomes that have been drawn from chapter four to seven respectively. The last section of this chapter includes the future scope of work.

8.1 Generalized Conclusions

- The range of tool rotation speed selected for drilling of microholes was 100 rpm to 500 rpm. Whereas, the range of tool rotation speed selected for fabrication of microchannels was 100 rpm to 600 rpm.

- An increase in tool rotation speed up to 300 rpm, the DOH increased owing to effective slurry circulation. Beyond 300 rpm, it started to decrease. The HOC and edge chipping decreased up to 300 rpm of tool rotation speed and thereafter both started to increase.

- An increase in tool rotation speed up to 300 rpm, both the DOC and form accuracy of machined microchannels increased and after that both started to decrease. The edge chipping decreased up to 300 rpm of tool rotation speed and thereafter it started to increase.

- The SS-304 tool suffered from plastic deformation and strain hardening which caused higher tool wear (i.e. longitudinal wear and edge wear) as compared to the WC tool in which no strain hardening was observed.

- The strain hardening of SS-304 caused poor dimensional and form accuracy of machined microchannels.

- The hardness, impact strength and acoustic property of tool material significantly affected the performance of rotary tool micro-USM process. Owing to superior properties over SS-304, the performance of WC tool material was found to be better in terms of higher MRR, DOC, lower WOC and better form accuracy.

- Both very high and low tool rotation speed, work feed rate and concentration diminished the performance of rotary tool micro-USM process by decreasing the MRR, DOC and increasing WOC of machined microchannels using both SS-304 and WC tool materials.

- An increase in power rating increased the MRR and DOC, but it simultaneously decreased the dimensional accuracy of machined microchannel.

8.2 Performance Evaluation of Rotary Tool Micro-USM Process

- In micro-USM process, rotary motion of tool provided easy replenishment of abrasive particles from machining zone and thereby, significantly improved the machining rate and form accuracy of both the microholes and microchannels. Further, rotary tool micro-USM process can be effectively used to fabricate other micro features of intricate shapes.

- The MRR increased continuously with an increase in power rating, slurry concentration, static load and abrasive size using both the rotary tool micro-USM and stationary tool micro-USM processes.

- The HOC initially increased and then decreased by increasing the power rating and static load in both rotary tool and stationary tool micro-USM processes. Both very coarse and very fine abrasives resulted in higher value of HOC. Slurry concentration of 20% resulted in lesser HOC owing to uniform distribution of abrasive particles in between tool and workpiece.

- Tool rotation in micro-USM provided effective circulation of slurry in between tool and workpiece resulting in lesser tool wear and better dimensional accuracy of microholes.

- With increase in work feed rate up to 20 mm/min, power rating up to 60% and concentration up to 20%, there was an increase in MRR and DOC machined by stationary tool and rotary tool micro-USM processes.

- Use of fine abrasive particles (i.e. #1000 mesh) yielded higher machining rate and DOC in stationary tool and rotary tool micro-USM processes owing to the availability of more number of abrasives in the machining zone.

- In micro-USM process, the tool wear significantly reduced by rotating the tool and enhanced its performance in terms of MRR, DOC and form accuracy by 155%, 147% and 19% respectively.

210

8.3 Investigations on Microhole Drilling

- The augmentation of rotary motion of tool in micro-USM process was found to be an effective solution to resolve the problem of debris accumulation in the machining zone. Hence, rotary tool micro-USM process can be employed for machining micro-holes in all types of hard and brittle materials.
- On increasing power rating, the MRR, DOH and HOC increased continuously.
- The MRR and DOH increased and HOC decreased by increasing the rotation speed up to 300 rpm, abrasive size up to #1200 mesh and concentration up to 20%.
- The maximum MRR and DOH were obtained when machining of silicon work material. However, HOC was also found to be maximum in silicon than that of glass and zircon.
- The fracture toughness as compared to hardness was found to be more significant factor affecting the machining rate in RT-MUSD process. Owing to low fracture toughness, silicon work material followed by glass and zirconia exhibited maximum MRR and DOH.
- The work material hardness significantly affected the tool wear in RT-MUSD process. Owing to the high hardness of zirconia, the tool wear was higher while machining of zirconia as compared to silicon and glass.
- Brittle facture was found to be the dominant mode of material removal in all three work materials (i.e. zirconia, silicon and glass) during RT-MUSD process.
- The parametric optimization for maximizing the MRR, DOH and minimizing the HOC revealed the parametric settings of rotation speed = 500 rpm, power rating = 42.22%, abrasive size = #1800 mesh and concentration of slurry = 23.92% for optimal responses. The maximum composite desirability observed was 0.8822.
- The rotary tool micro-USM process successfully machined a micro-hole of 4355 μm in glass using optimal parametric setting of process parameters.

8.4 Investigations on Tool Wear and its Effect on Form Accuracy of Microchannels

- In rotary tool micro-USM, two type of tool wear namely longitudinal wear and edge rounding wear were observed. Negligible lateral wear was noticed during machining using rotary tool micro-USM.

- The shape of the machined microchannel was greatly affected by tool wear. The form accuracy of machined microchannel is affected by the edge rounding wear, depth of microchannel is affected by the longitudinal wear of the tool.

- A novel geometrical model for quantification of 2-D tool wear to 3-D volumetric wear in rotary tool micro-USM process was developed. The developed model can be used to describe the form accuracy of the machined microchannels.

- The contribution of longitudinal wear was more as compared to edge rounding wear in TVW of tool.

- The desired depth of channel at the best possible form accuracy of the microchannel can be obtained by providing longitudinal wear compensation to the tool.

- A longitudinal wear compensation of 0.092 μm for each 1 μm depth of channel is recommended for rotary tool micro-USM process within the selected range of process parameters.

- The MRR and DOC was increased up to 500 rpm of tool rotation speed and after that both decreased owing to lesser interaction time between tool, abrasive particles and workpiece.

- Tool rotation speed of 300 rpm provided minimum WOC and TVW of tool and hence best possible form accuracy of machined microchannel.

- The DOC, WOC and MRR increased up to 20 mm/min feed rate and after that a decreasing trend was obtained in all owing reduction interaction time between tool, abrasive particle and workpiece.

- At a feed rate of 30 mm/min, minimum TVW of tool was obtained which resulted in best possible form accuracy of microchannel.

- The MRR and depth of microchannel were increased on increasing the power rating from 20% to 40% owing to increased ultrasonic energy. Beyond 40% of power rating, a decreasing trend was observed. The tool wearing out at faster rate at higher ultrasonic, thus decreasing the MRR and DOC.

- An increase in WOC was obtained when the power rating was increased from 20% to 60%.

- The TVW was increased continuously when the power rating was increasing 20% to 60%. The tool hit the abrasive particles with higher ultrasonic energy as the power rating increased, thus increased the TVW of tool.

- The best possible form accuracy of microchannel was observed at 60% power rating.

- The maximum MRR, TVW of tool, DOC and minimum WOC was obtained when #1200 mesh size abrasive particles were used.

- In case of machining with #1200 mesh size and #1800 mesh size abrasive particles, form accuracy of microchannel was better in comparison to form accuracy obtained when #1000 mesh size abrasive particles were used.

- The MRR and DOC were increased on increasing the slurry concentration from 10% to 20% owing to increased number of abrasive particle into the machining zone. Beyond 20% slurry concentration both decreased owing to multiple abrasive layers in the machining gap.

- The best possible form accuracy and minimum TVW and WOC were observed when 10% slurry concentration was used.

- The developed facility of rotary tool micro-USM process was used to fabricate different profiles of microchannels i.e. rectangular, circular and spiral etc. The fabrication of these profiles proved the capability of the developed facility.

- The measured responses of different profiles of microchannels i.e. MRR, WOC, DOC and surface roughness were quite close in magnitudes. This proved the interchange ability of micro fabrication of channels on the developed facility.

8.5 Development of Mathematical Model of Material Removal Rate

A mathematical model of MRR for rotary tool micro-USM process was developed by considering pure brittle fracture mode of material removal. The shape of abrasive particle was consider as regular tetrahedron. . The estimated results were compared with the experimental results and found to be in good agreement with each other. Additionally, statistical analysis was performed to check the prediction accuracy of the developed model. The results revealed that the model is adequate with a correlation coefficient of 0.9976 and a mean absolute percentage error

of 2.45%. Hence, the developed model can be used to estimate the MRR for RT-MUSM process of hard and brittle materials.

8.6 Future Scope of Work

The objective of present research work was to improve the performance of micro-USM process during machining of microfeatures such as microholes and microchannels. In order to achieve this, rotary motion of tool was introduced in the existing micro-USM system during present investigation. The effect of tool rotation was analyzed on the performance of rotary tool micro-USM process during machining of microholes and microchannels on hard and brittle materials such as glass, silicon and zirconia. But, still there is some scope of further improvement in the performance of micro-USM process to make it industrially viable. In future, following aspect needs to be explore to enhance rotary tool micro-USM process performance.

- The facility was developed for laboratory scale experimentation. This facility can be improved for industrial use by improving production capacity, consistency and reliability. In future work, developed facility can be used to perform different machining operations like turning and groove making by incorporating additional attachments.
- Adaptive feedback control tool feeding system can be a possibility to further improve rotary tool micro-USM process efficiency.
- In the present research work, only individual effect of variable process parameters were investigated on the rotary tool micro-USM process performance. In future, investigations on combined effect of rotary tool micro-USM process parameters on its performance can be conducted for better understanding of the process.
- In the present research work solid cylindrical tool was used for machining. In future, change in tool material and design are also a possibility to further improve rotary tool micro-USM process accuracy and efficiency.
- The present research work was conducted using water as a liquid medium for slurry. Further study can be carried out selecting other liquid mediums of slurry.
- The microchannels developed by rotary tool micro-USM process can be further processed by chemical etching to achieve super fine surface finish required in microfluidics area.

- In the present research work only feasibility study was carried out on fabrication of complex shape (serpentine, spiral, zig-zag etc.) microchannels on glass. In future, a detailed investigation can be carried out to develop fully dedicated lab on chip devices for microfluidic applications.

- A dedicated investigation can be performed on rotary tool micro-USM process by analyzing the behavior of abrasive particles in between the rotating tool and workpiece.

- An online tool wear measurement technique can be applied using high speed imaging. This shall be helpful in monitoring the tool wear before and after machining and report the dimensional change.

REFERENCES

1. Adithan M. (1974), "Tool wear studies in ultrasonic drilling", Wear, Vol. 29, pp. 81-93.

2. Adithan M. (1981), "Tool wear characteristics in ultrasonic drilling", Tribology International, Vol. 14 (6), pp. 351-356.

3. Adithan M. and Krishnamurthi R. (1978), "Structural alterations in the workpiece by ultrasonic drilling", Wear, Vol. 46, pp. 327-334.

4. Akhtar S.N., Sharma S., Ramakrishna S.A., and Ramkumar J. (2016), "Excimer laser micromachining of oblique microchannels on thin metal films using square laser spot", Sadhana, Vol. 41(6), pp. 633-641.

5. Alba-Baena N.G., Murr L.E., Loya-Puga A. and Salas W. (2007), "Use of WEDM in the characterization process of Al/2-phase systems consolidated by multilayers cylindrical dynamic compaction method", Materials Science Forum, Vol. 546-549, pp.1541-1546.

6. Algodi S.J., Murray J.W., Fay M.W., Clare A.T. and Brown P.D. (2016), "Electrical discharge coating of nanostructured TiC-Fe cermets on 304 stainless steel", Surface and Coatings Technology, Vol. 307, pp. 639-649.

7. Arif M., Rahman M., Wong Y.S. and Neha, D. (2011), "An experimental approach to study the capability of end-milling for microcutting of glass. The International Journal of Advanced Manufacturing Technology, Vol. 53(9–12), pp. 1063–1073.

8. Badar M. A., Raman S., and Pulat P.S. (2005[a]), "Experimental verification of manufacturing error pattern and its utilization in form tolerance sampling", International Journal of Machine Tools and Manufacture, Vol. 45(1), pp. 63-73.

9. Badar M. A., Raman S., Pulat P. S. and Shehab R.L. (2005[b]), "Experimental analysis of search-based selection of sample points for straightness and flatness estimation", Journal of manufacturing science and engineering, Vol. 127(1), pp. 96-103.

10. Baishya N.J., Sharma D. and Dixit U.S. (2014), "Optimization of pressure vessel under thermo-elastic condition", Journal of The Institution of Engineers (India): Series C, Vol. 95(4), pp. 389-400.

11. Baker R.W., (2012), "Membrane technology and applications", John Wiley & Sons.

12. Baroud C.N., Delville J.P., Gallaire F. and Wunenburger R. (2007), "Thermocapillary valve for droplet production and sorting", Physical Review E, Vol. 75, pp. 046302.

13. Bayer T., Himmler K. and Hessel V. (2003), "Don't be baffled by static mixers", Chemical Engineering, Vol. 5, pp. 2–9.

14. Becker H. (2009), "It's the Economy…", Lab on a Chip, Vol. 9, pp. 2759-2762.

15. Benedict G.F, "Nontraditional manufacturing processes", Marcel Dekker, Inc, New York & Basel, 1987.

16. Boy J.J., Andrey E., Boulouize A. and Malek C.K. (2010), "Developments in microultrasonic machining (MUSM) at FEMTO-ST", The International Journal of Advanced Manufacturing Technology, Vol. 47, pp. 37-45.

17. Brinksmeier E. and Preuss W. (2012), "Micro-machining", Philosophical Transactions of the Royal Society A: Mathematical, Physical and Engineering Sciences, Vol. 370(1973), pp. 3973-3992.

18. Byrne G., Dornfeld D. and Denkena B. (2003), "Advancing cutting technology", CIRP Annals - Manufacturing Technology, Vol. 52(2), pp. 483-507.

19. Casquillas G.V. (2014), "Microfluidics and microfluidic devices: a review", Elveflow Microfluidic Instruments RSS.

20. Chalker P., Clare A., Davies S., Sutcliffe C.J. and Tsopanos S. (2005), "Selective laser melting of high aspect ratio 3D nickel–titanium structures for MEMS applications", MRS Online Proceedings Library Archive, Vol. 890, pp. 1-6.

21. Chavoshi S.Z. and Luo X. (2015), "Hybrid micro-machining processes: A Review", Precision Engineering, Vol. 41, pp. 1-23.

22. Cheema M.S., Dvivedi A. and Sharma A.K. (2013), "A hybrid approach to multi-criteria optimization based on user's preference rating", Proceedings of the Institution of Mechanical Engineers, Part B: Journal of Engineering Manufacture, Vol. 227(11), pp. 1733-1742.

23. Cheema M.S., Dvivedi A. and Sharma A.K. (2015), "Tool wear studies in fabrication of microchannels in ultrasonic micromachining", Ultrasonics, Vol. 57(C), pp. 57-64.

24. Cheema M.S., Ph.D Thesis, "An ultrasonic micromachining approach to fabricate microchannels on glass", IIT Roorkee -2015.

25. Cheema M.S., Singh P.K., Tyagi O., Dvivedi A. and Sharma A.K. (2016), "Tool wear and form accuracy in ultrasonically machined microchannels", Measurement, Vol. 81, pp. 85-94.

26. Chen J.M., Huang P.C. and Lin M.G. (2008), "Analysis and experiment of capillary valves for microfluidics on a rotating disk", Microfluidics and Nanofluidics. Vol. 4, pp. 427-437.

27. Cherku S., Sundaram M.M. and Rajurkar K.P. (2008), "Experimental study of micro ultrasonic machining process", Proceedings of ASPE Annual Meeting, Oregon.

28. Cho H., Kim H.Y., Kang J.Y. and Kim T.S. (2007), "How the capillary burst microvalve works", Journal of Colloid Interface Science, Vol. 306, pp. 379-385.

29. Choi J.P., Jeon, B.H. and Kim B.H. (2007), "Chemical-assisted ultrasonic machining of glass", Journal of Material Processing Technology, Vol. 191(1-3), pp. 153-156.

30. Choi W.M. and Park O.O. (2003), "A soft-imprint technique for direct fabrication of submicron scale patterns using a surface-modified PDMS mold", Microelectronic Engineering, Vol. 70, pp. 131-136.

31. Crowley, T.A. and Pizziconi, V. (2005), "Isolation of plasma from whole blood using planar microfilters for lab-on-a-chip applications", Lab on a Chip, Vol. 5(9), pp. 922-929.

32. Dangayach G.S. and Deshmukh S.G. (2005), "Advanced manufacturing technology implementation: Evidence from Indian small and medium enterprises (SMEs)", Journal of Manufacturing Technology Management, Vol. 16(5), pp. 483-496.

33. Daridon A., Fascio V., Lichtenberg J., Wütrich R., Langen H., Verpoorte E. and de Rooij N.F. (2001), "Multi-layer microfluidic glass chips for microanalytical applications", Fresenius' Journal of Analytical Chemistry", Vol. 371(2), pp. 261-269.

34. Davim J.P., Rubio J.C. and Abrao A.M. (2007),"A novel approach based on digital image analysis to evaluate the delamination factor after drilling composite laminates", Composites Science and Technology, Vol. 67(9), pp. 1939-1945.

35. Derringer G., Suich R. (1980), "Simultaneous optimization of several response variables", Journal of Quality & Technology, Vol. (12) pp. 214-219.

36. Dhakar K., Ph.D. Thesis, "Investigations on near-dry EDM and analysis of process performance", Indian Institute of Technology Roorkee-2016.

37. Egashira K. and Masuzawa T. (1999), "Microultrasonic machining by the application of workpiece vibration", Annals of CIRP - Manufacturing Technology, Vol. 48(1), pp. 131-134.

38. Egashira K., Masuzawa T., Fujino M. and Sun X.Q. (1997), "Application of USM to micromachining by on-the-machine tool fabrication", International Journal of Electrical Machining, pp. 31-36.

39. Egashira K., Masuzawa T., Fujino M. and Sun, X.Q. (1998), "Application of USM to micromachining by on-the-machine tool fabrication", Proceedings of the 4th Korea-Russia International Symposium on the Science and Technology, Ulsan, Korea, Vol.3, pp.106-113.

40. Egashira K., Mizutani K. and Nagao T. (2002), "Ultrasonic vibration drilling of microholes in glass", CIRP Annals- Manufacturing Technology, Vol. 51(1), pp. 339-342.

41. Egashira K., Taniguchi T., Tsuchiya H. and Miyazaki M. (2004), "Microultrasonic machining using multitools", Proceedings of the 7th International Conference on Progress Machining Technology, Suzhou, China, Aviation Industry Press, Anwai, Beijing, China, pp. 297-301.

42. Ehrfeld W., et al. (1999), "Characterization of mixing in micromixers by a test reaction: single mixing units and mixer arrays", Industrial & Engineering Chemistry Research Vol. 38(3), pp. 1075–1082.

43. Elsayed S.M., Sarker R.A. and Essam D.L. (2014), "A new genetic algorithm for solving optimization problems", Engineering Applications of Artificial Intelligence, Vol. 27, pp. 57-69.

44. Fan W.H., Chao C.L., Chou W.C., Chen T.T. and Chao C.W. (2009), "Study on the surface integrity of micro-ultrasonic machined glass-ceramic material", Key Engineering Materials, Vol. 407, pp. 731-734.

45. Forster R., Schoth A. and Menz W. (2005), "Micro-ECM for production of microsystems with a high aspect ratio", Microsystem Technologies, Vol. 11(4-5), pp. 246-249.

46. Garg R.K., Singh K.K., Sachdeva A., Sharma V.S., Ojha K. and Singh S. (2010), "Review of research work in sinking EDM and WEDM on metal matrix composite materials", The International Journal of Advanced Manufacturing Technology, Vol. 50(5-8), pp. 611-624.

47. Gentili E., Tabaglio L. and Aggogeri F. (2005), "Review on micromachining techniques", Proceedings of 7th International Conference on Advanced Manufacturing System and Technology, CISM International Centre for Mechanical Sciences, Vol. 486, pp. 387-396.

48. Goel H. and Pandey P.M. (2017), "Experimental investigations into the ultrasonic assisted jet electrochemical micro-drilling process", Materials and Manufacturing Processes, Vol. 32(13), pp. 1547-1556.

49. Goldstine H.H. and Goldstine A. (1996), "The electronic numerical integrator and computer (ENIAC)", IEEE Annals of the History of Computing, Vol. 18(1), pp. 10-16.

50. Grover W.H., Skelley A.M., Liu C.N., Lagally E.T. and Mathies R.A. (2003), "Monolithic membrane valves and diaphragm pumps for practical large-scale integration into glass microfluidic devices," Sensors and Actuators B, Vol. 89, pp. 315-323.

51. Gudimetla P. and Yarlagadda P.K.D.V. (2007), "Finite element analysis of the interaction between an AWJ particle and a polycrystalline alumina ceramic", Journal of Achievements in Materials and Manufacturing Engineering, Vol. 23(1), pp. 7-14.

52. Guo Y., Wang L., Zhang G. and Hou P. (2017), "Multi-response optimization of the electric discharge machining of insulating zirconia", Materials and Manufacturing Processes, Vol. 32(3), pp. 294-301.

53. Gupta P.K., Dvivedi A. and Kumar P., (2015), "Developments on electrochemical discharge machining: a review of experimental investigations on tool electrode process parameters", Proceedings of the Institution of Mechanical Engineers Part B-Journal of Engineering Manufacture, Vol. 229(6), pp. 910-920.

54. Gupta P.K., Ph.D. Thesis, "Investigations on ECDM for subtractive micro-fabrication on glass", Indian Institute of Technology Roorkee-2015.

55. Gupta V. and Pandey P.M. (2016), "Experimental investigation and statistical modeling of temperature rise in rotary ultrasonic bone drilling", Medical engineering & physics, Vol. 38(11), pp. 1330-1338.

56. Guzzo P.L., Shinohara A.H. and Raslan A.A. (2004), "A Comparative study on ultrasonic machining of hard and brittle materials", Journal of Brazilian Society of Mechanical Science and Engineering, Vol. 26(1), pp. 56–61.

57. Harrington E.C. (1965), "The desirability function", Industrial Quality Control, Vol. 21(10), pp. 494-498.

58. Hassan, E.H., "Advanced machining processes", McGraw-Hill Company, 2005, pp. 15-31.

59. He J.F., Guo Z.N., Lian H.S., Liu J.W., Yao Z. and Deng Y. (2019), "Experiments and simulations of micro-hole manufacturing by electrophoresis-assisted micro-ultrasonic machining", Journal of Materials Processing Technology, Vol. 264, pp. 10-20.

60. He M., Edgar S., Jeffries G.D.M., Lorenz R.M., Shelby J.P. and Chiu D.T. (2005), "Selective encapsulation of single cells and subcellular organelles into picoliter- and femtoliter-volume droplets", Analytical Chemistry, Vol. 77, pp. 1539-1544.

61. Hessel V., Hardt S. and Lowe H. (2004), "Chemical micro process engineering: fundamentals, modelling and reactions", Wiley-VCH, Weinheim.

62. Hessel V., Lowe H. and Schonfeld F. (2005), "Micromixers-a review on passive and active mixing principles", Chemical Engineering Science, Vol. 60, pp. 2479-2501.

63. Ho K.H. and Newman S.T. (2003), "State of the art electrical discharge machining (EDM)", International Journal of Machine Tools and Manufacture, Vol. 43, pp. 1287-1300.

64. Hocheng H., Kuo K.L. and Lin J.T. (1999), "Machinability of zirconia ceramics in ultrasonic drilling", Materials and Manufacturing Processes, Vol. 14(5), pp. 713-724.

65. Hsu T.R. (2002), "Miniaturization–a paradigm shift in advanced manufacturing and education", In International conference on Advanced Manufacturing Technologies and Education in the 21st Century.

66. Hu X., Yu Z. and Rajurkar K.P. (2007), "Experimental study of tool wear in micro ultrasonic machining", In 35th North American Manufacturing Research Conference, Vol. 35, pp. 129-136.

67. Ichida Y., Sato R., Morimoto Y. and Kobayashi K. (2005), "Material removal mechanisms in non-contact ultrasonic abrasive machining", Wear, Vol. 258, pp. 107-114.

68. Ismagilov R.F., Ng J.M.K., Kenis P.J.A. and Whitesides G.M. (2001), "Microfluidic arrays of fluid-fluid diffusional contacts as detection elements and combinatorial tools", Analytical Chemistry, Vol. 73, pp. 5207-5213.

69. Jackson M.J. and Davim J.P. (2011), "Machining with abrasives", New York: Springer.

70. Jadoun R.S., Kumar P., Mishra B.K. and Mehta R.C.S. (2006), "Optimization of process parameters for ultrasonic drilling of advanced engineering ceramics using the Taguchi approach", Engineering Optimization, Vol. 38(7), pp. 771-787.

71. Jagannatha N., Hiremath S.S., Sadashivappa K. and Arun K.V. (2012),"Machining of soda lime glass using abrasive hot air jet: An Experimental Study", Machining Science and Technology: An International Journal, Vol. 16(3), pp. 459-472.

72. Jain A.K. and Pandey P.M. (2016), "Study of Peck drilling of borosilicate glass with µRUM process for MEMS", Journal of Manufacturing Processes, Vol. 22, pp. 134-150.

73. Jain A.K. and Pandey P.M. (2017), "Experimental investigations of ceramic machining using µ-grinding and µ-rotary ultrasonic machining processes: A comparative study", Materials and Manufacturing Processes, Vol. 32(6), pp. 598-607.

74. Jain V. (2014), "Application of Taguchi approach in the optimization of cutting Parameters in micro-ultrasonic drilling process", International Journal of Engineering Research and Applications, pp. 10-16.

75. Jain V., Ph.D Thesis, "Investigations on development of microchannels using micro ultrasonic machining", IIT Roorkee -2012.

76. Jain V., Sharma A.K. and Kumar P. (2011), "Microdrilling of difficult to cut materials for MEMS applications using ultrasonic micromachining", i-manager's Journal on Mechanical Engineering, Vol. 1(2), pp. 24-32.

77. Jain V., Sharma A.K. and Kumar P. (2011), "Recent developments and research issues in microultrasonic machining", ISRN Mechanical Engineering, Vol. 2011, pp. 1-15.

78. Jain V., Sharma A.K. and Kumar P. (2012), "Investigations on tool wear in micro ultrasonic machining", Applied Mechanics and Materials, Vol. 110-116, pp. 1561-1566.

79. Jain V.K., "Advanced machining processes", Book- Allied Publishers, Mumbai. 2009.

80. Jain V.K., "Introduction to micromachining", Oxford: Alpha Science International Limited, 2010.

81. Jain V.K., Dixit P.M. and Pandey P.M. (1999), "On the analysis of the electrochemical spark machining process", International Journal of Machine Tools and Manufacture, Vol. 39(1), pp. 165-186.

82. James S., and Sonate A. (2018), "Experimental study on micromachining of CFRP/Ti stacks using micro ultrasonic machining process," The International Journal of Advanced Manufacturing Technology, Vol. 95(1-4), pp. 1539-1547.

83. Jáuregui A.L., Siller H.R., Rodríguez C.A. and Elías-Zúñiga A. (2010), "Evaluation of micromechanical manufacturing processes for microfluidic devices", The International Journal of Advanced Manufacturing Technology, Vol. 48, pp. 963-972.

84. Ji R.J., Liu Y.H., Diao R.Q. Zhang Y.Z. Wang F. Cai B.P. and Xu C.C. (2014), "experimental research on electrical discharge machining characteristics of engineering ceramics with different electrical resistivities", The International Journal of Advanced Manufacturing Technology, Vol. 75(9–12), pp. 1743–1750.

85. Jin M., Feng X., Xi J., Zhai J., Cho K., Feng L. and Jiang L. (2005), "Super-hydrophobic PDMS surface with ultra-low adhesive force", Macromolecular Rapid Communication, Vol. 26, pp. 1805-1809.

86. Kainth G.S., Nandy A. and Singh K. (1979), "On the mechanics of material removal in ultrasonic machining", International Journal of Machine Tool Design and Research, Vol. 19, pp. 33-41.

87. Kandlikar S., Garimella S., Li D., Colin S. and King M.R. (2005), "Heat transfer and fluid flow in minichannels and microchannels", Elsevier, Amsterdam.

88. Kazantsev V.F. and Rosenberg L.D. (1965), "The mechanism of ultrasonic cutting", Ultrasonics, Vol. 3, pp. 166-174.

89. Kennedy D.C. and Grieve R.J. (1975), "Ultrasonic machining- a review", The Production Engineer, Vol. 54(1), pp. 481-486.

90. Khmelev V.N., Abramenko D.S., Barsukov R.V. and Lebedev A.N. (2008), "Usage features of contact and noncontact measuring methods of oscillation amplitude during adjustment process of ultrasonic devices", Proceedings of the 9th International Workshop and Tutorials on Electron Devices and Materials, Novosibirsk, Russia.

91. Klopfstein M.J., Ghisleni R., Lucca D.A. and Brinksmeier E. (2008), "Surface characteristics of micro-ultrasonically machined (1 0 0) silicon", International Journal of Machine Tools and Manufacture, Vol. 48, pp. 473-476.

92. Kohno T., Okazaki Y., Ozawa N., Mitui K. and Omada M. (1989), "In process measurement and a workpiece-referred form accuracy control system (WORFAC): concept of the method and preliminary experiment", Precision Engineering, Vol. 11(1), pp. 9-14.

93. Komaraiah M. and Reddy P.N. (1993), "Relative performance of tool materials in ultrasonic machining", Wear, Vol. 161(1-2), pp. 1-10.

94. Komaraiah M., Manan M.A., Reddy P.N. and Victor S. (1988), "Investigation of surface roughness and accuracy in ultrasonic machining", Precision Engineering, Vol. 10(2), pp. 59-65.

95. Koo N., Plachetka U., Otto M. Bolten J., Jeong J., Lee E. and Kurz H. (2008), "The fabrication of a flexible mold for high resolution soft ultraviolet nanoimprint lithography", Nanotechnology, Vol. 19, pp. 225304-225307.

96. Kremer D., Saleh S.M., Ghabrial S.R. and Moisan A. (1981), "State of the art of ultrasonic machining", Annals of CIRP, Vol. 30(1), pp. 107-110.

97. Kumar K., Zindani, D. and Davim J.P. (2018), Advanced machining and manufacturing Processes. Springer.

98. Kumar P. and Goel P. (2002), "Product quality optimization using fuzzy set concepts: a case study", Quality Engineering, Vol. (15/1) pp. 1-8.

99. Kumar V. and Singh H. (2019), "Rotary ultrasonic drilling of silica glass BK-7: microstructural investigation and process optimization through TOPSIS", Silicon, Vol. 11(1), pp. 471-485.

100. Kuriakose S., Patowari P.K. and Bhatt J. (2017), "Machinability study of Zr-Cu-Ti metallic glass by micro hole drilling using micro-USM", Journal of Materials Processing Technology, Vol. 240, pp. 42-51.

101. Kuriyagawa T., Shirosawa T., Saito O. and Syoji K. (2001), "Micro ultrasonic abrasive machining for three-dimensional milli-structures of hard-brittle materials", Proceedings of the 16th ASPE Annual Meeting 2001, pp. 525–528.

102. Kuriyagawa T., Shirosawa T., Saitoh O. and Syoji K. (2002), "Development of micro ultrasonic abrasive machining system: 1st report on studies in micro ultrasonic abrasive machining", JSME International Journal Series C Machine Elements and Manufacturing, Vol. 45(2), pp. 593-600.

103. Lavrik N.V., Sepaniak M.J. and Datskos P.G. (2004), "Cantilever transducers as a platform for chemical and biological sensors", Review of Scientific Instruments, Vol. 75(7), pp. 2229-2253.

104. Lawn B.R., Evans A.G. and Marshall D.B. (1980), "Elastic/plastic indentation damage in ceramics: the median/radial crack system", Journal of American Ceramic Society, Vol. 63(9–10), pp. 574–581.

105. Lawn, B., "Fracture of brittle solids", Cambridge University Press, Cambridge, 1993.

106. Lee H., "Thermal design: Heat sinks, thermo electrics, heat pipes, compact heat exchangers and solar cells", Hoboken, New Jersey: John Wiley & Sons, 2010.

107. Lee Y.H. and Choi K.J. (2010), "Analysis of silicon via hole drilling for wafer level chip stacking by UV laser. International Journal of Precision Engineering and Manufacturing, Vol. 11(4), pp. 501-507.

108. Lei S., Yu Z., Zhou K., Li J. and Kang R. (2019), "Influence of the planetary movement of tool on the aspect ratio of micro holes machined by micro-USM", Journal of Micro and Nano-Manufacturing, Vol. 7, pp. 1-7.

109. Li H., Wang Z., Wang Y., Liu H. and Zhao Z. (2018), "Micro-EDM and micro-USM combined milling of ZrB 2-SiC-graphite composite for 3D micro-cavities", The International Journal of Advanced Manufacturing Technology, pp. 1-11.

110. Lian H.S., Guo Z.N., Liu J.W., Huang Z.G. and He J.F. (2016), "Experimental study of electrophoretically assisted micro-ultrasonic machining. The International Journal of Advanced Manufacturing Technology, Vol. 85(9-12), pp. 2115-2124.

111. Lin Y.C., Lee, C.C., Lin H.S., Hong Z.H., Hsu F.C., Hung T.P. and Lyu Y.T. (2017), "Fabrication of microfluidic structures in quartz via micro machining technologies," Microsystem Technologies, Vol. 23(6), pp. 1661-1669.

112. Liow J.L. (2009), "Mechanical micromachining: a sustainable micro-device manufacturing approach", Journal of Cleaner Production, Vol. 17, pp. 662-667.

113. Lowe H., et al. (2000), "Micromixing technology", In: Fourth International Conference on Microreaction Technology, IMRET 4, Atlanta, USA. A.I.Ch.E. Topical Conference Proceedings, pp. 31–47.

114. Malek C.K., Robert L., Boy J.J. and Blind P. (2007), "Deep microstructuring in glass for microfluidic applications", Microsystem Technologies, Vol. 13, pp. 447-453.

115. Malviya M. and Desai K.A. (2019), "Build orientation optimization for strength enhancement of FDM parts using machine learning based algorithm", Proceedings of CAD'19, Singapore, pp. 232-236.

116. Mansur E.A., Mingxing Y.E., Yundong W. and Youyuan D. (2008), "A state-of-the-art review of mixing in microfluidic mixers", Chinese Journal of Chemical Engineering, Vol. 16(4), pp. 503-516.

117. Mark D., Haeberle S., Roth G., Von Stetten F. and Zengerle R. (2010), "Microfluidic lab-on-a-chip platforms: requirements, characteristics and applications", Chemical Society Reviews, Vol. 39(3), pp. 1153-1182.

118. Marshall D.B., Lawn B.R. and Evans A.G. (1982), "Elastic/plastic indentation damage in ceramics: the lateral crack system", Journal of American Ceramic Society, Vol. 65(11), pp. 561–566.

119. Masuzawa T. (2000), "State of the art of micromachining", CIRP Annals - Manufacturing Technology, Vol. 49(2), pp. 473-488.

120. Medis P.S. and Henderson H.T. (2005), "Micromachining using ultrasonic impact grinding", Journal of Micromechanics and Microengineering, Vol. 15(8), pp. 1556-1559.

121. Meijer M. (2004), "Laser beam machining (LBM), State of the art and new opportunities", Journal of Materials Processing Technology, Vol. 149, pp. 2-17.

122. Miller G.E. (1957), "Special theory of ultrasonic machining", Journal of Applied Physics, Vol. 28(2), pp. 149-156.

123. Mitchell-Smith J. and Clare A.T. (2016), "Electrochemical jet machining of titanium: overcoming passivation layers with ultrasonic assistance", Procedia CIRP, Vol. 42, pp.379-383.

124. Moges T.M., Desai K.A. and Rao P.V.M. (2017), "On modeling of cutting forces in micro-end milling operation. Machining Science and Technology, Vol. 21(4), pp.562-581.

125. Montgomery D., "Design and analysis of experiments", John Wiley and Sons New York, 2001.

126. Morgan C.J., Vallance R.R. and Marsh E.R. (2004), "Micromachining glass with polycrystalline diamond tools shaped by micro electro discharge machining", Journal of Micromechanics and Microengineering, Vol. 14(12), pp. 1687-1692.

127. Namba T., Sugimoto Y., Negishi M., Irie A., Ushikubi F., Kakizuka A. and Narumiya S. (1993), "Alternative splicing of C-terminal tail of prostaglandin E receptor subtype EP3 determines G-protein specificity", Nature, Vol. 365(6442), pp. 166.

128. Neils C., Tyree Z., Finlayson B. and Folch A. (2004), "Combinatorial mixing of microfluidic streams", Lab on a Chip, Vol. 4, pp. 342-350.

129. Neppiras A. (1964), "Ultrasonic machining and forming", Ultrasonics, Vol. 2, pp. 167-173.

130. Nguyen N.T. and Wu Z. (2005), "Micromixers- a review", Journal of Micromechanics and Microengineering, Vol. 15, pp. 1-16.

131. Nisar A., Afzulpurkar N., Mahaisavariya B. and Tuantranont A. (2008), "MEMS-based micropumps in drug delivery and biomedical applications", Sensors and Actuators B, Vol. 130, pp. 917-942.

132. Nitoi D., Petriceanu C., Severin I., Bogatu A.M. and Teodorescu O. (2016), "Semiautomatic high frequency ultrasonic testing system for welded plastic pipes", Applied Mechanics and Materials, Vol. 835, pp. 599-604.

133. Oh K.W. and Ahn C.H. (2006), "A review of microvalves", Journal of Micromechanics and Microengineering, Vol. 16, pp. 13-39.

134. Pandey P.C. and Shan H.S., "Modern machining processes", Tata McGraw-Hill, 1980.

135. Paul L. and Hiremath S.S. (2013), "Response surface modelling of micro holes in electrochemical discharge machining process", Proceedings of the Institution of Mechanical Engineers, Part B: Journal of Engineering Manufacture, Vol. 64, pp. 1395-1404.

136. Paul L., Hiremath S.S. and Ranganayakulu J. (2014) "Experimental investigation and parametric analysis of electro chemical discharge machining", International Journal of Manufacturing Technology and Management, Vol. 28(1-3), pp.57-79.

137. Pei W., Yu Z., Li J., Ma C., Xu W., Wang X. and Natsu W. (2013), "Influence of abrasive particle movement in micro USM", Proceedings of the 17th CIRP Conference on Electro Physical and Chemical Machining (ISEM), Vol. 6, pp. 552-556.

138. Pemble C.M. and Towe B.C. (1999), "A miniature shape memory alloy pinch valve", Sensors and Actuators A, Vol. 77, pp. 145-148.

139. Perveen A., and Molardi C. (2017), Machining of glass materials: an overview", In Advanced Manufacturing Technologies, pp. 23-47. Springer, Cham.

140. Petersen D.R. and Doorn J.A. (2004), "Reactions of 4-hydroxynonenal with proteins and cellular targets", Free Radical Biology and Medicine, Vol. 37(7), pp. 937-945.

141. Pham D.T., Dimov S.S., Bigot S., Ivanov A. and Popov K. (2004), "Micro-EDM—recent developments and research issues", Journal of Materials Processing Technology, Vol. 149(1-3), pp. 50-57.

142. Phillips RJ., "Microchannel heat sinks", Lincoln Lab, 1988, I, pp. 31–48.

143. Pilarski P.M., Adamia S. and Backhouse C.J. (2005), "An adaptable microvalving system for on-chip polymerase chain reactions", Journal of Immunology Methods, Vol. 305, pp. 48-58.

144. Qu N.S., Zhang T. and Chen X.L. (2018), "Surface texturing of polyimide composite by micro-ultrasonic machining", Journal of Materials Engineering and Performance, Vol. 27(3), pp. 1369-1377.

145. Rao R.V., Pawar P.J. and Davim J.P. (2010),"Parameter optimization of ultrasonic machining process using nontraditional optimization algorithms", Materials and Manufacturing Processes, Vol. 25, pp. 1120-1130.

146. Roy E., Pallandre, A., Zribi B., Horny M.C., Delapierre F.D., Cattoni A., Gamby J. and Haghiri- Gosnet A.M. (2016), "Overview of materials for microfluidic applications", In Advances in Microfluidics-New Applications in Biology", Energy and Materials Sciences. IntechOpen.

147. Ruszaj A. (2017), "Unconventional processes of ceramic and composite materials shaping", Mechanik, Vol. 3, pp.39-44.

148. Ruszaj A., Gawlik, J. and Skoczypiec S. (2016), "Electrochemical machining–special equipment and applications in aircraft industry", Management and Production Engineering Review, Vol. 7(2), pp.34-41.

149. Sahu R.K., Hiremath S.S., Manivannan P.V. and Singaperumal M. (2014) "Generation and characterization of copper nanoparticles using micro-electrical discharge machining", Materials and Manufacturing Processes, Vol. 29(4), pp.477-486.

150. Sarwade A., Master of Science Thesis, Study of micro rotary ultrasonic machining, University of Nebraska – Lincoln-2010.

151. Schmidt R. (2004), "Challenges in electronic cooling—opportunities for enhanced thermal management techniques—microprocessor liquid cooled mini-channel heat sink", Heat Transfer Engineering, Vol. 25, pp. 3–12.

152. Sharma D. and Deb K. (2014), "Generation of compliant mechanisms using hybrid genetic algorithm", Journal of The Institution of Engineers (India): Series C, Vol. 95(4), pp.295-307.

153. Sharma D., Deb K. and Kishore N.N. (2011), "Domain-specific initial population strategy for compliant mechanisms using customized genetic algorithm", Structural and Multidisciplinary Optimization, Vol. 43(4), pp.541-554.

154. Sharma L.K., Vikram V. and Singh T.N. (2017), "Developing novel models using neural networks and fuzzy systems for the prediction of strength of rocks from key geomechanical properties", Measurement, Vol. 102, pp. 158-169.

155. Sharma V., Srivastava I., Jain V.K. and Ramkumar J. (2019), "Modelling of wire electrochemical micromachining (Wire-ECMM) process for anode shape prediction using finite element method", Electrochimica Acta, Vol. 312, pp. 329-341.

156. Shaw M.C. (1956), "Ultrasonic grinding", Annals of CIRP, Vol. 5, pp. 25-53.

157. Shi K., Zhang D. and Ren J. (2015), "Optimization of process parameters for surface roughness and microhardness in dry milling of magnesium alloy using Taguchi with grey relational analysis", The International Journal of Advanced Manufacturing Technology, Vol. 81(1-4), pp. 645-651.

158. Shinozuka J. (2009), "Fabrication of multiple micro-grooves by ultrasonic machining with a tool that laminated thin hard-material and thin soft-material", Advanced Materials Research, Vol. 76-78, pp. 577-582.

159. Shoji S. and Esashi M. (1994), "Microflow devices and systems", Journal of Micromechanics and Microengineering, Vol. 4, pp. 157-171.

160. Singh A., Garg H. and Lall A.K. (2017), "Optical polishing process: analysis and optimization using response surface methodology (RSM) for large diameter fused silica flat substrates", Journal of Manufacturing Processes, Vol. 30, pp. 439-451.

161. Singh M., Jain V.K. and Ramkumar J. (2019), "Micro-electrical discharge milling operation", In Micro-electrical Discharge Machining Processes Springer, Singapore, pp. 23-51.

162. Singh N.K., Pandey P.M. and Singh K.K. (2017), "Experimental investigations into the performance of EDM using argon gas-assisted perforated electrodes", Materials and Manufacturing Processes, Vol. 32(9), pp. 940-951.

163. Skoczypiec S., Grabowski M. and Ruszaj A. (2016), "The impact of electrochemical assistance on the microturning process", The International Journal of Advanced Manufacturing Technology, Vol. 86(5-8), pp.1873-1880.

164. Smith T.J. (1974), "Parameter influence in ultrasonic machining", Ultrasonics, Vol. 11(5), pp. 196-198.

165. Soundararajan V. and Radhakrishnan V. (1986), "An experimental investigation on the basic mechanisms involved in ultrasonic machining", International Journal of Machine Tool Design and Research, Vol. 26(3), pp. 307-321.

166. Sreehari D. and Sharma A.K. (2018), "On form accuracy and surface roughness in micro-ultrasonic machining of silicon microchannels", Precision Engineering, Vol. 53, pp. 300-309.

167. Studer V., Hang G., Pandolfi A., Ortiz M., Anderson W.F. and Quake S.R. (2004), "Scaling properties of a low-actuation pressure microfluidic valve", Journal of Applied Physics, Vol. 95, pp. 393-398.

168. Subramonian S., Kasim M.S., Ali M.A.M., Abdullah R.I.R. and Anand T.J.S. (2015), "Micro-drilling of silicon wafer by industrial CO_2 laser", International Journal of Mechanics and Materials Engineering, Vol. 10(1), pp. 2-6.

169. Sun X.Q., Masuzawa T. and Fujino M. (1996[a]), "Micro ultrasonic machining and its applications in MEMS", Sensors and Actuators A, Vol. 57, pp. 159-164.

170. Sun X.Q., Masuzawa T. and Fujino M. (1996[b]), "Micro ultrasonic machining and self-aligned multilayer machining/assembly technologies for 3D micromachines", Proceedings of IEEE, MEMS '96, pp. 312-317.

171. Takayama S., Ostuni E., LeDuc P., Naruse K., Ingber D.E. and Whitesides G.M. (2001), "Subcellular positioning of small molecules", Nature, Vol. 411, pp. 1016.

172. Takeuchi Y., Sawada K. and Sata T. (1996), "Ultraprecision 3-D micromachining of glass", Annals of CIRP, Vol. 45(1), pp. 401-404.

173. Tateishi T., Yoshihara N., Yan J. W. and Kuriyagawa T. (2009), "Fabrication of high-aspect ratio micro holes on hard brittle materials-study on electrorheological fluid-assisted micro ultrasonic machining," Key Engineering Materials, Vol. 389, pp. 264-270.

174. Terry S.C., Jerman J.H. and Angell J.B. (1979), "A gas chromatographic air analyzer fabricated on a silicon wafer", IEEE Transactions on Electron Devices, Vol. 26(12), pp.1880-1886.

175. Thoe T.B., Aspinwall D.K. and Wise M.L.H. (1998), "Review on ultrasonic machining", International Journal of Machine Tools and Manufacture, Vol.38(4), pp.239-255.

176. Thomas Jr. L.J. and Bessman S.P., Micropump powered by piezoelectric disk benders, US patent 3,963,380, USA, 1975.

177. Thomson J.A., Itskovitz-Eldor J., Shapiro S.S., Waknitz M.A., Swiergiel J.J., Marshall V.S. and Jones J.M. (1998), "Embryonic stem cell lines derived from human blastocysts", Science, Vol. 282(5391), pp. 1145-1147.

178. Tyagi A., Sharma V., Singh Patel D., Jain V.K. and Ramkumar J. (2019), "Experimental and analytical investigations into wire electrochemical micro turning", Journal of Micromanufacturing, Vol. 2(1), pp. 42-58.

179. Visvakarma U., Ph.D. Thesis, "Development of EDM process variants and analysis of their effects on performance measures", Indian Institute of Technology Roorkee-2014.

180. Visvanathan K., Li T. and Gianchandni Y.B. (2011), "3D-SOULE: A fabrication process for large scale integration and micromachining of spherical structures ", Proceedings of 24th International Conference on Micro Electro Mechanical Systems (MEMS), IEEE, pp. 45-48.

181. Viswanath A., Li T. and Gianchandni Y. (2014), "High resolution micro ultrasonic machining for trimming 3D microstructures", Journal of Micromechanics and Microengineering, Vol. 24(6), pp. 65017 (1-8).

182. Wang J., Shimada K., Mizutani M. and Kuriyagawa T. (2018), "Effects of abrasive material and particle shape on machining performance in micro ultrasonic machining," Precision Engineering, Vol. 51, pp. 373-387.

183. Wang J., Shimada K., Mizutani M. and Kuriyagawa T. (2018), "Tool wear mechanism and its relation to material removal in ultrasonic machining", Wear, Vol. 394, pp. 96-108.

184. Wang M., Zhang Y., Xu X., Chen G., Clare A.T. and Ahmed N. (2019), "Effects of tool intermittent vibration on helical internal hole processing in electrochemical machining", Proceedings of the Institution of Mechanical Engineers, Part C: Journal of Mechanical Engineering Science, Vol. 233(12), pp.4102-4111.

185. Weibel D.B. and Whitesides G.M. (2006), "Applications of microfluidics in chemical biology", Current Opinion in Chemical Biology, Vol. 10, pp. 584-591.

186. Wensink H., Berenschot J.W., Jansen H.V. and Elwenspoek M.C. (2000), "High resolution powder blast micromachining", Proceedings of 13th International Workshop on Micro Electro Mechanical Systems (MEMS 2000), Miyazaki, Japan, pp. 769-774.

187. Wheeler D.B., Carpenter A.E. and Sabatini D.M. (2005), "Cell microarrays and RNA interference chip away at gene function", Nature Genetics Supplement, Vol. 37, pp. 25-30.

188. Xiao X., Zheng K. and Liao W. (2014), "Theoretical model for cutting force in rotary ultrasonic milling of dental zirconia ceramics", The International Journal of Advanced Manufacturing Technology, Vol. 75(9-12), pp. 1263-1277.

189. Yadav R.S. and Yadava V. (2017), "Experimental investigations on electrical discharge diamond face surface grinding (EDDFSG) of hybrid metal matrix composite", Materials and Manufacturing Processes, Vol. 32(2), pp. 135-144.

190. Yang B.Z. and Lin Q. (2007), "A latchable microvalve using phase change of paraffin wax", Sensor and Actuators A, Vol. 134, pp. 194-200.

191. Yarlagadda P.K.D.V, Christodoulou P. and Subramanian V.S. (1999), "Feasibility studies on the production of electro-discharge machining electrodes with rapid prototyping and the electroforming process", Journal of Materials Processing Technology, Vol. 89-90, pp. 231-237.

192. Yu Y.Z., Rajurkar K.P. and Tandon A. (2004), "Study of 3D micro ultrasonic machining", ASME Journal of Manufacturing Science and Engineering, Vol. 126, pp. 727-732.

193. Yu Z., Hu X. and Rajurkar K.P. (2006), "Influence of debris accumulation on material removal and surface roughness in micro ultrasonic machining of silicon", CIRP Annals Manufacturing Technology, Vol. 55(1), pp. 201-204.

194. Yu Z., Ma C., An C., Li J. and Guo D. (2012), "Prediction of tool wear in micro-USM", CIRP Annals- Manufacturing Technology, Vol. 61(1), pp. 227-230.

195. Zarepour H. and Yeo S.H. (2012[a]), "Predictive modeling of material removal modes in micro ultrasonic machining", International Journal of Machine Tools and Manufacture, Vol. 62, pp. 13-23.

196. Zarepour H. and Yeo S.H. (2012[b]), "Single abrasive particle impingements as a benchmark to determine material removal modes in micro ultrasonic machining", Wear, Vol. 288, pp. 1-8.

197. Zarepour H., Yeo S.H, Tan P. and Aligiri E. (2010), "A new approach for force measurement and workpiece clamping in micro-ultrasonic machining", The International Journal of Advanced Manufacturing Technology, Vol. 53, pp. 517-522.

198. Zhang C., Brinksmeier E. and Rentsch R. (2006), "Micro-USAL technique for the manufacture of high quality microstructures in brittle materials", Precision Engineering, Vol. 30, pp. 362-372.

199. Zhang C., Rentsch R. and Brinksmeier E. (2005), "Advances in micro ultrasonic assisted lapping of microstructures in hard–brittle materials: a brief review", International Journal of Machine Tools & Manufacture, Vol. 45, pp. 881-890.

200. Zhang C., Xing D. and Li Y. (2007), "Micropumps, microvalves, and micromixers within PCR microfluidic chips: Advances and trends", Biotechnology Advances, Vol. 25, pp. 483-514.

201. Zhang S. (2004), "Beyond the petri dish", Nature Biotechnology, Vol. 22, pp. 151-152.

202. Zhong Z.W. (2003), "Ductile or partial ductile mode machining of brittle materials", The International Journal of Advanced Manufacturing Technology, Vol. 21(8), pp. 579-585.

203. Ziaie B., Baldi A., Lei M. Gu Y. and Siegel R.A. (2004), "Hard and soft micromachining for Bio-MEMS: review of techniques and examples of applications in microfluidics and drug delivery", Advanced Drug Delivery Reviews, Vol. 56(2), pp. 145-172.

APPENDIX-A

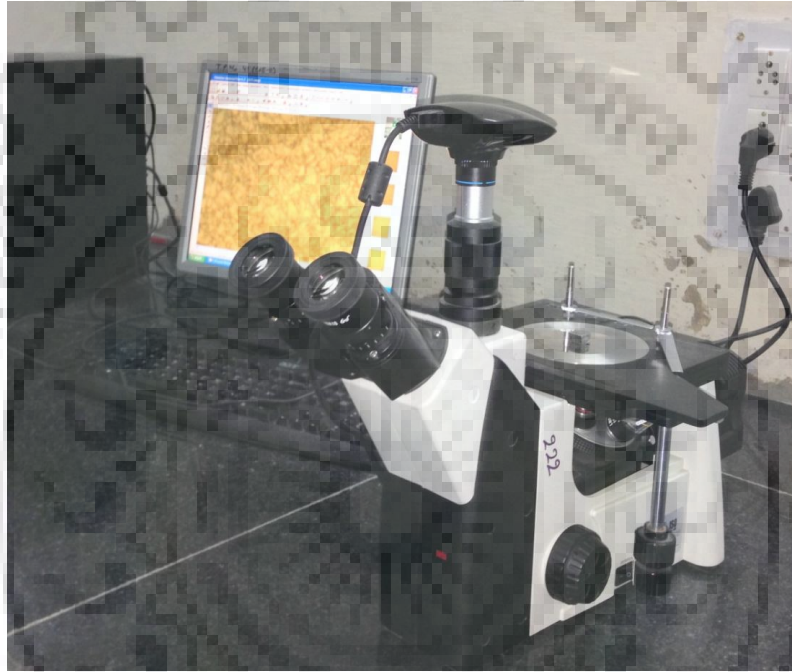## A.1 Equipments

A.1.1 Optical Microscope

Figure A.1 Optical Microscope

Make	Dewinter
Model	DMI Premium
Eyepiece	Wide field eyepiece 10X (Paired) FOV 18mm
Objectives (infinity corrected)	M Long Working Distance Plan Achromatic 5X to 50X
Trinocular Observation Head	- Side and top of observation head inclined at 45°. - Vertical phototube for micro photography light split (80:20). - Diopter adjustment ring on binocular tube (±5). - Interpupillary distance from 54mm to 75mm.

A.1.2 Electronic Balance

Figure A.2 Electronic Balance

Make	SHIMADZU
Model	AUW220D
Measuring capacity	220 g
Least count	0.01g

A.1.3 Ultrasonic Cleaner

Figure A.3 Ultrasonic Cleaner

Make	Citizen
Model	YJ5120-1
Capacity	5 Ltr
Frequency	40 KHz
Temperature Range	0-80 °C
Adjustable Time	1-99 min
Ultrasonic Power	120 W

A.1.4 Optical Microscope

;
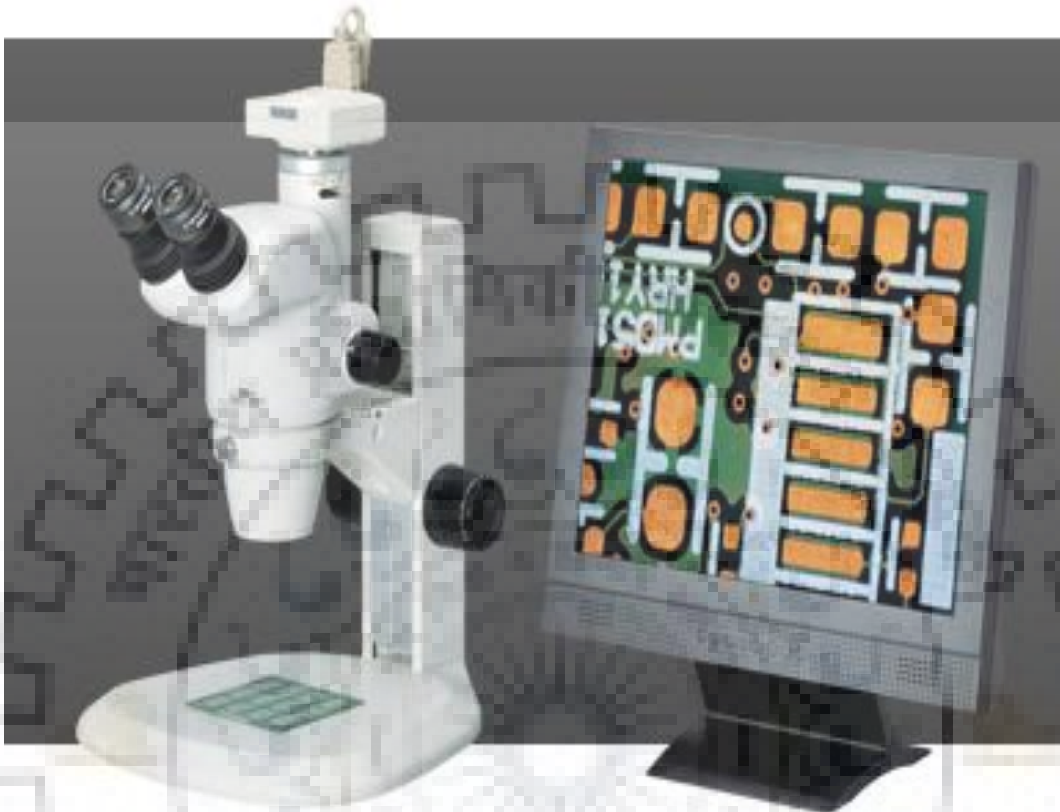
Figure A.4 Optical Microscope

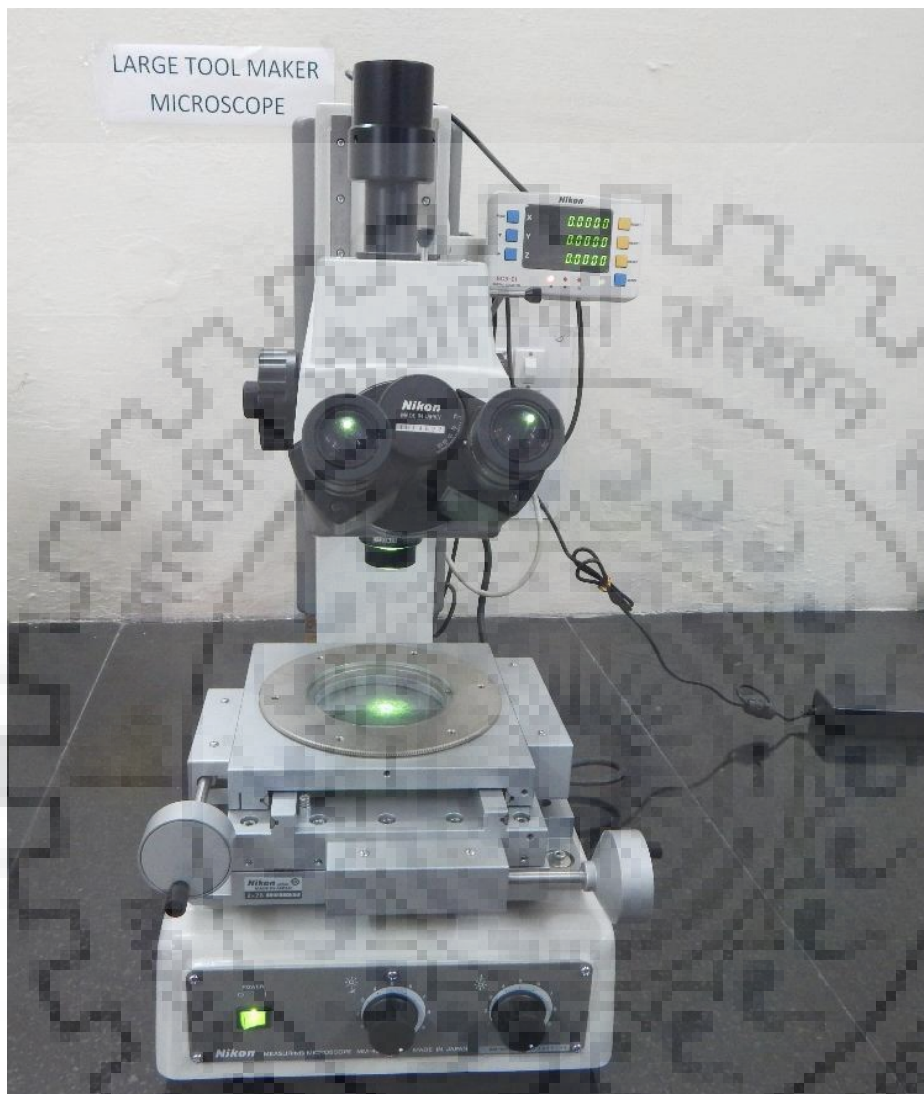| Make	NIKON
Model	SMZ745T
Optical System	Greenough optical system
Total Magnification	3.35-300 X
Zoom Range	0.67-5 X
Zoom Ratio	7.5:1
Working Distance	115 mm
Interpupillary distance adjustment	52-75 mm
Eyepiece Tube	Fixed type

A.1.5 Digital Tool Maker's Microscope

Figure A.5 Digital Tool Maker's Microscope

Make	NIKON
Model	MM-400
Z-axis movement	Manual (dual side coarse/fine focus knob)
Eyepiece	CFWN10x (Field No. 20)
Max. workpiece height	150mm
Light source : Diascopic	LED diascopic illuminator (standard)
: Episcopic	LED episcopic illuminator

A.1.6 Field Emission Scanning Electron Microscope (FE-SEM)

Figure A.6 Field Emission Scanning Electron Microscope

Make	FEI
Model	QUANTA 200F
Spatial Resolution	20 kV
Magnification	100X-1000X
Operating Voltage	5-30 kV
Gun	Field Emission Gun (FEG)

LIST OF PUBLICATIONS

1. **S. Kumar** and A. Dvivedi (2019) "On Machining of Hard and Brittle Materials using Rotary Tool Micro-ultrasonic Drilling Process", Materials and Manufacturing Processes, Vol. 34(7), pp.736-748. (**Impact factor: 3.35**)

2. **S. Kumar** and A. Dvivedi (2019) "Micro-ultrasonic drilling of monocrystalline silicon: An experimental investigation on machined surface topography and optimization using User's preference rating based TOPSIS", Materials Science in Semiconductor Processing, Vol. 102. (**Impact factor: 2.72**).

3. **S. Kumar** and A. Dvivedi (2019) "On effect of tool rotation on performance of rotary tool micro-ultrasonic machining", Materials and Manufacturing Processes, Vol. 34(5), pp. 475-486. (**Impact factor: 3.35**)

4. **S. Kumar** and A. Dvivedi (2019)"On effect of tool material properties of performance of rotary tool micro-USM", Journal of Brazilian Society of Mechanical Engineering, 41:432. (**Impact factor: 1.74**)

5. **S. Kumar** and A. Dvivedi (2018) "Fabrication of microchannels using rotary tool micro-USM: An experimental investigation on tool wear reduction and form accuracy improvement", Journal of Manufacturing Processes, Vol. 32, pp. 802-815. (**Impact factor: 3.46**)

6. **S. Kumar** and A. Dvivedi, (2017) "Experimental investigation on drilling of borosilicate glass using micro-USM with and without tool rotation: a comparative study", International Journal of Additive and Subtractive Materials Manufacturing, Vol. 1(3-4), pp. 213-222.

7. **S. Kumar** A. Dvivedi and P. Kumar (2017) "On tool wear in rotary tool micro-ultrasonic machining", Proceedings of the 3rd Pan American Materials Congress (pp. 75-82). Springer, Cham.

8. **S. Kumar** and A. Dvivedi "On development of predictive model for material removal rate and performance evaluation of ultrasonic turning process", Journal of Manufacturing Processes, (**Impact factor: 3.46**) (**Under review**)

9. **S. Kumar** and A. Dvivedi "On predictive modeling of tool wear in rotary tool micro-ultrasonic machining", International Journal of Machine Tools and Manufacture. (**Impact factor: 6.01**) (**Under review**)

10. S. Kumar and A. Dvivedi "On predictive modeling of tool wear in rotary tool micro-ultrasonic machining", Measurement (**Impact factor: 2.79**) (**Under review**)

11. **S. Kumar** and A. Dvivedi (2019) "Parametric investigations and optimization of rotary tool micro-USM using Taguchi methodology", Proceedings of the 6th International Conference on Production and Industrial Engineering (CPIE-2019) NIT Jalandhar.

12. **S. Kumar** and A. Dvivedi (2018) "On performance evaluation of helical grooved tool during rotary tool micro-ultrasonic machining", Proceedings of the 7th International and 28th All India Manufacturing, Design and Research (AIMTDR-2018) Conference at College of Engineering Guindy, Anna University, Chennai.

13. **S. Kumar** and A. Dvivedi (2016) "On comparative study of micro-ultrasonic drilling with and without tool rotation", Proceedings of the 4th International Conference on Production and Industrial Engineering (CPIE-2016) NIT Jalandhar.

14. **S. Kumar** and A. Dvivedi (2016) "Investigations on fabrication of microchannels using rotary tool micro-ultrasonic machining", Proceedings of the 6th International and 27th All India Manufacturing, Design and Research (AIMTDR-2016) Conference at College of Engineering Pune, pp. 444-447.